EFFECT OF MICROSTRUCTURAL MODIFICATION ON THE ENERGY ABSORPTION CAPACITY OF ALUMINIUM FOAM

Ph.D. THESIS

by

VINOD KUMAR JEENAGER

DEPARTMENT OF METALLURGICAL AND MATERIALS ENGINEERING
INDIAN INSTITUTE OF TECHNOLOGY ROORKEE
ROORKEE- 247 667 (INDIA)
June, 2014

EFFECT OF MICROSTRUCTURAL MODIFICATION ON THE ENERGY ABSORPTION CAPACITY OF ALUMINIUM FOAM

A THESIS

Submitted in partial fulfilment of the requirements for the award of the degree of

DOCTOR OF PHILOSOPHY

in

METALLURGICAL AND MATERIALS ENGINEERING

by

VINOD KUMAR JEENAGER

DEPARTMENT OF METALLURGICAL AND MATERIALS ENGINEERING
INDIAN INSTITUTE OF TECHNOLOGY ROORKEE
ROORKEE- 247 667 (INDIA)
June, 2014

INDIAN INSTITUTE OF TECHNOLOGY ROORKEE
ROORKEE

CANDIDATE'S DECLARATION

I hereby certify that the work which is being presented in the thesis entitled **"EFFECT OF MICROSTRUCTURAL MODIFICATION ON THE ENERGY ABSORPTION CAPACITY OF ALUMINIUM FOAM"** in partial fulfilment of the requirement for the award of the Degree of Doctor of Philosophy and submitted in the Department of Metallurgical and Materials Engineering of the Indian Institute of Technology Roorkee, Roorkee is an authentic record of my own work carried out during a period from July, 2009 to July, 2014 under the supervision of **Dr. B.S.S. Daniel, Professor and Dr. Vivek Pancholi, Associate Professor**, Department of Metallurgical and Materials Engineering, Indian Institute of Technology Roorkee, Roorkee.

The matter presented in this thesis has not been submitted by me for the award of any other degree of this or any other Institute.

(VINOD KUMAR JEENAGER)

This is to certify that the above statement made by the candidate is correct to the best of our knowledge.

(B.S.S. DANIEL)
Supervisor

(VIVEK PANCHOLI)
Supervisor

Date:

The Ph. D. Viva-Voce Examination of **Mr. Vinod Kumar Jeenager**, Research Scholar, has been held on …….

Signature of Supervisors **Chairman, SRC** **Signature of External Examiner**

Head of the Department/Chairman, ODC

Dedicated

To

My beloved Grandparents

(Late Shri and Smt. Kistur chand jeenager

&

Late Shri and Smt. Ramjas jeenager)

ABSTRACT

With the advancement in technology, there is increasing scientific and industrial interest in the development of material with excellent properties intended for automotive, structural and lightweight applications. Metal foam is a class of material offers a unique combination of mechanical and physical properties such as light weight, good energy absorption and sound absorption capacity. Potential applications of metal foams include light weight cores for sandwich panels, shells and tubes, where the foam can increase the resistance to local buckling, increase the impact resistance and improve the energy absorbing capacity of the structure. Energy absorption capacity offers potential applications in transportation applications where damage due to impact load result in damage, for example, foam-filled hollow sections in automobiles (such as crash box, door assembly and wings) may reduce damage and injuries resulting from impact. For this type of application, closed cell metal foam is more suitable than the bulk alloy, because it deforms plastically under the impact without spring back, preventing further damage. Thus, there is a need to develop the effective and practical ways to improve mechanical properties of closed cell aluminium foam in order to improve energy absorption capability of aluminium foam.

From above brief introduction, it is convincible to state that the aluminium foam has the potential to be used in different field of applications mainly related to energy absorption. Therefore, it is necessary to strengthen the closed cell aluminium foam so that it can sustain the compressive loads and absorb maximum energy. In general, load applied on closed cell metal foam is sustained by the cell wall; therefore, it is necessary to strengthen the foam cell wall material. Generally, the strength of the metal foam is refers to plateau stress, which is the extended constant stress domain beyond the elastic limit. Therefore, it is reasonable to state that the strengthening of the metal foam cell wall at microscopic level helps to improve the energy absorption capacity.

Strengthening can be achieved through refinement of the cell wall structure. Refined structure can be achieved either by post processing technique or by adding suitable grain refiner which change growth mechanism from dendritic to nucleation and growth. Post processing techniques (mainly related to thermal treatment) and several techniques (i.e. addition of grain refiner, mechanical vibrations, and mechanical stirring) are employed for the modification of the cell wall microstructure. In foaming process due to process limitations, only some of the techniques (stated above) can be used to change the microstructure. Use of the mechanical

vibration and stirring is less feasible in the foaming process, whereas addition of grain refinement, reinforcement and post processing technique (i.e. thermal treatment) known to improve microstructure, as well as, mechanical performance of the alloy can be employed.

Although the current state of research on the foaming technology and the property improvement is on high, still researchers struggles to find out the way to improve the mechanical property and the stability of the liquid melt (to minimize the drainage problem). Hence, there is an urgent need to establish a serious attention to modify the cell wall microstructure, so that the energy absorption capacity can be improved. Similarly, drainage phenomenon should be addressed property to improve the stability of the foam. Therefore, in the present thesis work a serious effort has been made to deal with the different aspect (i.e. grain refinement, distribution of the intermetallic phases) of cell wall microsturctural modification in order to improve the energy absorption capacity with less drainage.

The **Chapter 1** presents introduction to the topic and gives a brief idea about the aim and scope of the work. It also provides an insight into the type of foam used in the present work.

The **Chapter 2** outlines a brief review of literature, discussing the basic description of the foam (**Section 2.1-2.2**), exist metal foam processing techniques with corresponding overview (**section 2.3**). Selection of the matrix material (**section 2.4**), physics of foaming (**section 2.5**), the factor affecting the stability of the foam structure (**section 2.6**) and the effect of the cell wall structure on the stability of the foam (**section 2.7**) are presented in the respective section. Properties and applications of the foam (**section 2.8-2.9**) followed by various strengthening techniques (**section 2.10**) are presented in their respective section. On the basis of the literature review, the proposed formulation of the problem is discussed in **section 2.11**.

The **Chapter 3,** titled experimental details: material and methods, presents materials used in the work (**Section 3.1**), experimental setup for foam processing, different characterization techniques adopted in the present work are discussed in the subsequent section (**Section 3.2-3.5**).

Chapter 4 describes the modification of the cell wall material of the produced closed cell foam at optimized parameters (i.e. stirring time, stirring speed, amount of blowing agent and holding time) through microsturctural modification using post processing technique (i.e. thermal treatment). Chapter four is divided into four main sections with respective subsections. The chapter begins with the raw material characterization, including compositional analysis, TGA

analysis of the TiH_2 and master alloy characterization. It is found that the blowing agent decompose in the range of 490- 575 ^oC. Master alloy characterization mainly shows the importance of Cu addition, it is found that the Cu addition results into proper foaming and this behaviour is attributed to the network like structure distributed evenly throughout the alloy matrix, which helps in lowering the drainage at the time of foaming [1]. Further, to analyze the macrosturctural, microsturctural behaviour and phase present in produced closed cell aluminium foam, a detailed study of produced foam has been carried out in the second section. From the analysis, it has been noticed that the formation of second phase network like structure retard the sever drainage and results in adequate pores structure, however, microstructure evaluation of the cell wall matrix shows the presence of thick dendritic structure. Dendritic structure may results in deterioration of the performance of the metal foam, therefore, to reduce the dendritic structure foam sample further thermally treated at different temperature and duration.

The effect of thermal treatment on the cell wall microstructure is discussed in the next section (third) of the chapter 4. The reduction in the dendritic structure has been observed with the thermal treatment. The thermal treatment process is carried out in two steps, first solutionising of the sample followed by water quenching, whereas, in second step sample further aged to evaluate the effect of precipitation hardening on the cell wall microstructure. It is found that solutionising results in homogenized structure with some eutectic phases, whereas, further aging results in precipitation, however, as aging time and temperature increased grain become coarser. The effect of microsturctural modification on the mechanical behaviour of the foam is discussed in the last (fourth) section of the chapter 4. It is observed that after solutionising, microhardness of the foam decreased, which further increased when sample aged, shows that aging results in precipitation hardening. The compressive properties of the foam sample improved after thermal treatment, solutionised sample shows highest property gained, whereas, aging result in moderate improvement in compressive behaviour when compared with sample in as-cast condition.

In order to check the grain refinement effect on the energy absorption capacity, a study of the effect of grain refinement has been carried out in the **chapter 5**. Chapter formation is similar to chapter 4 i.e. master alloy characterization, foam characterization, evolution of the effect of grain refinement and finally compressive behaviour analysis. Scandium is used as grain refiner, the different amount of scandium added (in the form of master alloy) during master alloy formation; using stirring and melting. It has been observed that with the use of grain refinement, the stability of foam improves. Drastic improvement has been observed in the stability of the

foam, macrostructure shows negligible, or in other words, no drainage after the scandium addition. Through microsturctural analysis effect of Sc addition in terms of grain refinement is observed, grain size is reduced up-to 27μm, which is approximately 200% lower as compared to the foam without scandium addition (82 μm). Microstructure analysis shows that the grain refinement is related to the distribution of the alloying element and their distribution in the cell wall, which in-turn affects the hardness and improves the compressive behaviour of the foam. Mechanical property analysis of the produced foam shows that the maximum hardness value for Al-Sc foam is observed at 1 wt. % of scandium addition, which is 154 VHN with minimum grain size (27μm). It has been observed that compressive behaviour of the Al-Sc foam also support the microsturctural improvement. Yield strength, plateau stress and energy absorption capacity improves as grain is refined. The improvement in the performance of the foam may be attributed to growth mechanism which changes from dendritic to nucleation and finally growth, results in grain refinement.

To check the effect of reinforcement on the energy absorption capacity, reinforcement method with different amount of reinforcement is explored in **Chapter 6.** Chapter formation is similar to chapter 4 and chapter 5. Short steel fibre (SSF) is used for reinforcement; reinforcement has been done at the time of foaming. SSF is coated using electroless coating technique, which improves wetting behaviour of the SSF. Improvement in the stability of the foam is observed after foam reinforced with CCSSF. Through microsturctural analysis it is found that reinforcement has significant effect on cell wall microstructure. Secondary phases developed after reinforcement is distributed along the plateau boarder and within the alloy matrix. Stability of the foam may be attributed to this distribution, which in-turn affects the hardness and improves the compressive behaviour of the foam. Mechanical property analysis of the reinforced foam shows that the microhardness value improved moderately at small amount of reinforcement (0.5 wt. %) and improves significantly (20-30%) as reinforcement amount is increased. The results of the axial compression test indicates that the compressive properties (i.e., yield strength, plateau stress and energy absorption capacity) improves after the reinforcement. From results it is observed that reinforcement after 1 wt. % result in unreacted fibre surrounded by porosity which in turn reduces the effect of reinforcement.

Finally **chapter 7** draws the conclusion and contribution made in this thesis and suggestion for future work is presented in **chapter 8.**

ACKNOWLEDGEMENTS

Without the Sun, this world, solar power, this thesis work have not been possible.

So I start by offering a prayer to the GOD Sun:

ॐ विश्वानि देव सवितर्दुरितानि परासुव। यद् भद्रं तन्न आसुव।

यजुर्वेदः, ३०: ३

(O God, the creator of the universe (The Sun) and the giver of all happiness, keep us far from bad habits, bad deeds, and calamities. May we attain everything that is auspicious.)

My first acknowledgment goes to the most important person my mother, for her support, sacrifice and love. I would like to thank my father for providing freedom to be myself. I am utterly grateful to my maternal uncle P.M. Jeenager (source of inspiration), my elder sister Nand Kanwar and his husband Hanuman Jee who is like elder brother to me, and my younger brothers Er. Pawan Kumar, Shambhu Lal and bahu Ekta Rathore and Manbhar Parihar for their extended support and making me free from my social responsibilities during my Ph.D. work.

I express sincere gratitude to my thesis supervisors Prof. B.S.S. Daniel and Dr. Vivek Pancholi, MMED for the encouragement and guidance.

I would like to express thanks to Prof. S. K. Nath, Head, MMED for his invaluable discussions and suggestions, despite his busy schedule. The help rendered by him is invaluable and unforgettable. His motivation and energy has always been a driving force for successful completion of this thesis work.

I am also thankful to faculty members of the department for their help and support throughout the course of my research work. I am highly grateful to the members of my Student Research Committee, Prof Anjan Sil (Chairman), Dr. Inderdeep Singh (External member) and Dr. G.P. Chaudhari (Internal member) and specially Dr. B.V. Manoj Kumar, Dr. Suhrit Mula, Dr. Sadan Ghosh for their invaluable suggestions, encouragement and motivation to improve the quality of my research work. A special thanks to all technical and administrative staff of MMED and IIC for their assistance in preparation and characterization of my samples.

I greatly enjoyed working with my friends Dr. Keshao Prasad, Mr. Anupam Saini, Dr. Vineet Agotia, Mr. Neeraj Gupta, Mr. Dharmendra Singh, Mr. Aashish Selokar, Mr. Maruff

Husain, Mr. Chaitanya Sharma, Mr. Vikash Kumar, Mr. Akshay kausal, Mr. Shiv Kumar, Mr. Paritosh Dubey and all research scholars in MMED.

I would like to express my reverence and admiration to my wife Deepshikha for her sacrifice and providing me constant encouragement. I am thankful to my son Lakshya Partap and nephew Vadika Kanwar whose smiling, loving and innocent face have always refreshed me and their innocently naughty activities relieved the stress of my research work.

Special thanks to Mr. Fareed Ahemad, Mr. Bhingole P.P., Dr. Pavan Kumar Kankar , Mr. Vaibhav Bajpayi , Mr. V.N. Shukla, Mr. Iftkhar Bhai, Mr. Sandeep Sharma, Ms. Reena and staff of sports complex for providing me unconditional support during my stay at Roorkee.

I would like to thank everyone who is directly or indirectly involved to the successful completion of my thesis, I would also like to express sincere apology, if I could not mention anyone here. This could be due to lack of space but not due to lack of appreciation.

Above all, I express my sincere thanks to the GOD from the core of my heart for bright guiding light: Jai Bajarang Bali.

(Vinod Kumar Jeenager)

CONTENTS

LIST OF FIGURES

Figure **Figure description** **Page**

LIST OF TABLES

ρ	Density	kgm^{-3}
ρ_s	Base alloy density	kgm^{-3}
ρ^*	Base alloy density	kgm^{-3}
σ	Engineering stress	Pa (Nm^{-2})
σ_{pl}	Plateau stress	Pa (Nm^{-2})
ε	Engineering strain	-
ε_d	Densification strain	-
σ_y	Yield strength	Pa (Nm^{-2})
σ_o	Frictional strength	Pa (Nm^{-2})
k	Locking parameter	-
d	Average grain size	mm
σ_{ss}	Solid solution strength	Pa (Nm^{-2})
λ	Wavelength	-
d	The distance between atomic layers in a crystal	A^o
θ	angle of incident	^{o}, rad

EPMA	Electron probe micro-analyzer
TGA	Thermo gravimetric analysis
XRD	X-ray diffraction
SEM	Scanning electron microscopy
BSE	Backscattered electron imaging
EDX	Energy dispersive X-ray spectroscopy
TEM	Transmission electron microscopy
SAED	Selected area energy diffraction
VHN	Vickers hardness number
SSF	Short steel fibre
CCSSF	Copper coated short steel fibre

LIST OF PUBLICATION (Articles in Journals)

1. V.K. Jeenager, Vivek Pancholi, B.S. S. Daniel "The Effect of Aging on Energy Absorption Capability of Closed Cell Aluminum Foam" Advanced Materials Research, 585, 327-331 (2012).

2. V.K. Jeenager, Vivek Pancholi "**Influence of cell wall microstructure on the energy absorption capability of aluminium foam**" *Materials & Design, Volume 56, April2014, Pages 454-459.*

LIST OF PUBLICATION (Paper presented in conferences)

1. V.K. Jeenager, Vivek Pancholi, B.S. S. Daniel, International conference on Advances in Materials and Processing Challenges and Opportunities November 2-4, 2012, held at IIT Roorkee, India.

2. V.K. Jeenager, Vivek Pancholi, B.S. S. Daniel, International conference on Advancement & Futuristic Trends in Mechanical & Materials Engineering October 3-6,2013, held at PTU Jhalandhar, India.

The frequent economical global crisis and the current unstable prices of oil and raw materials have tended the automotive manufacturer to reduce the weight of automobile parts for better the efficiencies of the engines. The double threat of dwindling oil and gas reserves and ever increasing demand for energy has put a heavy premium on growing economies worldwide. Similarly, legal regulation regarding air pollution also restrict on the weight of the automotive parts. Therefore, weight saving possibilities in automobiles will be seriously considered and investigated by the automobile manufacturer, which reflected in the recent (2014) European environment agency data, according to that vehicle mass is reduced 9.2 kg in last year whereas the average engine capacity decreased by 6.7 % (measured in $cm.^3$) since 2007. Light weight vehicle design along with improved aerodynamics and improved engine efficiency are recognised approaches to lower the fuel consumption.

Due to specific properties, such as, light weight, environmental compatibility as well as higher energy absorption capability derived from the cellular structure, Al foam material demand is increased in numerous areas such as transport, aerospace, automobile industry, as well as, in building and construction engineering applications owing the exclusive combination of properties (i.e. thermal, damping, mechanical and physical (Xia et al., 2012). Compared with polymeric foams which are widely used, metal foams offer superior properties, such as metal foam can operate at elevated temperatures, fully recyclable without any pollution or waste problem. Similarly, Al foams can absorb more energy, reduce noise and vibration under high deformation loads when compare with the other foams. The high specific strength of metal foam makes it most suited candidate for weight structural applications in sandwich form (Demsetz and Gibson, 1987; Schwingel et al., 2007), whereas, due to its good energy absorption capacity Al foams also used for crash safety applications (Miyoshi et al., 1999; Nemat-Nasser et al., 2007; Ramachandra et al., 2003; Wallentowitz and Adam, 1996).

Despite many studies on Al foam, which are reviewed in chapter 2 of this thesis shows that mechanical properties have been widely studied in recent years (Jeon et al., 2009; Kishimoto et al., 2014; Konstantinidis et al., 2005; Sugimura et al., 1997), still the performance of foam is not promising due to existing of the variation in the cell structure and morphological defects in the form of nonuniform cell structure, such as local drainage, cell wall rupture (Gibson and Ashby, 1997; Rabiei et al., 2000; Sugimura et al., 1997). These deficiencies caused by the inability to control the drainage. Hence, to control these defects it is necessary to fully understand the microstructural behaviour, as cell wall microstructure can play an

important role in optimisation of mechanical properties. By the strengthening of the cell wall microstructure, the deformation and collapse of the foam will be delayed, which increases the strength of foam.

Generally, strength defines as the lattice resistance to plastic shear but strength has different connotations in different classes of materials, such as, strength for metals and polymers refers to yield strength, for ceramics the modulus of rupture, for elastomers tear strength and for composites and wood it is tensile strength. The word 'strength' for foam subjected to compressive loads, refers to plateau stress, which is the extended constant stress domain beyond the elastic limit.

Hence, the properties and stability of foam can be improved through either the cell wall geometry alteration or strengthening of the cell wall. Steps have already taken in first area (i.e. alteration of the foam cell geometry), which was mainly concerned on relative density, geometry of cells and morphological defects (Aguirre-Perales et al., 2012; Duarte and Oliveira, 2012; Hossein Elahi et al., 2012; Jeenager and Pancholi, 2014; Jeenager et al., 2012; Jiménez et al., 2012; Kamm et al., 2013; Kumar et al., 2013; Lázaro et al., 2013; Xu et al., 2012; Zhao et al., 2011a; Zhao et al., 2011b). However, work on the strengthening of Al foam (produced through melt route using TiH_2 as a blowing agent) is scanty. In literature some experimental data are available through which some of the aspect of the effect of thermal treatment can be understand, Y. Feng et al (Feng et al., 2003b) reported thermal aging result in to improved mechanical properties under static and dynamic loading. Similarly, (Wang et al., 2009) reported that the thermal treatment result in to improve the strength and energy absorbing capacity of foam (Al-Mg-Si).

The effects of various strengthening mechanism on the cell wall microstructure are also not available for Al foam. Therefore, an experimental investigation has been carried out to study the effect of cell wall microstructural modification using strengthening techniques (solution treatment, grain refinement and reinforcement). The motivations of the present thesis include assessing the effect of microstructural modification on the energy absorption capacity of metal foam. It is believed that with the results of this thesis, many aspects of the Al foam microstructure will be clarified.

In the recent years, synthesis and characterization of aluminium foam has been the main area of interest. The present chapter consist of the literature review available in the area of metallic foam related to property improvement, which aimed at to identify the gaps in the literature. In the light of gap identified, different studies concerning the effect of the different parameters on the properties of metal foam, the research problem formulated. Finally, the chapter concludes with an outline of the research plan taken up in the present research work.

2.1 Metal foam

In rapidly grow technical world a variety of materials are available, however, there is consistent interest to develop specific application oriented materials which meet the specific requirement. In the automobile field, a material with light weight and good energy absorption capacity is a prime concern as light weight improves the mileage of the vehicle whereas energy absorption capacity good for safety. Hence, it would not be an exaggeration to say that metal foam due to its dual properties (i.e. light weight and high specific strength) becomes the centre of attraction in the field of rail, aerospace and automobile industries.

2.2 Development of the metal foams

A through literature review suggest that the metallic foams have been developed since 1926. Later in 1943,B. Sosnik added mercury to molten aluminium to create pores and in 1948 he proposed a technique to produce metallic foam (Sosnick, 1948). Therefore, 1950 can be considered as the starting epoch in the field of metallic foam. In 1956, mercury was(JC, 1956) replaced with the blowing agents, which generating gas by thermal decomposition. Up to the date many researchers used this technique to produce metallic foam. In year 1963, (B.C., 1963) invented technique (similar to PM (powder metallurgy) route) to develop the metallic foams. Literature(Ashby, 2000) suggests that up to the late 1980 little amount of work has been done. In the early 1990s, some research work especially on the manufacturing process methods were started (Gergely et al., 2000). In the late 1990s, some UK, US and German universities initiate some research and interdisciplinary which was related to metallic foam, but large scale of production in industrial application has stated recently. In recent years, a variety of cellular and foamed metals have been fabricated by researchers and in industries. Substantial progress in theoretical, as well as, in the experimental study of the foaming behavior at macro, micro and nano level can be attributed to the development of caliber in experimental technology through which wide range of possibilities in production, as well as, in characterization is observed.

Broadly, materials with more than 70% porosity are classified as cellular solids(Gibson and Ashby, 1997), whereas, (Banhart, 2001)reported that the dispersions of one phase into second phase results in to nine possible intermediate combination where phase may be either of the state of the matter (i.e. solid ,liquid or gas). Hence, metal foam can be simply defined as the heterogeneous composite of solid (i.e. metal) and gaseous (H_2) phase. If the gaseous phase is completely enclosed with solid phase and there is no interconnection between the cells then it is called as closed cell foam (as shown in Fig. 2.1). If the cells are interconnected to each other then it is called as open cell foam.

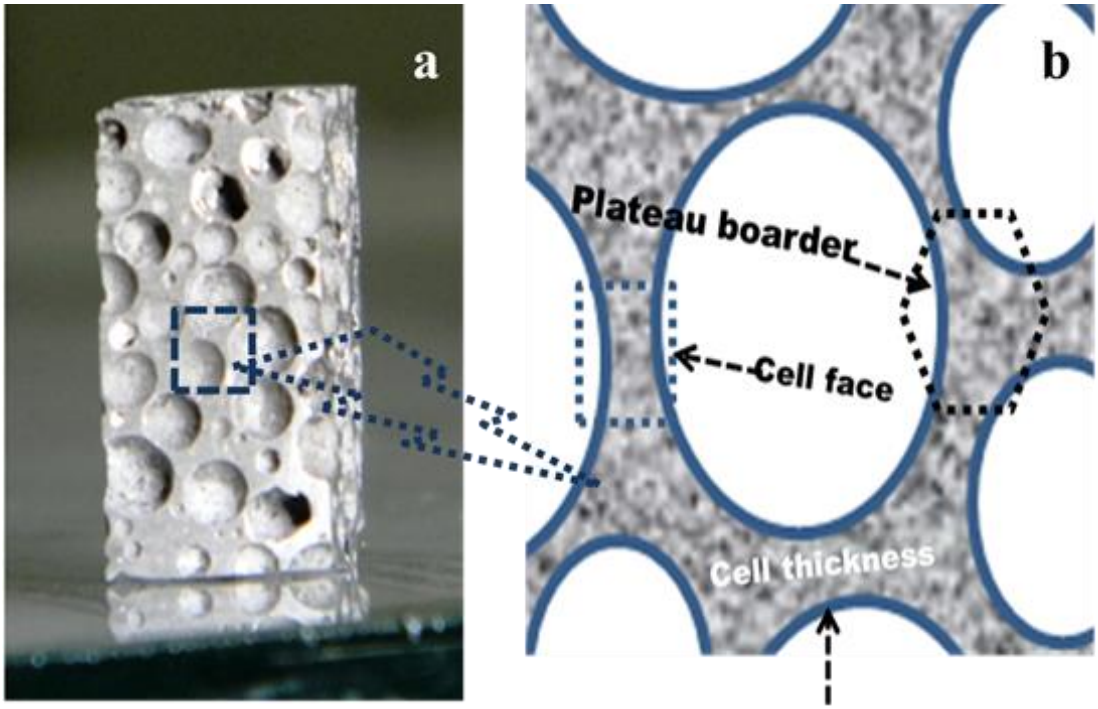

Fig. 2.1 (a) Cross sectional view of closed cell foam and (b) schematic representation of cell structure showing terminology and notation.

2.3 Various fabrication methods of closed cell metal foams

In recent years, technical advancement in the research field made it is easy to develop and investigate the process feasibility more precisely and quickly, which further outcome in the form of development in the wide range of fabrication methods.

Under this section (2.2) of the chapter, an overview of fabrication methods is explored. Each technique is used to produce foam with a set of parameter used to control the structure of foam, some of the most common methods used to develop and produce metal foam are summarised in the following Table 2.1:

Table 2.1The most commonly used foaming process with respective family of alloy.

Process used	Material	Reference
Foaming with blowing agent method	Al, Zn	(Elliott 1961, Hardy 1967, JC 1956, Polonsky et al 1961)
Powder metallurgical (PM) route	Al, Zn, Pb	(Elliott 1961, Hardy 1967, JC 1956, Polonsky et al 1961)
Investment casting technique	Al, Zn	(Banhart 2001)
Gas injection method	Al, Zn	(Banhart 2001)
Casting around space holder technique	Al, Zn, Pb, Cu	(Banhart 2001)
Vapour deposition technique	Ni, Cu	(Banhart 2001)
Electro-deposition technique	Ni, Cu, Ni-Cr	(Banhart 2001)
Gas entrapment technique	Ti	(Banhart 2001)
Solid-gas eutectic solidification (Gasars) route	Al, Ni, Mg, Cu	(Banhart 2001)

First seven of the above mentioned process (as shown in the Table 2.1) are used to produce foam commercially (Banhart, 2001). The processing techniques based on liquid melt route and powder metallurgical route are most popular, both the processes are detailed in below subsections. As the simplicity and feasibility of the process lends itself to large-scale manufacturing with trade name "Alporas" and "Alulight" respectively.

2.3.1 Powder metallurgy route

The method is often known as ''PM route'' because the process starts with powder. Although, the fundamental idea behind the PM route is quite old (B.C., 1963; J.F., 1960) but this method was well developed at Fraunhofer-Institute, Bremen (Germany) (Baumeister J., 1996, 1997; Baumeister J., 1991; J., 1990, 1992; Wadley et al., 2003). Now this method is up to a level of sophistication and through this technique foam and foam components are commercially manufactured with the trade name "Alulight".

From this method net shaped complex parts, sandwich panels and foam filled hollow profiles can be easily developed, which is the most attractive part of this technique. In the PM

route, porosities are either developed by using blowing agent or with the help of some other techniques (where chemical reactions or solid parts are used to create pores) during the process. The selection of the foaming agent depends on sintering and melting temperature of the matrix material. Some of the reported combination of foaming agent with the respective matrix material is given in the Table 2.2.

Table 2.2 Some of the foaming agent with respective material

Foaming agent	Matrix material
TiH_2	Al (Von Zeppelin et al 2003)
ZrH_2	Zn (Von Zeppelin et al 2003)
$MgCo_3$	Steel (Park & Nutt 2001)
SrO_3	Steel (Park & Nutt 2001)
$BaCo_3$	Cu (Kelley et al 1993)
$PbCO_3 \cdot Pb(OH)_2$	Lead and lead alloy (Irretier & Banhart 2005)
MgH_2	Lead and lead alloy (Irretier & Banhart 2005)

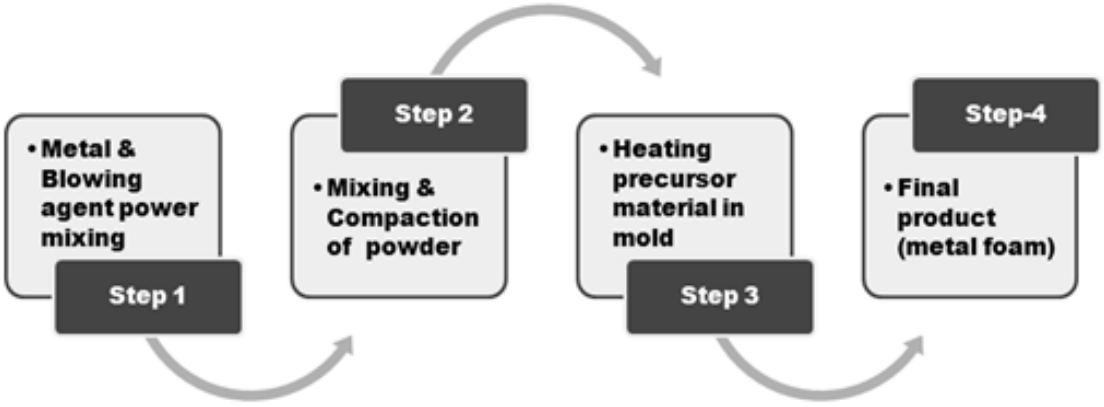

Fig. 2.2 The schematic diagram shows the steps used for foam production through PM route.

Steps used in the foam production through PM route are schematically presented in the Fig. 2.2. In general, the final density of foam depends on the decomposition rate of the blowing agent and the stability of the cell wall structure. Hence, for good foaming in PM route blowing

agents are pre heat treated so that the decomposition of the blowing agent and the melting of the matrix took place simultaneously, which further results in a uniform cell structure.

2.3.2 Liquid melt route

Literature reported that numerous attempts have been made to develop foam through liquid melt route using aluminium, magnesium, zinc or aluminium alloys as base material (Berry, 1972; Bjorksten J., 1972; Hardy, 1967; LM, 1970; Niebylski LM, 1974, 1976; W.S., 1965). In this method of foaming process, gas is the main source to develop pore and gas mainly introduced in the melt either of the following techniques:

1. Shoot gas into the melt during foaming using an external source (gas injection method).
2. Gas generated by some blowing agent.
3. Dissolved gases in melt.

2.3.2.1 Foaming by the gas injection method

The gas injection method was first patented in Nov. 1990 by Alcan International and Cymat Aluminium (Canada) for commercial production (Jin I., 1990) and in this technique one metal matrix composite can be as a base metal to produce metal foam. In the gas injection method, gas (O_2, N_2 or air) is injected in liquid metal through external sources. The use of impellers and nozzles as an external source also ascertains uniformity of gas bubble in the liquid melt which in turn result into fine and uniform gas pore distribution.

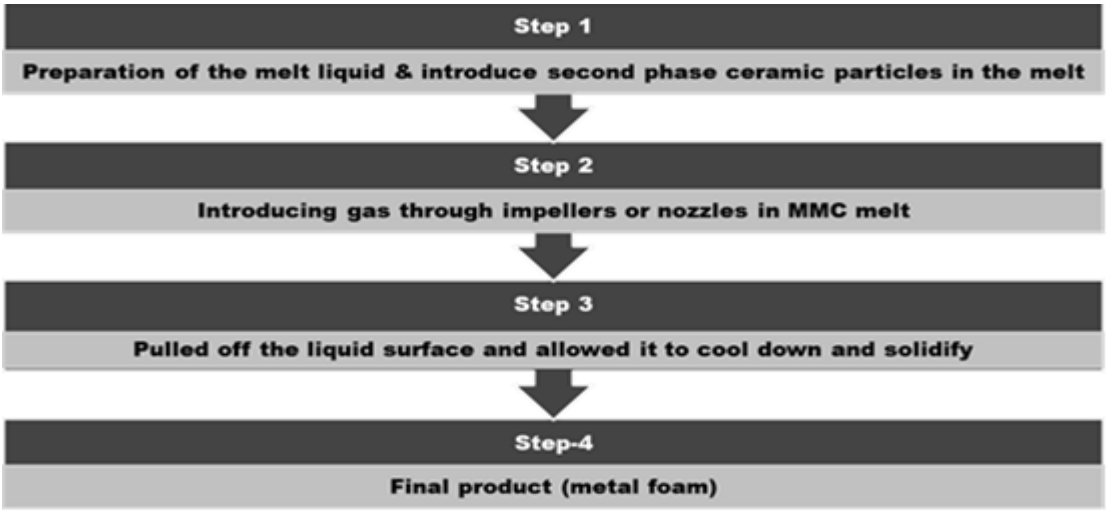

Fig. 2.3 Schematic diagram shows the steps involved in foam processing through gas injection method.

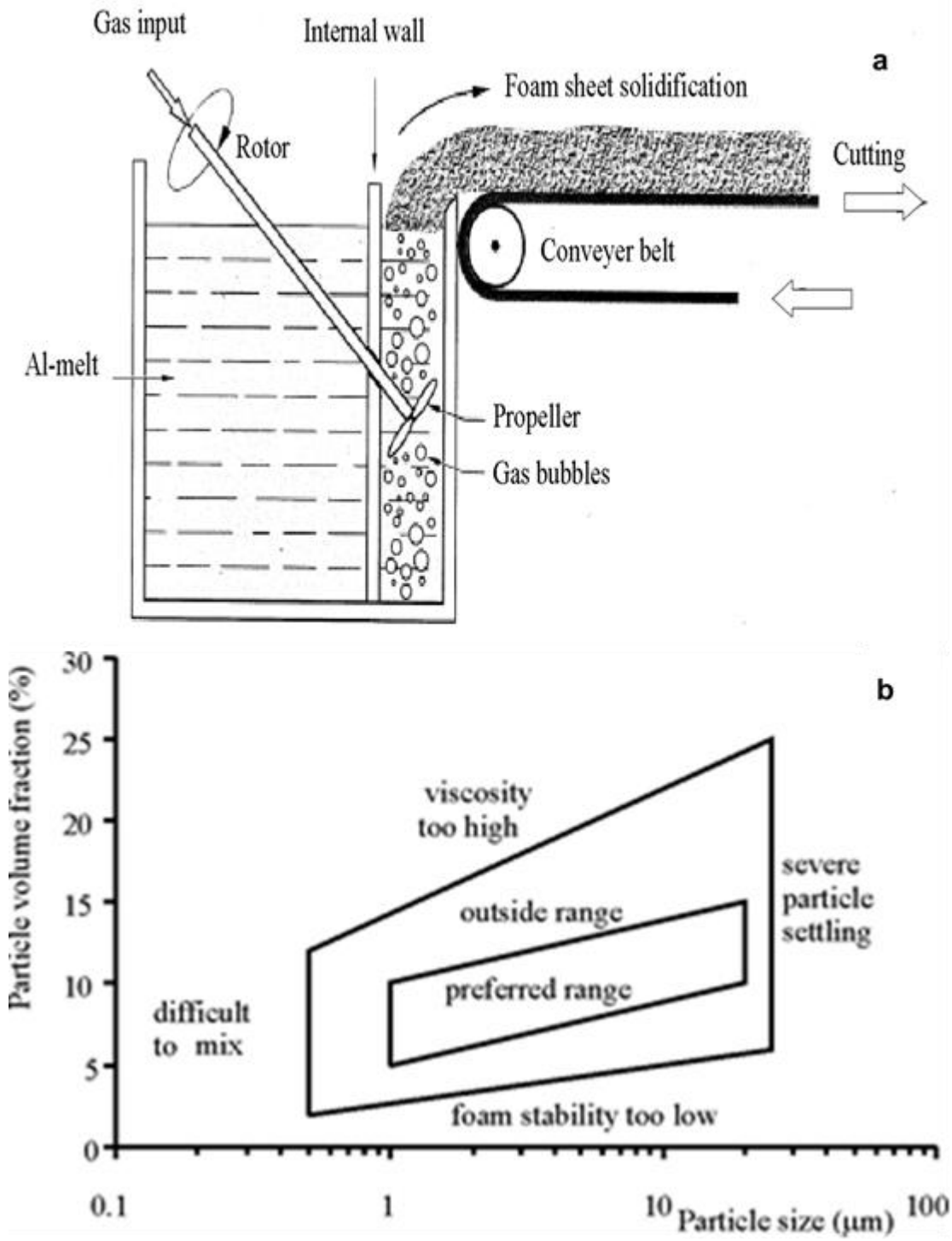

Fig. 2.4 (a) Direct foaming of melts by gas injection method for foaming (Jin I., 1990) and (b) empirical guide for selection of the particle size for stabilization of melts(Deqing and Ziyuan, 2003).

However, to produce defect free metal foam structure, stability of the process is the prime concern and in this method stability is achieved through the introduction of the second phase particles in the melt. Most commonly used second phase ceramics are: Al_2O_3, Sic, and MgO. Although, second phase ceramic particle helps to stabilise the melt still,

it is also necessary to assure that the added particles have not been stripped of from the cell wall. General steps used to produce the metal foam through gas injection method are depicted in Fig. 2.3. Hence, it is necessary to consider the wetability of the added particle before introduce it in the liquid melt. Literature (Banhart 2001) suggests that too much lower contact angle also result in lower stability of foam.

The particle size is selected on the basis of established empirical relation (as shown in Fig. 2.4 (Banhart, 2000; Fang and Fan, 2007; Prakash et al., 1995)). From the Fig. 2.4, it is clear that the particle with smaller size (<1 μm) are difficult to mix whereas bigger particle size (>20 μm) results into the severe particle setting, Therefore, 5-20 μm is the most suitable particle size.

2.3.2.2 Foaming with blowing agent

In this method, gas is generated by particles (generally known as foaming agent), which are added in the liquid melt during foaming (Berry, 1972), which further decompose in the liquid melt. Chemical blowing agent is a compound of low molecular weight gaseous product (H_2) and other by-product (Ti) which are formed by a chemical reaction(s) and promoted by reacting polymer's exothermic heat. TiH_2 in powder foam, is generally used (also used in the present research work) as a foaming agent in the production of metal foams. At the elevated temperature TiH_2 decomposes and form titanium and hydrogen (equation 2.1) (Elliott, 1961; Hardy, 1967; JC, 1956; Polonsky et al., 1961) :

$$TiH_2 \rightarrow Ti + H_2 \quad \ldots\ldots\ldots\ldots\ldots\ldots\ldots\ldots\ldots\ldots \quad (2 \cdot 1)$$

Following steps are used (in the present work) to produce foam through liquid melt route using TiH_2 as a blowing agent (as a gas source):

1. Melting of the master alloy (in this step of the process, master alloy is melted in furnace at elevated temperature (730^{o}C in present work)).
2. Thickening of the melt, this step of the process includes introduction of the thickening agent in the liquid melts which stabilize the melt and raises the foam against collapse (Ca is used as the thickening agent in the present work).
3. Addition of blowing agent (TiH_2), this step involves addition of the foaming agent at constant stirring (for a proper dispersion of foaming agent).
4. Hold the melt inside the furnace without stirring for the different holding time varying from 60 to 180 sec.
5. Finally, the crucible (contain melt) is quenched in water to solidify the liquid foam.

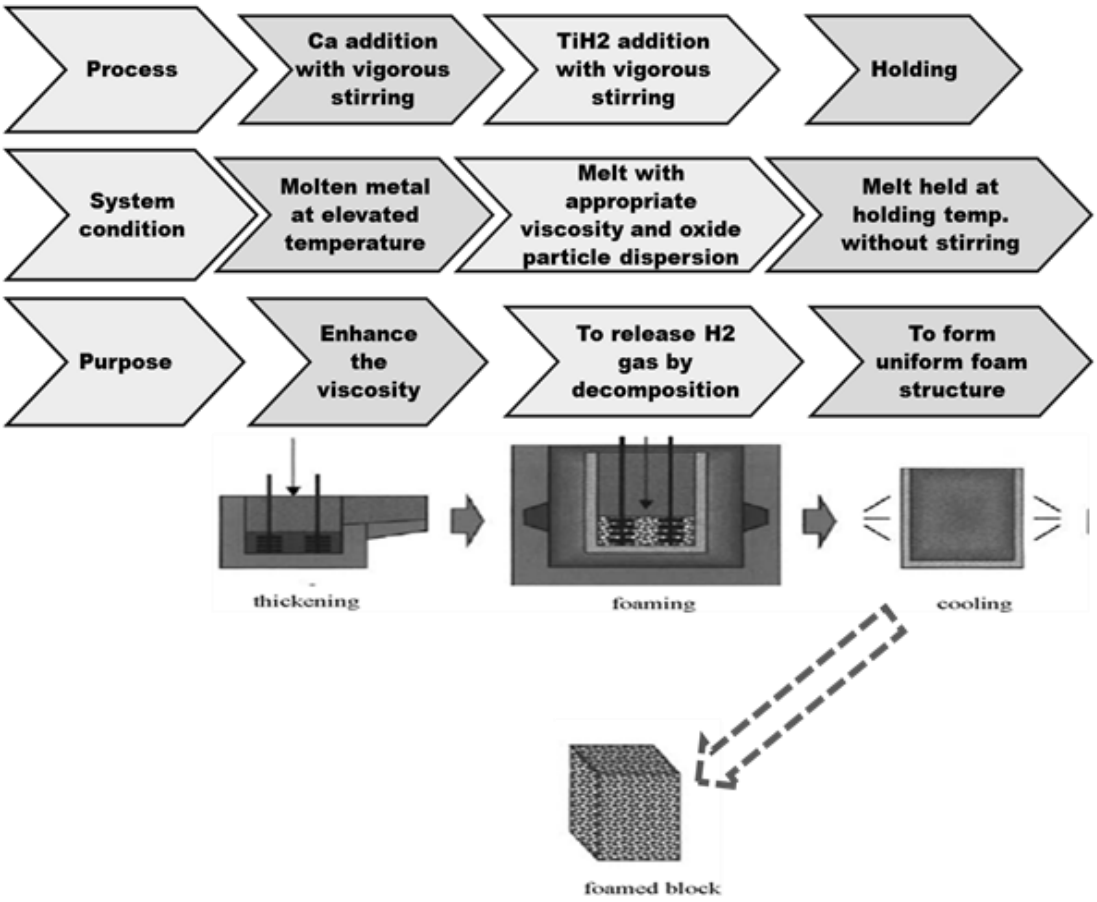

Fig. 2.5 schematic representation of the foaming process shows the step involved in production of foam via melt route using blowing agent as a gas source (Miyoshi et al., 2000)

The whole process is schematically present in the Fig. 2.5. This process is used commercially to produce Alporas™ (Miyoshi et al., 2001; Miyoshi et al., 2000) and commercially exploited by Shinko Wire (Japan). In this method of foam processing, melt viscosity is a prime concern which is accomplished by the incorporation of calcium (in present work), ceramic reinforcements, aluminium dross and manganese dioxide (Augustin and Öchsner, 2009; Gibson et al., 2010; Nadler, 1999). For example, addition of Ca metal in the Al melts form oxides and intermetallic (CaO, $CaAl_2O_4$ and Al_4Ca) which increase the viscosity by thickening of the melt. To achieve high viscosity of the melt ($(6–7)\times10^{-3}$ Pa·s), a continuous stirring (up to 8–12 min) is required for calcium content of 1.8 wt. % (Ma and Song, 1998).

Process parameters such as uniform melt temperature, viscosity and distribution of TiH_2 particles is the main variables which control the whole foaming process, hence to produce homogeneous cell structure it is necessary to carefully handle these variables. The foaming is

generally carried out at 680–720 ºC and ZrH2 (0.5–0.6 wt. %) can also be used as blowing agent instead of TiH_2 to produce metal foam from this route.

Generally, densities of such Al foams have been determined to be around 0.18–0.24 g/cm^3. In some cases, it becomes difficult to mix the blowing agent in the liquid metal as it decomposes very fast at the liquids temperature. To avoid such situations, a low melting point precursor (such as Al–Si, Al–Cu or Al–Mg) with eutectic composition is prepared with dispersion of the blowing agent without decomposition and subsequently added to the high temperature melting liquid in the second stage. As reported in the literature, ferrous alloys have also been attempted to process by this route using tungsten powder (as foam stabilizer) and $MgCO_3$ or $SrCO_3$ (as a blowing agent) (Park and Nutt, 2000, 2001a, b, 2002), which decomposes around 1300^oC.

The main drawback of this process is the higher cost of the foaming agent and the calcium. In this process, to disperse the foaming agent throughout the volume, stirring is required; therefore, this process can not be used to produce complex net-shape components and blocks of foam in regular shapes.

Recently, an attempts have been made to develop injection techniques using metallic foams, whereby a melt is injected into a die as it foams, but with only limited success as achieved as in this process heating and cooling rates are difficult to control across the sample and the injection pressure is also necessarily kept at low to avoid crushing of the molten foam, favouring irregular cell structures with density markedly decreasing with distance from the injection point (Banhart, 2012; Schorghuber et al., 1999).

2.4 Matrix material

It is expected that the metallic foam retains the properties of the base material. In this section of the chapter, reviews of the literature related to the selection of the base aluminium alloy among different aluminium alloys are reviewed. A wide range of literature exists in the area of aluminium and its alloy. Some of the important series of aluminium alloy related to present work are reviewed in following subsections:

2.4.1 Aluminium and aluminium alloys

Metal foam poses superior quality when compare with the polymer and other foam. Therefore, the selection of the metal for foam production is one of the most important steps in foam processing. Aluminium alloys possess lots of desirable properties, such as, high strength to weight ratio, good ductility, good thermal and electrical conductivity, high fracture

toughness and splendid resistance to corrosion (Handbook, 1992). All above properties make aluminium alloys highly desirable in numerous application fields (i.e. as industrial, aerospace, transportation and rocket engines (Pandey and Spowart, 2010)). Wrought aluminium alloys are available in standard forms such as plates, sheet, bar, tube, rod, wire, extrusion, forgings and foils (Polmear, 1995). On the basis of strengthening mechanism, aluminium alloys can be broadly classified in to two categories i.e. non-heat treatable and heat treatable alloys (which are depicted in the Fig. 2.6). In non-heat-treatable (1xxx, 3xxx, 4xxx and 5xxx) alloys, manganese (Mn), silicon (Si), magnesium (Mg) are used as alloying elements and these series of aluminium alloy can not be strengthened by heat treatment process, hardening of these series is done with the help of cold working process. Heat-treatable (i.e. 2xxx, 6xxx and 7xxx series) alloys can be strengthened by hardening effect. Alloying elements (such as Cu in 2xxx series, Mg and Si in 6xxx series and Zn in 7xxx series) found in the respected series are responsible for hardening effect. Hardening of these elements entirely depends on the temperature; therefore, hardening of these series can be easily done by heat treatment, also known as precipitation hardening. On the basis of above brief discussion, it is reasonable to state that in heat treatable alloys the combination of alloying elements and thermo-mechanical processing contributes to achieve desirable properties. Therefore, in the present work 6061 alloy chose as a starting material to produce foam.

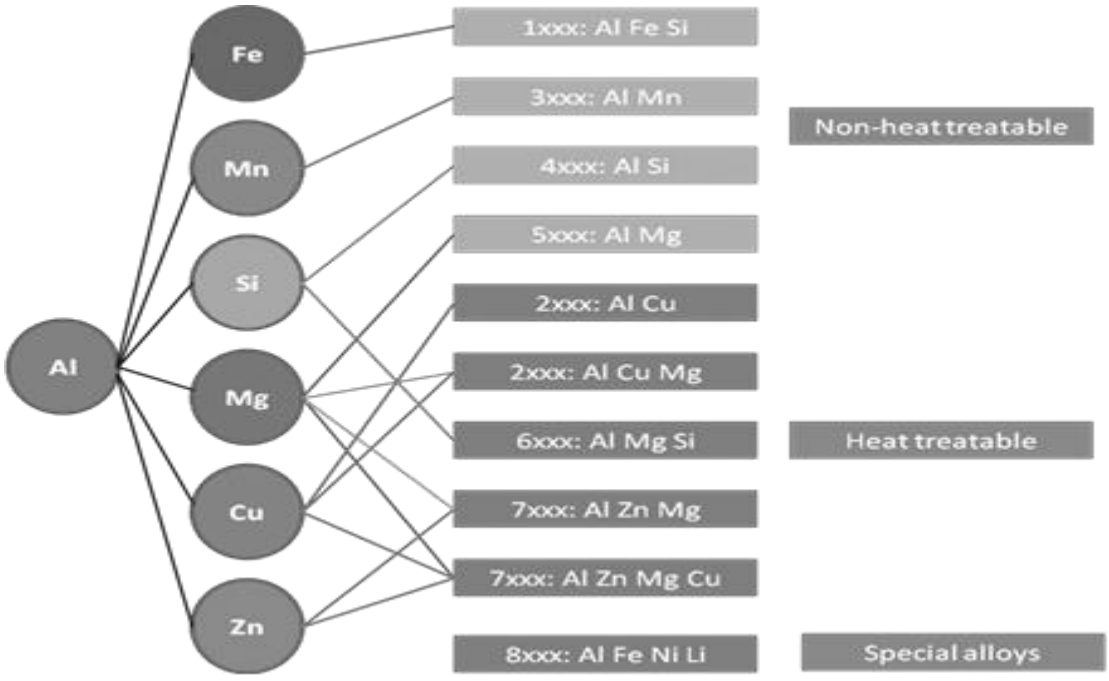

Fig. 2.6 Classification of wrought aluminium alloys (Hatch, 1984)

2.4.2 Chemical composition of the cell wall base material (6xxx series aluminium alloy)

The main constituents in 6xxx series aluminium alloys include: alloying elements, additives and impurities. Mg is the major alloying element in the amount of 0.8-1.2% followed by Si in the range of 0.4-0.8%. As discussed in the previous section that Mg, Si helps in lowering viscosity, however, Cu is the best suitable candidate for precipitation hardening. Therefore, Cu is added in the 6061 alloy for stability of foam, as well as, cell wall strengthening through precipitation hardening. The additives or minor (< 1%) addition of alloying element is used to improve weldability and recrystallization nature of the alloys.

2.5 Physics of foaming

It is mainly associated with stabilisation of foam and variety of drainage. The stability of the foam is mainly defined as the absence of cell wall rupture, as well as, restricts the drainage of the melt in during foaming. Several factors affect the stability of foam, such as geometry and thickness of the cell wall, surface tension and gravity. Viscosity is also influence the foam stability. For the foam structure to be retained in the solid, the life-time of the cell wall should be comparable to the time for solidification. For this reason, the foam stability is an important parameter which is explained as the delayed rupture of cell walls and subsequent retardation in melt drainage (Ashby, 2000). It is common practice to introduce a solid second phase either in-situ or ex-situ to enhance stability by increasing melt viscosity. Cell wall rupture is an irregular and spontaneous process as the drainage of liquid melt induced by local pressure differences within the cell wall and by gravity. So, metal foam stability can be understood as a slowing down of the cell wall rupture and drainage process.

2.5.1 Stages in the progress of a foam structure

2.5.1.1 Cell growth

First step in the foam evaluation after the addition of blowing agent is the development of cell wall structure, which is illustrated in the Fig. 2.7 schematically. When we add TiH_2, it decomposes in Ti and H_2. H_2 gas entrapped in the matrix material and it is the first step when the pore is developed, the shape of the cell is controlled by surface tension. With the advancement of holding time pore expand further, the effect gravity as well as surface tension work simultaneously on the pore, which results in the shape distortion and the shape becomes angular and finally, it results into three dimensional network structure (Degischer et al., 2003). Some of the terms used to characterise foam cell wall cell wall structures are labelled and illustrated in Fig. 2.1(b). Schematic diagram Fig. 2.7 (a), (b) and (c) shows the development

stage of the pore development, as shown in Fig. 2.7 (a) pores are starts to developed as time progress initial dispersion of pores further expand result in expansion of the cell wall and finally, low density cell structure was developed.

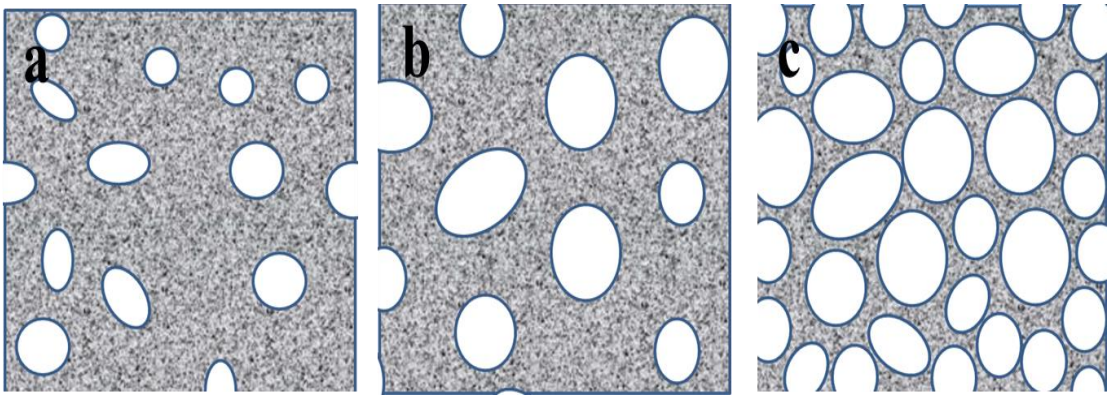

Fig. 2.7 Schematic representation of the pore expansion during foaming of a melt by a blowing agent (TiH_2): (a) initial dispersion of pores, (b) expansion of the cell, (c) low density cell structure.

2.5.2 Drainage and cell wall

Drainage is the single most challenging and common phenomenon results in density gradient, which finally result in the form of cell wall collapse. Sometimes, cell wall collapse is so severe that it is seen as local features in foam casting. Schematic representation of the coalescence of neighbouring cell wall is illustrated in Fig. 2.8. Thinning of cell faces at the middle point of the cell wall is usually the result of surface tension which makes the cell wall more rounded and result into drainage of the material. In the early stage of structure evolution means that the foams are subjected to interrupted foaming (Degischer et al., 2003). In recent years, some of work and techniques are under the development stage which made it easy to understand the effect of the process parameter and the composition of matrix material on the structure of the cell wall.

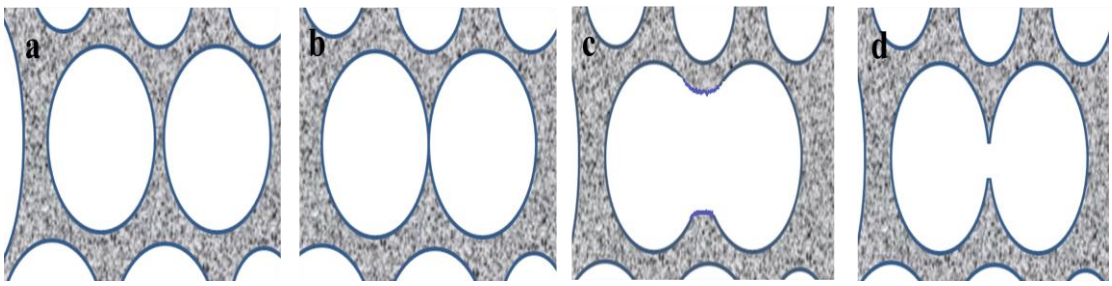

Fig. 2.8 Schematic representation of the stages of the cell wall calescence: (a) neighboring pores (b) thinning of the cell wall (c) rupture of the cell wall (d) rounding of cell and formation of the new cell.

(Stanzick et al., 2002a) used neutron radioscopy to measure the effect of drainage evolution of the metal foam and found that the data obtained through this technique is qualitatively in agreement with the data of the foam produced, similarly, the cell wall structure can be easily evaluated with the help of the use of high-intensity synchrotron X-ray radioscopy and through this technique drainage, as well as, cell wall coalescence processes (such as drainage and cell coalescence) to be observed in real time (Banhart, 2001; Stanzick et al., 2002b). Above techniques enable the investigation of the effect of holes and defects in foamable precursor material on the cell structure obtained. Numerical process modelling (comprises of growth and interaction of cells in a molten foamable precursor material) is also offers the potential to evaluate the effect of a range of material properties and process parameters (Diop et al., 2011; Korner and Singer, 1999; Körner et al., 2005b). However, all these techniques remain under development.

2.6 Factors affecting the stability of foam structure

2.6.1 Gas diffusion

By definition, closed cell foam is a heterogeneous composition of solid and gaseous phase where gas is enclosed with solid phase. In metal foam when metal is in the aqueous stage, pressure difference between cells is expected, which results in cell wall coarsening and gas diffuse through the cell wall. Due to the curved outer surface, gas loses in the air from the outer edge of the bubble. However, gas diffusion can be controlled to some extent through the diffusivity and solubility of the gas in the molten metal. Most of the gases are less soluble in the melt, whereas the solubility of the H_2 is significant in Al (Lin and Hoch, 1989). Gas diffusivity can be reduce significantly through alloying specially Si (Brandes and Brook, 1992). As in metal foam, cell faces are comparatively thicker and cell surfaces tends to align with the solid wetting agent which further restrict the diffusion of gases through the cell wall. As in the metallic foam, metal hold for a small duration (holding time- 80-120 sec.), therefore, it is reasonable to assume that in metal foam effect of gas diffusion on the cell structure is negligible.

2.6.2 Melt viscosity

To get uniform foam structure, it is necessary that the gas bubble held within melt up to the solidification of foam. Therefore, uniform distribution of the cell is necessary and can be easily acquired through the reduction of the velocity of the bubble by which it is rise. Velocity

of the bubble can be optimized through balancing the buoyancy of the bubble with the viscous drag of the melt.

As discussed earlier (in section 2.2.2.1) particle size greatly affect the stabilisation, which can be attributed to colloidal interactions between small particles. Colloidal interaction results in to the higher viscosity of the melt whereas larger particle also increase the viscosity through loss of angular momentum, when they collide. Therefore, viscosity plays an important role to stabilize the foam and it can be increased by particle addition in the melt. Increase in the viscosity can also be attributed to the networks of solid particle which formed due to loose particle agglomeration.

2.6.3 Surface tension

As literature suggest that as aqueous liquids form with the help of some surfactant which lowers the surface tension, similarly phenomenon is also expected for molten metal (Wilde et al., 1999). Due to the surface tension, it is expected that the cell wall leads to progressively rounder with wider plateau boarder and thinner cell faces which finally result into the drainage of the melt from cell faces to plateau boarder. Therefore, to reduce this phenomenon use of species prefers which expected to migrate at the gas-liquid interface and resists the change in surface area. By limiting the effect of surface tension on bubbles abbreviates the driving force for the flow of material from cell faces to plateau boarders, and results in the lower rate of thinning and reduce the collapse of cell faces. Optimisation of the quantity of the surfactant is necessary because too low quantity may be insufficient for uniform distribution, whereas, if the quantity is too high, there will be insufficient surfactant to cover the surface regardless of the movement of the cell faces.

2.7 The influence of the cell structure on stability of the foam structure

2.7.1 Cell face thickness

There seems to be a minimum cell face thickness, below which films will rupture, in literature (Banhart et al., 2001; Long and Khanna, 2003; Stanzick et al., 2002b), reported cell face thickness range is 50-80 μm for Al-Si alloys and as high as 100 μm in pure aluminium foams. In literature, it is also suggested that this may be a critical thickness below which cell faces are not stable, even though the reason behind such characteristic (critical thickness) is not certain (Duarte and Banhart, 2000). In general, thickness of the cell face is limited by the shape, size and volume fraction of the solid phase present, geometry of the foam structure, master alloy, processing time and temperature. Some evidence of a loose correlation between the size

of solid stabilising particles and the thickness of cell faces are reported by (Gergely and Clyne, 2004; Ip et al., 1999b).

2.8 Properties of the foam

2.8.1 Mechanical properties

For metallic foam, the mechanical properties mainly depends on the relative density (Bafti and Habibolahzadeh, 2013; Edwin Raj and Daniel, 2011; Jiang et al., 2007; Li et al., 2003; Liu et al., 2014; Surace et al., 2009; Wicklein and Thoma, 2005) of the foam. (Ashby et al., 2000), reported that a simple scaling relationship is exist between relative density and mechanical properties. The relative density of foam is defined as the ratio of foam density (σ^*) to the density of the master alloy (σ_s). The fraction of pore space or porosity in the foam is given as:

$$\text{Fraction of porosity} = \left(1 - \sigma^* / \sigma_s\right) \ldots\ldots\ldots\ldots\ldots\ldots (2 \cdot 2)$$

Behaviour of the metal foam under the tensile and compressive load is different from the bulk alloy system (Banhart, 2001), it is evident from the Fig. 2.9 that the tensile behaviour of the metallic foam is more or less similar to the solid metal whereas compression behaviour of metallic foam is different.

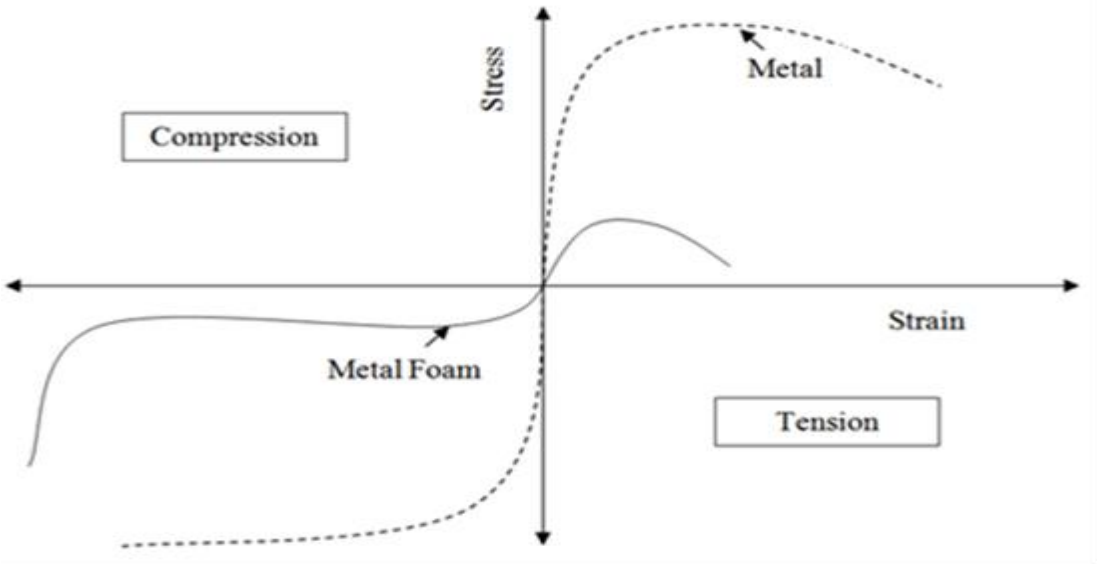

Fig. 2.9 Stress-strain diagram of bulk metal and foam metal in compression and tension (Banhart, 2001).

2.8.1.1 Compressive behavior of the metal foam

Compression behaviour of metal foam is the most important research area and several recent publications are available in literature (Alizadeh and Mirzaei-Aliabadi, 2012; Chen and McKittrick, 2011; Jeon et al., 2009; Kishimoto et al., 2014; Li et al., 2014; Luong et al., 2013; Májlinger and Orbulov, 2014; Mondal et al., 2013a; Mondal et al., 2013b; Mu et al., 2011; Orbulov and Ginsztler, 2012; Pinto et al., 2014; Sahu et al., 2014; Sulong et al., 2014; Sun et al., 2014). Fig. 2.10 shows the schematic representation of the compressive stress strain curve for metal foam sample, compression properties that can be determined from the stress-strain curve also elaborate schematically. There are three regions identified in the compression stress-strain curve, the initial linear elastic region, an extended plateau region and the final densification region. In the initial recoverable linear region, Hook's law is valid.

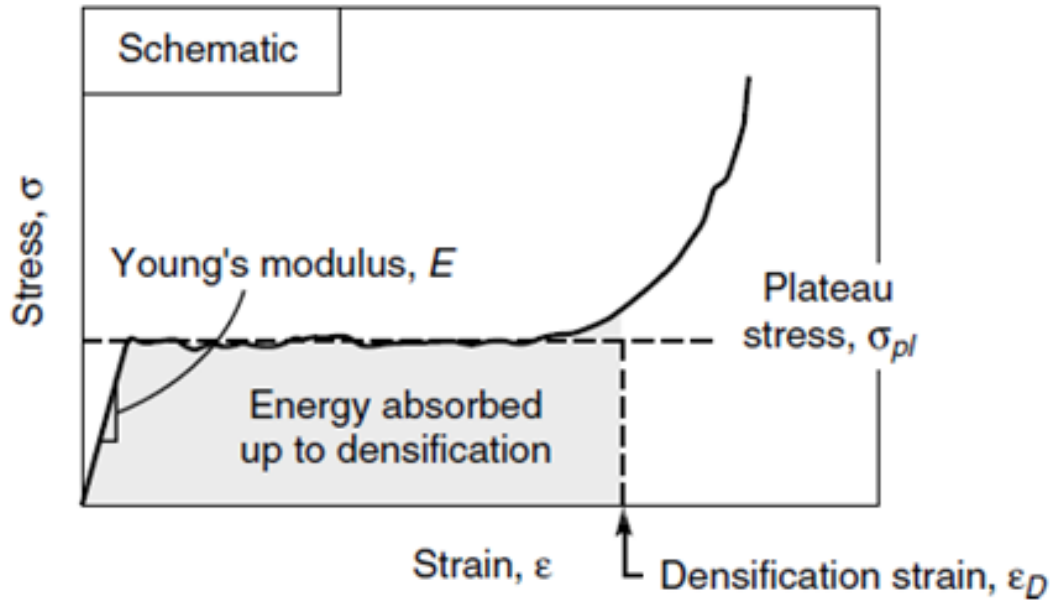

Fig. 2.10 A schematic representation of the compressive stress-strain curve showing the linear elastic, stress plateau and densification regions in foam.

In the foam sample stress strain curve elastic region is followed by an extended region known as plateau region. Plateau region can be further differentiated into two regions, the initial collapse stage and successive collapse stage. Initial collapse stage is marked by sudden collapse of the cell wall after the first peak stress also known as yield stress of the foam, whereas successive collapse stage in the stress-strain is characterised by serration with more or less constant stress level. Average stress in the successive collapse stage is known as plateau stress denoted by σ_{pl} and generally (in this work) taken as the average compressive stress for compressive nominal strain in the range of 5-30%. Formerly, Alporas foam samples have tested in relative density range 0.08-0.15 and found the plateau stress to fall in the range 1.39-2.46

MPa. The structural variation in the foam is results into the yielding, cell buckling and the compaction of cell layer, which occurs from the weakest region of the cell wall and proceeds to the next weaker layer. This successive layer by layer collapse of the cells is the reason for the serration in the stress-strain curve. The actual stress-strain behaviour varies from foam to foam depending on the fabrication methods and presence of the amount and type of particles in the cell wall. Third region of the stress curve is found after plateau region, when all the cell walls have completely collapsed and touch each other with a small increment in strain and appreciate increment in the stress is observed. This region at the end of the plateau region is also known as the densification region and corresponding strain associated with the commencement of this region is called densification strain and denoted as εd (Ashby, 2000).

The extended plateau stress in compression is unique to foam applications where the stress remains constant and the foam collapse layer by layer. Young's modulus and yield strength of foam are lower than that of the fully dense material, but the specific properties are significantly higher. The densification region is characterised by the dramatic build-up of stress for incremental strain, which is signifying the complete collapse of foam into a dense material.

2.8.1.1.1 Energy absorption capacity

As detailed in the previous section, metallic foams pose large compressive strains at nominally constant stress levels up to densification. This extended plateau region, which is mainly made metal foam capable to absorb large energy at constant stress and used in crash and blast protection systems (Ahmad and Thambiratnam, 2009; Edwin Raj and Daniel, 2011; Greene et al., 2002; Hanssen et al., 2000; Jung et al., 2014; Miyoshi et al., 1999; Montanini, 2005; Motz and Pippan, 2001; Nemat-Nasser et al., 2007; Ramachandra et al., 2003; Reglero et al., 2010; Sriram et al., 2006; Sun et al., 2013; Thiyahuddin et al., 2014; Zhang et al., 2014). Generally, damage occurred during the impact depends on the capacity of the structure to withstand the load. Hence, to avoid the damage during the impact load, it is necessary that the allowable stress level should be designed on the basis of plateau stress such that the impact stress level remains below the plateau stress.

When foam is compressed or loaded, work is done on the foam. The work done per unit volume (W) to deform the foam up to densification strain (ε_d) is known as energy absorption capacity, which is generally the area under the stress-strain curve up to the densification strain (ε_d) and is given by following equation 2.3:

$$W = \int_0^{\varepsilon_d} \sigma \, d\varepsilon \qquad (2.3)$$

The plateau stress value depends on the cell wall material, relative density and the strain rate. Several deformation mechanisms are involved in absorbing energy (such as elastic, plastic or brittle, the compression and flow of fluid within the cells (Feng et al., 2003b). The deformation mechanism is vastly differ for open-cell and closed-cell foam. In open-cell foam, the energy is absorbed by the elastic buckling, plastic yielding or brittle crushing of the cell edges (V., 2011). However, in closed-cell foams, along with the above, bending and stretching of cell walls along with compression and flow of fluid within the cells also contribute in the energy absorption. Sometimes, a higher plateau stress is reported at the higher strain rate, which is useful when foam is intended for energy absorption at higher velocity impact. Higher energy absorption capacity at high strain rate is a very desirable property while using foam for light weight impact energy absorption applications.

2.8.1.2 Tensile behaviour of metal foam

Generally, mechanical properties of the metallic means compressive strength, whereas, analysis under tensile loading is rare. Lack of interest in the tensile testing is governed by its pore, which find within foam and act as crack initial site. Literature suggests that even ductile material foam did not perform well, when it is tested under tensile load (Fusheng and Zhengang, 1999). Andrews et al.(Andrews et al., 1999; Andrews and Gibson, 2001; Olurin et al., 2000) tested aluminium foam under tension and reported that the ductility as 0.17%, whereas, defects in the cellular structure result into bending of the cell wall, which in turn results in low tensile strength, approximately half of its compressive strength. In tensile load due to the defects found in the microstructure of foam, tensile loading of foams is almost entirely avoided (Ashby, 2000). Degradation in properties due to microstructural defect found in foam material are usually diminished by incorporating them as sandwich or filled structures, foam in sandwich form result into better properties and high specific strength (Contorno et al., 2006; Demsetz and Gibson, 1987; Schwingel et al., 2007; Triantafillou and Gibson, 1987). These added benefits often lead to substantial improvements in foam properties with only a small increase in overall material density (Contorno et al., 2006; McCormack et al., 2001; Mostafa et al., 2013) and are therefore, extremely important for the future development of foam applications.

2.9 Applications of metal foam

Open cell foam poses some specific properties, such as open pore voluminous structures, large surface area, good thermal conductivity and electrical conductivity. All these properties

with very fine cell structure open cell foam used in special applications such as in chemical industry as a high temperature filters and in compact heat exchangers where heat transfer is increased through pressure drop (Ashby, 2000; Banhart, 2001; Nakajima, 2007). Higher cost of the material is a constraint in open cell foam which reduces the scope of the open cell foam in advanced technology, aerospace and in advance manufacturing. Hence, it is reasonable to state that the main applications of the closed cell metal foams are impact absorber and light structural material. In general, metal foam have some physical properties of their base material and can be recyclable back to its base material but the thermal conductivity likely to be reduced (Banhart, 2001). Ship buildings, aerospace, railway and sporting equipment are some less known areas in which foams are increasingly used. Biomedical industry is another area where the porous layer of foam can ensure the in growth of tissue for titanium or cobalt-chromium alloys.

Regarding functional applications of foam, the major breakthrough is in the area of open-cell foam for heat exchanger design, filtration devices and electrodes for batteries. Details about heat exchanger design using metal foam are given in (Evans et al., 1998). Fire arresting capability, silencer design, acoustic control, decoration and arts are other areas where foams have the potential as a functional material. Even though metallic foams have great potential to use but the complexity and sensitivity of the process directly affect the cost of the end product which remain formidable obstacles in their widespread use (Maine and Ashby, 2000).

2.10 Strengthening of the cell wall material

Generally, the strength of metallic foam refers to the plateau stress, the extended constant stress domain beyond the elastic limit as discussed in the previous section (2.7.1.1). When the load is applied on the closed cell foam it is mainly sustained by the cell wall. Therefore, to improve the performance of the closed cell foam it is necessary to enhance the strength of the cell wall. Cell wall material strengthening can be achieved through the different strengthening mechanism used in alloy system (i.e. strain hardening, solid solution strengthening, grain refinement, dispersion hardening and precipitation hardening) (Dieter, 1962).

Above stated mechanisms can be used to improve the strength of the cell wall, which in turn improves the plateau stress. In metallic foam, strengthening can be achieved either pre (in-situ alloying and reinforcement) or post processing (thermal treatment) treatment. The combined effect of the above stated mechanism may be results into strengthening of the cell wall material.

In present work, in master alloy Cu is added in 6061 alloy, therefore Cu is the main alloying element in the used master alloy. As shown Fig. 2.11(Al-Cu indicative phase diagram), it is observed that the maximum solubility of the Cu is about 5% at eutectic temperature, lower at room temperature. This nature of the Cu atoms make it suitable candidate for precipitation hardening, as Cu get precipitated in the form of Al_2Cu, distributed randomly in Al matrix, as well as, at grain boundary.

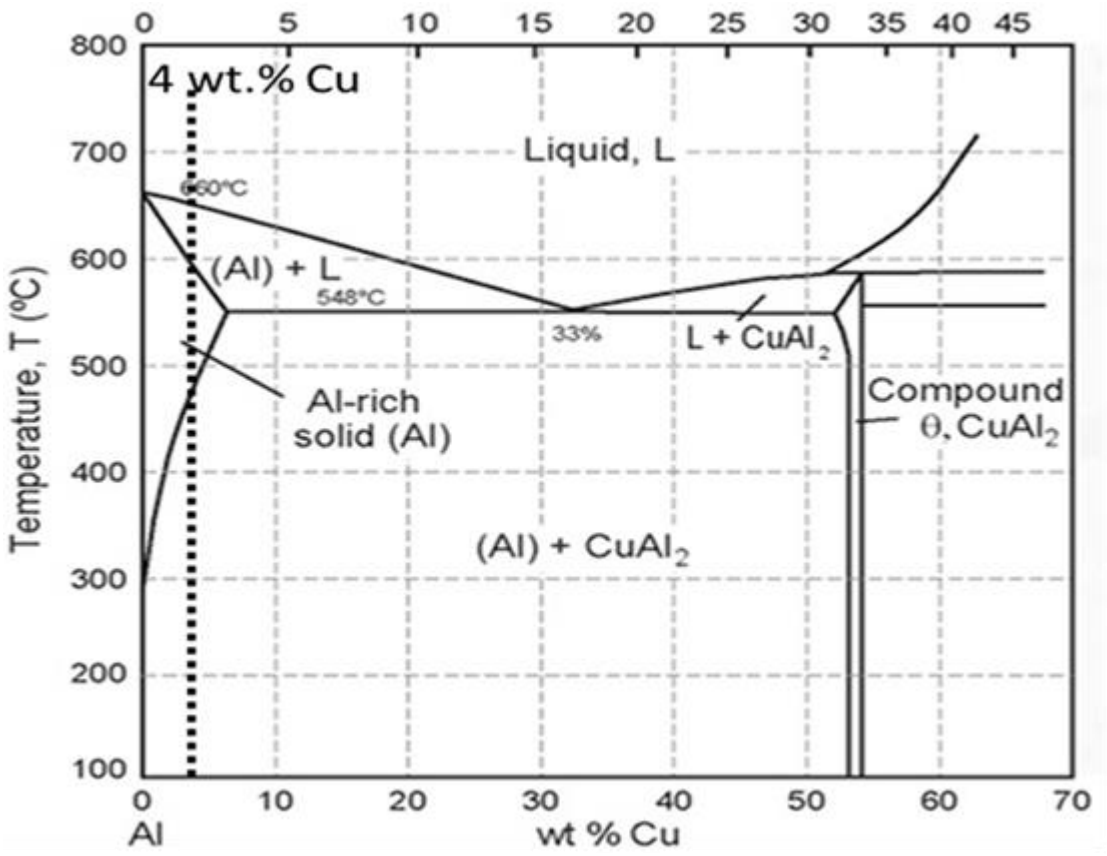

Fig. 2.11 Indicative phase diagram shows an approximate composition of master alloy (used in the present study) through aluminum-rich end Al-Cu system.

2.10.1 Strengthening mechanisms in aluminium alloys

Due to good strength to weight ratio high-strength aluminium alloys are of great interest in the research field and a substantial amount of work has been reported on strengthening of the aluminium alloys (Tellkamp et al., 2001; Youssef et al., 2006; Zhao et al., 2004). Dislocation movement under external stresses decides the deformation behaviour of any material, therefore, to improve the strength of the material, dislocation motion should be restrained in such a way that an extra load required to initiate the plastic deformation. Dislocation movement can be restricted within the microstructure by dislocation density improvement in the alloy matrix. In literature, various strengthening mechanisms are reported to produce high strength aluminium

alloys, such as in single phase metallic system grain size reduction, solid solution strengthening and strain hardening mechanism applies for strengthening (V., 2011), whereas, in the multi-phase system dispersion hardening, fibre strengthening and precipitation hardening are mainly used to strengthen the matrix material (Huskins et al., 2010). In the next section 2.8.1.1 to 2.8.1.3, most of the discussion will be centred on the interaction of dislocations with different obstacles. Reviews of the strengthening mechanisms are described in below subsections.

2.10.1.1 Strengthening by grain size reduction

In polycrystalline materials, orientation of the grain changes with the movement of one grain to the next across the grain boundary. Therefore, the movements of dislocation became more difficult if there is any misalignment in the grain orientation. Reduction in grain size results in the dense grain boundary area, hence, the mean distance travelled by the dislocation decreases, which in turn results into pile up of dislocations at grain boundary. Hence, reduction in grain size strengthens the grain boundary and grain boundary strengthening generally described by the Hall-Petch relation. According to Hall-Petch relation "variations in the yield strength (σ_y) with respect to grain size (d) have following relationship (Hall, 1951; Huskins et al., 2010; Petch, 1953) (equation 2.3):

$$\sigma_y = \sigma_o + kd^{-1/2} \quad \ldots\ldots(2.4)$$

Where; σ_o is the friction stress, k is the locking parameter, d is the average grain diameter. The yield strength (σ_y) is inversely proportional to grain size; therefore, the fine grained materials are stronger than the coarse grained materials.

2.10.1.2 Solid solution strengthening

The introduction of the solute atoms in the crystalline lattice of base metal mainly diffuses to a matrix solid solution and goes into interstitial or substitution positions in solution. The alloying element atoms cause lattice distortion, which restrict the dislocations motion and result into increase in the strength. Solid solution strengthening depends on size, concentration and shear modulus of solute atoms. The relation between solute strengthening increment $\Delta\sigma_{ss}$, and concentration (C) of a solute atom is given by:

$$\Delta\sigma_{ss} = HC_{\alpha} \quad \ldots\ldots(2.4)$$

Where α and H are constants. A higher concentration of solute atoms hinder dislocations, hence, result into higher strength(Suzuki, 1990).

2.10.1.3 Precipitation hardening

Precipitation hardening is used to strengthen almost all heat treatable aluminium alloys. In general, heat treatment follows the path: solution treatment, quenching and aging (Polmear, 1995) , which can be presented schematically on temperature-time scale (as shown in Fig. 2.12).

Precipitation hardening mainly depends on solid solubility of the metal matrix at elevated and lower temperature. For better results, solubility should be significantly higher at elevated temperature, whereas, partially soluble at lower temperature. The parameters (i.e. cooling time, soaking time and temperature) are used in the heat treatment process are greatly affect the final properties of the alloy (Rajan and Sharma, 2012). In solution treatment process, the alloy is heated near solidus temperature and holding at same temperature for sufficient time for homogenisation.

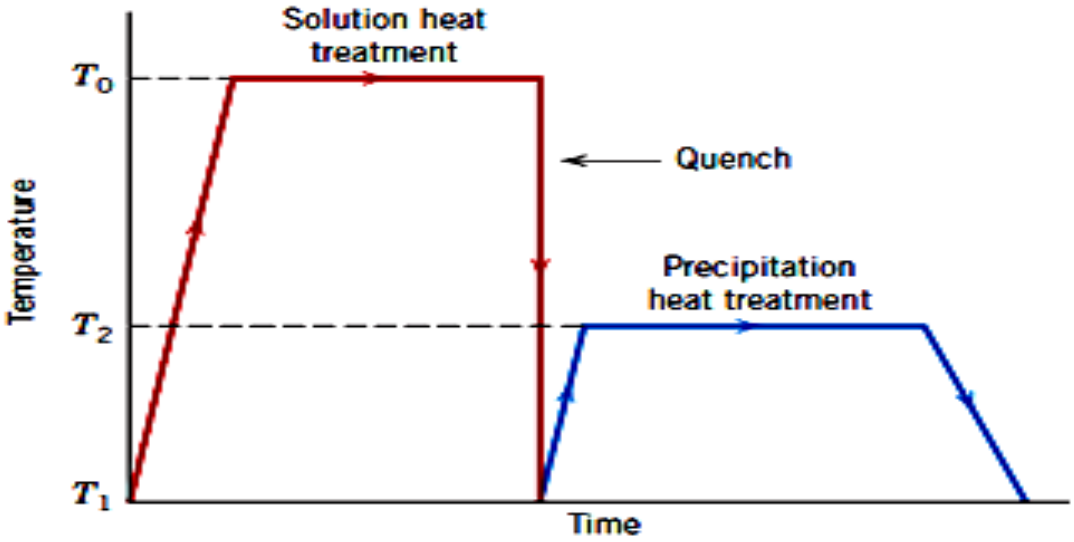

Fig. 2.12 General steps followed in precipitation strengthening.

After solution treatment, alloy is quenched in water to create a supersaturated solid solution in single phase with maximum saturation of the alloying element for subsequent aging. The cooling rate determines the degree to which supersaturated solid solution is prevented from precipitate out the stable phases. The degree of precipitation (slow or fast) depends on alloy composition, time and tempering temperature. Slow precipitation occurred at room temperature; whereas, it is more prompt at elevated temperature also known as artificial aging. Precipitation hardening or age hardening is most widely used strengthening mechanisms in aluminium alloys specially in 2xxx (Al-Cu), 6xxx (Al-Mg) and 7xxx (Al-Zn) series, where formation of the fine second phase particle in the super saturated solution is more prompt and

results in improved hardness and strength. These extremely fine precipitates hinder the dislocation movements, which provide resistance to slip, thereby, strengthen the alloy. After solution treatment, alloy is quenched in water to create supersaturated solid solution in single phase with maximum saturation of the alloying element for subsequent aging. The cooling rate determines the degree to which supersaturated solid solution is prevented from precipitate out the stable phases. The degree of precipitation (slow or fast) depends on alloy composition, tempering time and tempering temperature. Slow precipitation occurred at room temperature; whereas, it is more prompt at elevated temperature. Precipitation hardening relies on the changes occurred in the solid solubility with temperature variation. The precipitation process can be monitored with the help of the hardness measurement, which furnish a good indication of the strength of a material. Therefore, the effect of the aging treatments can be evaluated by hardness testing and metallography.

The addition of Cu in to aluminium improved the hardening behaviour; therefore, further thermal treatment results in good strength and the improvement in the strength attributed to precipitation hardening. Phase diagram at the aluminium rich end is shown in Fig. 2.11, from phase diagram, it is observed that in the range of 500^{o}C approximately 5% of Cu dissolved in the solid solution whereas at lower temperature solubility is much lower (< 0.1%). As solubility limit of Cu exceeded, the rich amount of Cu forms a compound with aluminium which is designed as θ (Al_2Cu). Precipitation sequence of the supersaturated solid solution in Al-Cu alloys is as follow (Wang and Starink, 2005b).

$$\text{super saturated solid solution} \rightarrow \theta''(Al_3Cu) \rightarrow \theta'(Al_2Cu) \rightarrow \theta(Al_2Cu) \quad \ldots\ldots (2 \cdot 5)$$

Hence, it is clear that an alloy with 4 wt. % Cu held at 500^{o}C for sufficient time so that all the copper to be taken into solution followed by rapid quenching in water to room temperature. Cu completely retained in solid solution and remains in this state for short period of time at room temperature. This state of the alloy is known as super saturated solid solution. The quenched alloy is in a well-known metastable condition and metastable condition structure stable only at a higher temperature.

In this condition, if the temperature of the supersaturated solution increases slightly to a level well below where all the copper will go back into solution and excess copper atoms diffuse and cluster together. These clusters of copper atoms form regions of vivid strain in the crystal lattice of the Al-Cu solution and hinder the dislocation movement results in an increase in hardness and strength. Further diffusion of Cu results into formation of discrete particles compound of Al_2Cu. Nucleation and growth of $CuAl_2$ can not take place at room temperature

which is favourable condition and increase in strength is sufficiently permanent to be used in the design of engineering components. However, the structure is still highly unstable again allowed nucleation and growth process continue.

2.10.1.4 Dispersion hardening

In dispersion-hardening mechanism, presence of the fine (with less than 0.1μm size) second phase particles results in to higher strength and hardness. These particles are uniformly dispersed and found within the metal matrix with very little solubility (even at elevated temperature) in the matrix. Particle can be added through either mixing or consolidated as precipitate in solid solution; these dispersed fine particles restrict the dislocation motion and result in improved strength of a material. Strengthening through dispersion hardening depends on the size, shape and amount of the second phase present in the alloy. The dispersed particles are much harder than the matrix material and it is hard to deform them even at higher stress. Dislocations moving through the matrix can either be cut through the precipitate particles or bend around to bypass them. Therefore, dislocation can not cut through the particles and the moving dislocation arc bypass instead of cutting through the particles. With increase in the applied shear stress the dislocation bends adequately and when it reached to a critical curvature the sections of the dislocation meet at the other side of the particle and moves forward, which results in a dislocation loop around each particle. This is best known as Orwan mechanism (Orowan, 1948), used to describe dispersion hardening as shown in Fig.2.14.

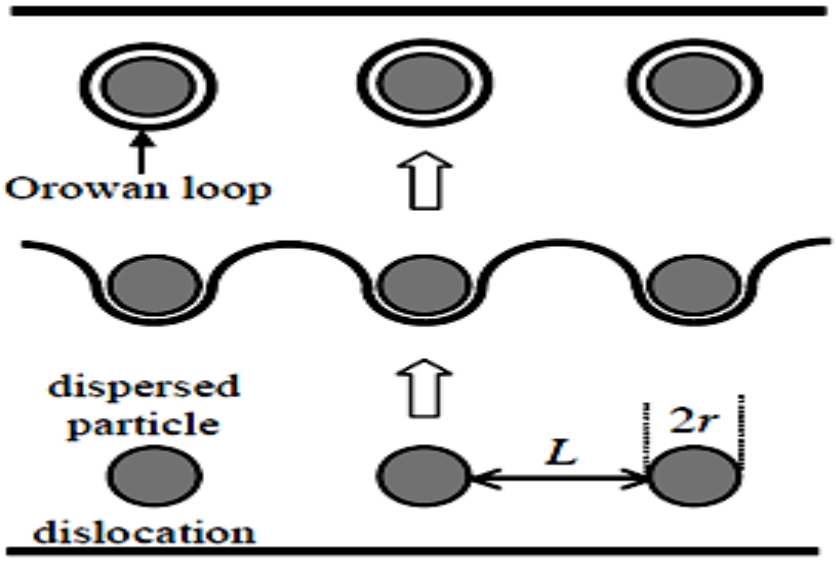

Fig. 2.13Sschematic representation of orwan mechanism used for dispersion hardening (Orowan, 1948).

2.10.1.5 Reinforcement strengthening

This is an approach of metal matrix strengthening, which involves extrinsic modification by introducing additional (external) phases. In this approach, the strength is improved by second phase reinforcement that has higher strength than the metal matrix. Aluminium based discontinuous reinforcement poses better properties as compare to the unreinforced alloy (Quigley et al., 1982; Surappa and Rohatgi, 1981). High strength materials can be produced by the introducing fine fibers in a metal matrix. For good results, it is necessary that the strength of the fibre must have high enough then the matrix material, while, the matrix must be nonreactive with the fibers. Because of very high strength, whiskers of materials (such as Al_2O_3, ceramic particles, metal carbides) have been used for reinforcement. The reinforced fibers may be long and continuous, or they may be discontinuous. When the uniaxial load is applied on the discontinuous and random fibre reinforced material, it undergoes axial, as well as transverse normal strains, whereas, in a continuous fibre reinforced material an additional shear strain is also developed. As reported in literature, fiber reinforced materials poses anisotropic mechanical properties and these properties depends on the fibre orientation in the matrix. Following are the main observation during the strengthening effects of reinforcement (Clyne and Withers, 1995):

1. Load transfer from the matrix to fibers
2. Geometrical and thermal mismatch between matrix and fibers, results in improved dislocation density.
3. The presence of the fiber in the matrix also contribute to Orowan strengthening (Orowan, 1948).

The section (2.9.2), presents the possible strengthening mechanism for the master alloy used in the present work, strengthening mechanism review helped in understanding the various mechanisms. After reviewing these strengthening mechanisms, it has been concluded that dispersion strengthening, grain size reduction and reinforcement can be employed and investigated for cell wall material of foam. Hence, on the basis of above literature review, these approaches are used in the present work presented in the following sections.

Mechanical properties of the metallic foam can be improved either by changing the foam cell geometry or employed pre (thermal treatment) and post processing techniques (alloying, particle addition etc.), much of the work performed related to alteration of the cell geometry including which includes relative density, cell geometry and morphological defects with subsequent effect on the mechanical properties of foams has been extensively investigated

(Aguirre-Perales et al., 2012; Duarte and Oliveira, 2012; Hossein Elahi et al., 2012; Jiménez et al., 2012; Kamm et al., 2013; Kumar et al., 2013; Lázaro et al., 2013; Zhao et al., 2011a; Zhao et al., 2011b). However, there are some data related to post processing treatment (especially heat treatment) is available to understand the change in mechanical behaviour after treatment. (Feng et al., 2003a) studied the quasi static, as well as, dynamic compressive behaviour of T6 aged aluminium foam and found that the T6 aging treatment result in improved yield stress and 34%-63% improvement in the energy absorption capacity but aging treatment did not show any effect on the densification strain at different strain rate. Wang et al (Wang et al., 2009) examined Al-Mg-Si foam T6 strengthened treatment, as hardened and as fabricated sample at 10^{-3} to 2000 s^{-1} strain rate he found that T6 strengthened treatment can raise the strength and energy absorbing capacity. Foams that were fully heat treated performed best with an increase of strength by 60%-75% over the untreated sample. Aging treatment increased the elastic limit and the plateau stress level and consequently the energy absorbed during crushing.

On the basis of literature review, it is noted that stabilisation of the foam processing is still a main hurdle in the defect free foam, so it is necessary to know the reason behind the defect generated (Matijasevic and Banhart, 2006) in the foam at macro level (in the form of local drainage) as well as microstructure level. In order to achieve stabilisation, particles are added in the foam of oxides (Al_2O_3, $MgAl_2O_4$, TiO_2 etc.(Babcsán et al., 2004; Banhart, 2006; Chakraborty et al., 2011; Deqing and Ziyuan, 2003; Ip et al., 1999a; Kadoi et al., 2010; Körner et al., 2005a; Mahmutyazicioglu et al., 2013; Wübben and Odenbach, 2005)), carbides (SiC, B_4C, TiC, etc. (Banhart, 2006; Golestanipour et al., 2011; Haesche et al., 2008; Haibel et al., 2006; Kumar and Gokhale, 2012; Prakash et al., 1995; Ravi Kumar et al., 2014; Ravi Kumar et al., 2010; Yu et al., 2008)), borides (such as TiB_2), fly ash(Mu et al., 2010b) and suspended solid particles (Babcsán et al., 2003; Cao et al., 2006; CAO et al., 2005; Deqing and Ziyuan, 2003; Gergely and Clyne, 2000; Guden et al., 2007; Kaptay, 2003; Mukherjee et al., 2010; Stocco et al., 2011; Wübben and Odenbach, 2005). In recent years, some researchers use carbon fibers for stabilisation purpose(Cao et al., 2008; Mu et al., 2011; Mu et al., 2010b; Mu et al., 2013) and found that the use of fibres improved the stability of the melt, Mu et al (Mu et al., 2013) find that the presence of fibres stimulates mechanical barrier and disjoining pressure within the melt.

2.11 Gaps in literature

A literature review did not reveal any systematic study on the following aspects related to Al alloy foam produced through melt rout using TiH_2 as a foaming agent:

1. There is acute scarcity of literature available on the effect of microstructural modification on Al foam.
2. Limited information is available in the literature on the influence of heat treatment on microstructural and mechanical behaviour of Al foam.
3. No systematic information is available in the literature on the influence of grain refinement on the mechanical behaviour of Al foam.
4. There is acute scarcity of literature available on the fracture behaviour of Al foam.
5. No proper guidelines and data are available for the selection of initial foam temper, and process parameters.
6. No systematic information is available in the literature on the influence of reinforcement on the mechanical behaviour of Al foam.

2.12 Objectives

In the light of the above stated facts and constraints in the processing of al foam, following objectives have been framed in the thesis work:

1. To synthesize stable Al foam by the melt foaming method using TiH_2 as a foaming agent.
2. Study of evolution of microsturctural features resulting during in situ processing of foam.
3. To improve the energy absorption capacity of produced foam.
4. To investigate the effect of thermal treatment on cell wall microstructure and energy absorption capacity of foam.
5. To investigate the effect of scandium addition on microstructural behaviour and energy absorption capacity of foam.
6. To investigate the effect of reinforcement on microstructure and compressive properties of al foam.

In order to achieve above objectives of the study considering the constraints, in present work; heat treatment, alloying and reinforcement used to modify the microstructure and a systematic attempt has been made to investigate the microstructure and mechanical properties of aluminium foam in different conditions. It is expected that investigation in present work will provide the basis for improvement in energy absorption capability which is beneficial to

extending the practical applications of metallic foam. The foam specimens were heat treated at different temperature for different durations. The thermal behaviour, including the microstructural development during thermal treatment, which followed by measuring the hardness and tested under compression to determine the properties such as plateau stress, yield stress and energy absorption. Same course of action is followed in the scandium inoculated foam, as well as, in fibre reinforced foam. Different characterization techniques are used to evaluate the effect of microstructural modification on the energy absorption capacity. The result demonstrated that all are the approaches used in this study to improve the mechanical properties of closed cell aluminium foam are effective. The plan of the proposed work is schematically presented in the following Fig. 2.15.

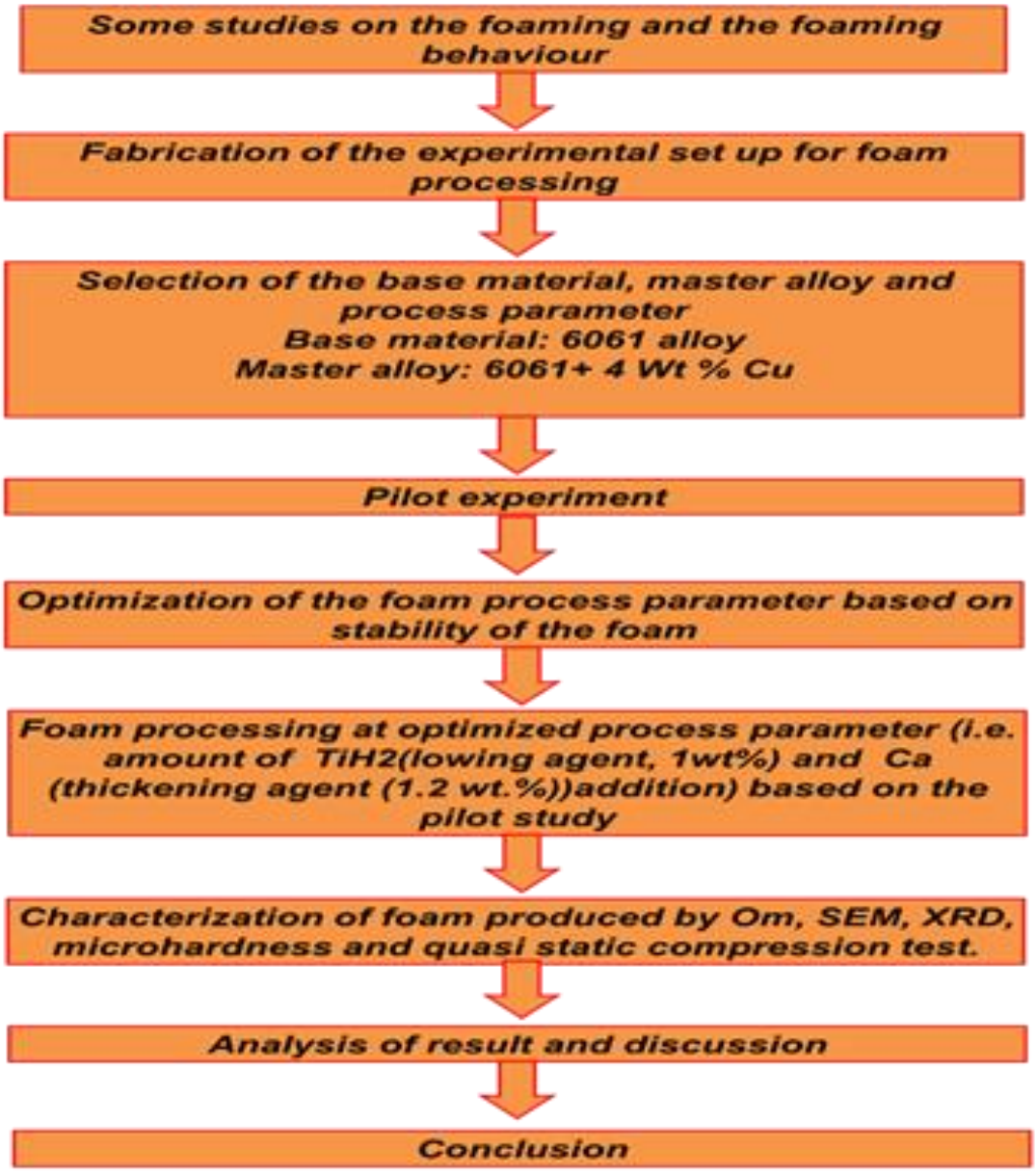

Fig. 2.14 The flow chart of the proposed work

In the present chapter, selection of matrix material, fabrication of the experimental set up (to prepare aluminium foam), techniques used for microstructural and mechanical characterisation are discussed. The foaming agent is studied by thermo gravimetric analysis (TGA). Closed cell foams are characterised by optical microscope, XRD (X-ray diffraction), scanning electron microscope (SEM) and transmission electron microscopy (TEM). Mechanical tests are carried out and used to correlate the effect of microstructural modification and the energy absorption capability of the foam.

3.1 Raw material and master alloy

The first step in the casting route is selection and preparation of the master alloy. Aluminium 6061 alloy (procured from Hindalco Industries Ltd, Mumbai, India) with the chemical composition (as shown in the Table 3.1) has been taken as initial material for the present work, which further alloyed with 4 wt.% Cu to prepare master alloy. Master alloy was prepared by heating initial material at 900^{o}C for an hour and further furnace cooled. Prepared master alloy is used for all the foaming experiments.

Table 3.1 Chemical composition of 6061 aluminium alloy used as a base material in present work.

Alloy	Chemical composition (wt. %)								
	Si	Fe	Cu	Mn	Zn	Mg	Cr	Ti	Al
Wt. %	0.4-0.8	0.7	0.15-0.4	0.15	0.25	0.8-1.2	0.04-.35	0.15	balance

3.2 Experimental setup

Designed experimental set-up consists of muffle furnace (top opening box type), removable stirrer system arrangement (for powder addition at the time of foaming), voltage stabiliser and variable voltage supplier (to control the stirrer speed). The set-up was designed for at least 1 Kg of casting capacity). As shown in Fig. 3.1, set-up is attached with temperature controller, stirrer speed controller and water quenched bath with continuous flow so that the water bath temperature can be maintained. The set-up was fabricated and modified in-house. The foaming process employed in the present work follows the melt foaming method using TiH_2 as a foaming agent (as discussed in the literature review section). The apparatus used in

the synthesis of the foam is illustrated schematically in Fig. 3.1; the muffle (a heating chamber of size 200 × 200 × 300 mm.) encircled by an electrical element, Kanthal A-1 wire of gauge 16 SWG).

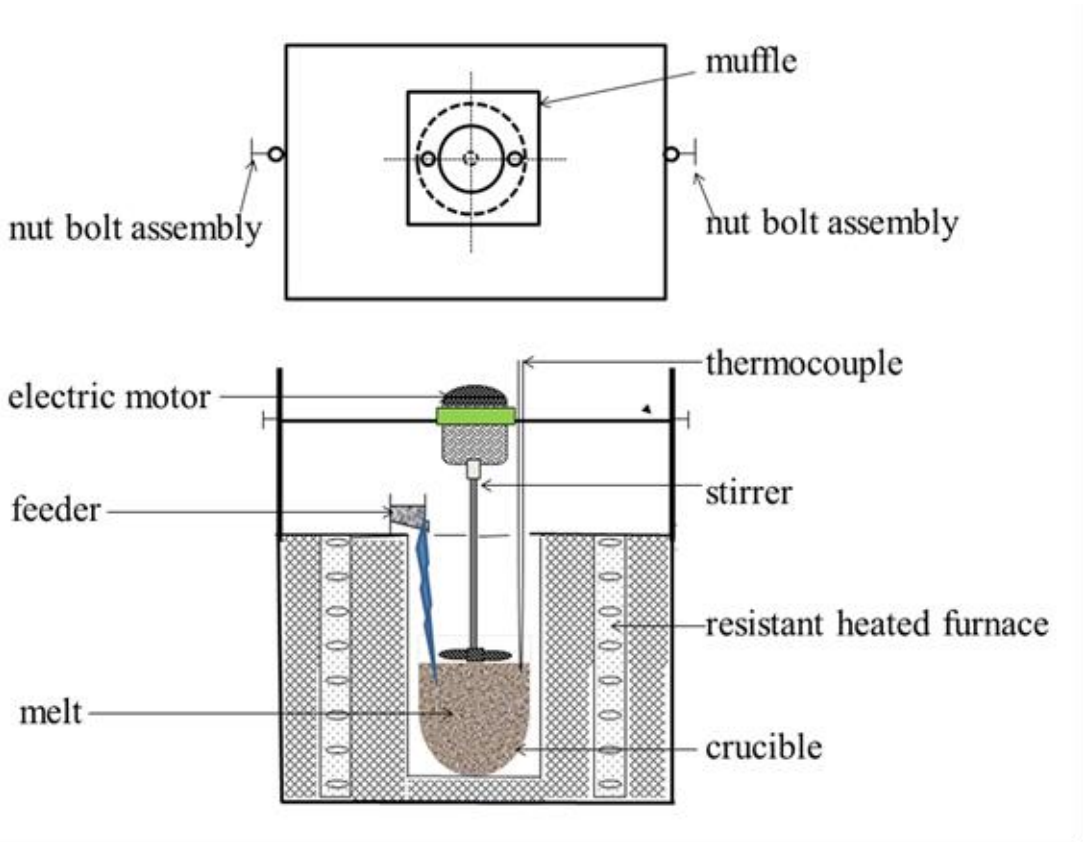

Fig. 3.1 Schematic representation of the experimental set up used in present study for closed cell foam processing.

Except the top end, all the sides of the furnace are permanently insulated to avoid heat loss. The muffle opening is covered with two lids made of the steel frame fastened with fire-clay brick, which also facilitate the passageway for the attachment (i.e. stirring assembly), powder pouring and thermocouple holes are provided on the lids. The power is supplied through voltage stabilizer to automatically maintain the constant voltage level. Furnace, power supply equipped with PID controller (with a calibrated chromel-alumel thermocouple) for temperature control. The stirrer is powered by an electric motor (capacity 0.5 HP) with a maximum speed of 1200 rpm. The speed of the stirrer is maintained and controlled by variable voltage stabilizers. A stirrer motor assembly fixed in a frame mounted on two solid rods welded on the side of the furnace, which can be fixed at various heights with the help of a nut bolt assembly. The speed continuously monitored by a non-contact type tachometer placed at some distance to the stirrer rod.

3.3 Foaming Procedure

In the present study, the melt foaming method was employed to produce closed cell metal foam. A clay (graphite coated) crucible contain about 0.5 kg master alloy placed in a muffle furnace (maintained at 730ºC) and a stirrer motor assembly (as shown in Fig. 3.1) was introduced to the melt though a sliding frame assembly, and the speed of the stirrer was increased to 850 rpm. After some time (2-3 minutes) thickening agent (Ca granules (98.8 % metal basis and 16 mesh)) was added in the liquid melt while stirring at 750 rpm (for 10-12 min), which in turn increase the melt viscosity. When melt viscosity was achieved, TiH_2 (blowing agent) was added in the melt and stirrer at 1020 rpm for sufficient time (60-90 Sec.), to disperse blowing agent in the melt immediately. After proper dispersion of blowing agent stirring was stopped and stirrer removed from melt and melt subsequently hold in the furnace for sufficient time (90-120 Sec.) to ensure proper dispersion (without losing at the surface of the melt), as well as, decomposition of the blowing agent. After holding time, the clay graphite crucible containing the metal foam was taken out of the furnace and immediately cooled in water bath to arrest the produced foam.

Foam processing technique remain same in whole dissertation work, as per strengthening mechanism used to improve the properties of the produced foam master alloy master alloy composition is altered as described below.

- To stabilise the metal foam and measure the effect of thermal treatment (i.e. improve the strength of cell wall microstructure through the thermal treatment) master alloy was prepared with 4 wt. % Cu addition in the initial material (6061 Al alloy).
- To measure the effect of the grain refinement (i.e. improve the strength of the cell wall through grain refinement), master alloy was prepared by addition of scandium (0.6-1.0 wt. %) in initial master alloy (i.e. 6061+4 Cu).
- To measure the effect of the reinforcement on the cell wall microstructure and energy absorption capacity same master alloy was used (6061 +4 Cu) which is further reinforced by CCSSF during foam processing.

3.4 Characterization techniques

3.4.1 Macrostructural characterisation

To quantify the macrostructure of the casted foam, digital micrograph of the bisected sample has been taken (to evaluate the structural homogeneity and local drainage).

Macrostructural analysis in this dissertation work is used to optimize the process parameter through evaluations of the defect generated in the structure (i.e. cell wall collapse, rate of drainage).

3.4.2 Thermal analysis

TGA is fundamentally a microbalance inside a small furnace (furnace is tubular so it can measure higher temperatures), which is principally based on the measurement of the mass loss of the sample placed in the microbalance with respect to time. Sample to be analysed placed inside the furnace and the temperature is cranked up. As temperature rise and when the sample react, burns up or evaporated, the mass is determined. A constant temperature of the sample indicated that the sample boils up and if the sample burns the heating rate inside the furnace increased which can be easily measured in the oven. Through TGA analysis, it is easy to get information regarding thermal stability, decomposition behaviour (in this work blowing agent), and kinetics. Working principle shortly described above and the schematic diagram of the working principle of the same is shown in the Fig.3.2. In the present work, thermo-gravimetric analysis is carried out on the TiH_2 powder to know the thermal decomposition behaviour with the approaching temperature of hydrogen gas development. To avoid oxidation effects, the TGA analysis was executed in inert atmosphere. The heating rate in present work is 10°C/min and the argon gas flow was maintained at 200 ml/min. Weight loss due to the evolution of the H_2 gas indicates the decomposition of TiH_2.

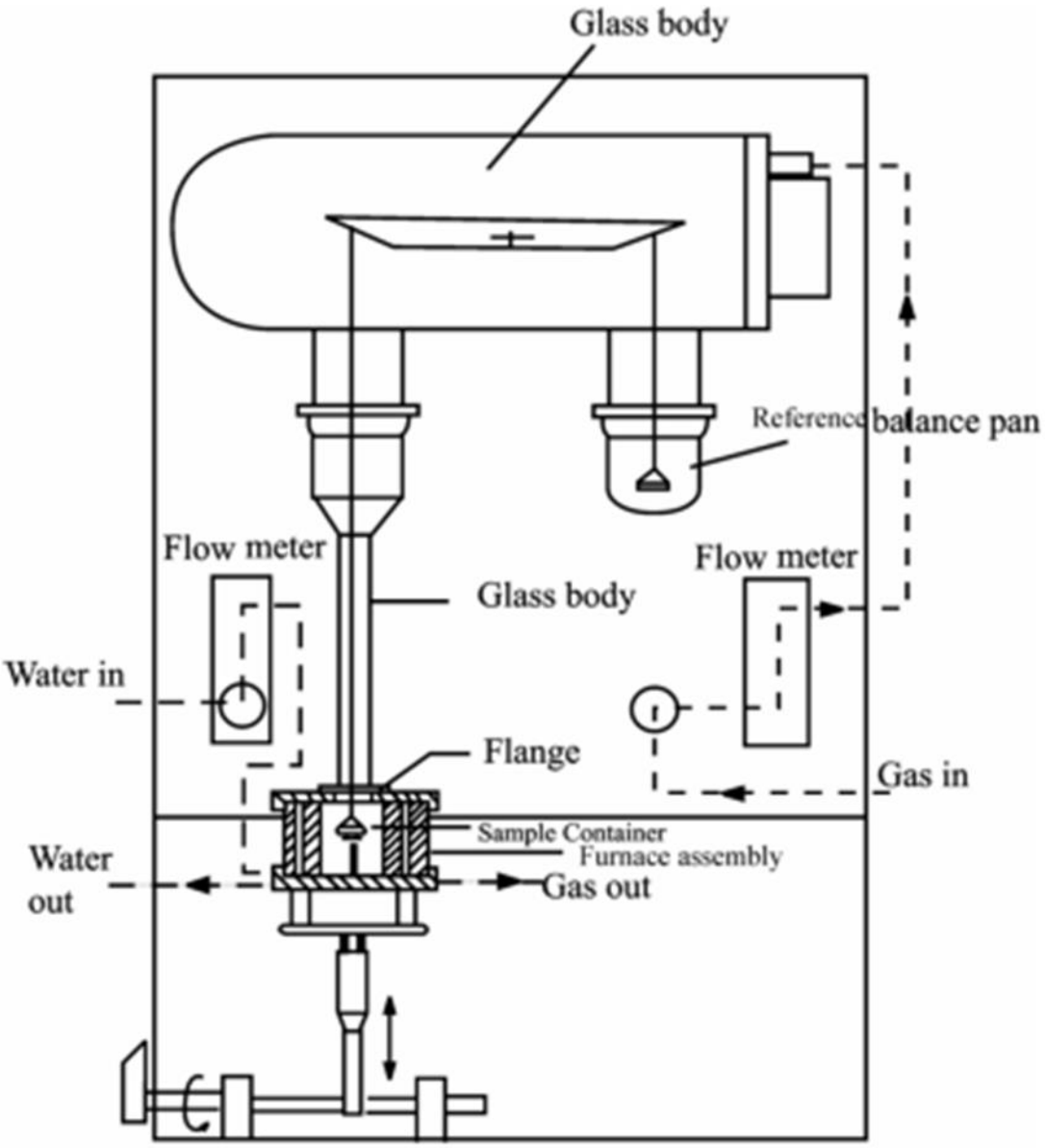

Fig. 3.2 Schematic representation of the working principle of TGA used to measure decomposition behaviour of TiH_2.

3.4.3 Structural characterisation

Samples for basic microstructural and mechanical characterization were prepared from produced foam. Pore size at different location in foaming direction, as well as, in transversal direction was measured using travel microscope with a 0.01 mm order resolution. Average pore size was measured using line intercept method. For compression testing, all samples were prepared with approximately square section (10×10 mm^2) and the height twice to base (20 mm).

3.4.4 Optical microscopy

Optical microscopy renders micrograph of specimens for preliminary microstructural examination. The foam samples in different condition (i.e. as-cast, aged, solutionised, alloyed and reinforced) were characterized to examine the change in microstructure with respect to change in parameters using an optical microscope (LEICA DMI5000 M).

Initially, the sample was prepared from cast foam and then cut on the diamond cutter with proper lubrication to avoid a rise in temperature at the time of cutting of the samples. After cutting, the samples were mounted on the sample holders and polished it mechanically up to 2000 grit size on water proof SiC emery papers. To avoid embedding of abrasive particles into the soft aluminium foam, continuous flow of water was maintained so that particle flushes away with water. The final mirror polish of the mechanically polished samples was done on polishing machine using a fine velvet cloth, magnesium oxide and 1 micron size diamond paste. The polished samples were etched with Keller's etchant. After etching, proper rinsing and drying, preliminary microstructural examination of the sample (at different location) was done under an optical microscope with different magnifications in polarized light.

3.4.5 Scanning electron microscopy (SEM)

After the preliminary microstructure evaluation with optical microscope, samples were prepared for SEM analysis. Scanning electron microscope Quanta 200 FEG (FEI Company, the Netherlands) equipped with field emission source and EDS (Genesis 2000i) with the resolution of 135 eV is shown in Fig.3.3 (a). The working of the SEN is presentenced schematically (as shown in Fig. 3.3 (b)). To avoid charging due to non-conducting phases present in the samples, samples were coated with a thin layer of gold. SEM analysis used for microstructural analysis (i.e. morphology, fracture surface morphology, dispersal of the intermetallic and oxides) of the cell wall material. For SEM analysis, samples were prepared follow the standard metallographic procedure. SEM studies were conducted with an electron beam accelerating potential of 15 or 20 kV.

To increase the contrast between the different elements, the backscattered electron image mode is preferred, similarly, the secondary electron mode were preferred for surface morphology and used for observation of the dispersion of the various phases in the metal matrix.

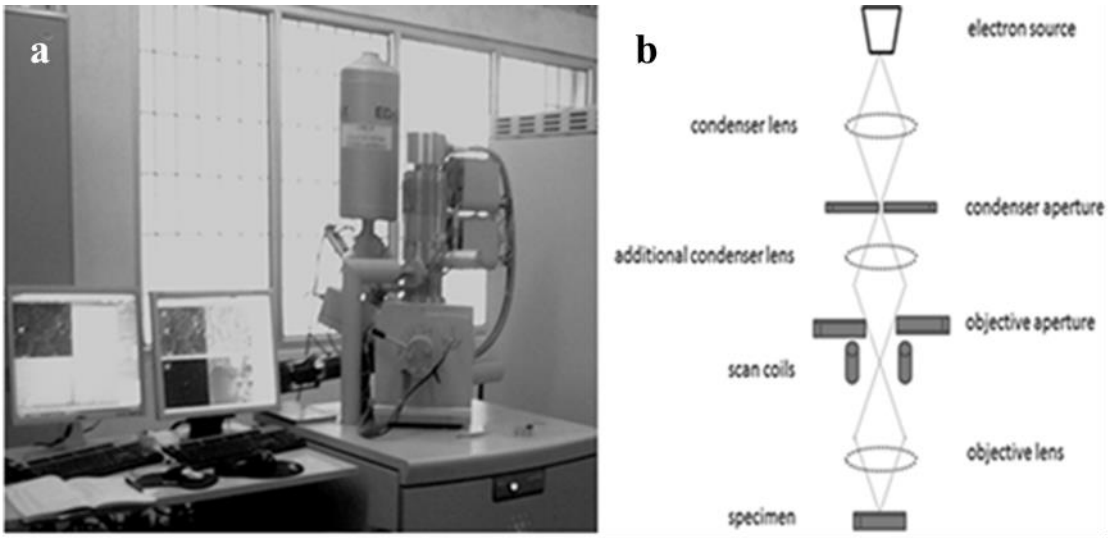

Fig. 3.3 (a) Photograph of FEI Quanta 200 FEG-SEM and (b) schematic diagram represents the typical working principle of SEM.

Compositional analysis is done with localized energy dispersive X-ray spectroscopy (EDX), elemental mappings and line analysis. Al the elemental analysis was executed on the cell wall surface and across particles.

3.4.6 Transmission electron microscopy (TEM)

In the present work, investigation of the cell wall microstructure (at lower scale) in as-cast, aged, solutionised, reinforced and grain refined foam samples were carried out using FEI Technai 20 TEM, operated at 200 kV. The photograph of the TEM is shown in Fig. 3.4 (a) with a schematic diagram (as shown in Fig. 3.4 (b)) represents the typical working of TEM. The basic working principle of the TEM microscope is similar to the optical microscope, the only difference in optical microscope and TEM is in TEM electron replaced photons whereas electromagnetic lenses replace glass lenses. In TEM the image is viewed on the screen rather than through eyepiece. In transmission electron microscope (TEM), energetic electrons are used to get the complete information (i..e. compositional, morphological and crystallographic) of the sample. TEM is the most powerful microscopes and due to utilisation of high energy focussed beam for imaging, TEM unveils the information that can not be accessed through an optical microscope and SEM. TEM is mainly used to characterize the grain size, crystal structures, specimen orientation, chemical compositions of phases, dislocation density, and precipitation morphology present in the sample through diffraction pattern, X-ray and electron-energy analysis.

TEM is a characterization technique wherein a beam of electrons interacts with the specimen in a high vacuum chamber. Interaction of the electrons transmitted through the

sample and results into the image formation. Image is further magnified and focused to have an enlarged version on a fluorescent screen or to be detected by a sensor such as a CCD camera.

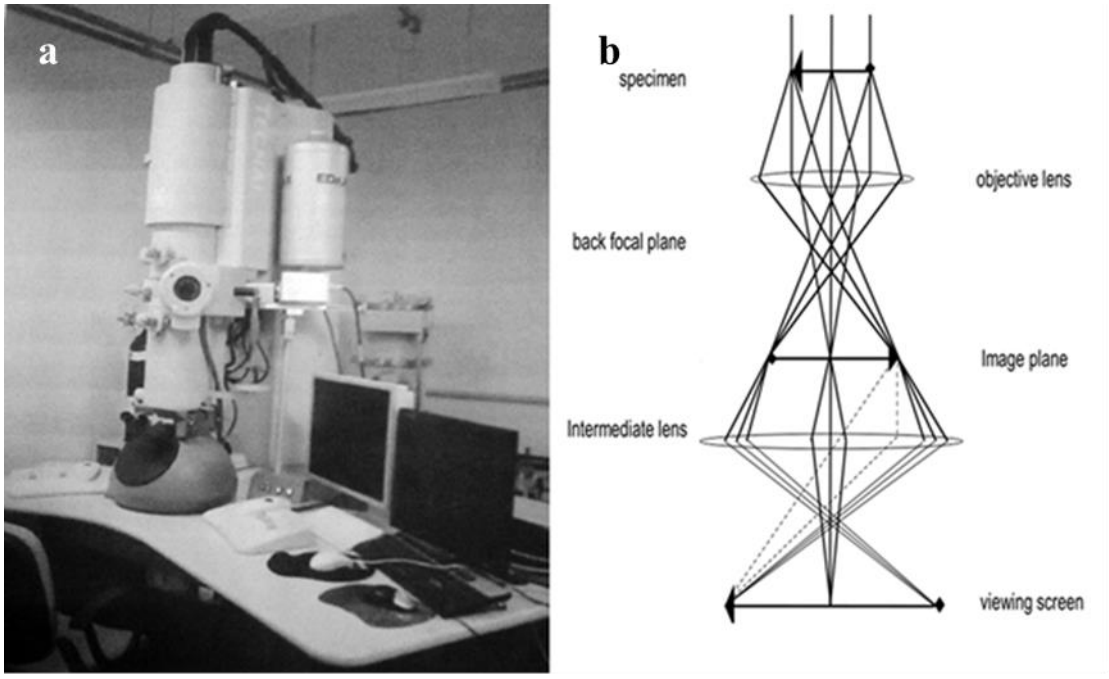

Fig. 3.4 (a) Photograph of FEI Tecnai-20-TEM and (b) schematic diagram represents the typical working principle of TEM.

For simplicity, TEM is divided into three sections: (1) illumination section, (2) Objective (lens/stage) section and (3) imaging section. The illumination section comprises an electron gun equipped with either a LaB_6 (lanthanum hexaboride) or tungsten filament source. When the high voltage source (100-300 kV) connected to the gun, it emitted an electron beam which passes through the set of condenser lenses and produces a beam side which interacts with the sample, the interaction of the beam and the sample results in image and diffraction patterns, all the operations take place in a vacuum.

For sample preparation for investigation through TEM, extra care requires. To prepare a thin section, initially thick slices (approx. 500 μm) were cut from the foam sample using slow speed diamond cutter. Now samples were thinned up to 100 μm using emery papers down to 2000 grit size through mechanically polishing. Both sides of the sample were polished and subsequently punched to 3mm diameter discs. After that thin sample were cleaned (using acetone), which further thinned using twin-jet electro polishing unit with a 15:85 solution of perchloric acid and methanol at -40^{o}C temperature and 40 volts potential. To ensure the clean

surface without any layer of an etchant, sample were rinsed thoroughly in ethanol and water. Thus, samples were ready for microsturctural characterisation using TEM.

3.4.7 X-ray diffraction

Quantitative and qualitative analysis of the foamed samples were done using XRD technique. In present investigation, XRD analysis was used to identify any crystalline phases present in the sample, similarly sample were also characterize by X-ray diffraction to find out the different phases present in the foam sample in different conditions. D8 (Bruker AXS, Karlsruhe, Germany) advance instrument with computer control, analysis software and Cu Kα radiation was used to perform X-ray diffraction measurements for all the foamed samples. The photograph of Bruker AXS D8 XRD equipment is shown in Fig. 3.5 (a). The XRD patterns of the calcium, TiH_2 powders checked for purity and degradation effects. Foamed samples of the cell wall material are taken to carry out phase identification. A diamond file is used to make powder samples while avoiding contamination. To suppress the aluminium peaks by increasing the relative quantity of the intermetallic, the foam sample selectively leached using diluted hydrochloric acid. All XRD analysis was carried out in the range of 20°-90° using Cu-Kα radiation of $\lambda = 1.5413\ A^o$. The Goniometer speed is maintained at 1°/min. Peak identification has been carried out by comparing with the relevant JCPDS X-ray diffraction data cards.

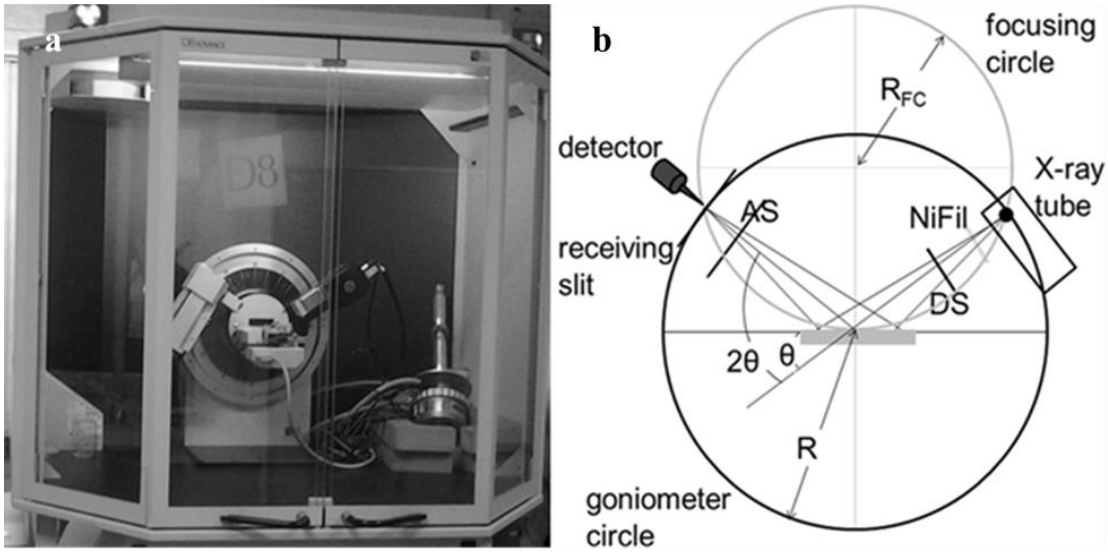

Fig. 3.5 Photograph of D8 Advance, Bruker AXS, X-ray diffractometer used for X-ray powder analysis and (b) schematic representation of diffraction in Bragg–Brentano geometry.

Filtered monochromatic X-rays produced by a cathode ray tube are collimated and directed toward the sample. X-ray diffractometer is designed in such a way that when the sample rotate by an angle θ in the path of the collimated X-ray beam, the X-ray detector is rotated by an angle of 2θ which is mounted to collect the diffracted X-rays. The working principal of the XRD is shown schematically in the Fig. 3.5 (b). When the Bragg's condition (i.e. $2d \sin \theta = n\lambda$) is satisfied, the incident X-ray beam is diffracted at the specimen and constructive interference occurs resulting in intense peak.

X-ray signals are recorded by a detector; in the present instrument (Bruker D8 Advance diffractometer) Nal scintillation counter is used as a detector with the capacity for detection of radiations in the wavelength ranges of 0.5 to 3 Å. The information such as inter planar spacing, unit cell size or lattice parameters, crystallite size and strain in the sample can be acquired through diffraction pattern.

3.5 Mechanical testing procedures

To correlate the microstructural and mechanical properties of foam in terms of compressive behaviour in different conditions mechanical testing has been conducted to accommodate the results obtained through microstructural characterization techniques. Mechanical properties of the close cell foam were determined by compressive and microhardness tests at room temperature. The samples for axial compression and microhardness test were taken from a direction parallel to foaming direction. Interrupted compression (compression up-to 30%) test has been carried out to evaluate the fracture behaviour in terms of crack initiation and further growth in each condition.

3.5.1 Micro hardness test

Resistance to plastic deformation (generally through indentation or scratch) is well known as hardness. In the Vickers hardness test method, both soft and hard materials can be tested and their accurate results are widely acclaimed. The hardness tests were performed to evaluate hardness values (VHN) of as-cast, aged, solutionised, alloyed and reinforced foamed samples. The hardness testing method is the conventional way to get an idea to evaluate the change in material properties due to change in microstructure.

Photograph of microhardness tester ((VHM-002V Walter UHL, Germany), as shown in Fig. 3.6) is used to measure the microhardness of closed cell metal foam. Foamed samples are well polished and flatten before microhardness testing. At least eight readings were taken to obtain an average hardness (VHN) of the sample. Indentations to measure microhardness

were done at a load of 5 gm. (49.03 mN) and loading time of 10 s at the junction of the cell wall of the foam sample. Generally, spacing between two consecutive indentations should be more than 2-5 times of the indentation diagonal.

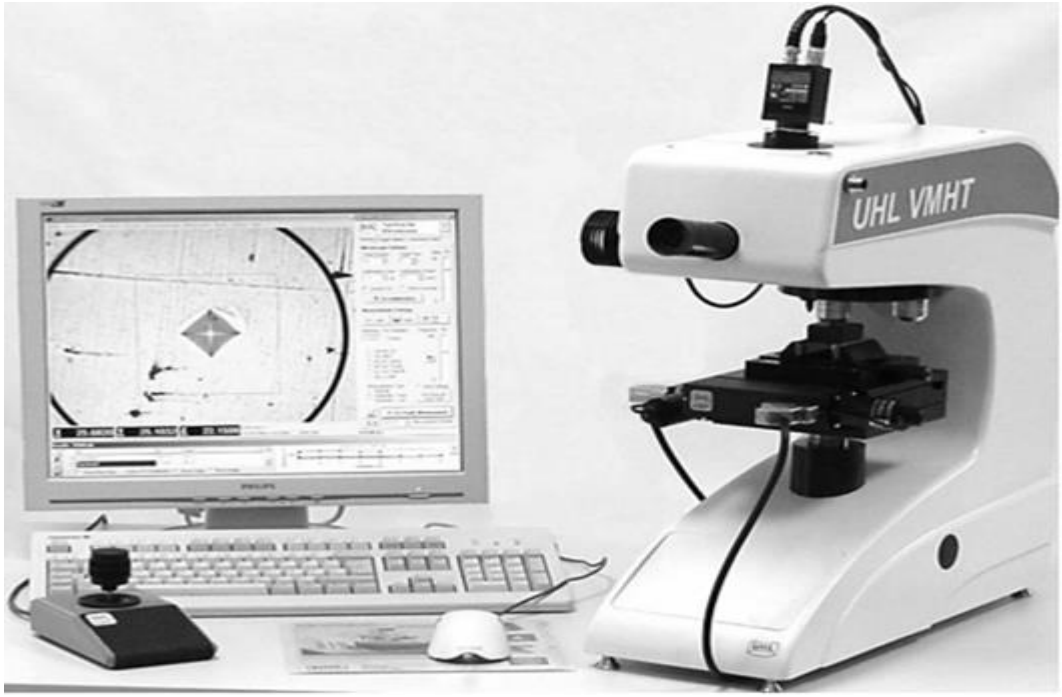

Fig. 3.6 Photograph of VHM-002V-Vickers microhardness tester.

3.5.2 Compression test

Investigation of the mechanical behaviour of the closed cell aluminium foam sample was done by performing axial compression tests at ambient condition. To estimate the densification behaviour, plateau stress and energy absorption capacity of the samples in different conditions (i.e as-cast, solutionised, aged and reinforced) are tested under axial compression load at the constant strain rate of 1×10^{-3}. Samples for compression test were prepared by slow speed diamond cutter with the regular square base and height twice that of the base. Sample prepared for compression test is also shown in Fig 3.7 marked as 1. Dimensions and weight of each sample was recorded. The axial compression test was performed on the computerized universal testing machine with a load capacity of 25 kN ((H25K-S, Hounsfield, UK) as shown in Fig. 3.7) at a constant strain rate of 1×10^{-3}, while vacuum grease was applied to take care of friction between the specimen and the plunger. Post-test analysis of the data has been done on the data recorded at Q Mat software (Version 5.35). At least three samples were tested in each condition and the averages of the three were used for discussion throughout the thesis.

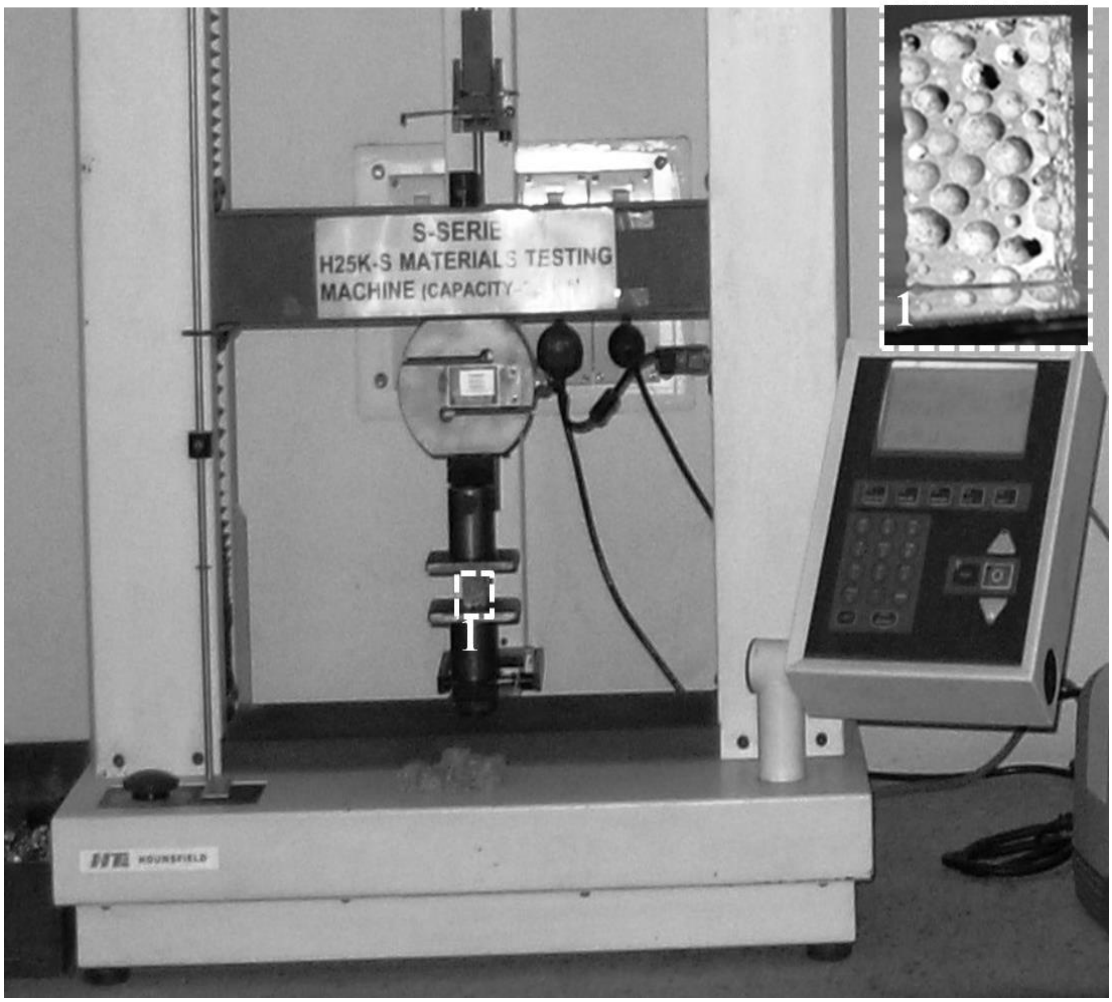

Fig. 3.7 Photograph of H25K-S, Hounsfield, UK universal testing machine used for compression test, foam sample (10×10×20 mm^3) prepared for compression test is also shown (marked as 1).

The yield stress ($\sigma_{y)}$ in the thesis is taken as an upper limit of the elastic region beyond which the cells undergo plastic deformation. The plateau stress (σ_{pl}) was taken as the average value of the stress from 5 to 30% strain.

The area under the stress-strain curve up to densification strain is termed as energy absorption per unit volume (W) and given by the equation (3.1):

$$W = \int_{0}^{\varepsilon_d} \sigma(\varepsilon) d\varepsilon \qquad (3.1)$$

Where: ε_d is the densification strain where cell wall of the foam completely collapse and flattened out, as well as, the slope of the stress-strain curve increases abruptly. Layer by layer collapse occurred when compression load is applied on the closed cell foam.

To examine the failure mode, fracture characteristic and the stages of the failure at different regions of the sample an interrupted compression test were performed where the compression test were stopped at 30% strain.

CHAPTER 4: MICROSTURCTURAL AND MECHANICAL BEHAVIOUR OF AS- CAST FOAM: EFFECT OF THERMAL TREATMENT

Synthesis of aluminium foam usually involves the development of foam, followed by microstructure characterisation and mechanical characterisation. Microstructure characterisation of foam is important, so that structural behaviour of the form may be detected. In this chapter, firstly, aluminium foam (produced based on optimum process parameter), is presented along with the description on raw material characterisation, and the basis of the characterisation. The structural characterisation of the produced foam, microstructural and mechanical characterisation and influence of process parameters, structural heterogeneity, heat treatments on the microstructural and mechanical behaviour of closed cell aluminium foam is also presented. Aluminium foam has been synthesized at optimum process parameters through melt route using TiH_2 (as blowing agent). Evolution of microstructure has been done using optical microscopy, SEM and TEM, whereas mechanical properties have been determined by performing compression and microhardness tests. The results of microstructural analysis have been used to affirm the findings of the axial compression test and microhardness tests. Fractography of the foam sample has been done using an interrupting method and used to acknowledge the mode of fracture in different condition during compression tests.

4.1 Raw material characterisation

4.1.1 Base material characterisation

In this section of the chapter, characterisation of the base metal has been explained. The chemical composition of 6061 aluminium alloy procured from Hindalco Industries Ltd, Mumbai, India as determined by electron probe micro-analyser (EPMA) is shown in Table 3.1.

In this section of the chapter, first decomposition behaviour of TiH_2 (used as a blowing agent) is explained. The release of hydrogen resulting from the thermal decomposition of TiH_2 has been investigated by thermo gravimetric analysis (TGA) at the scan rate of 10^oC/min, which indicates that the decomposition starts at 490°C and is completed at 574°C, which is also supported by work reported earlier (Raj, 2008). The results of TGA for TiH_2 have been shown in Fig. 4.1. The onset temperature for hydrogen release was found to depend on the heating rate. With the variation in the amount of TiH_2 and the stirrer time, pore size, as well as, relative density can be altered (Alinejad and Zakeri). It is also reported in literature that the amount of TiH_2 addition decides the amount of hydrogen release, as well as, it also helps in to improve the viscosity of the melt by the formation of intermetallic, which in turn stabilise the foam.

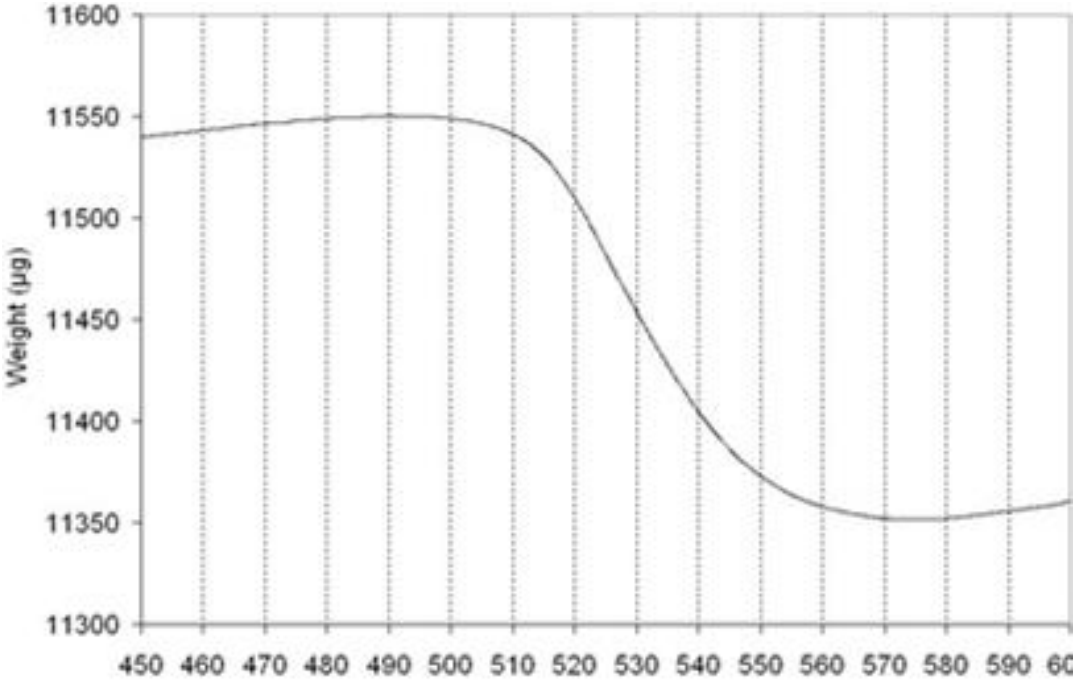

Fig. 4.1 TGA analysis graph showing the decomposition behaviour of blowing agent (TiH_2), which takes place between 490°C to 574°C.

It is observed that foaming with 0.5 wt. % of TiH_2 result in release of insufficient amount of hydrogen gas and which is not sufficient to create enough porosity, similarly the relative densities of produced foam (with 0.5 wt. % TiH_2) are usually greater than 0.3. However, uniform cell structure with less drainage is obtained when the foaming has been done with around 1.0 wt. % TiH_2. With the help of optimisation techniques (Raj and Daniel, 2008b) has also reported that the 1.2 wt. % of TiH_2 is sufficient to produce good foam, as well as, amount of blowing agent greatly impact the foam quality.

4.1.2 Master alloy characterisation

4.1.3 Master alloy characterisation

As reported in (Raj, 2008), the use of the 6061 Al alloy (as a base material) for foaming will result into improper foaming, one of the such casting is shown in Fig 4.2 (a) with the optical micrograph in Fig. 4.2 (b) showing that no foaming has occurred.

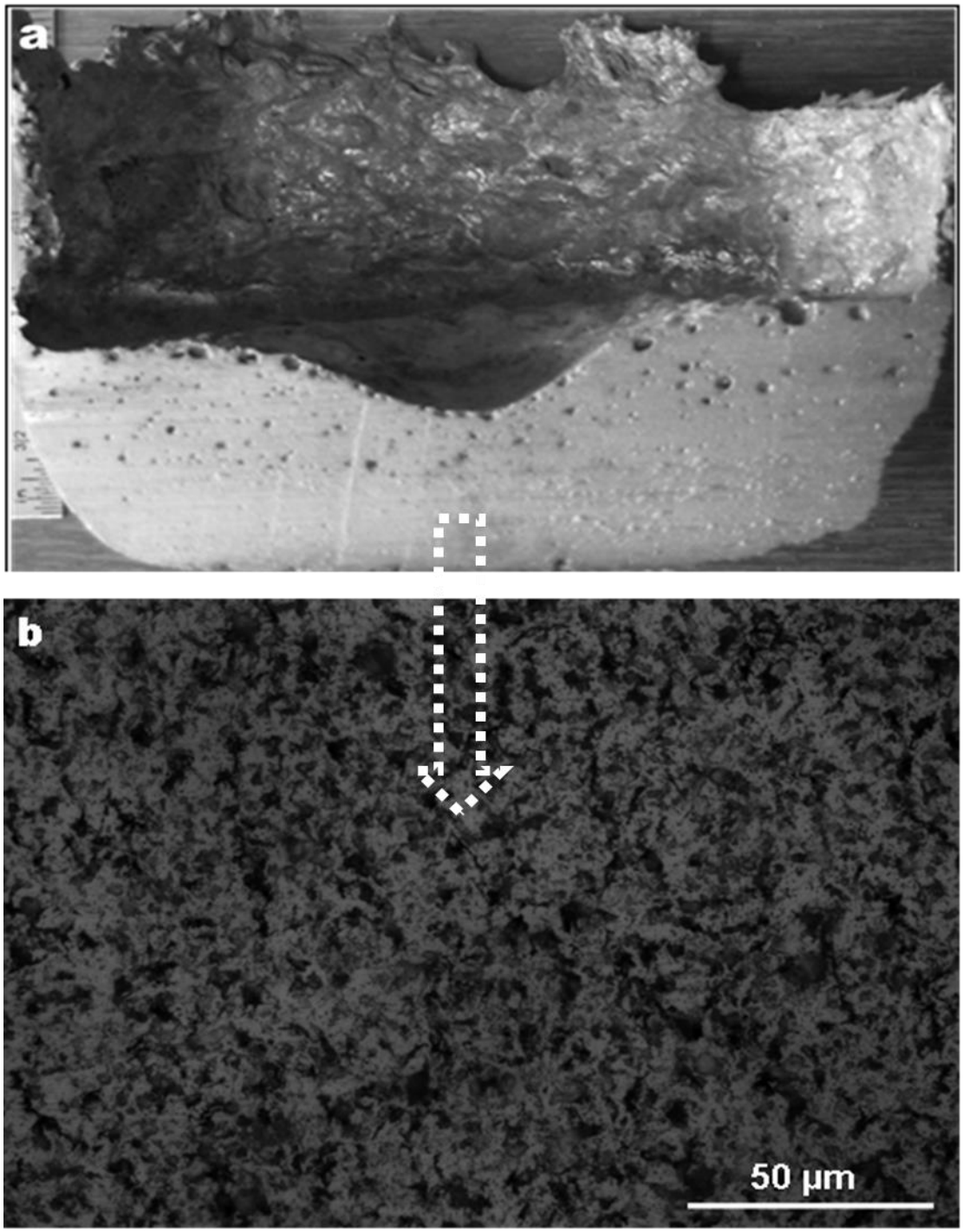

Fig. 4.2 (a) Photograph of the cast foam showing cross section of foam casting produced by melt route using TiH_2 as a blowing agent shown at approximately real size (without Cu addition) and (b) optical micrograph of the cell wall taken from the

Above Fig. 4.2 (a) represents the cross section of the foam produced without Cu addition, from the cross-section of the casting, it is observed that there is no foam structure except some pores at the top portion of the casting and remaining material is completely freed porosity.

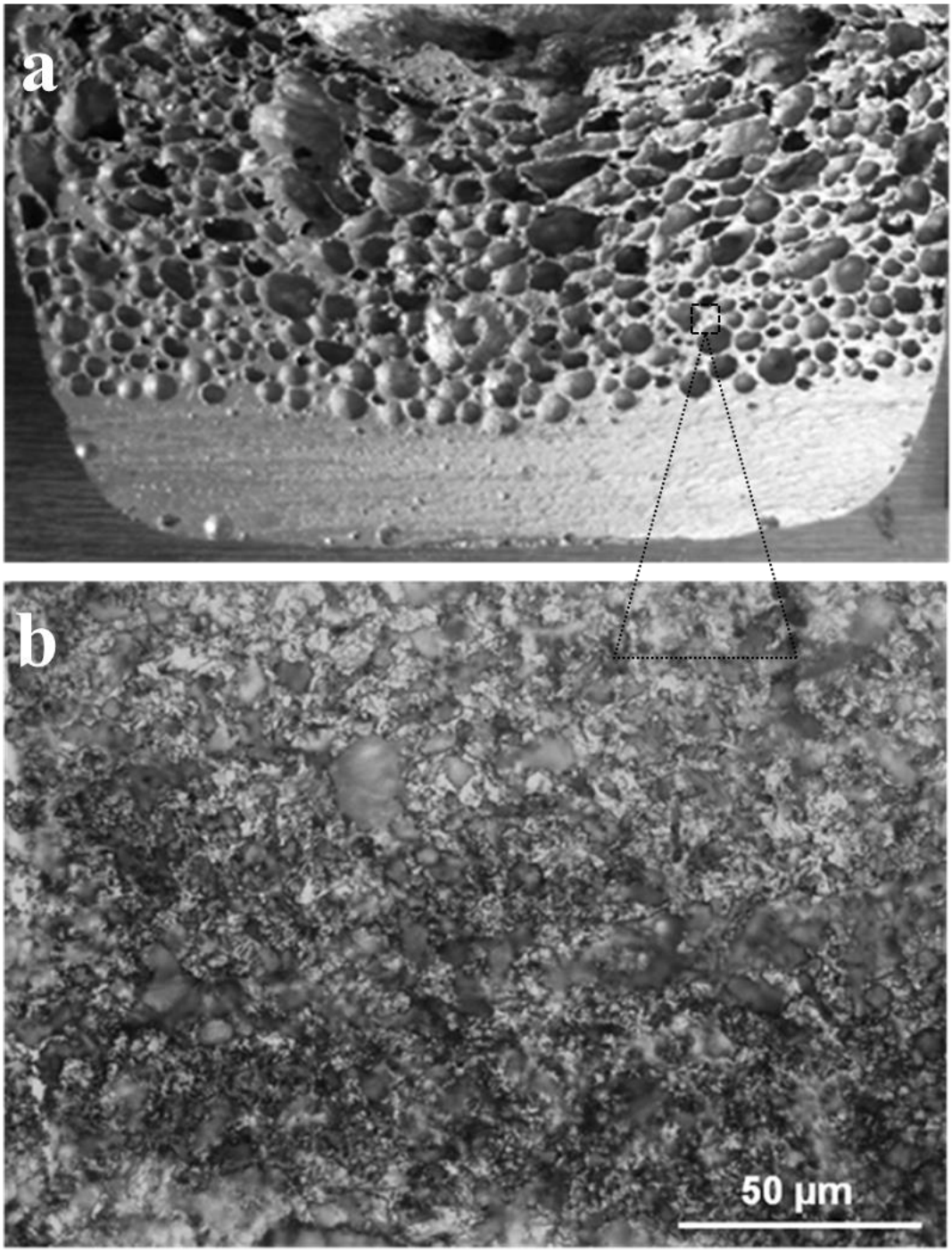

Fig. 4.3 (a) Photograph of the cast foam showing cross section of foam casting produced by melt route using TiH_2 as a blowing agent shown at approximately real size (with Cu addition) and (b) optical micrograph of the cell wall taken from the cross section of the same cast foam.

Therefore, from above observation it has been concluded that for proper foaming, it is necessary to stabilise the metal to minimise the material drainage at the time of foaming. It is

common practice to introduce a solid second phase through particle addition (either in-situ or ex-situ) to improve the stability of foam through melt viscosity improvement (Golestanipour et al.). As observed from the cross section of cast foam produced directly from 6061 alloy (without copper addition) did not produce foam. Earlier reported work (Raj, 2008), suggested that the addition of Cu results in the formation of some intermetallic phase, which forms the network like structure in the matrix, which further helps in lowering the drainage at the time of foaming. On the basis of the reported work (Raj, 2008), in present work 4 wt. % Cu is used to prepare master alloy. It has been found that when the alloy is modified by adding 4 wt. % of copper, foam could be synthesized. One of the casting prepared with the master alloy (Al 6061+ 4wt. % Cu) is shown in the Fig. 4.3 (a) and corresponding optical micrograph is shown in the Fig. 4.3 (b). It is evident from the macrostructure of the cross section of the casting that the addition of the Cu has assisted in the foaming.

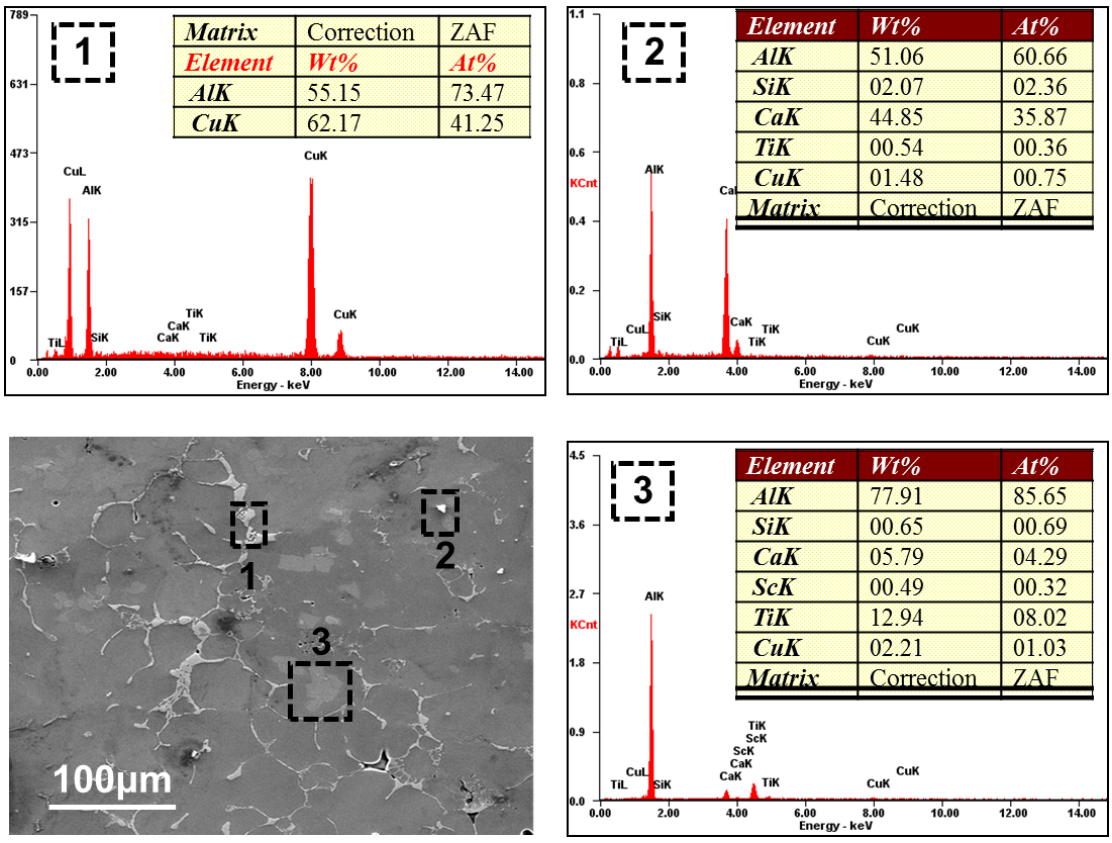

Fig. 4.4 Cell wall microstructure along with the EDS analysis at marked point 1, 2 and 3.

From the optical micrographs (4.2, 4.3), it is found the Cu addition results in the bright structure, whereas foam produced without Cu does not incorporate any structure. To reveal the structure and composition of the network arm after the addition of the 4 wt. % Cu, SEM image has been taken in back scattered electron imaging mode. From the SEM micrograph (Fig. 4.4)

it is found that after 4 wt. % Cu addition aluminium form dendrite arms of Al-Cu which is distributed throughout the cell wall. To identify the elements of the dendrite arm, EDS analysis has been done, which in turn affirm the presence of the Al_2Cu intermetallic in lamellae form (Fig. 4.4 (indicated as point 1)), these network structures contribute in the foam formation. Some solid intermetallic formed (Fig. 4.4 (indicated as point 3)), when TiH_2 is added. The presence of Al_2Cu as lamellae is also expected to help in the stabilization of the foam. On the basis of above observations, in the entire dissertation work, the composition (6061+ 4 wt. % Cu) has been used as the master alloy for all foaming experiments. As reported in the literature (Wang and Starink, 2005b), addition of Cu results in intermetallic formation, which further helps in precipitation hardening. Therefore, it is expected that the addition of Cu also helps in the cell wall strengthening through post processing treatment (i.e. thermal aging process).

4.2 Characterisation of the synthesised as-cast foam

Since the width of cell faces is often comparable to the scale of features of the metallographic structure, the distribution of phases can be significant. Therefore, microstructural characterisation of the produced foam is an important part followed by structural characterisation. The synthesis of metal foams, in general, comprises of addition or generation of finely divided solid phases in the liquid melt which act as stabilisers or surfactants and affect the quality of the foam, as well as, mechanical performance. The properties of the closed cell metal foam depend on the structural aspects, such as; the relative density, pore size distribution and cell wall thickness. To produce the foam with the desired pore size is a challenging task due to the irreversible nature of the process (i.e. cell wall collapse due to continuous drainage).

There are some processing challenges to produce specified foam structure, such as, stochastic phenomenon which leads to cell wall collapse. Therefore, it is necessary to retard the drainage through introducing some solid second phases or ceramic particle during the process either in-situ or ex-situ.

4.2.1 Macrostructure

Low magnification digital macrograph of the as cast foam (cross section parallel to the foaming direction) is shown in Fig.4.5, from the macrograph it has been observed that the synthesised foam has more or less equal pore size. It is also found that cell wall thickness is less towards the centre of the casting, whereas near the crucible wall and bottom of the casting thickness is more (as evident from the Fig. 4.5). The progressive thinning of the cell wall

observed towards the upper portion of the casting might be driven by the local drainage (indicated and numbered as 1), as shown in the Fig. 4.5. Due to drainage, a bulk material is found at the bottom of the casting (indicated and numbered as 4). From macrostructure, as in Fig. 4.5, it is observed that in the upward direction from the bottom of casting, initially, a fairly thick cell wall develops a curvature (indicated and numbered as 3).

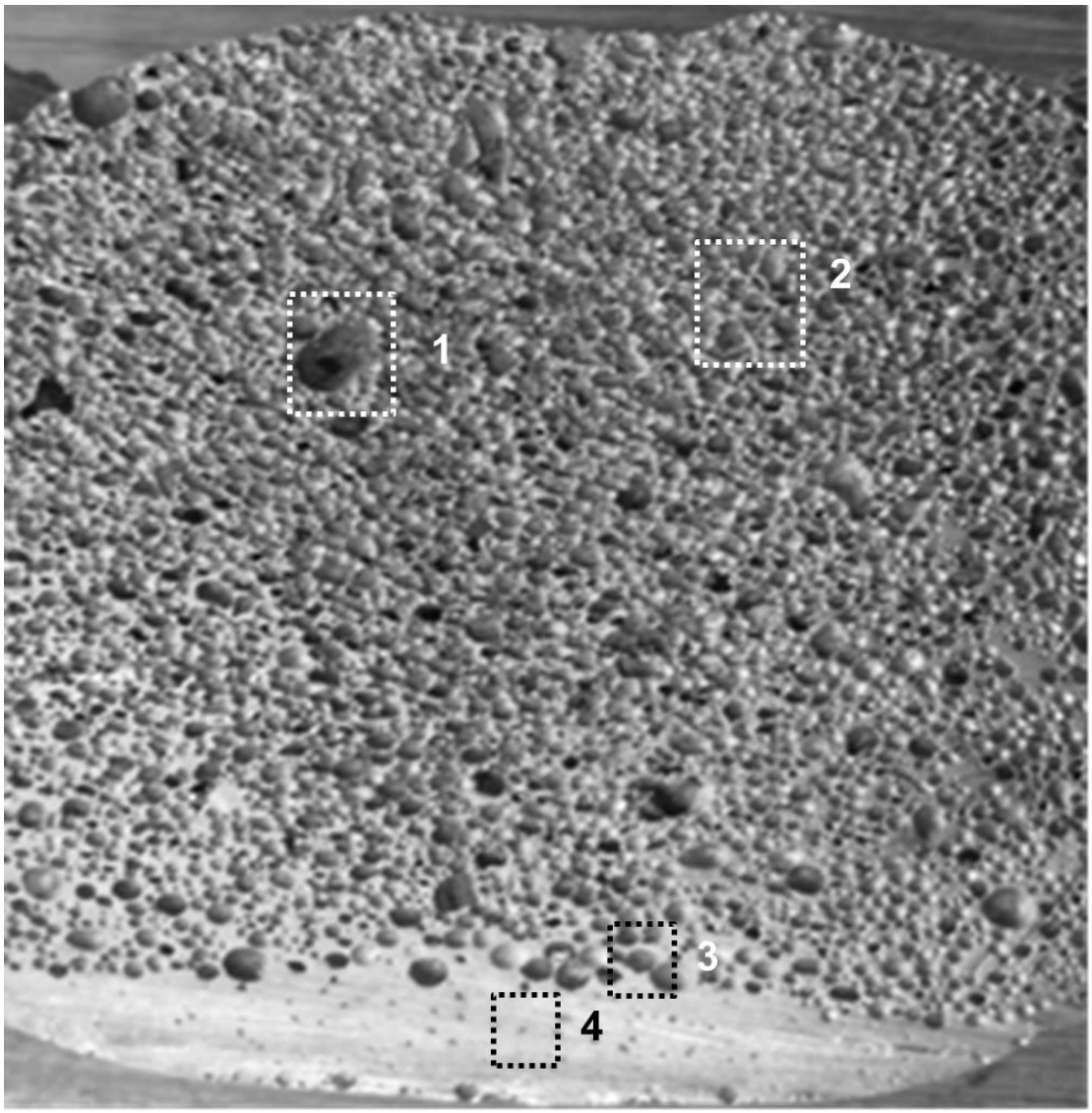

Fig. 4.5 Macrograph showing cross section of cast foam produced by melt route using TiH_2 as a blowing agent shown at approximately real size, which exhibits several features resulting from foam drainage.

This curvature progressively drives metal away from the cell face towards the cell edge, which leads to thinning of the cell wall (indicated and numbered as 2) and results in the rupture of the cell wall. Due to thinning of the cell wall (as discussed in literature review section) some of the cell wall collapse and co-join neighbouring cells into a big pore. If the collapse occurs at a later stage, then there is not enough time for readjustment, the co-joined cells display a

pronounced aspect ratio. The most common reason behind collapse of the foam is gravity which results in density gradients, and in uttermost cases the local features (indicated and numbered as 1 in Fig. 4.5). An overall view of the foam casting phenomenon such as coalescence of neighbouring cells, local drainage etc. are illustrated in Fig. 4.5.

4.2.2 Microstructure

The optical micrograph of cell wall in cast foam condition is shown in Fig. 4.6 (a) and Fig. 4.6 (b). Unetchad sample is shown in Fig. 4.6 (a), which reveals the presence of some tiny spots, spotted as black in the micrograph. Tiny spots may be intermetallic or secondary phase particle in the range of 0.3μm size. To find out the actual structure of the cell wall and position of the second phase particles in the aluminium matrix, etching has been done with Keller's etchant at room temperature. During etching, the aluminium is dissolved and significant structure is observed, as shown in Fig. 4.6 (b).

In Fig. 4.6 (b), microstructure of the etched sample shows α-Al as a major phase with secondary phases. The positions of the second phase particles are clearly visible, regardless of the grain boundary, which reveals the development of grain structure. As observed from the Fig. 4.6 (b), microstructure of synthesised foam predominately consists of thick coarse dendrite structure with the average arm spacing of 10-15 mm. The foam sample further analysed with SEM (back scattered electron image Fig. 4.6 (d)), from the backscattered image, net like structure is observed, which is distributed throughout the matrix with the combination of some coarse grains. To examine the composition of the netlike structures EDS has been done, from the elemental analysis; it was found that the net like structures in white colour corresponds to Al_2Cu particles. The EDS of the netlike structure is shown in Fig. 4.6 (c), these net like structures are much brighter than the aluminium matrix as shown in SEM images (Fig. 4.6 (d)), due to their larger effective atomic number as compared to the aluminium matrix. On the contrary, oxygen having an effective atomic number lower than the aluminium matrix seen black corresponds to the oxide phase (Al_2O_3). Along with these two particles, fine grey colour particles distributed throughout the matrix rich in Ti are Al3Ti intermetallic, which concurs well with the result of the previous work reported earlier (Raj, 2008). (Raj, 2008) reported that the thin plate white in colour is Al_2Cu whereas other intermetallic particles grey in colour is $Al_{20}CaTi_2$ and evenly distributed along the cell wall. From the high magnification optical micrograph (Fig.4.6 (b)), it is observed that the "smaller grains" appear on the surface of the dendritic structure in the aluminium matrix. These "smaller grains" growth may be the effect of solidification of the liquid during the cooling of casting.

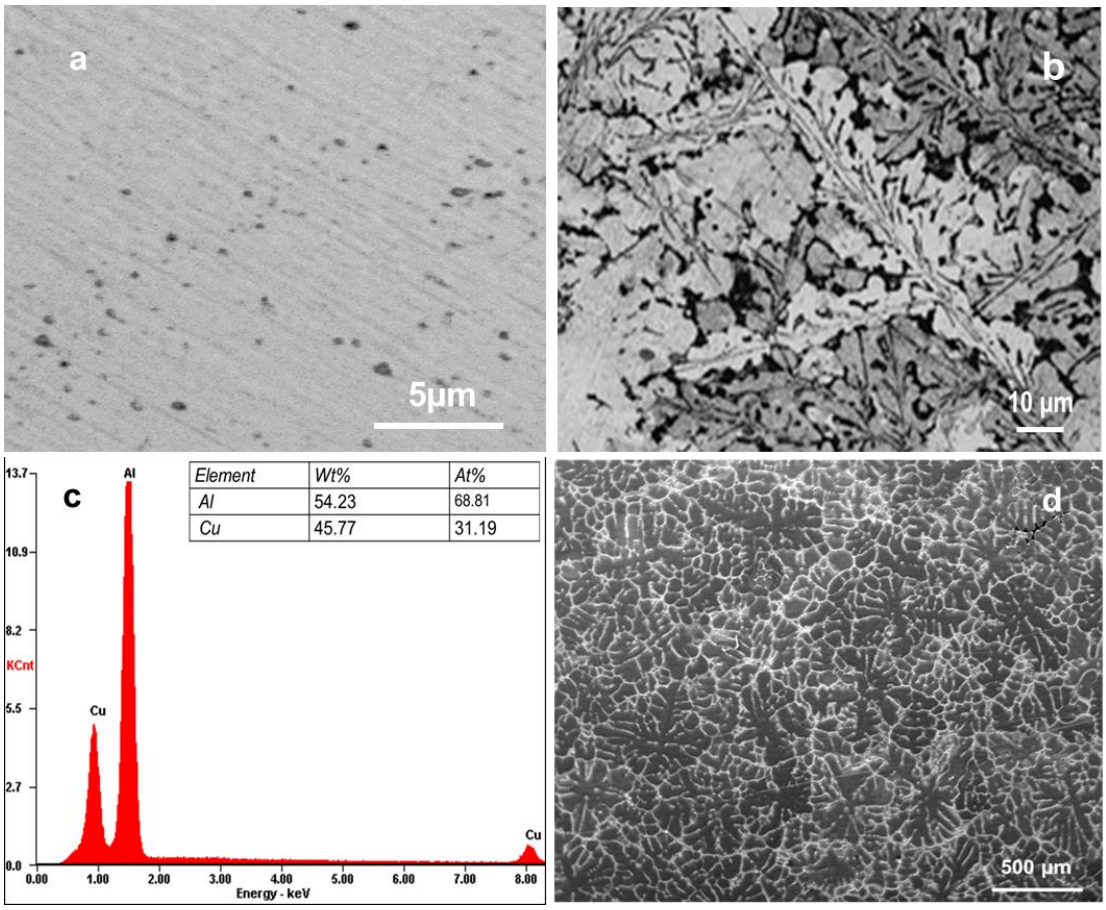

Fig. 4.6 (a) Optical micrograph of un-etched foam sample, (b) Optical micrograph of etched foam sample, (c) EDS analysis of the net like structure and (d) SEM image of the cell wall showing net like structure.

From above discussion, it is concluded that the cell wall microstructure consists of various phases, including intermetallics and oxides, which is dispersed in aluminium matrix. However, cell wall microstructure (as shown in Fig. 4.6 (b) and (d)) consists of thick dendrites, which in turn result in to impairment the mechanical properties of the foam; hence to enhance the property of the aluminium foam it is necessary to refine the microstructure of the cell wall.

4.2.3 X-ray Diffraction Analysis

A distinctive XRD pattern of the synthesized aluminium foam is shown in Fig. 4.7. The measured X-ray integrated intensities of various planes of Al are in agreement with the JCPDS standard data.

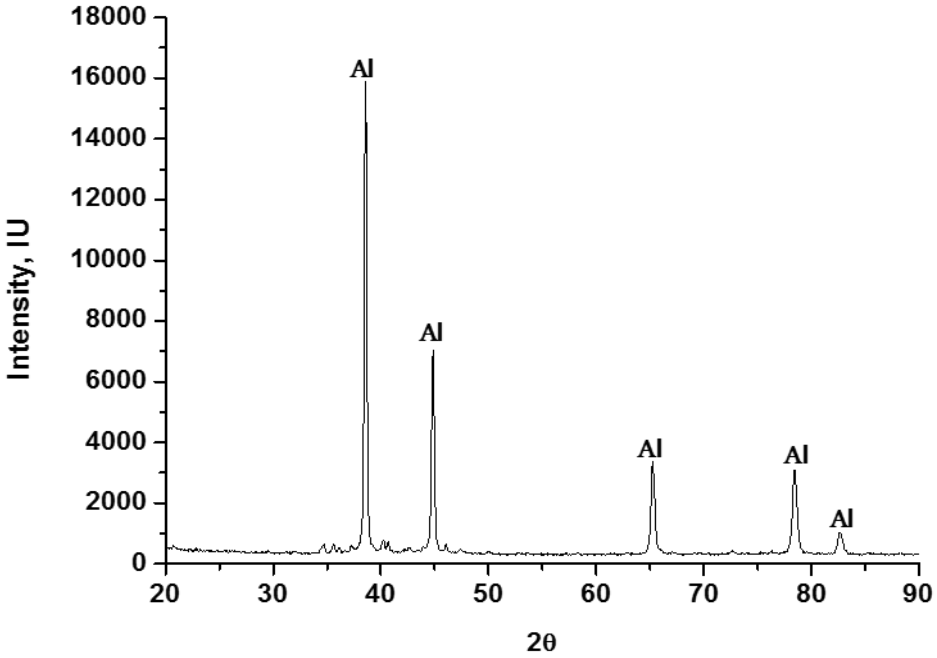

Fig. 4.7 The powder XRD pattern of synthesized as-cast foam.

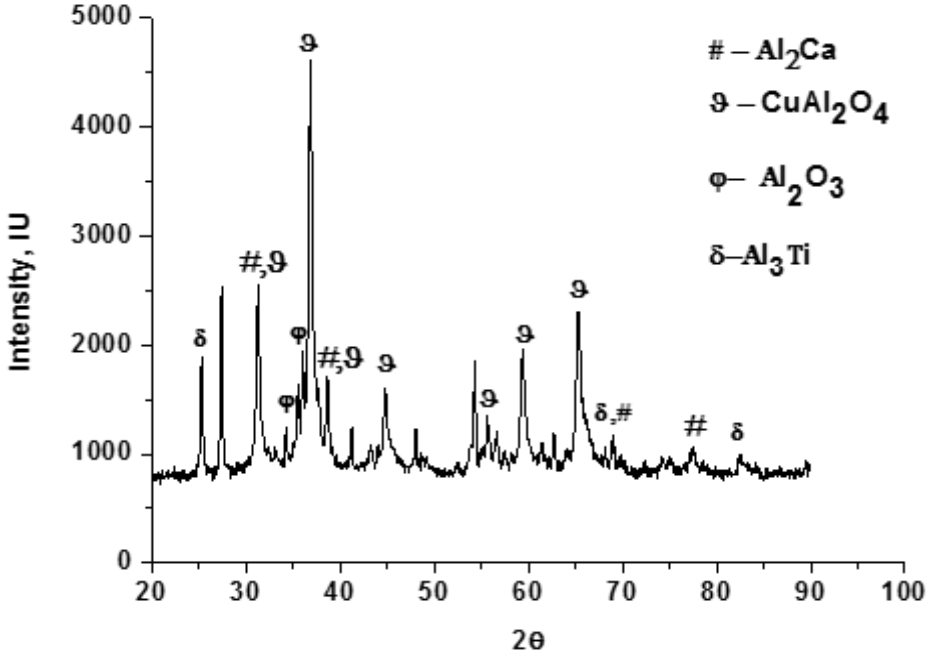

Fig. 4.7 The powder XRD pattern of the extracted particles from the as-cast foam after leaching with dilute hydrochloric acid.

The peaks in the XRD pattern indicates the primary solid solution of aluminium, which is also reported earlier (Raj and Daniel, 2008a). Some other peaks with low intensity have been observed in the XRD pattern, indicating a small volume fraction of the other elements or their fine size distribution in the base aluminium matrix. To identify the particle with low intensity in

XRD, the synthesized foam is selectively leached by week hydrochloric acid. The main purpose behind the selective leaching is to dissolve primary aluminium and resolve the particle peaks. Result of the XRD has been supported by earlier work (Raj, 2008), where the presence of Al_2Ca, Al_3CuO_4, Al_3Ti and Al_2O_3 has been reported, as shown in Fig. 4.8. (Raj, 2008) also report that the partial oxidation of the sample at the time of selective leaching results in Al_2CuO_4 phase instead of Al_2Cu phase. The addition of blowing agent TiH_2 and Ca granular to the melt formed an intermetallic after reacting with aluminium and results in the strengthening of the foam cell wall material. At low intensity, peak shows broadening points (as shown in Fig. 4.8). Dispersion of the fine intragranular in the melt is expected to improve the viscosity of the melt and improve the strength of the cell wall, which in turn helps to improve the stability of the liquid melt (Neu et al., 2012).

4.3 Post processing treatment of the synthesised foam

The general, property of the foam refers to energy absorption capability. Hence, when the foam is subjected to the compressive load, it required a good strength to sustain the applied load. Generally, strength of the metal foam refers to the plateau stress, which is the extended constant stress domain beyond the elastic limit. The compression load is mainly held by the metal foam cell wall; therefore, to improve the strength of the metal foam, it is necessary to modify the strength of the cell wall. The cell wall microstructure can be altered by heat treatment process, which in turn will alter the mechanical properties of as-cast foam.

It is also of interest to know that how the property modification of the cell wall materials will influence the mechanical property of the aluminium foam as a whole, and more specifically, energy absorption capacity during compressive loading. For strengthening the cell wall material through heat treatment, it is necessary to understand the strengthening mechanism of the master alloy, which is used to develop the foam. In the present work, master alloy used to produce foam consists of 4 wt. % Cu. As discussed in the literature review (chapter 2) section, aluminium contain Cu can be easily strengthen by precipitation hardening, which further helped to strengthen the alloy matrix through precipitation hardening. In the present work, master alloy employed with 4 wt. % Cu and the solidification behaviour of the same is presented in the equilibrium phase diagram (as shown in Fig. 4.9 (a)). In the Fig. 4.9 (a), the dashed vertical line shows the approximate composition of master alloy used in the present work. Heat treatment cycle adopted in the present work is also illustrated in the Fig. 4.9 (b), which schematically represent the heat treatment cycle used in the present work.

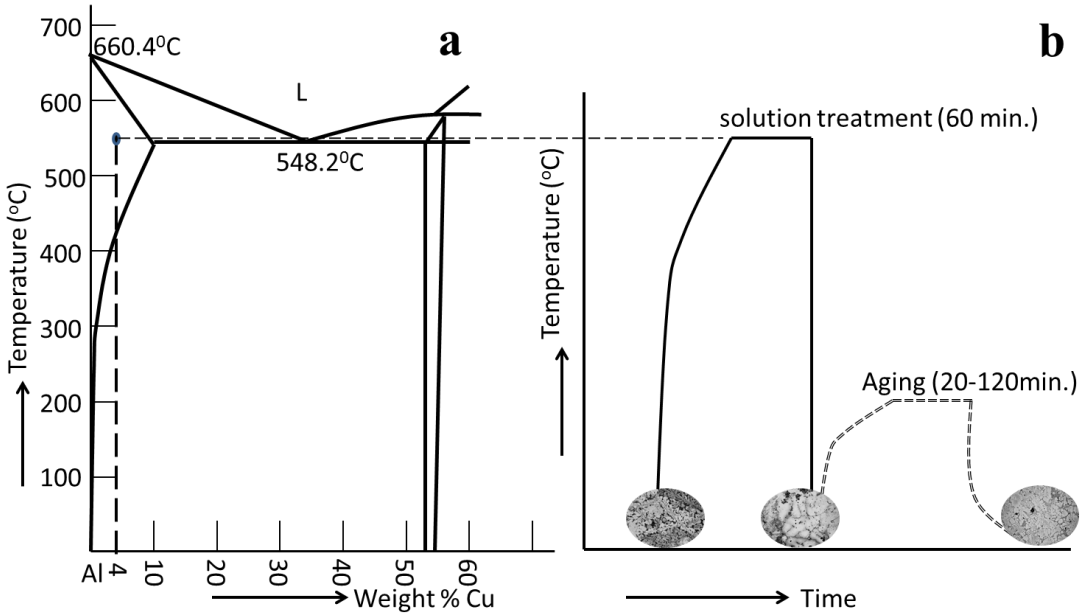

Fig. 4.8 (a) Schematic (Al-Cu) phase diagram, showing the approximate composition of master alloy and (b) schematic representation of heat treatment cycle.

4.3.1 Solutionising of the as-cast foam at 550°C

Rapid cooling of the cast material results in the incomplete solidification and the incomplete solidification results in multi-phase eutectic structure in the spaces between the dendritic structures (Guy, 1962). In the present work, the above state phenomenon is clearly observable in the optical micrograph of the as-cast foam sample (as shown on Fig. 4.6 (b)), where dendrite structure with Al_2Cu is clearly visible.

From the Al-Cu phase diagram, it is observed that the aluminium alloys with 4% Cu has eutectic point at 548.2°C. Therefore, thermal treatment of the alloy at this temperature results into the equilibrium structure, whereas some particles merge into the solid solution of the matrix which partially form intermetallic particle. In the present work, as-cast foam sample solutionised at 550°C for one hour to obtain the equilibrium structure. Through the solutionising process, the secondary phases go in the solution, which homogenize the structure of the as-cast foam material and the solutes dissolve back to solution for further processing.

In the present work, we employed the solution heat treatment to uphold the solute in the aluminium matrix solution as much as possible. The alloy in this state is best known as the solid solution.

4.3.1.1 Microsturctural evaluation

In the present work, sample in as-cast condition is shown in Figs. 4.6 ((b) and (d)). From high magnification optical micrograph (Fig. 4.6 (b)), it is observed that the sample in as-cast condition consists of the thick dendrite structure. The dendrite structure may work as crack initiation sites, as well as, helps in further crack propagation when the load applied on the sample (i.e. at the time of compression test). Hence, to get better result, it is necessary to minimise the dendrite structure. To eliminate the dendritic structure, solutionising process plays an important role. Therefore, it is necessary to understand the kinetics of the homogenisation in the metal foam.

Figs. 4.8((a) and (b)) shows high magnification optical micrograph of the cell wall microstructure (at two different magnification), which has been solutionised at 550^{o}C for 1 hr. followed by water quenching. From optical micrographs it is observed that after solution treatment cell wall microstructure get homogenised and there is no dendrite structure, which shows that when the as-cast foam sample is solutionised and quenched from the single phase region (i.e. at 550^{o} C) to below liquids, it results in supper saturated solid solution of Cu atom in the Al matrix (also observed in the optical micrograph).

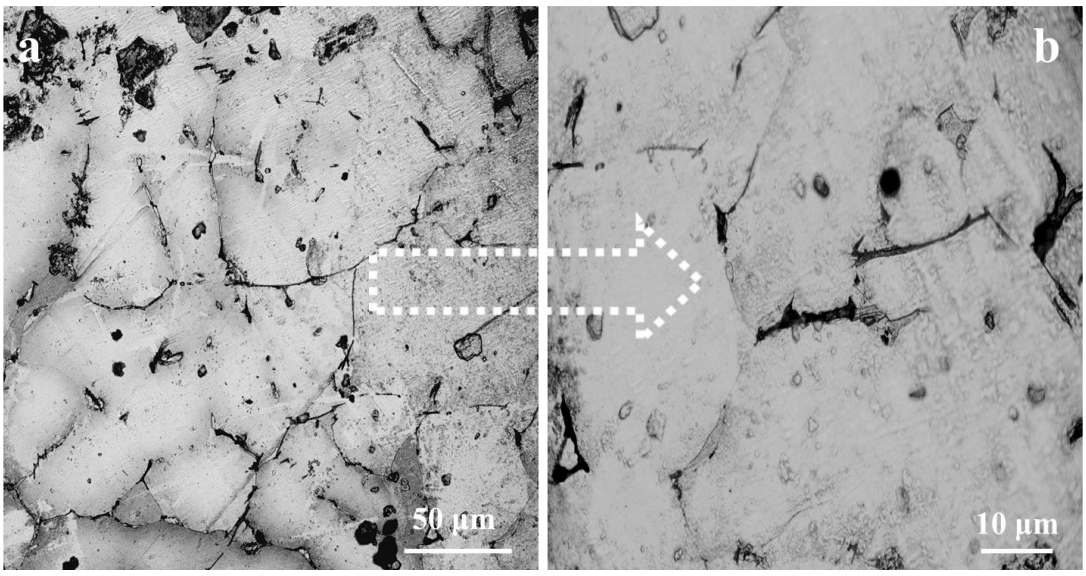

Fig. 4.9 Optical micrograph of the foam cell wall solutionised at 550^{o}C at two different magnifications of (a) 50 µm scale and (b) 10µm scale, which showing homogenized structure.

It is observed from optical micrograph that the microstructure mainly consist of α-Al (as a major phase) with some fine eutectic phases i.e. aluminium matrix and Al_2Cu. For more clear information regarding eutectic phases, image further magnified, although eutectic phase can not

resolved optically, still overview of the particle distribution in the alloy matrix is clearly visible. In optical micrographs (Fig. 4.10 (a) and (b)), it is observed that the particle appears in the micrographs is either brighter or darker compared to the aluminium matrix. It is believed that Al_2Cu phase (which is seen in the optical micrograph as a net plate like structure) is unstable and might be the result of microsegragation during solidification process. Some fine particles are clearly visible in the higher magnification optical micrographs (i.e. Fig. 4.10 (b)), the chemical composition of the particles has been studied using EDS analysis (as shown in the Fig. 4.11). The EDS result reveals the presence of Mg, Al, Ca, Ti, Cu and O.

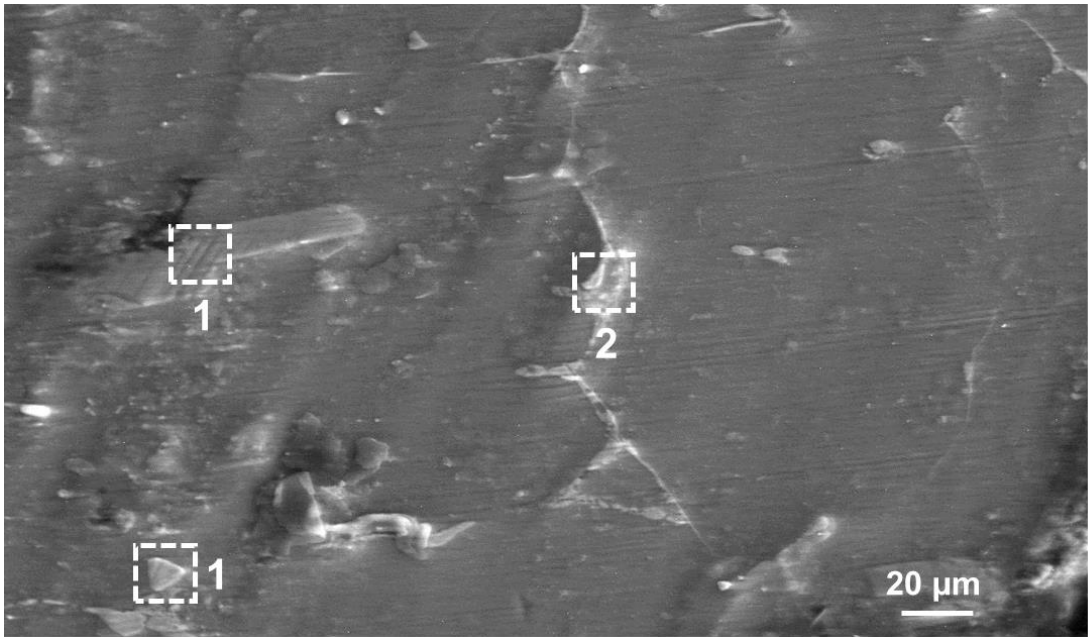

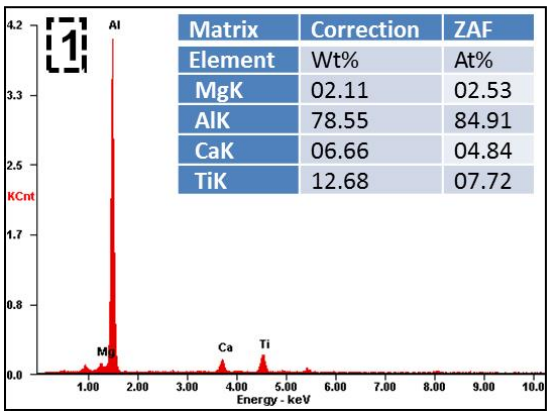

Matrix	Correction	ZAF
Element	Wt%	At%
MgK	02.11	02.53
AlK	78.55	84.91
CaK	06.66	04.84
TiK	12.68	07.72

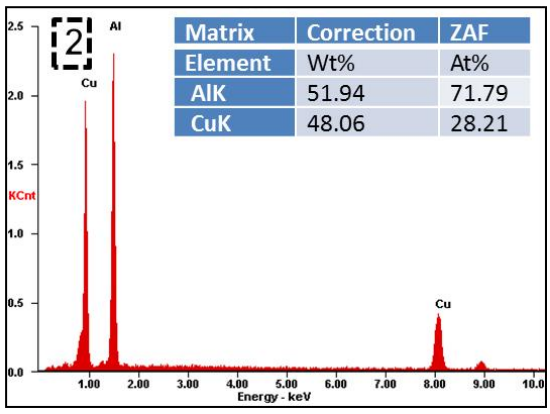

Matrix	Correction	ZAF
Element	Wt%	At%
AlK	51.94	71.79
CuK	48.06	28.21

Fig. 4.10 SEM image of foam cell wall solutionised at 550^{o}C showing the presence of second phase particles with corresponding EDS of the specify points numbered as 1 and 2.

The EDS result of the first type of the particle (shown as the solid particle, numbered as 1) with plate like structure reveals the presence of the Ca, Ti and Mg element and identified as

$Al_{20}CaTi_2$. Similarly, the second type of structure (numbered as 2), reveals the presence of Al-Cu intermetallic and identified as Al_2Cu phase.

4.3.2 Precipitation hardening of the as-cast foam at different temperature and time cycle

As discussed in the literature review section, age hardening treatment is commonly used to obtain the optimum combination of strength and ductility. It involves rapid cooling to retain the maximum concentration of age-hardening constituent (Al_2Cu) in solid solution combined with artificial and over-ageing to obtain the desired mechanical properties. These changes in microstructure include the dissolution of precipitates, the homogenization of the cast structure, such as, the minimization of alloying element segregation, spheroidisation, coarsening and the precipitation of finer hardening phase. The precipitation sequence in the present work is based on the formation of Al_2Cu, which is described as(Wang and Starink, 2005a):

$$\alpha_{ss} \rightarrow \text{GP zones} \rightarrow \theta' \rightarrow \theta(Al_2Cu) \qquad (4 \cdot 1)$$

The aging process sequence begins, when the supersaturated solid solution (α_{ss}) gives away small coherent precipitates called GP zones. These particles are invisible in the optical microscope but macroscopically this change can be observed through the increase in hardness and strength of the alloy. As the process proceeds, the GP zones start to dissolve, and θ′ begins to form, which results in increase in the hardness, as well as, strength of the alloy. Continued aging causes the θ′ phase to coarsen and the θ (Al_2Cu) precipitate to appear.

It is observed in the bulk alloy system that constituent phases (coarse intermetallic phases), which formed by a liquid–solid eutectic reaction during solidification get transformed on further heat treatment. Further, heat treatment (also referred as precipitation hardening) is one of the most frequent techniques used to strengthen the alloy. In the present work, Cu is the main alloying element and it is well known that Al-Cu is most suitable age-hardenable alloy. As mentioned earlier, aluminium foam property is refers to the strength of the cell wall and hence, through the precipitation hardening of the matrix material results in strengthens the foam. In the present work, the age hardening technique is employed to evaluate the effect of the precipitation hardening on the cell wall microstructure of the foam sample. Therefore, solutionised sample is further heated below 200^oC at different temperature and different duration which is called aging temperature and aging time respectively.

4.3.2.1 Microsturctural evaluation

The Al-Cu eutectic and intermetallic phases formed during the rapid cooling retains the maximum concentration of age-hardening constituent in solid solution. However, further thermal treatment results in hardening and coarsening of the constituents. The brief review of the age hardening process and the steps involved has been already explained in literature review. Therefore, to understand the kinetics of precipitation in the aluminium foam we examine the changes occurred in the cell wall structure through microstructural analysis at different temperature and duration.

Fig. 4-12(a-d) shows the optical micrograph of the aged samples. Samples were aged at 100^{o}C for 20, 40, 60 and 120 minutes duration respectively followed by solutionising and quenching. It is found that aging results in cluster formation. As discussed earlier, further increase in aging time results in an increase in the clustering, as well as grain coarsening.

Cell wall microstructure of the aged (at 100^{o}C for 20 minute) sample is shown in Fig. 4.12 (a), which shows α-Al as a major phase and the Al-Ca-Ti intermetallic, which is surrounded with some precipitate clusters. This result is well supported with literature as literature suggest that cluster precipitation is the first step in the precipitation hardening sequence specially in 6xxx series alloy (Miyoshi et al.).

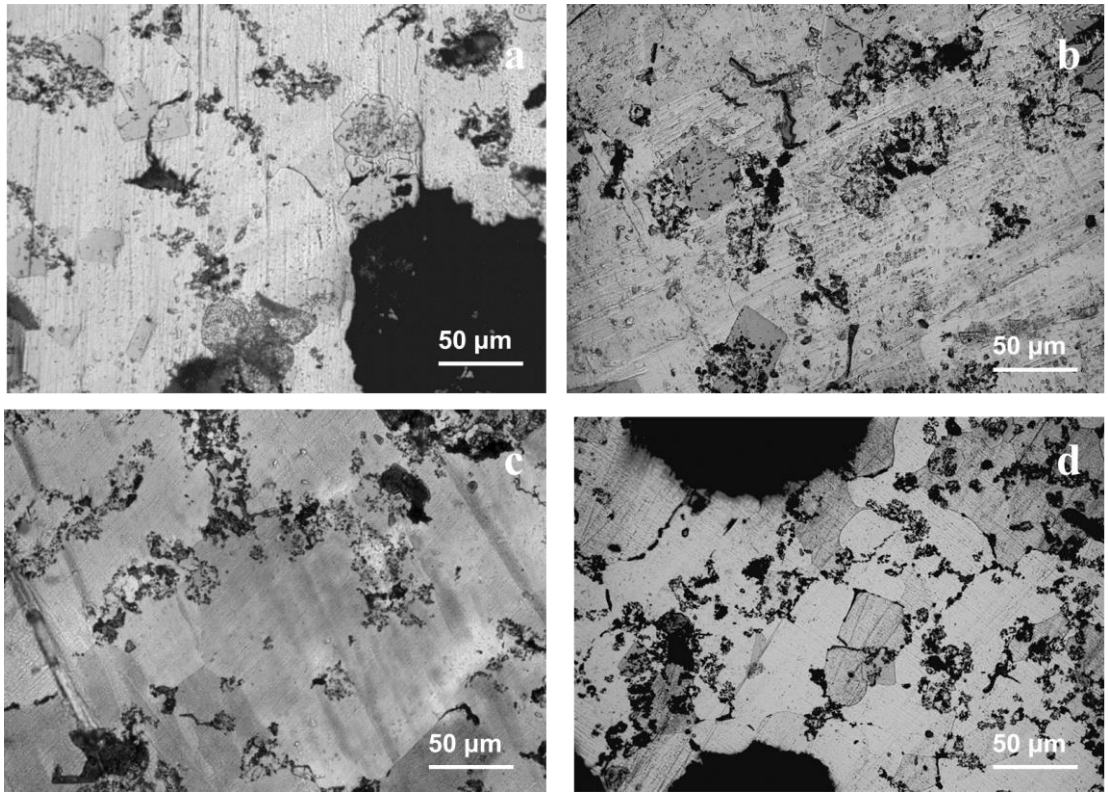

Fig. 4.11 Optical micrograph of foam cell wall aged at 100^{o}C for (a) 20 min., (b) 40 min., c) 60 min., and (d) 120 minute aging time.

With the increase in aging time from 20 minute to 40 minute (at same temperature), it is found that the cell wall structure is more or less similar to the previous microstructure (Fig. 4.12 (a)). Although, it is not possible to clearly decide from optical micrograph, still from the overview of the particle distribution in the alloy matrix it has been observed that precipitate size is also increased as aging time advanced, which in turn is evident from optical micrograph (Fig. 4.12 c). Increase in the precipitate size may be the result of the clotting of existing clusters, which is further responsible for formation of big clusters. It is also apparent from the micrographs that increases in aging time results in some visible grain boundary, as well as, grain coarsening that is the result of growth of the precipitate cluster.

Figs. 4.13 (a), (b), (c) and (d) show the optical micrograph taken at the cell wall samples aged at 150^{o}C for 20, 40, 60 and 120 minutes respectively followed by solutionising and quenching. It is evident from the optical micrograph that aging at 150^{o}C results into some Al Cu eutectic phase at short aging time of 20 minutes (Fig.4.13 a). With increase in aging time from 20 to 40 (Fig. 4.13 b) minutes these precipitate grow, as well as, dense clustering formation take place at grain boundaries with some embedded particles within matrix, as well as, at grain boundaries. This phenomenon may be attributed to precipitation growth.

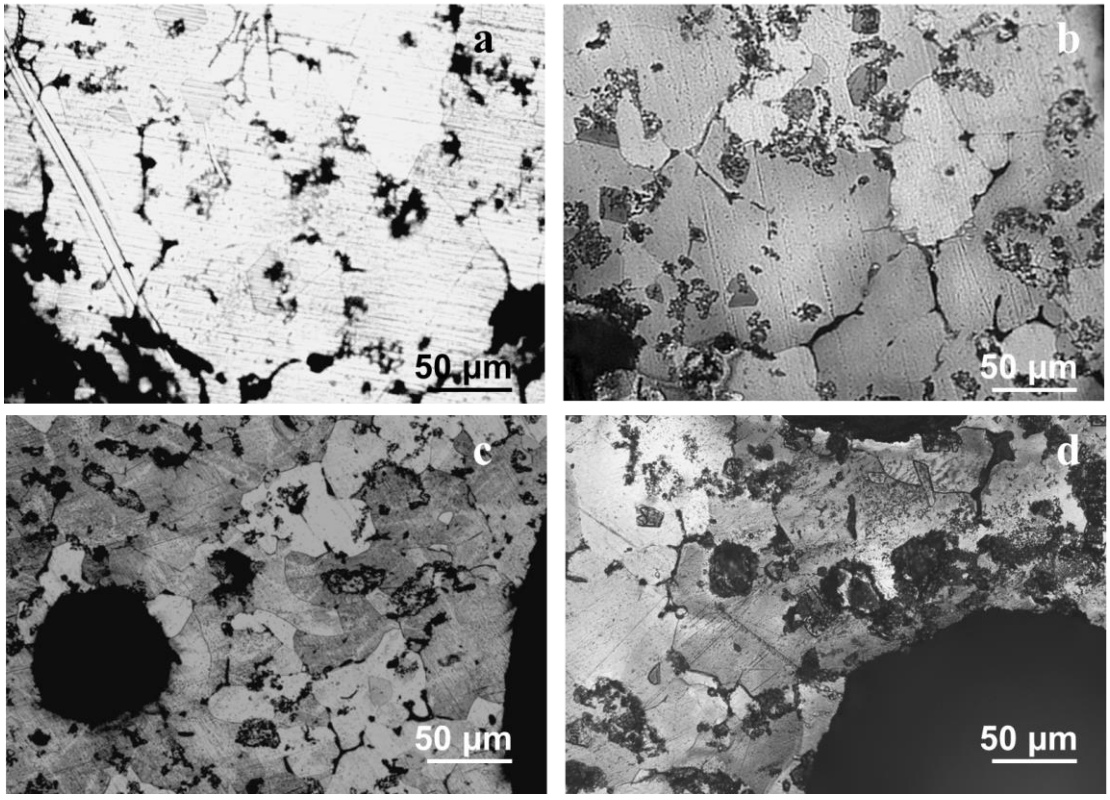

Fig. 4.12 Optical micrograph of foam cell wall aged at 150^{o}C for (a) 20 min., (b) 40 min., c) 60 min., and (d) 120 minute aging time.

From the optical micrograph of the sample aged at 150^{o}C for 60 (Fig. 4-13 c) minute, it is observed that the rate of the growth of precipitates from supersaturated solid solutions are higher when compare with 20 and 40 minute aging time. Further, prolonged aging (i.e. 120 minute) results into the grain coarsening (as observed in Fig. 4-13 (d)), which further deteriorate the properties.

Figs 4.14 (a), (b), (c), and (d) shows the optical micrographs of the sample aged at 180ºC for different aging time of 20,40,60 and 120 minute respectively. It is observed from the optical micrographs that aging at this temperature results in the stable phase of Al-Cu, as well as, over aging of aluminium. It is evident from the all micrograph that at this temperature, effect of the aging time is not that much effective because of grain coarsening (as observed in all the micrographs). It is evident from the micrographs that grain coarsening demise the second phase precipitate strengthening.

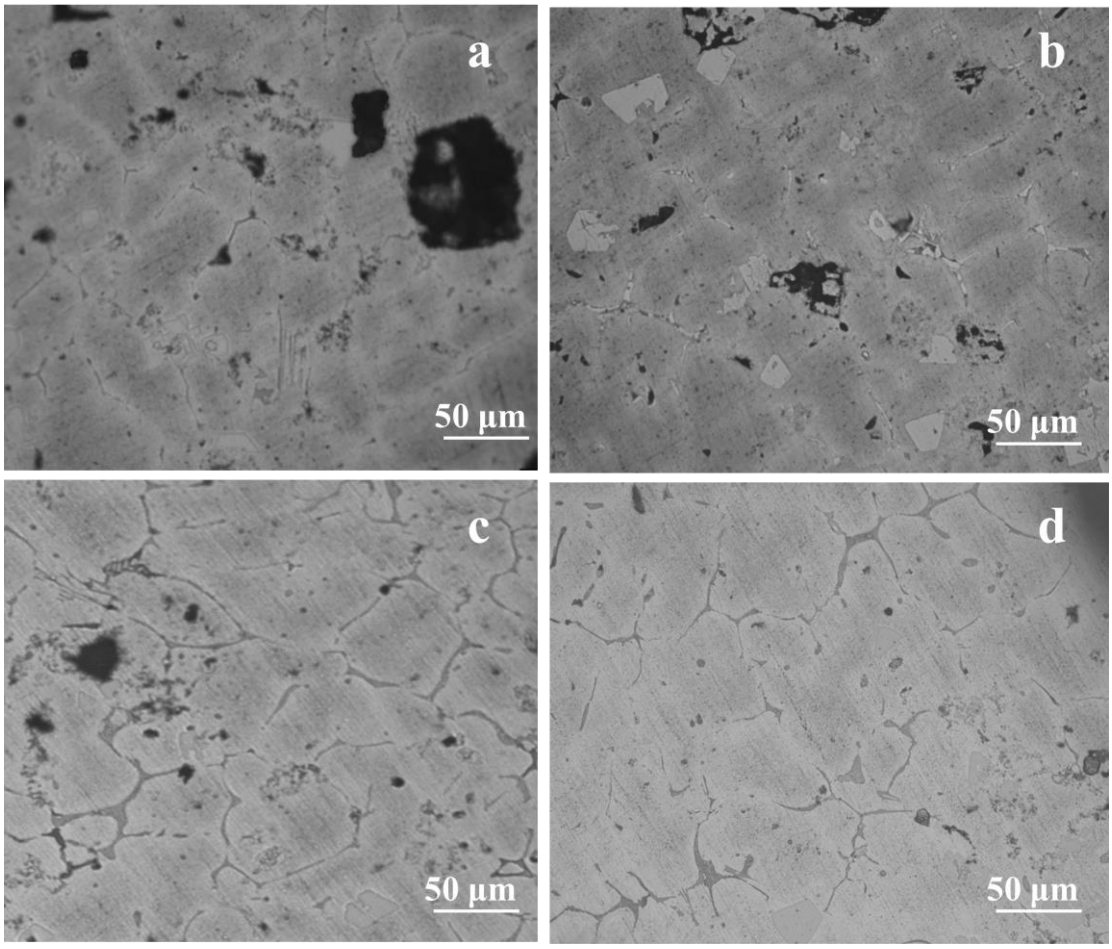

Fig. 4.13 Optical micrograph of foam cell wall aged at 180^{o}C for (a) 20 min., (b) 40 min., c) 60 min., and (d) 120 minute aging time.

For more detail (especially precipitation) analysis, TEM specimens were prepared from synthesised foam in as-cast, solutionised and aged condition (Figs. 4.15, 4.16 and 4.18). The bright field TEM micrograph provides information on a length scale of more than two orders of magnitude lower than that of the SEM images. The particular image refers to the structure of the aluminium cell wall material between the intermetallic particles seen in the SEM micrographs.

Fig. 4.15 shows the bright field TEM micrograph (Fig. 4.15(a)) with corresponding STEM EDS (Fig. 4.15(b)) and SAED pattern (Fig. 4.15(c)) for the as-cast foam sample respectively.

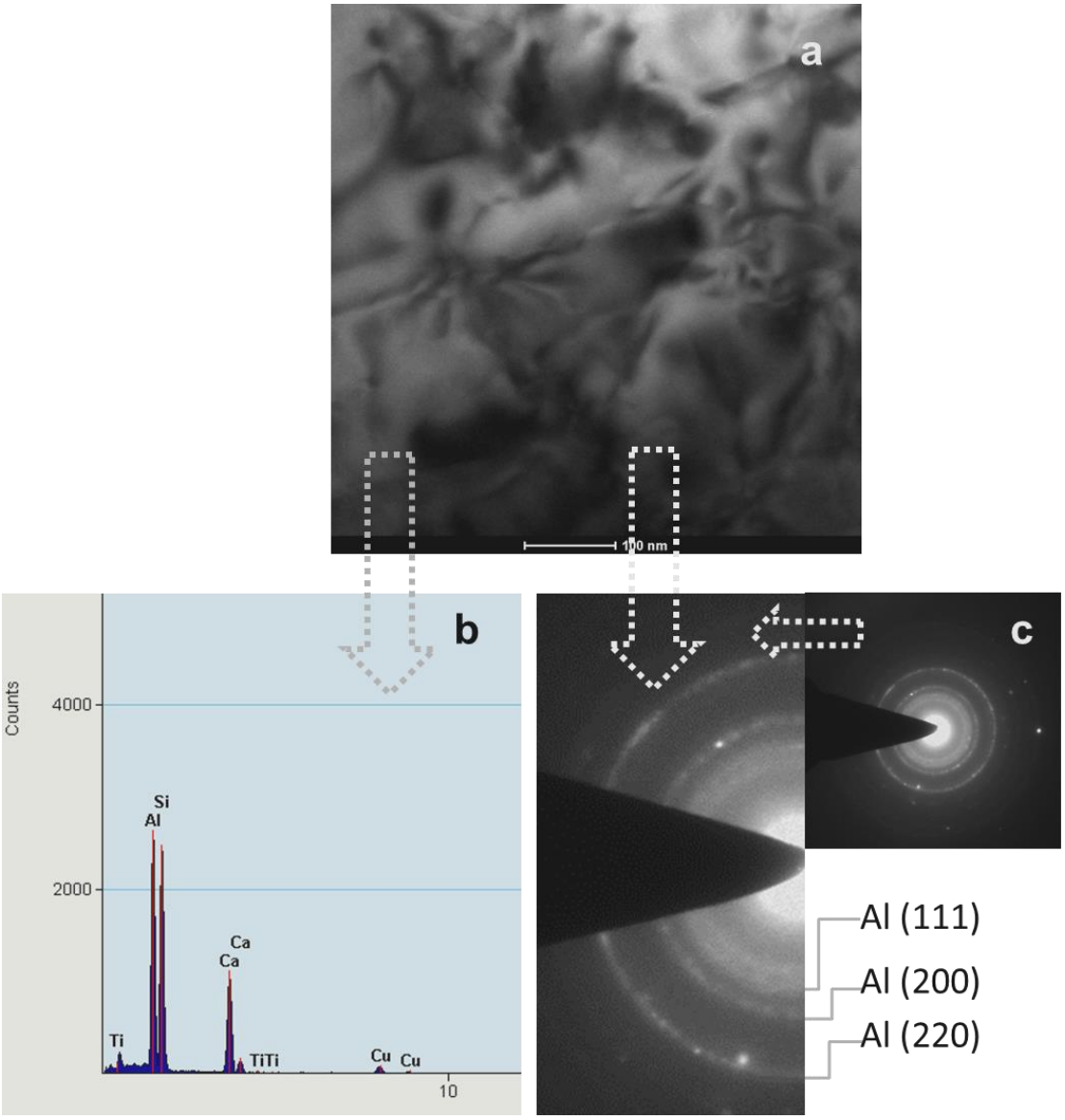

Fig. 4.14 (a) Bright field TEM image of the foam cell wall in as-cast condition with respective (b) STEM EDS and (c) SAED pattern.

Bright field TEM micrograph had shown in the Fig. 4.15 (a), which shows the presence of the fine aluminium grain substructure on the scale of 200 nm. The diffraction pattern of the as-cast foam confirms the multi-crystalline nature. The SEM micrograph reveals the presence of 30 µm sized particles within the cell wall material. On the other hand, the TEM micrograph shows the presence of less than 100 nm sized single-crystalline intermetallic particles embedded in the aluminium matrix between the coarse intermetallic particles. The particles that are present within the aluminium grain are expected to enhance the strength of the cell wall material. The EDS in STEM mode is shown in the Fig. 4.15 (b), indicating that this region is predominantly aluminium but also reveals the presence of Ti, Ca and Cu. The diffraction pattern is indexed (Fig. 4.15 (c)) using JCPDS Card No. 001-1179 (Al).

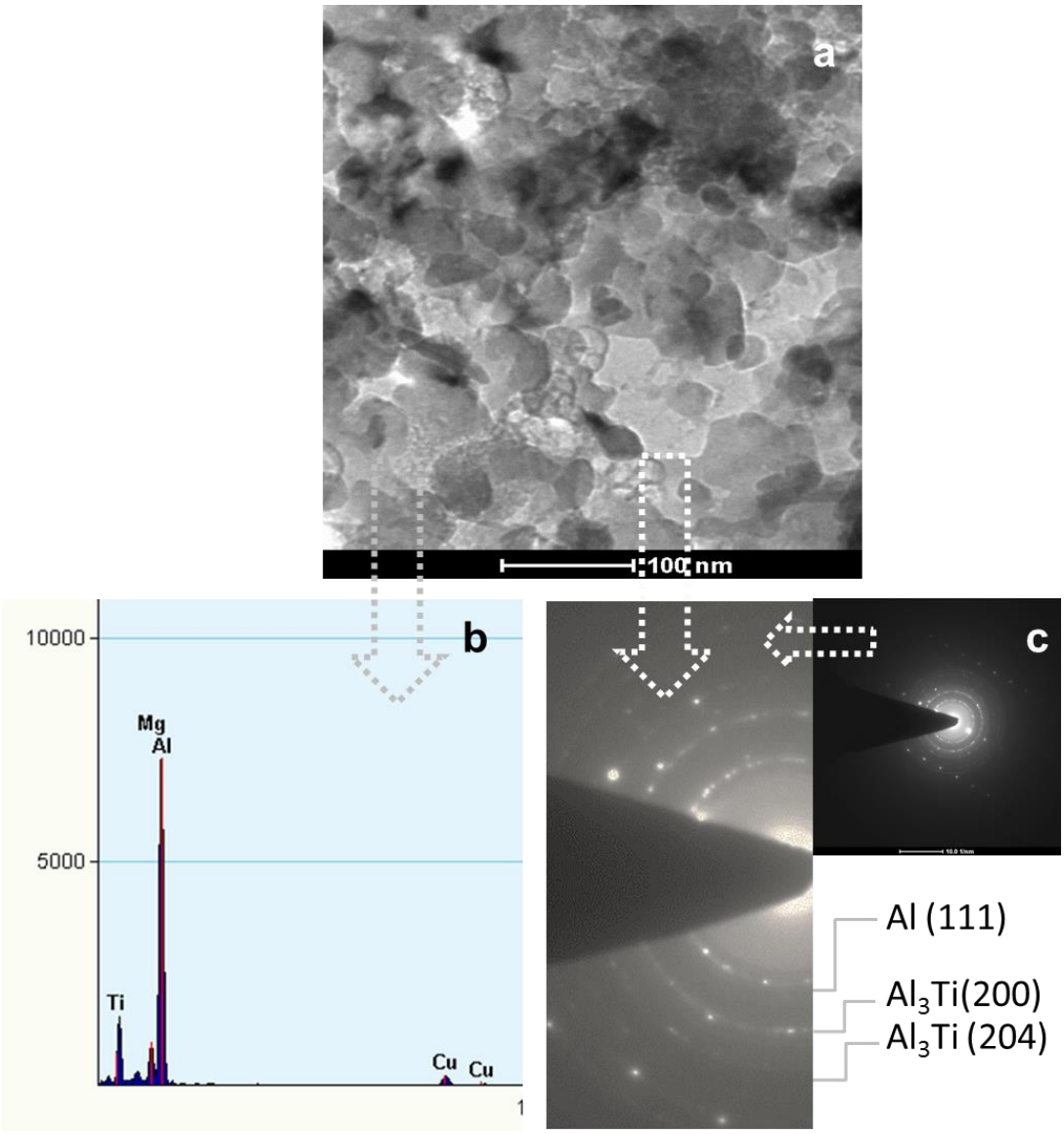

Fig. 4.15 (a) Bright field TEM image of the solutionised foam cell wall with respective (b) STEM EDS and (c) SAED pattern.

TEM image of synthesised foam after solutionising treatment followed by quenching is shown in Fig. 4.16 (a), respective EDS taken in STEM mode and SAED pattern is shown in Fig. 4.16 (b) and (c). Although, the crystallite nature of the sample has not been changed, the pore morphologies are strongly affected by the heat treatment at 550^{o} C. From TEM micrograph, it is found that some undissolved particle observed in the structure, which is also reflected in SAED pattern. EDS analysis indicates that this region is still predominantly aluminium but also contains titanium, which indicates the presence of Al-Ti intermetallic in the solutionised samples. Indexing of the SAED pattern affirms the presence of Al_3Ti intermetallic. The diffraction pattern is indexed (Fig. 4.16 (c)) using JCPDS Card No. 001-1179 (Al), 002-1121 (Al_3Ti).

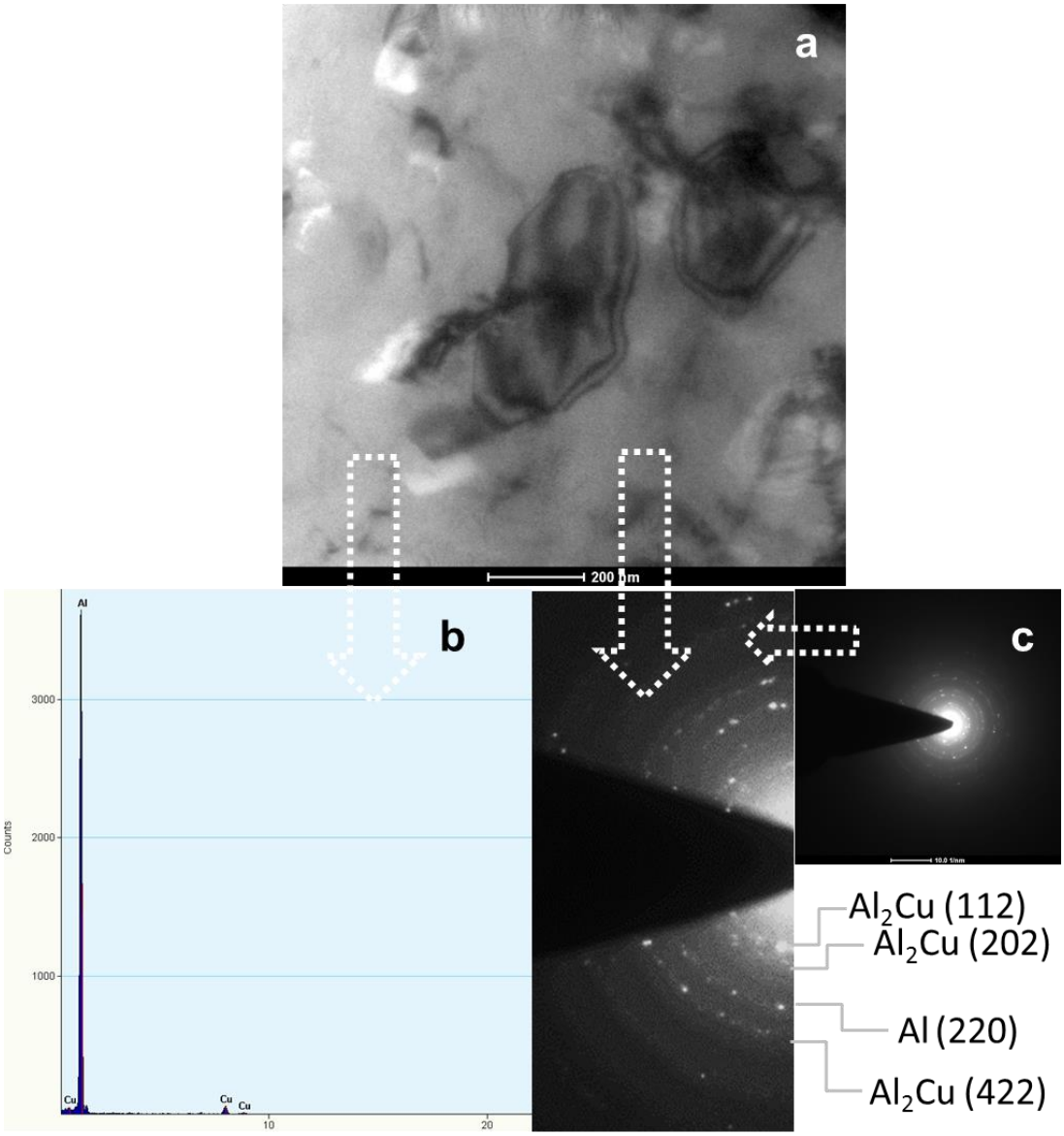

Fig. 4.16 (a) Bright field TEM image of the foam cell wall in peak aged condition with respective (b) STEM EDS and (c) SAED pattern.

Bright field TEM image of the peak aged sample is shown in Fig. 4.17(a) with respective STEM EDS (Fig. 4.17(b)) and SAED pattern (Fig. 4.17(c)). Similar to the solutionising treatment, the aging treatment results in morphological changes, which are mainly attributed, as well as, explained by the age hardening behaviour of the matrix alloy. It is worth to note that in the case of aged condition, the structural change was more pronounced and aging treatment significantly coarsens the precipitate. Grain with approximately average grain size of 125nm is found. The corresponding pattern shows a ring pattern with some diffraction spots, which indicates the fairly larger grain size with little misorientation.

Indexing of the SAED pattern affirms the presence of Al_2Cu intermetallic. The diffraction pattern is indexed (Fig. 4.16 (c)) using JCPDS Card No. 001-1179 (Al), 002-1121 (Al_3Ti).

XRD analysis of the as-cast, solutionised and aged foam sample is shown in the Fig. 4.18 ((a), (b) and (c)), which shows the presence of Al_2CuO_3, Al_2O_3, Al_3Ti and TiO_2. Fig. 4.18 (b) and (c) show the presence of Al_2Cu phase in the cell wall, which confirms the precipitation. Peaks corresponds to the oxide of the same phase is present in the as-cast foam in the foam of Al_2CuO_3 with Al (Al_2O_3) and Ti (TiO_2).

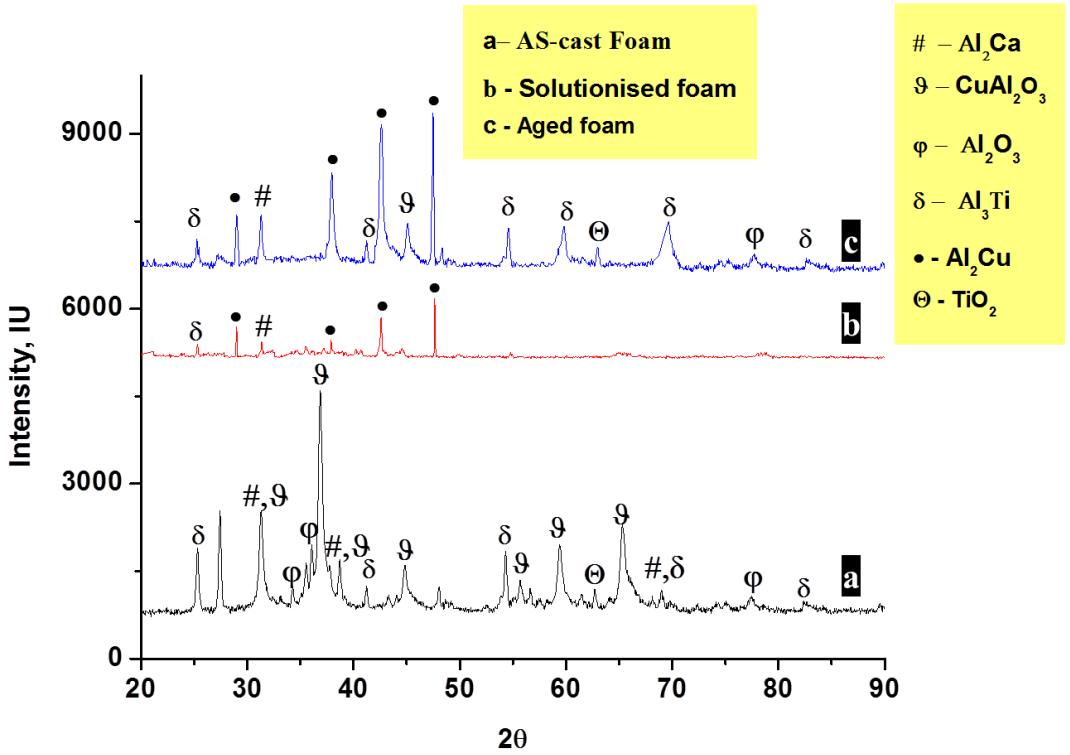

Fig. 4.17 The powder XRD pattern of the extracted particles from the: (a) as-cast, (b) solutionised and (c) peak aged foam sample after leaching with dilute hydrochloric acid.

4.3.2.2 Inference from microstructural studies

Most of the metal foam properties (the nature of the porosity, scale of the porosity) can be defined by the process used to produce metal foam. Tailoring of process parameters including holding time, amount of blowing agent, stirrer speed offers some scope for fine-tuning the structure for a given application. The foaming process is slightly more sensitive to a very small variation in process parameter. The degree of reproducibility of a process is also important and susceptible to the presence of flaws and defects. Another very important phenomenon in the foam processing (to achieve optimum mechanical properties) is the stabilization of the melt. Stabilization in the foaming process refers to prevention of the cell wall collapse during holding and solidification. Hence, to achieve a fine pore size with equal distribution, stabilisation plays an important role. Melt viscosity is also important to control the pore size and density of the foam, the ceramic particles (i.e. SiC/Al_2O_3/MgO) are generally used to stabilize the gas bubble in producing foam through the gas injection melt route (Chethan et al.). In melt foaming method, to increase the viscosity, calcium metal is used, which is well dispersed in the melt and form CaO, $CaAl_2O4$ or even Al_4Ca and improved melt viscosity.

Drainage along the cell edge is goaded by gravity which progressively makes the foam drier. In fact, there is a European Science Foundation initiative to carry out experiments in space to understand the drainage phenomena neglecting gravitational effects. Edwin et al (Raj, 2008) also suggests that progressive thinning of the cell wall is driven by local drainage and ultimately, result in cell wall collapse. The collapsed cell wall co-joins with neighbouring cells and form a big pore. If the collapse occurs at a later stage there is not enough time for readjustment and the co-joined cells display a pronounced aspect ratio.

Post processing technique may also plays an important role in the property modification of the produced foam through microstructural alteration, such as, thermal treatment. Thermal treatment after foaming process refers to modification of the microstructure of the cell wall and further improvement in the microstructure through solutionising and thermal aging. Therefore, thermal treatment can be used as a post treatment technique for property enhancement. The reported work refers to foams processed by powder metallurgy route. Such foams were solutionised above 500^{o}C and aged at about 165^{o}C for varying durations followed by quasi-static compression testing. It has been reported that energy absorption has improved from 25 to 75% for thermally aged samples over the as-foam condition (Feng et al., 2003b) (Campana and Pilone, 2009). Furthermore, (Lehmhus and Banhart, 2003)has made the distinction between samples aged after solution treatment and those that are heat treated without the solutionising

step and reported that the samples that were only aged demonstrate more ductility and perform better for energy absorption application. In our previous work, it has been found that there is a significant improvement in energy absorption capacity with peak aging due to finer precipitation of second phase particles instead of thick dendrite structure.

Improving the cell wall microstructure of the produced foam allows better control on the foam structure, which in turn influences the foam properties. The proposed post-processing technique of thermal treatment has the scope to improve foam property and subsequently mechanical properties of foams, synthesized by liquid melt route. The heat treatment technique to the problem is to demise the dendrite structure and strengthen the cell wall through solutionising and precipitation hardening, so that the cell wall collapse is further delayed, when load is applied on it. The objective is met by introducing thermal treatment at different time and temperature.

4.4 Mechanical Property Analysis

In section 4.3, the effect of the process variables on the foaming behaviour and the impact of post process technique (i.e. thermal treatment) on the microsturctural behaviour of produced foam are described. The change in microstructure with respect to heat treatment variables and tailoring them for the requirements are discussed in details along with the results obtained in previous section. Stochastic nature of the foam makes it more sensitive to the slight change in the variables. Therefore, to nullify the variance in results, a minimum of five specimens are tested for each set of experiment under each process variables. The course of action used to calculate the mechanical properties i.e. energy absorption capability, plateau stress, etc. is given in the previous chapter. It should be noted that the process variable decides the morphological and microstructural features of foam, which are in turn are responsible for the mechanical properties. In the initial part, microhardness of produced foam and thermal treatment is compared. Later, as-cast foam, solutionised and peak aged sample are only considered for all the mechanical property analysis. As observed in the previous section, changes in the microstructure in each aging condition are more or less. Therefore mechanical testing has been done for peak aged sample.

The main purpose of the thermal treatment is to measure the effect of thermal treatment on the microstructure and further investigate its effect on the structural properties. Hence, the main focus of the investigation is structure-property correlation and the assessment of the mechanical properties of the thermally treated sample in comparison to the as-cast foam sample

based on the experimental results obtained. The mechanical properties investigated are present in subsequent sections

4.4.1 Microhardness

Vickers hardness number (VHN) is measured for as-cast foam, solutionised and aged sample at different aging temperature at a load of 5g. Microhardness for as-cast foam, solutionised and aged sample with respective aging time is tabulated in the Table-4.1.

The aging behaviour of the respective condition in terms of the microhardness value is shown in Figs. 4.19 (a), (b) and (c). The hardness value of the foam sample in as-cast, as well as, solutionised foam condition sample is used for reference in each aging condition in respective figures. From the hardness value of the as-foam and solutionised sample, it is observed that the hardness value of solutionised sample is marginally lower than the as-cast foam sample. The samples showed typical response to ageing treatment at the different aging time i.e. 100, 150 and 180^{o}C. As shown in Fig. 4.19 (a), sample aged at 100^{o}C shows the hardness values greater than both the as-foam and solutionised sample. Sample at this aging temperature shows typical aging behaviour which means that as aging time increases hardness value also increases up to 60 minute and after that decrease in hardness value is observed.

Table 4.1 The microhardness values of untreated and thermally treated samples.

Sample condition v/s Microhardness, VHN						
As-cast	Solutionised	Aged sample				
		Aging temperature	Aging time			
			20	40	60	120
105±6	87±4	100	126±7	134±11	146±6	125±2
		150	144±6	160±6	146±7	120±6
		180	96.63±2	130.08±4	102.53±7	108.78±3

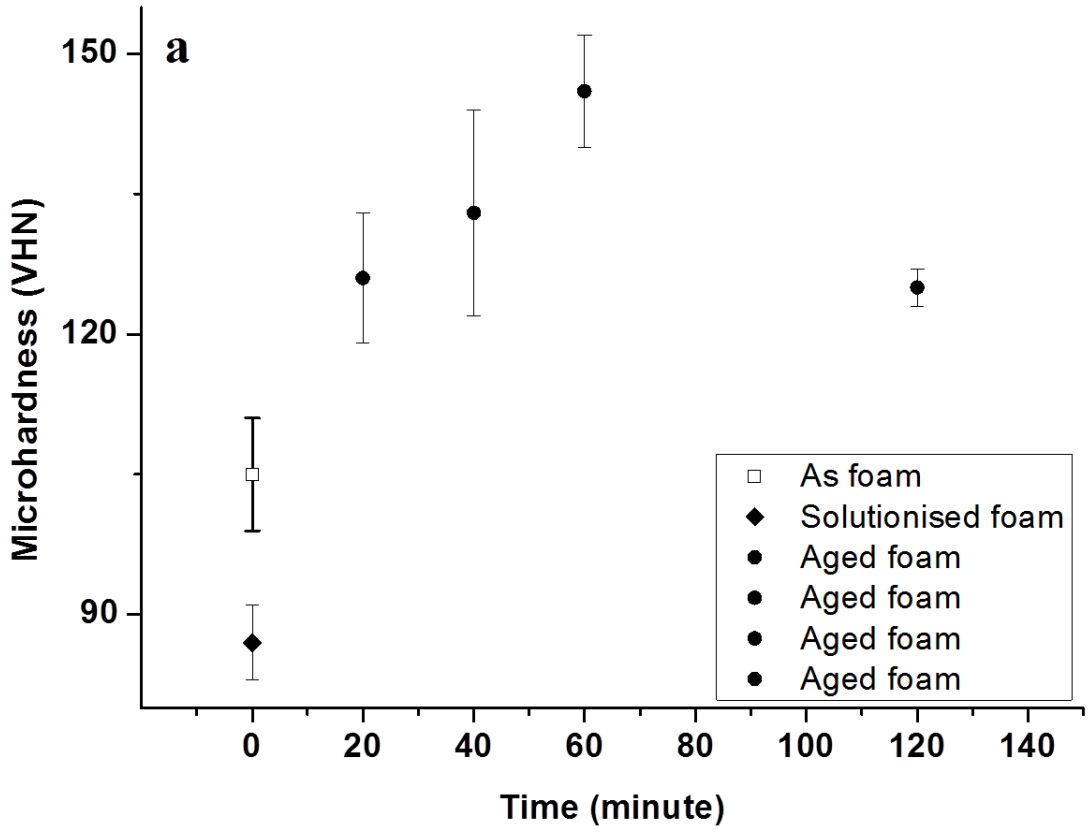
a
150
120
90
Microhardness (VHN)
0
20
40
60
80
100
120
140
Time (minute)
As foam
Solutionised foam
Aged foam
Aged foam
Aged foam
Aged foam

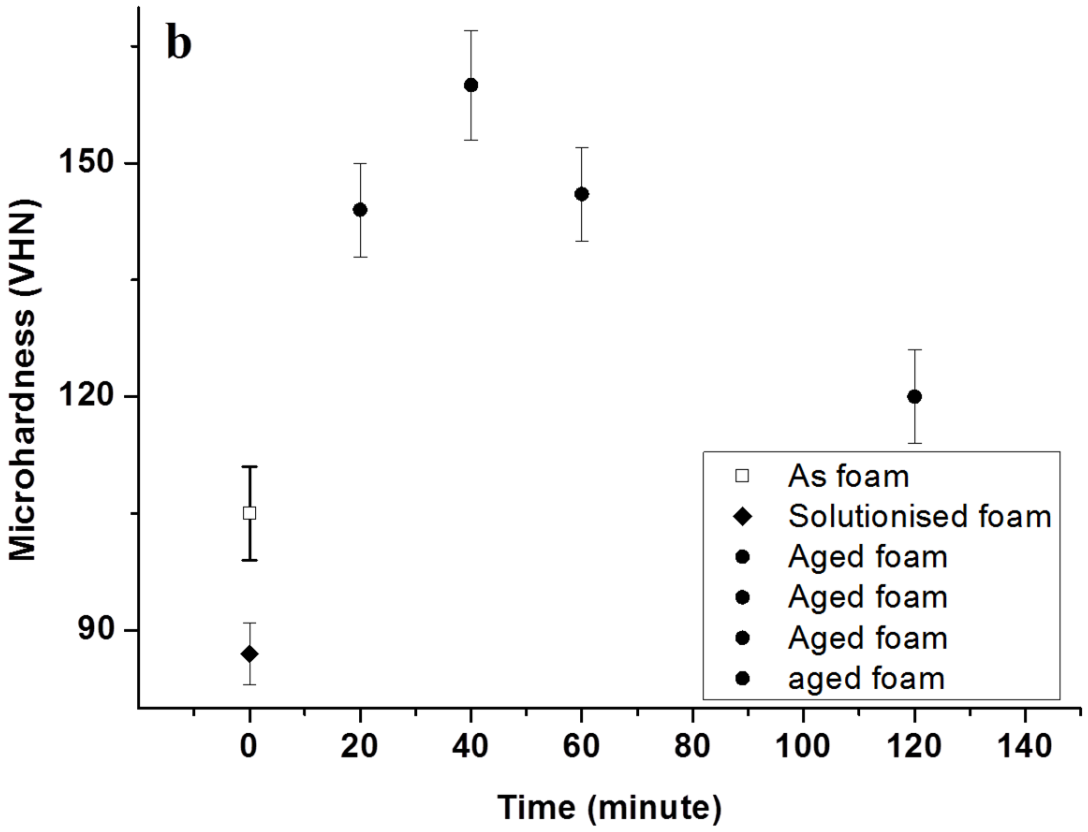
b
150
120
90
Microhardness (VHN)
0
20
40
60
80
100
120
140
Time (minute)
As foam
Solutionised foam
Aged foam
Aged foam
Aged foam
aged foam

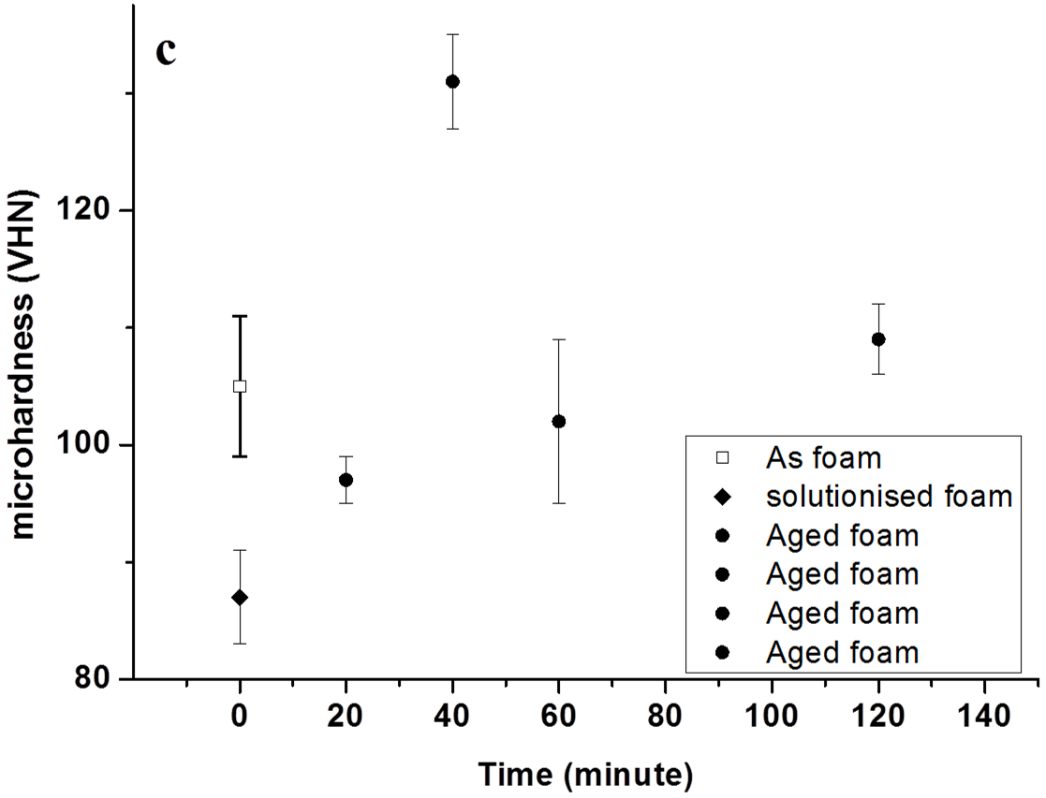

Fig. 4.18 Variation in microhardness with aging time for foam sample aged at (a) 100^{o}C, (b) 150^{o}C and (c) 180^{o}C.

The sample aged at 150^{o}C (as shown in Fig. 4.19 (b)) shows the higher hardness value as compared to solutionised as well as-foam sample. It is interesting to note that at 150^{o}C peak hardness value found at 40 minutes instead of 60 minutes, as observed in 100^{o}C. This observation is due to co-cluster formation and subsequent precipitation hardening.

Sample aged at 180^{o}C (as shown in Fig. 4.19 (c)) shows entirely different behaviour at the lower aging time i.e. 20 minute and it also shows hardness value lower than the as-cast foam. Peak ageing at this temperature (found at 40 minutes) is similar to the 150^{o}C but the value of the hardness is lower than the value found at 150^{o}C. This behaviour indicates that the synthesised foam shows over-aging behaviour at 180^{o}C.

4.4.2 Quasi-Static Compression Test

The microstructures of the cell wall material of the as-foam, solutionised and aged sample are analysed in the previous section and it is expected that the microstructural changes in each condition will reflect in compression behaviour. In consequence, the as-cast foam sample had dendritic structure, whereas the solutionised sample had $Al_{20}CaTi_2$, Al_2Cu and Al_2Ca intermetallic particle. Aged sample comprise of large amount of brittle cluster, in addition to, intermetallic particles.

During the quasi-static compression test, the collapse of the foam cells is observed and progresses layer-by-layer from one end until full densification occurs. The compressive stress-strain curve has been obtained by plotting the applied load divided by the original specimen cross-sectional area, to obtain the applied nominal stress against the percentage compressive strain. The compression curves of samples in as-foam, solutionised and peak aged condition are plotted in Fig.4.20.

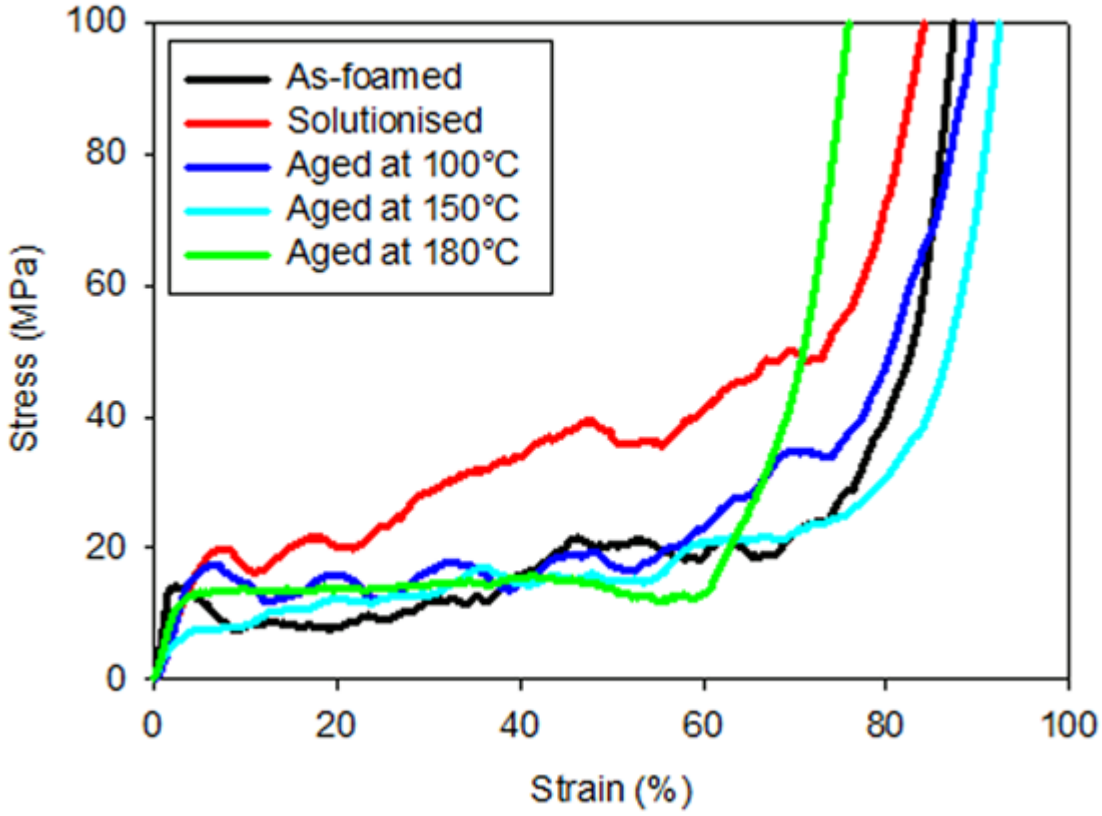

Fig. 4.19 Stress–strain curves for as-foam, solutionised and peak-aged aluminium alloy foam samples under compressive loading at 1×10^{-3} s^{-1} strain rate.

The values of yield stress, plateau stress and energy absorption of the respective samples are shown in Table 4.3. The values of plateau stress and energy absorption for as-foam and peak-aged samples are approximately similar, whereas, that of solutionised condition are significantly higher. The reduction in these compressive properties with increase in aging temperature can be attributed to the presence of brittle intermetallic and grain coarsening. This leads to early collapse of the cell wall and results into poor performance. Another interesting aspect worth notice is the absence of strain softening in the case of sample aged at 150^{o}C (as shown seen in Fig. 4.17). Foam aged at this temperature does not have a sudden drop in the compressive strength after yielding. This phenomenon can be attributed to the ductile nature of sample aged at 150^{o}C in comparison with the more brittle 180^{o}C.

Table 4.2 Values of mechanical properties of as-cast, solutionised and aged foam samples.

Heat treatment Condition	Yield stress (MPa)	Plateau stress (MPa)	Energy absorption (MJ/m3)
As-cast foam	14±4	10±3	13±3
Solutionised foam (at 550^{o}C for 60 minute)	20±1	23±3	29±3
Aged (at 100^{o}C for 60 minute)	18±5	11±1	16±2
Aged (at 150^{o}C for 40 minute)	8±3	10±3	15±2
Aged (at 180^{o}C for 40 minute)	13±2	13±1	12±1

It can also be visualized that at this aging temperature (150^{o}C) longer and more prominent densification plateau is observed. Sample aged at 180^{o}C shows slight decrease in stress level at the plateau region. This phenomenon of decreasing stress level in the plateau region is reflective of the brittle nature of the cell wall. Again this finding supports the phenomenon of over aging and grain coarsening at this temperature. In order to explain ductile/brittle nature of the foam in all conditions, deformed samples were sectioned and examined under SEM.

4.4.3 Fractography

Fractography provides information about the nature of the fracture. In the present work, fractography is refers to the interpreted compression test. Interrupted compression test means the sample is compressed up to 30% compression and then SEM of the fracture sample has been taken to analyse the fractured surface. Back scattered SEM image of the fractured sample obtained from interrupted compression test at different condition i.e. as-cast, solutionised and aged condition are shown in Figs. 4.21 (a), (b) and (c) respectively.

Fig.4.21 (a) shows the backscattered electron micrograph of the fracture surface of as-cast foam sample.

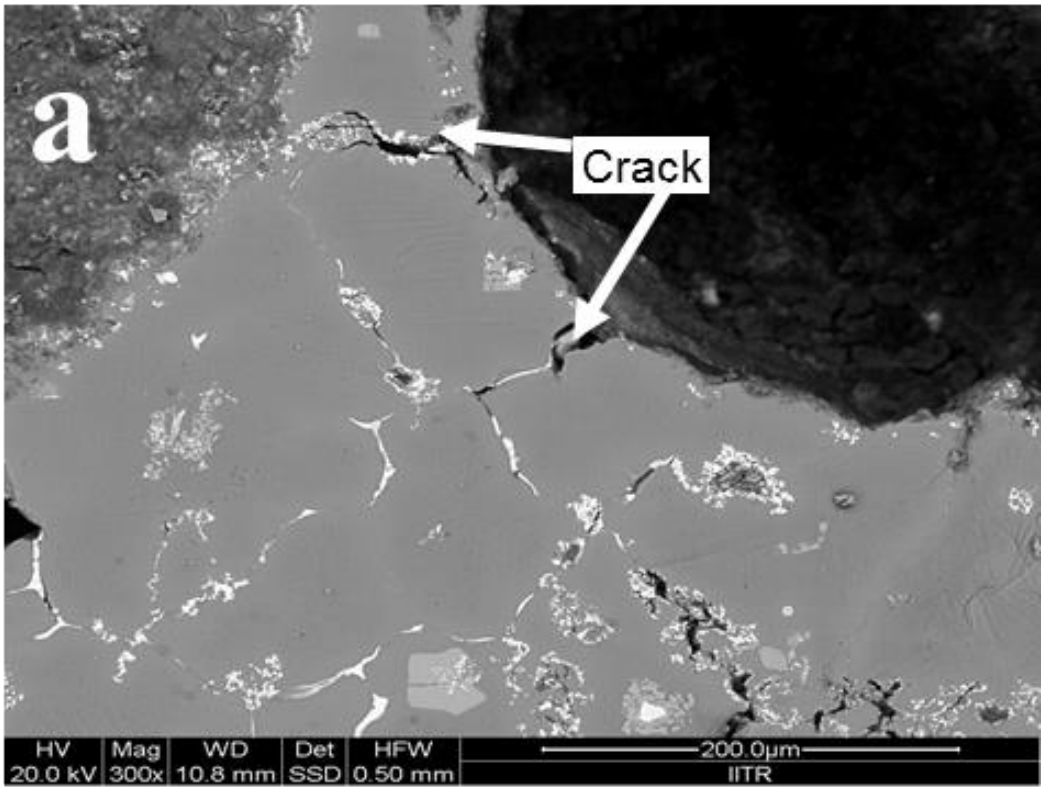
a
Crack
HV
20.0 kV
Mag
300x
WD
10.8 mm
Det
SSD
HFW
0.50 mm
200.0µm
IITR

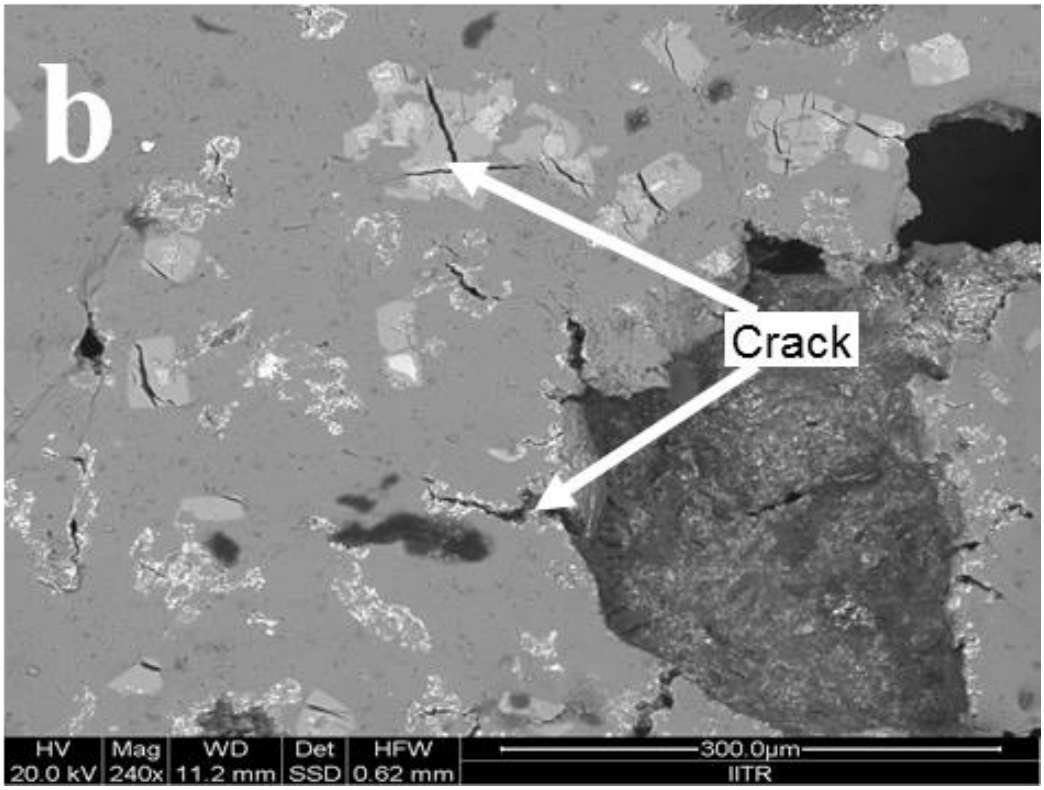
b
Crack
HV
20.0 kV
Mag
240x
WD
11.2 mm
Det
SSD
HFW
0.62 mm
300.0µm
IITR

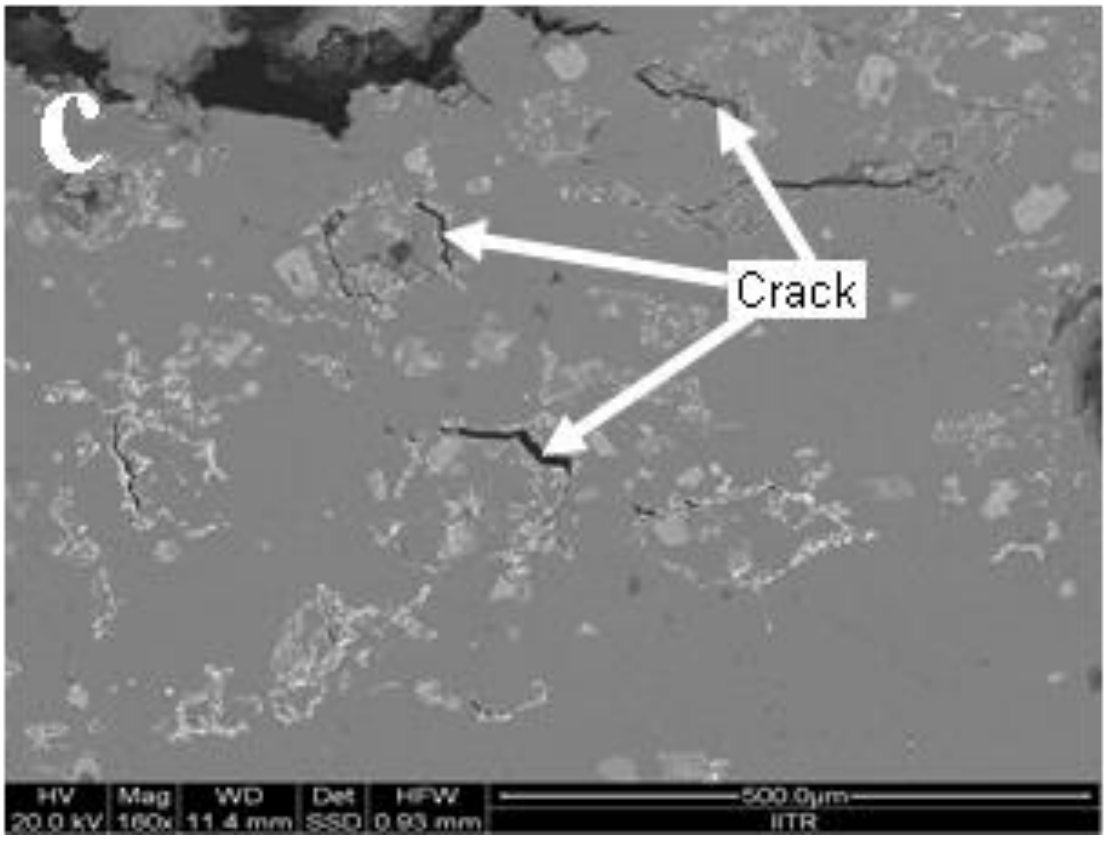

Fig. 4.20 SEM micrograph of fractured surface of interrupted compression sample in (a) as-cast, (b) solutionised and (c) peak aged sample.

From this micrograph it is evident that dendritic structure is present in the as-cast foam condition and crack starts from the cell wall and further propagates through the path given by dendrite structure. It is observed from the Fig.4.21 (a) that the embedded particle of the Al-Ca-Ti intermetallic phases also act as a crack initiation sites.

Fig. 4.21 (b) shows the crack behaviour of the solutionised sample. Through the backscattered image, it is found that the crack propagation behaviour in solutionised sample is quite different from the as-cast foam sample. It can be seen that the inter-dendritic region is rather discontinuous, which means that there is no easy path for crack propagation. However, the undissolved Al-Ca-Ti intermetallic particle acts as the crack initiation site. These embedded particles are less in number at the plateau border of the foam. Hence, crack initiation and further propagation of the same is also tough, as compared to as-cast foam sample.

Fig. 4.21 (c) shows the fracture micrograph of peak aged sample. From this micrograph, it is clear that there is no dendrite structure present, however, some cluster, co-cluster and precipitate are found. During the aging, formation of cluster and precipitate (which is brittle in nature) allows easy path for crack initiation and further propagation.

Investigations of the mode of failure, crack initiation and propagation in aluminium foam are reported in the literature. Increase in size and fraction of precipitates is reported to increase the occurrence of cracking in aluminium foam (Amsterdam et al., 2006). The failure modes of closed cell foams under compression load can be characterized as Mode I, compressive bending and fracturing at ‘‘hinges”; Mode II, direct brittle fracturing due to induced tension or shear; Mode III, cracking in the cell face; and Mode IV, friction and shear between fractured cells (Onck, 2001). The micro- mechanism of deformation observed in closed cell aluminium foam includes cleavage, deboning of clustered precipitates located around the grain boundaries, bending of cell edges, stretching of the cell faces and buckling of the cell wall (Deqing et al., 2005; Edwin Raj et al., 2009; Mu et al., 2010a; Paul and Ramamurty, 2000).

The failure mechanisms of the as-foam, solutionised and aged samples are clearly different from one another. In the as-foam condition, the cracks nucleate at precipitates near the pore and connect to neighbouring intermetallic particles along the dendritic structure (Fig. 4.18 a). Fracture propagates by linking up several of these micro-cracks, which are initiated in the neighbourhood of intermetallic precipitates. The cell wall failure mode is predominantly brittle in nature, as the interconnected interdendritic Al_2Cu provides an easy path for the crack propagation along the aluminium-Al_2Cu interface. On the other hand, in solutionised samples, the cracks after 30% compression found to be within the intermetallic particles all across the cell wall. Even the cracks that have nucleated on the cell walls are limited to the intermetallic phase.

4.5 **Summary**

Thermal treatment technique has been used as a post processing technique to alter the microstructure and the cell wall microstructure has been characterised for macrosturctural and microsturctural features and change in the microstructural features are correlated with the compressive properties. The findings and conclusion of the present chapter are:

1. Thermal treatment in the foam has significantly affected the microstructure of the metal foam i.e. thermal treatment results into non dendritic structure.

2. The micro-hardness (VHN) of the treated sample is highest in aged condition and this phenomenon of increasing hardness is mainly attributed to the precipitation hardening.

3. From the quasi static compression test results, it is observed that the yield stress, plateau stress, and energy absorption capacity has been improved after the thermal treatment when compared with the foam without reinforcement. The compressive property improvement can be interrelated to the morphology of the cell wall and the presence of precipitates.

4. These compression test results shows that property enhancement is maximum in the solutionised sample, although property also enhanced after aging treatment but it is lower than the solutionised sample.

CHAPTER 5: MICROSTURCTURAL AND MECHANICAL BEHAVIOUR OF Al-Sc FOAM: EFFECT OF SCANDIUM ADDITION

Grain refinement can be used to improve the quality of the casting as grain refinement results into fine equiaxed grain. In the previous chapter, we discussed about the processing of foam, property enhancement through the post processing technique i.e. thermal treatment. Present chapter comprises of master alloy characterisation, synthesis of the Sc added (in the form of master alloy) foam using different wt. % of Sc, microstructural and mechanical property characterisation. Microstructure characterisation of foam enabled the proper understanding of the structural behaviour of the Sc added form. The evaluation of the phase (present in the cell wall) and their chemical composition at micro and macro level has been done. The obtained result has been compared with the foam (without Sc) to evaluate the effect of the Sc addition on the properties of aluminium foam. Furthermore, the optimum condition in terms of the grain size and casting condition were identified. Finally, correlation among microstructural features, physical and mechanical properties are discussed.

It is reported in the previous chapter that through the thermal treatment, property of the foam can be altered. In this chapter, to strengthen the cell wall material, grain refinement technique is used. The grain size is refined through grain refinement so that the dislocation movement can be retarded. As reported earlier in (Chandrashekar et al., 2009), use of grain refiner convert the columnar structure into equiaxed grain. The formation of equiaxed structure results in improved mechanical properties, good machinability, improved feeding to get rid of shrinkage porosity, better surface finish, less ingot crack formation, enhanced resistance to hot tearing. All the above stated improvements in the casting and structural behaviour results in: prolonged fatigue life, good corrosion resistance, improved toughness and strength.

Literature suggests that chemical grain refining is one of the most effective methods of grain refinement; other method used for grain refinement is dynamic nucleation and inoculation technique, where grain refiner is added to the melt for nucleation. Inoculation techniques have a greatest industrial importance for grain refinement (Greer, 2003), due to its simplicity (Chandrashekar et al., 2009; Murty et al., 2002). It is reported in the literature that a fine equiaxed material grain structure pose an excellent properties such as high yield strength, high toughness, excellent formability, wear resistance (Alipour et al., 2013) and also improves

machinability of castings (Birol, 2013; Cibula, 1949; Ohno et al., 1983). For large casting grain size is mainly controlled by the use of master alloy contain grain refiner (McCartney, 1989; Murty et al., 2002). In the present study master alloy (Sc added, as a grain refiner) is used. Norman et al (Symposium held April 13-15) reported that the scandium is an effective grain refiner and also show precipitation hardening behaviour if it further treated thermally (Chandrashekar et al., 2009; Monachon et al., 2011; Van Dalen et al., 2005; van Dalen et al., 2011).

As reported earlier, grain refinement in the casted and as well as in wrought alloys is equally important from numerous viewpoints as it helps to improve the strength of the alloy, distribution of porosity, machining, ingot homogeneity and better formability. Similarly, grain refinement reduce shrinkage defects and susceptibility to hot cracking(Irving, 1997; Mousavi and Cross, 1999). Therefore, it is well established fact that the grain refinement is best suited technique for aluminium and its alloys, in the present work, scandium (in the form of master alloy) was used as a grain refiner to evaluate the grain refinement effect on the cell wall (i.e. cell wall alloy) strengthening which expected to result in enhanced energy absorption capability.

5.1 Master alloy characterisation

5.1.1 Master alloy chemical composition

As discussed in the chapter 3 the starting materials used in the preparation of the master alloy is 6061 alloy (table 4.1) added with 4 wt. % Cu. To analyse the effect of grain refinement on microsturctural and mechanical behaviour of the foam, Al-Sc master alloy (Al-2wt% Sc (Table 5.1) is added in the starting master alloy (6061+ 4 wt. % Cu). The normal composition of the used Al-Sc master alloy is shown in below Table 5.1.

Table 5.1 Chemical composition of the Al-Sc master alloy used to prepare master alloy for Al-Sc foam synthesis.

Master alloy	Chemical composition (wt. %)			
	Si	Fe	Sc	Al
Al-2.0 Sc	0.15	0.14	2.00	balance

5.1.2 Microstructural Analysis

The closed cell metallic foam properties mainly depends on the structural properties (as explained in the literature review section) such as the relative density, pore size and the distribution of pore in the matrix which decide the cell wall thickness. As, it is an established fact that the foaming process is irreversible in nature, therefore, to produce good foam it is necessary to minimise the melt drainage during foaming process as drainage results into the thinning of cell wall which further reduce the overall performance of the foam. As discussed in previous chapter, Cu addition helps in foaming, but drainage is still there as discussed and shown in the macrostructure (Fig.4.5).The secondary and backscattered SEM image of the master alloy (6061 + 4 wt. % Cu) alloy after addition of 1 wt. % scandium (in the form of master alloy) is shown in Fig. 5.1 (a) and Fig. 5.1 (b) respectively. With the addition of the scandium, it has been found that structure is more refined as compared to the primary master alloy ((Fig.4.2 (b), without scandium addition). It is observed (Fig. 5.1(b)) that the structure is consist of dense fine Al_2Cu network as well as lamellae, which is distributed throughout the structure with a very fine grain boundary (numbered as 1 and enclosed within the ellipse). Some very small primary particles are also seen at the centre of a grain (indicated by an arrow and numbered as 3).

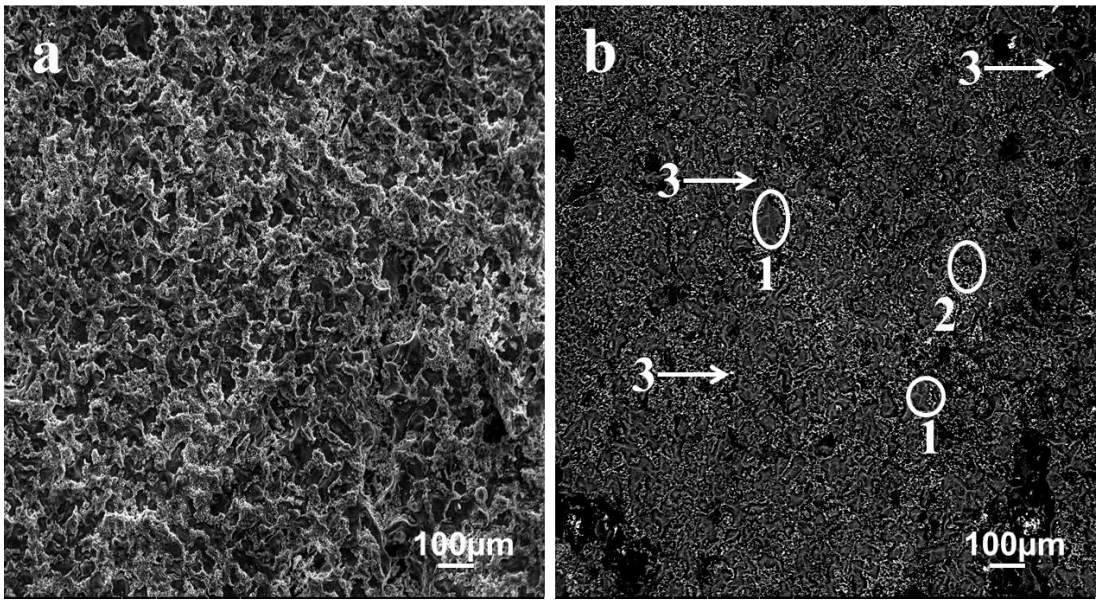

Fig. 5.1 (a) Secondary electron SEM image and (b) backscattered SEM image of Sc added (in the form of master alloy) master alloy.

It is expected that these primary particles may act as nucleant at the time of foaming and result in to more refine cell wall microstructure.

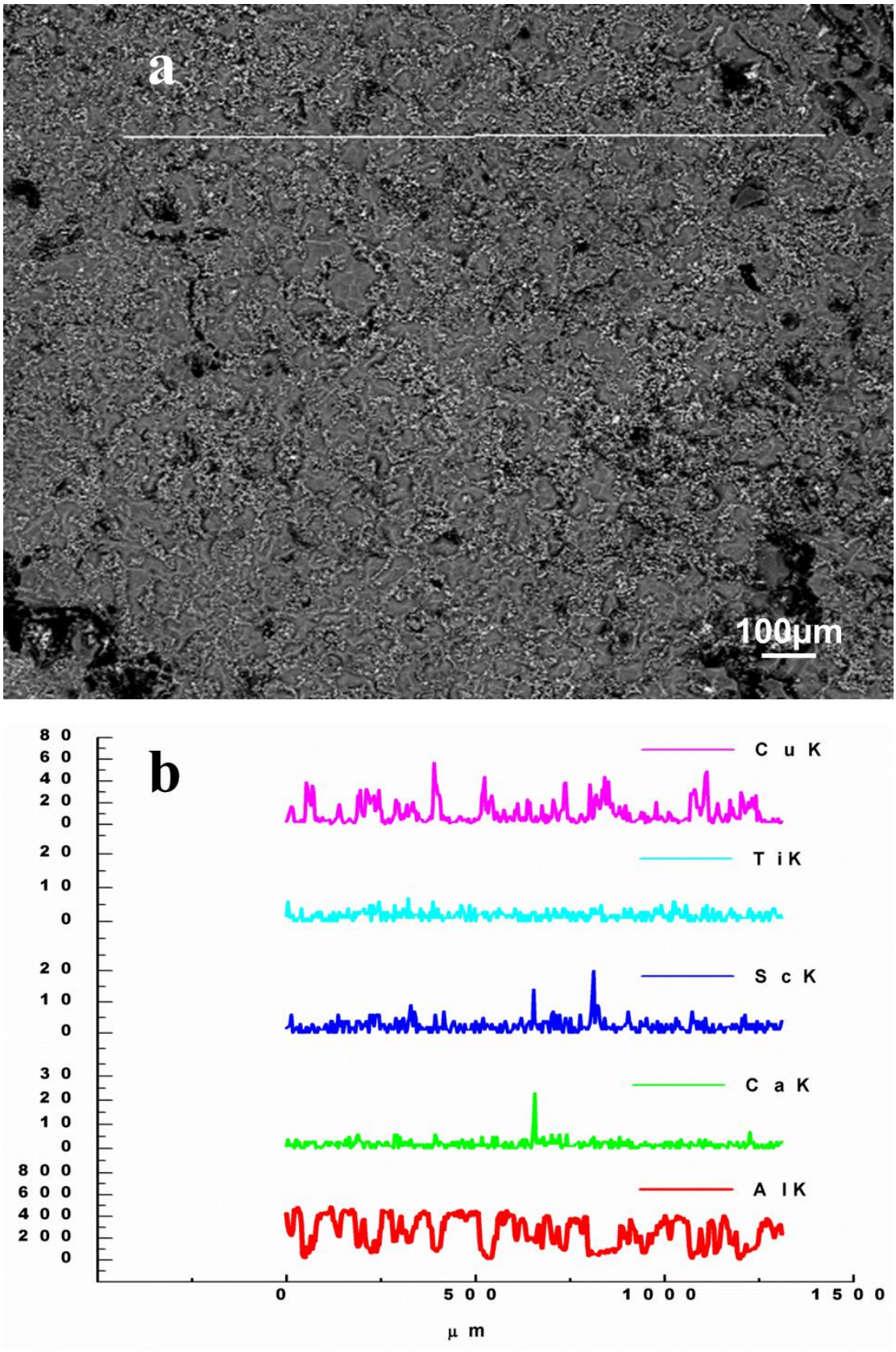

Fig. 5.2 (a) Backscattered SEM image of Sc added master alloy and (b) EDS line scan of Cu, Ti, Sc, Ca and Al.

As shown in the above Fig. 5.1 (a) and Fig. 5.1 (b), some cluster (of primary particles) is observed (numbered as 2 and indicated by the ellipse) at the grain boundaries which might be forced ahead of the advancing solid–liquid interface. Hyde et al reported that some of the primary particle from these clusters nucleated at the later stage of the solidification as the scandium content of the melt increases (Hyde et al., 2001). The SEM image, EDS line scan of Cu, Ti, Sc, Ca and Al for the master alloy prepared with 1 wt. % Sc addition are shown in Fig. 5.2 (a) and (b). In Fig. 5.2 (b) all the features, which described above are also clearly visible. The line scan of Al and Sc indicates the possibility of Al-Sc intermetallic. It is clear that in prepared master alloy structure, the distribution of Ca, Sc and Ti is random. No obvious co-segregation of Sc is present.

5.2 General characterization of the Al-Sc (Sc added) foam

This section of the chapter discussed (general discussion i.e. apply to all wt. % Sc addition) about the effect of the scandium addition observed at macroscopic and microscopic level. Foam produced following the melt route as described earlier. Characterisation is mainly consisting of macroscopic and microscopic examinations. The first part contains an overall evaluation of the change at the macro scale level such as level of drainage, local drainage, and cell wall collapse. The second part of this section mainly consists of microstructure analysis of the produced foam and general structural changes (after scandium addition), corresponding EDS, EDS line scan and elemental area mapping has been done to affirm the findings (changes occurred due to the scandium addition in the master alloy). Microstructure analysis reveals the change occurred in the features of the metallographic structure and the distribution of particle and dispersoids in the aluminium matrix.

5.2.1 Macrostructure

Low magnification digital macrograph of the cross section (parallel to foaming direction) of scandium added foam is shown in Fig. 5.3. It is observed from the macrostructure that pore size is equally distributed throughout the synthesised foam casting with more or less equal pore size. It has been found that after the addition of the Sc thinning of the cell wall towards the centre of casting is relatively less as compared to the foam without Sc, whereas, near the crucible wall and at the bottom of the casting thickness is reduced and tends to normal cell wall thickness. The progressive thinning of the cell wall towards the upper portion of the casting mainly driven by the local drainage, which is reduced after the Sc addition. Similarly, from the macrostructure it is clearly evident that there is a very small or in other words no drainage

collection is found at the bottom of the casting. From macrostructure of the produced scandium added aluminium (as shown in Fig. 5.3), it is observed that in the upward direction from the bottom of casting, initially a fairly thick cell wall is observed, which develops a curvature similar to the foam produced without Sc. This curvature progressively drives metal away from the cell face towards the cell edge, which leads to thinning of the cell wall and results in to collapse of the cell wall. The low rate of drainage as observed in Sc added foam is partly the result of the smaller pore size, and corresponding higher effect of surface viscosity. Cell coalescence in the foam without Sc addition (Fig. 4.5) is linked with rapid melt rejection from the cell faces to the adjacent plateau borders, which will widen them and force melt flow and redistribution(Raj, 2008).

The digital micrograph shown in the Fig. 5.3 shows the absence of drainage and the stability of cell faces in Sc added foam. The stability of the cell wall is a clear indication of the narrow cell faces which is influenced by surface viscosity and results into complete absence of forced melt flow and redistribution.

Fig. 5.3 Photograph of cast foam showing cross section of Al-Sc foam produced by melt route using TiH_2 as a blowing agent shown at approximately real size, which exhibits several features resulting from Sc addition, such as uniform pore distribution and no drainage collection at the bottom.

Cross sections of the cell structure of foam also shows that although, drainage of metal has occurred during the extended foaming time but the effect on the cell structure is relatively small. The cell size has increased at the top of foam.

5.2.2 General microstructural analysis of the scandium added foam

Cell wall structure of the produced foam is of main concern as it bears the load applied on the foam; hence, to enhance the property of the cell wall tends to change the property of the metallic foam. In the whole chapter, discussion is about the effect of scandium addition on the cell wall microstructure, therefore, in this section of the chapter, overall view of changes observed in the cell wall structure after Sc addition at microscopic level such as, change in the microstructure, phases present in cell wall microstructure etc. are collected and used as a reference throughout the chapter.

The optical micrograph of the cell wall of scandium added foam produced follows the same technique as described in the previous chapter are shown in Fig. 5.4 (a), (b), (d) and Fig.5.4 (d). The unetched sample at two different magnifications is shown in Fig. 5.4 (a) and Fig. 5.4 (b) which reveals the presence of different plate like, tiny spots and bulky structure spotted in black, grey and dark grey colour. These different types of particles are marked with the unique number. Tiny spots marked as no. 6 (shown in the Fig.5.4 (a)) at the different location in the aluminium matrix (in the form of cluster and mainly in the range of 0.25- 3µm size). It may be intermetallic or the secondary phase particle of scandium and aluminium. Other structure which is mainly present in the foam of lamella and triple junction and marked as no. 3 and 5 may be the intermetallic of the aluminium and copper (as it also found and discussed in the previous chapter 4) as Al_2Cu. As observed, in the cell wall microstructure (Sc added) lamella structure is not continuous, which indicates the presence of the scandium due to that the structure is not continuous as well as dendritic. Moreover, some bulky structure (grey in colour) is also observed in the micrograph and marked as no. 1 and 4 is the intermetallic of Al-Ti-Ca (as discussed and identified as $Al_{20}CaTi_2$ in the previous chapter). Some black particles (one of which is marked as no. 2) could be either oxygen or porosity. To find out the actual structure of the cell wall and position of the second phase particles in the aluminium matrix etching has been done with Keller's etchant at room temperature. During etching, the aluminium is dissolved and the clear structure is observed (as shown in Fig.5.4 (c).

Optical micrograph of the etched sample at different magnification (as shown in Fig. 5.4(c), and (d)), which shows the microstructure of the cell wall (Sc added foam), and it unveils the presence of α-Al as a major phase with secondary phases. The positions of the second phase

particles are clearly visible regardless of the grain boundary, which reveals the refinement of the grain structure with Sc addition.

As shown in Fig. 5.4(c), microstructure of scandium added foam predominately consists of solid particles grey in colour and some cluster like structure at grain boundary, as well as, in the matrix. For more detailed information, microstructure has been analysed at higher magnification, which shows the presence of bulky intermetallic, as well as, tiny particles and dispersoids at the grain boundary. From high magnification optical micrograph, it is also observed that the cluster like structure is in fact dispersoids of very small particles and may be contain scandium.

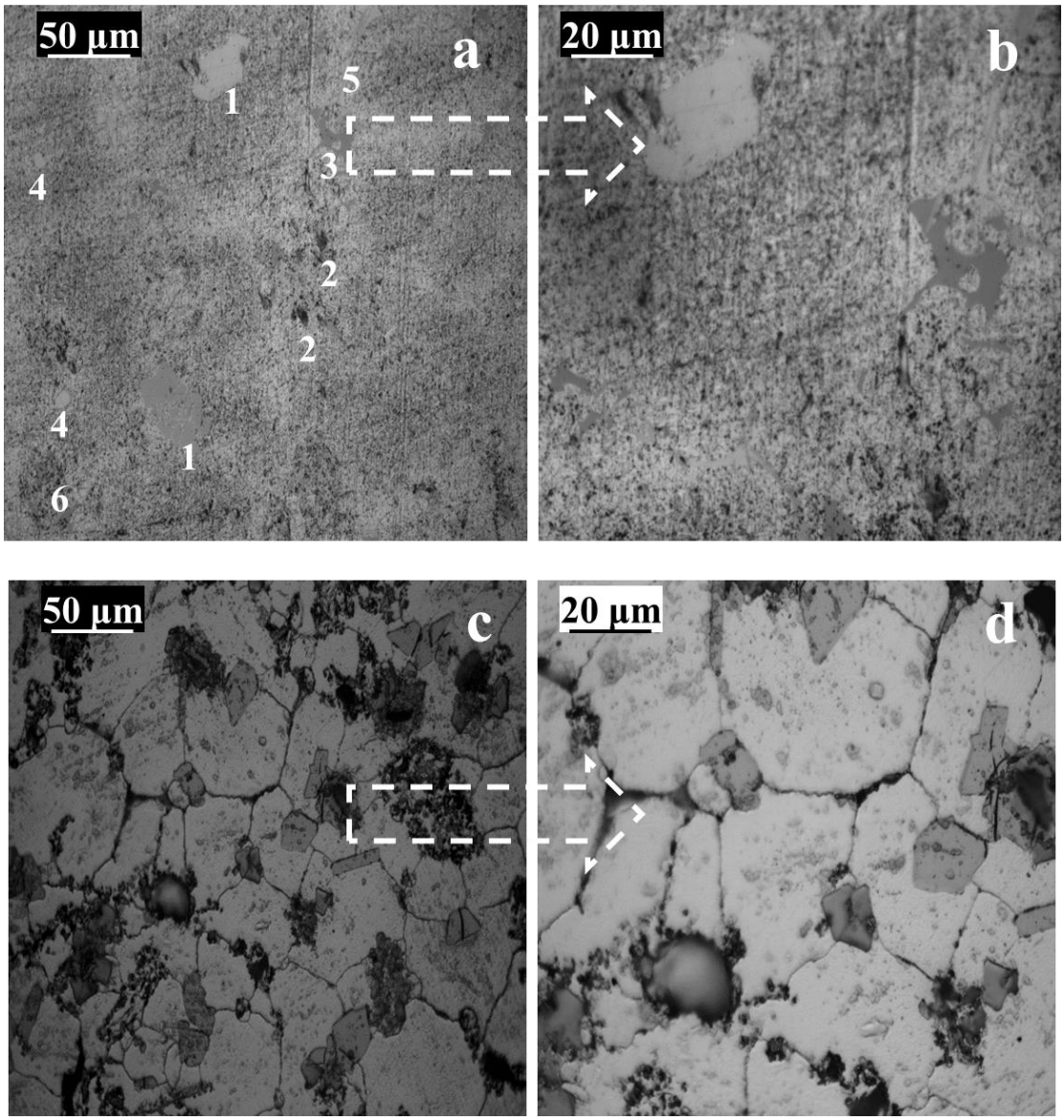

Fig. 5.4 Optical micrograph showing the microstructure of unetched (a, b) and etched (c, d) sample of the scandium added (in the form of master alloy) foam

To obtain more structural information (resulting from Sc addition), sample further analysed with SEM. Fig. 5.5 (a) show the back-scattered electron SEM image of scandium added foam. It is observed that the image consist of bright discontinuous lamella structure, which is distributed throughout the matrix (mostly at the grain boundaries) with the combination of some coarse grains. Lamellas (marked as no.3) are accompanied with some tiny particles (marked as no.4) with an approximate size of 1 µm.

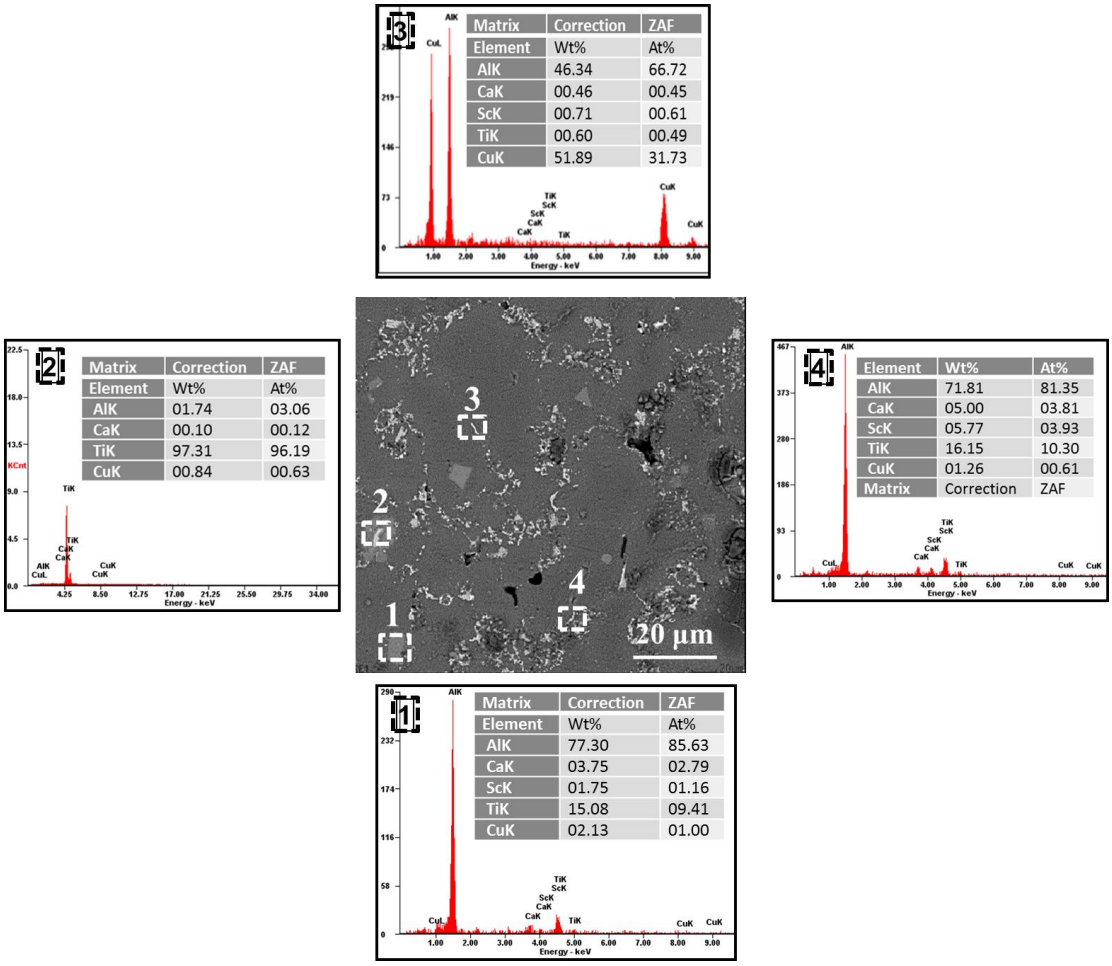

Fig. 5.5 Back scattered electro SEM micrographs showing the morphology of Sc added foam with corresponding EDS.

Based on energy dispersive X-ray spectroscopy (EDS), it is found that the lamellas and the triple junction like structures are mainly Al_2Cu which is also presented in the previous chapter with respective chemical composition (Fig. 4.4 b). From energy dispersive X-ray spectroscopy (EDS), it is observed that the bulky structure grey in colour (marked as no.1) consists of mainly Al-Ca-Ti (which is $Al_{20}CaTi_2$ as reported earlier, Edwin et al). From the micrograph, presence of porosity is observed, which appears black in the image, whereas, the

presence of some Ti is also observed (marked as no.2). Some black particles are also displayed in the back scattered image, which indicates the presence of oxygen (as reported in the previous chapter (Al-O).

The SEM image, EDS line scan and EDS elemental mapping of Cu, Sc, Ti, Ca and Al for the Sc added foam are shown in Figs.5.6, 5.7 and 5.8 respectively. The SEM image accompanying line scans of corresponding element (i.e. Al and Cu) for scandium added foam are shown in Fig. 5.6 (a) and (b) respectively. It can be seen that the coarse primary Al_2Cu is formed at the interface of the matrix in the Sc added foam, resulting in complex discontinuous, sharp-angled morphologies (Fig. 5.6 (b)–(d)). Fig. 5.6 (c) and (d) shows the elemental mappings of scandium added foam. A large number of lamellas and triple junction like structure are observed in the foam cell wall.

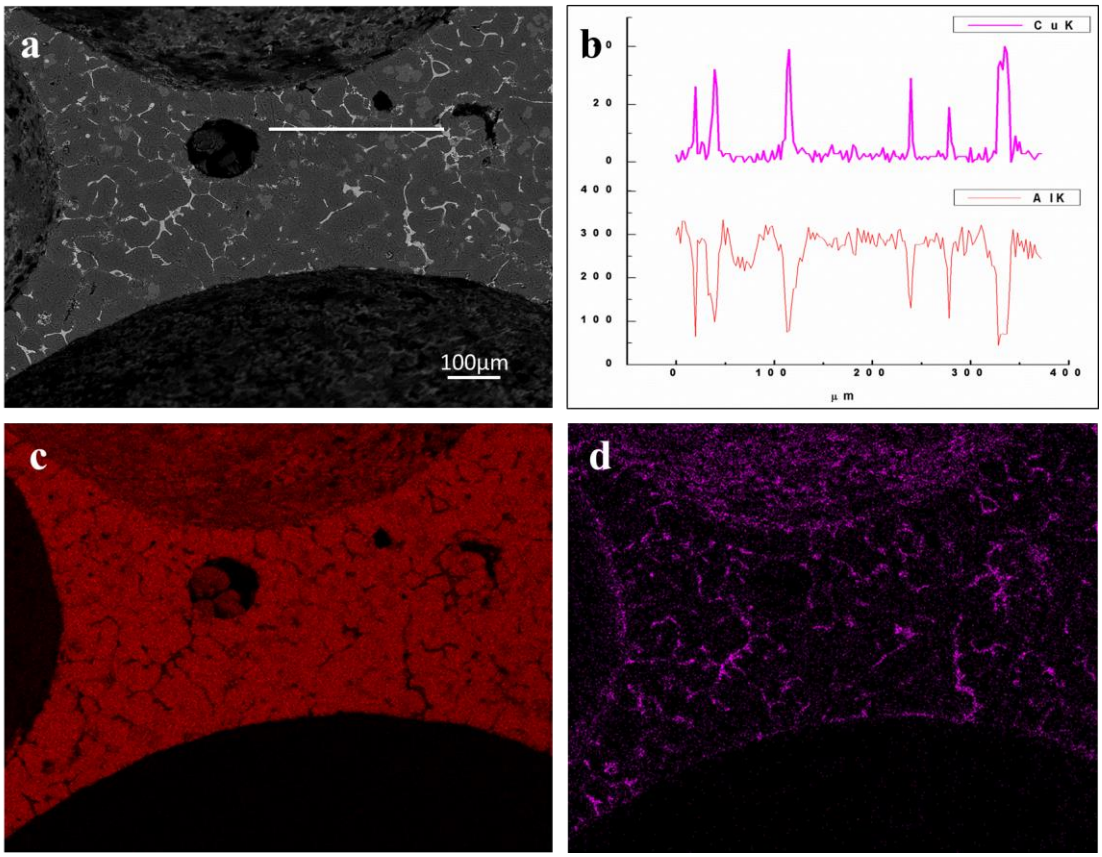

Fig. 5.6 SEM micrograph, (b) EDS line scan of Al and Cu, (c) EDS elemental mapping of Al and (d) EDS elemental mapping of Cu for investigated scandium added foam.

Elemental mappings in Fig.5.6 indicates that these lamellas are enriched with Al and Cu, which affirms that the lamellas in the alloy belongs to Al–Cu that in turn demonstrates that the Al_2Cu is formed at the grain boundaries (in the form of lamella and triple junction) of the alloy. Fig. 5.7 (a) shows SEM image of the cell wall microstructure of the scandium added foam with the corresponding line scan (Fig. 5.7(b)) and the element distribution (as Al (Fig. 5.7(c)) and Sc (Fig. 5.7(d)). However, distribution of Sc is not homogeneous in the alloy matrix (Fig. 5.7 (d)), which indicates that the major part of the scandium has been used for the dispersoids formation.

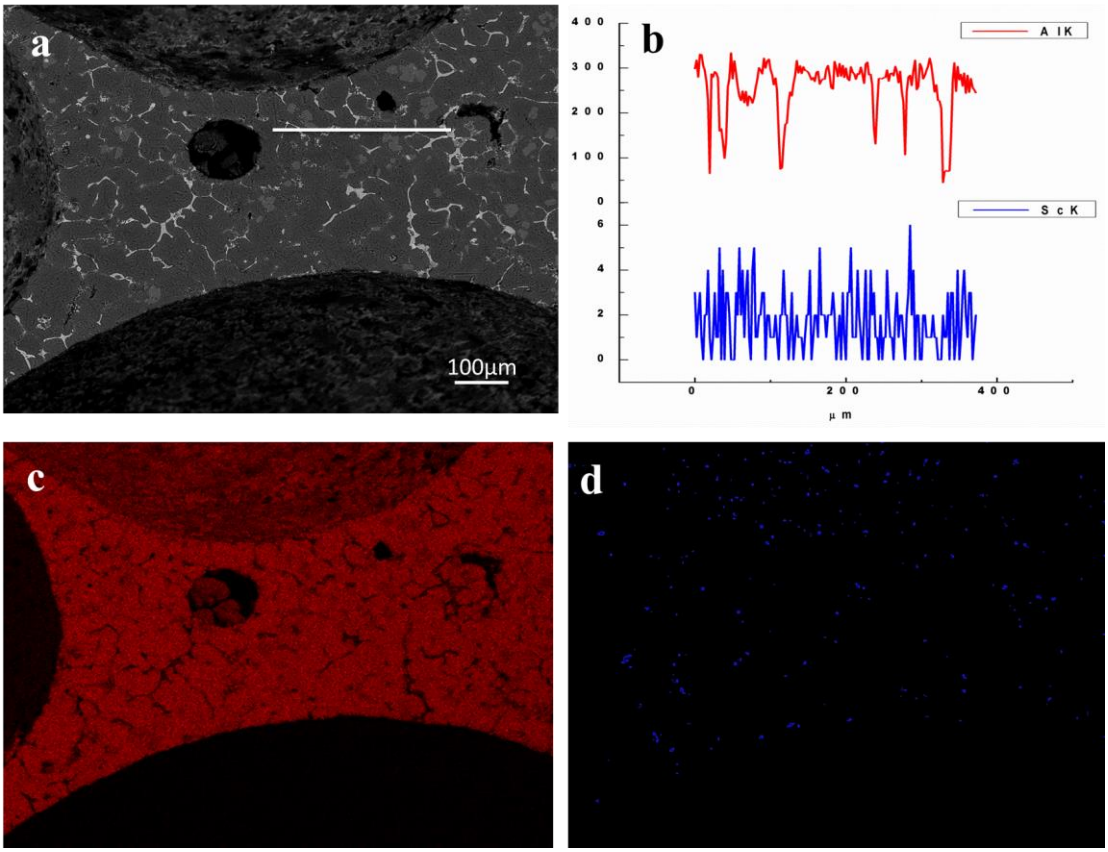

Fig. 5.7 (a) SEM micrograph, (b) EDS line scan of Al, Sc and (c,d) EDS elemental mapping of Al, Sc for investigated scandium added foam.

Fig. 5.8 (a), (b), (c), (d) and (e) shows SEM image of the cell wall microstructure with corresponding line scan and element distribution such as Al, Ti and Ca. It can be seen form Fig 5.8 (a) that there are plenty of second phase particles in the micrograph. These second phase particles are larger in size and distributed in the cell wall at the grain boundary, as well as, within the grain. However, distributions of these large particles are not homogenous (as shown in the Fig. 5.8 (c) and (d). From line scan it is found that Ca and Ti are distributed in the liquid matrix area and locate at the same place. The EDS line scan also confirms the formation of Al-

Ca-Ti containing phase, which again affirm the formation of the $Al_{20}CaTi_2$ and in agreement the earlier reported work (Raj, 2008).

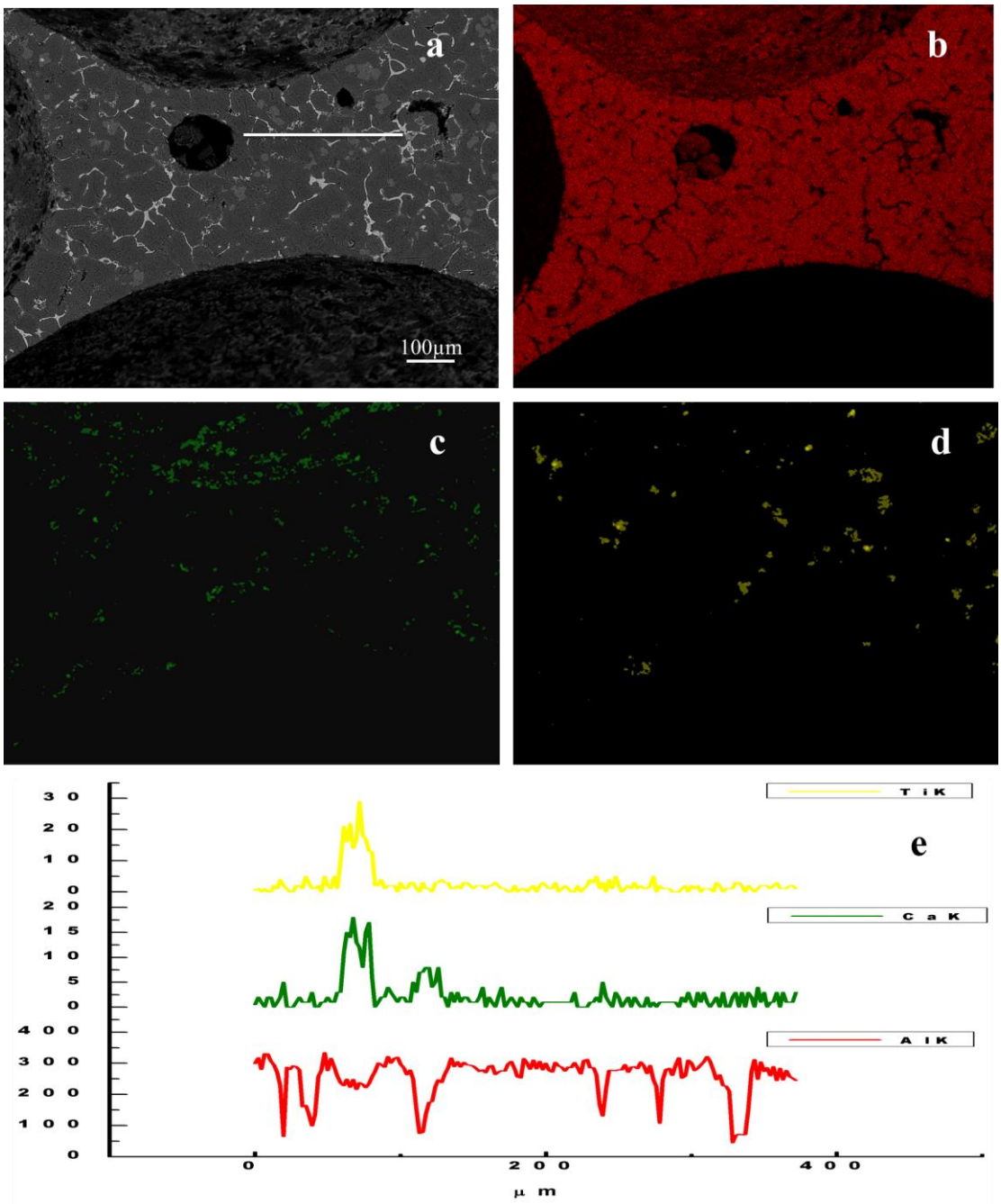

Fig. 5.8 (a) SEM micrograph, (b) EDS elemental mapping of Al, (c) EDS elemental mapping of Ca, (d) EDS elemental mapping of Ti and (e) EDS line scan of Al, Ca and Ti for investigated scandium added foam.

An overall microsturctural view with EDS line scan and elemental mapping of the produced scandium added foam is clear from above discussion. From above overview of the microsturctural studies, it is reasonable to state that the cell wall of the Al-Sc foam is different from the foam without Sc addition in terms of cell wall microsturctural featuring Al-Sc

dispersoids. Presence of the Al-Sc dispersoids with unique features (such as intermetallic crystalline structure and particle morphology) helps to regulate the structure and properties of the produced foam, more effectively than the foam without Sc addition.

In the present study, hyper-eutectic composition is used so that further processing is not required to improve the properties, as less than 0.55% (i.e. hypoeutectic composition) scandium addition results into dendritic structure and required further post processing to reduce the dendritic structure (Huang et al., 2012).

5.2.3 X-ray Diffraction Analysis

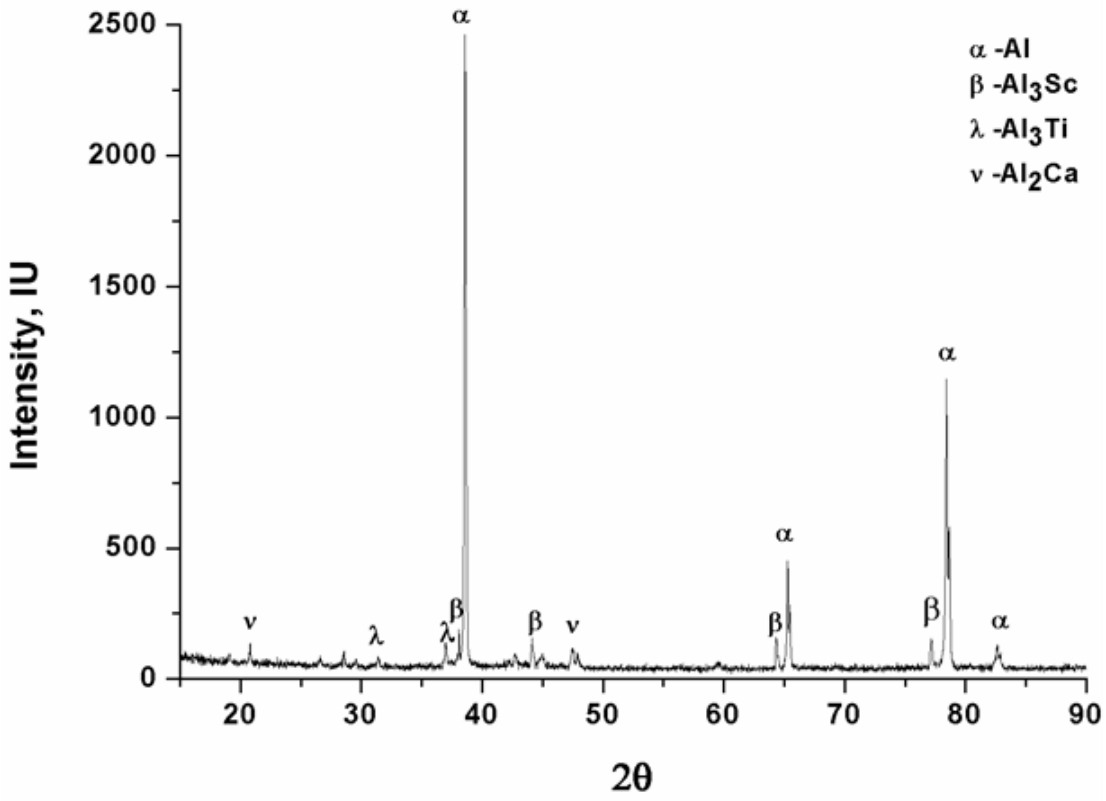

Fig. 5.9 The powder XRD pattern of scandium added foam.

The XRD pattern of the synthesized aluminium foam is shown in Fig. 5.9. The measured X-ray integrated intensities of various planes of Al is in agreement with the computed JCPDS standard data. Some of the peaks in the XRD pattern belongs to the primary solid solution of aluminium (Raj, 2008). Some other peaks with low intensity has also been observed in the XRD pattern, which indicates a small volume fraction of the other elements or their fine size distribution in the base aluminium matrix. The presence of Al_3Sc, Al_2Ca and Al_3Ti is shown in Fig. 5.9.

5.3 Effect of the variation in the scandium content on the grain size

The optical micrographs of produced foam samples without scandium and with scandium addition are shown in Figs. 5.10 (a-d).

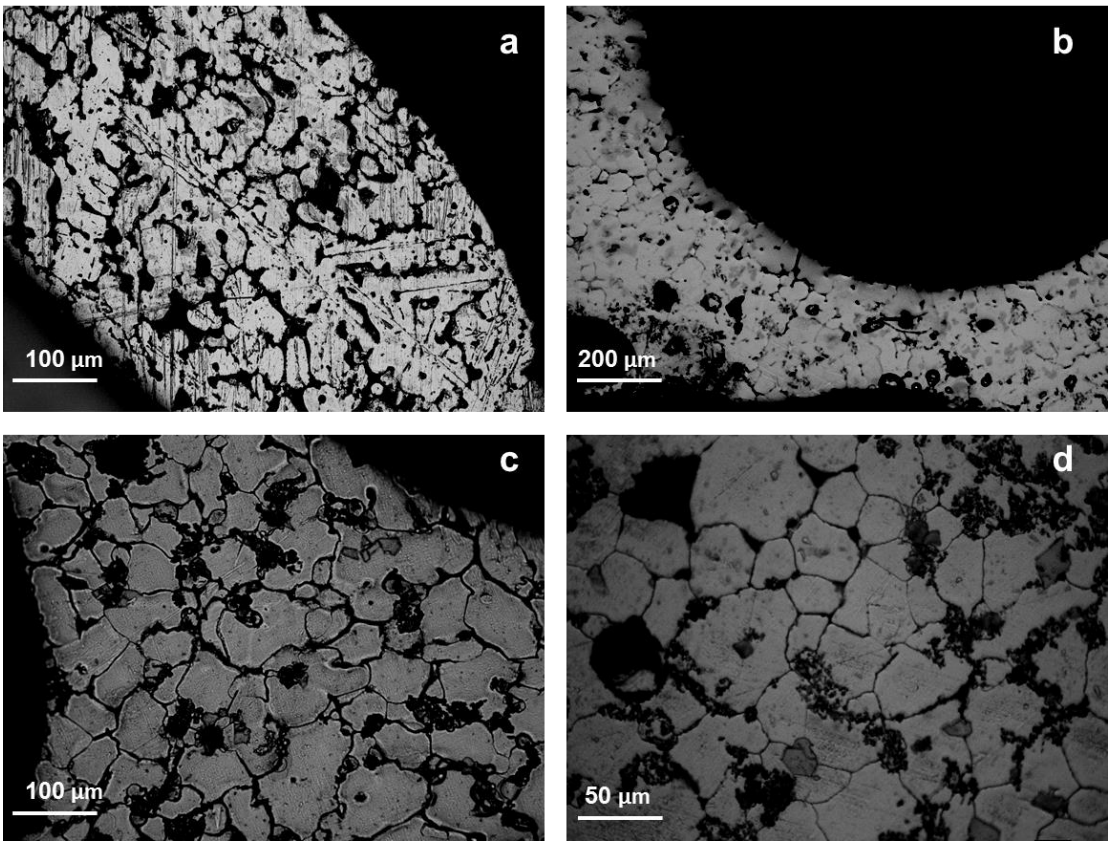

Fig. 5.10 Optical micrograph of the foam cell wall indicating grain size for (a) 0% Sc, (b) 0.6%, (c) 0.8% and (d) 1% Sc addition.

Table 5.2 Variation in average grain size of Al based foam with scandium addition.

Sample condition v/s Grain size, µm			
As-cast	Addition level of scandium, % wt.		
	0.6	0.8	1
82±4	69±3	53±5	30 ±3

For each addition level of scandium and corresponding grain size is presented in Table 5.2 and Fig. 5.11 (error bar length in the graph is indicate the standard deviation in the grain size taken at the different location of micrograph). As observed from the Table 5.2, the as-cast foam (without scandium addition) was observed to have an average grain size of 82µm (Table 5.2). However, increase in the addition level of scandium results in the grain size reduction as presented in Table 5.2. These micrographs were used to carry out the grain size measurements. The mean linear intercept method (Pickering, 1975) is used to calculate the average grain size.

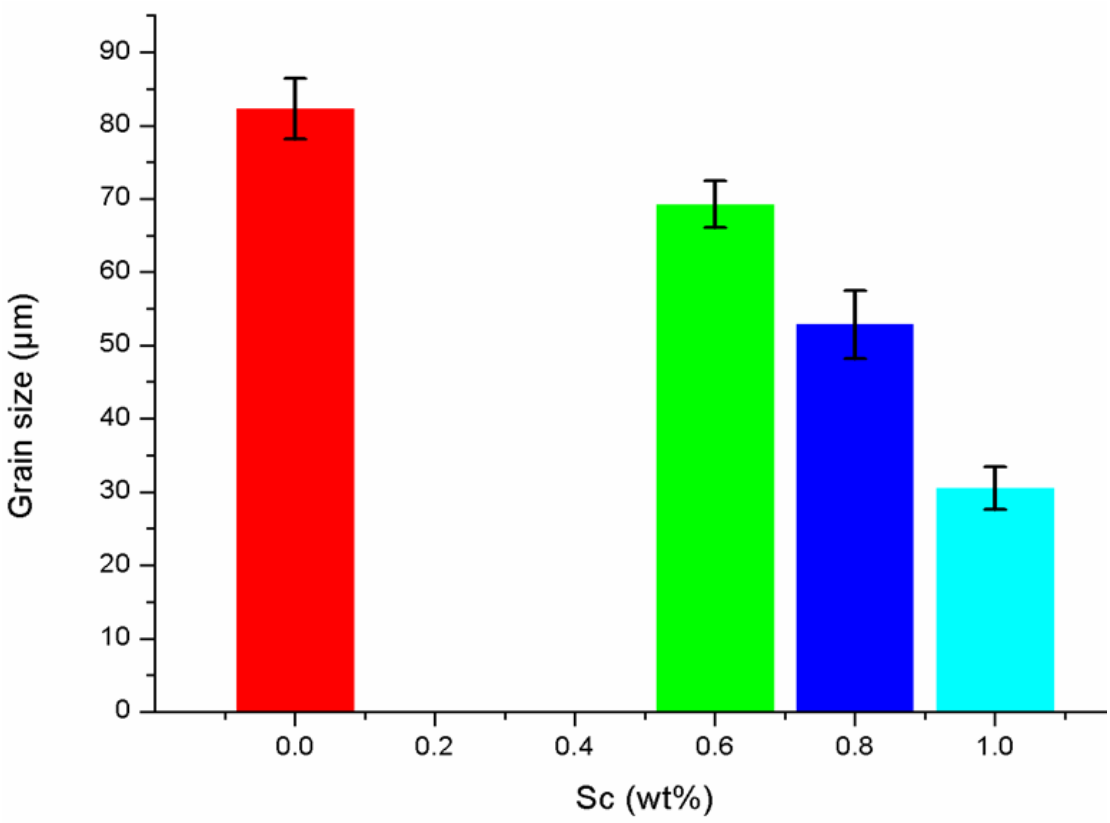

Fig. 5.11 Effect of Sc addition on the average grain size of foam.

In the present study, it has been observed from the micrograph that a maximum reduction in grain size has been achieved at the highest addition level (1 wt. % Sc). At this level, there is approximately 31% of the reduction in grain size is achieved as compared to the foam produced without scandium, resulting in an average grain size of 30 µm. Earlier studies for aluminium alloys showed that an increase in the Sc content in the alloy results in the grain refinement as scandium is the good refiner among the other (Monachon et al., 2011; Tolley et al., 2005; Van Dalen et al., 2005; van Dalen et al., 2011). Addition levels of scandium up-to hypoeutectic (i.e.<0.55 wt.%) composition did not cause a significant change in grain size due to the presence of dendritic structure in the alloy which is further required thermal treatment for significant improvement. Norman et al (Norman et al., 1998) also investigated the effect of the

scandium addition on the grain size of aluminium alloy and found that addition level beyond hypoeutectic composition is required to form the Al_3Sc particle during solidification, just after casting which mainly worked as grain refiner. It has been reported in the literature that 1% of the grain refiner addition is more effective and beyond this level of addition, impurities are observed in the alloy matrix (Greer, 2003).

From the above result and subsequent literature support it is adequate to state that the reduction in grain size mainly attribute to the change in growth mechanism from dendrite to nucleation and growth. The scandium intermetallic grains present in the master alloy serve as nuclei. For more clear reasoning behind the grain refinement, study has been done on lower magnitude, for this, TEM analysis is employed. TEM specimens of the scandium added foam at different locations were prepared. In the TEM study, information has been collected to support the findings of the work.

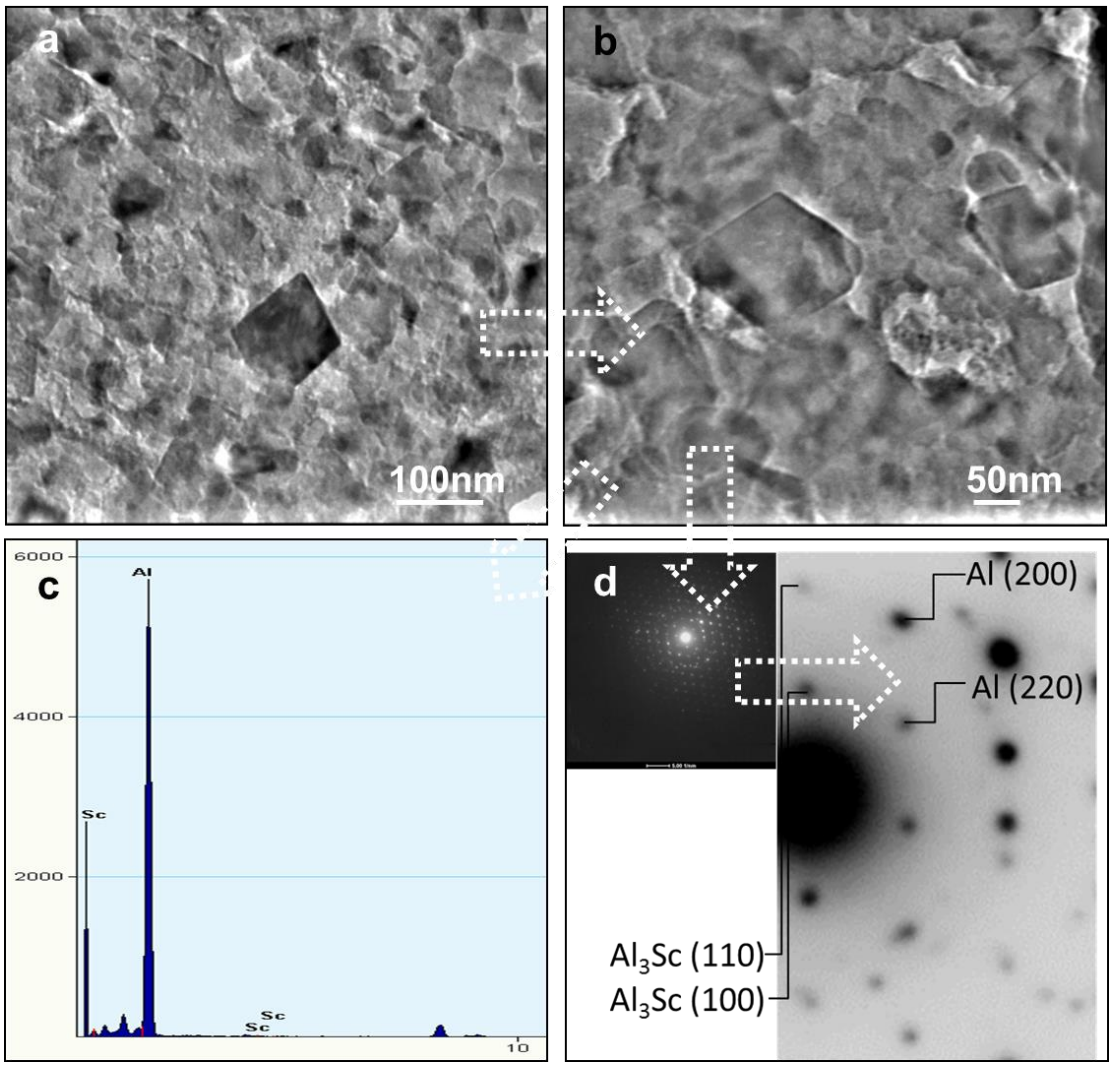

Fig. 5.12 Bright field TEM image ((a) and (b)), SAED pattern with indexing (c) and STEM EDS of scandium Added foam.

TEM images at two different location and magnification refer to the structure of the scandium added aluminium foam cell wall material between the intermetallic particles seen in the SEM micrographs. Figures 5.8 a), b), c) and d) shows the bright field TEM micrograph, SAED pattern and STEM EDS of the scandium added foam sample respectively. The bright field TEM micrograph (as shown in the Fig. 5.8 (a) and (b)) disclose the presence of the fine aluminium grain substructure on the length scale of 100 and 50nm. The diffraction pattern of the scandium added foam confirms the multi-crystalline nature on a fine scale. Through SEM analysis, it is observed that the grain size is reduced after scandium addition, which further confirmed through TEM analysis.

5.3.1 Inference from microstructural studies

As an overview of the results obtained for scandium added foam, changes in microstructure in the foam of grain size reduction has been observed at different level of scandium addition. The addition of scandium results into the reduction in grain size, related to the distribution of alloying elements and their distribution. Furthermore, increase in the scandium further refine the grain effect is observed on refining aluminium foam. For the effect of grain refinement, it is suggested that available primary nuclei site act as nucleation sites which stimulate nucleation at the time of solidification reduces the melt surface tension and following activation of microscopic refinement.

By comparing the results of produced foam at the different level of scandium i.e.0.6, 0.8 and 1wt. %, it is inferred that in the foam (0%Sc), where the scandium intermetallics are not available, growth mechanism is dendritic, although oxides are available as nucleant which is formed on the surface to nucleate α-Al. However, in scandium added foam, the growth mechanism is changed from dendritic growth to nucleation and growth, due to formations of Sc intermetallic which serve as nuclei and refinement is considerable. At 1wt. %, the amount of Sc intermetallic (which acts as nuclei) is optimum which in turn leads to reduction in grain size. The effect of various amounts of Sc has been tested under different microscopic techniques and it is concluded that Sc additions change the grain size (i.e. reduce). In the bulk alloy system, it was suggested that the scandium decomposes directly to the equilibrium cubic Al_3Sc phase that is fully coherent with aluminium matrix. This structure alleviates homogeneous nucleation and slows growth of fine, uniformly distributed particles. Finding of the microstructural characterization of the scandium added foam confirms that the results obtained are well versed with previously reported work for bulk alloy system ((Gao and Chen, 2010; Jordens et al.,

2013)).Therefore, much enhanced grain (fine) structures are observed after scandium addition, which is attributed to the nucleation and growth mechanism.

5.4 Mechanical Property Analysis

In the section 5.2 and 5.3, the effect of scandium addition on the macrostructural and microstructural behaviour of Sc added foam has been described. In general, mechanical property study of metallic foams is related to the load bearing capacity as from microsturctural behaviour it is expected that the cell wall of the Sc added foam produced have sufficient mechanical strength (attributed to grain refinement) and it can sustain more load without any damage and subsequent failure. To evaluate the mechanical strength after Sc addition, Sc added foam sample tested under the compression load. The course of action used to choose the sample i.e. number of sample for each test, dimension and the subsequent calculation of the mechanical properties (i.e. energy absorption capability, plateau stress, etc.) are given in the previous chapter. It should be noted that the process variable decides the morphological and microstructural features of foam, which are in turn responsible for the improvement in mechanical properties.

Next section comprises of the mechanical property evaluation to assist the changes found in microstructure, after scandium addition with the help of results obtained with mechanical testing. In the initial part, microhardness of produced foam and scandium added foam (different addition) are compared. Finally, assessment of the mechanical properties of the scandium added foam in comparison with the s-cast foam was carried out based on the experiment results obtained. Hence, the main focus of the investigation is the structure-property correlation. The following sections describe the mechanical properties investigated in the present study.

5.4.1 Microhardness

Vickers hardness number (VHN) is measured at the parameters used in the previous chapter for the sample without scandium and with the different amount of scandium (0.6, 0.8 and 1 Wt %).

The effect of scandium addition on the metallic foam in terms of the microhardness values is shown in Fig.5.13.As observed from the Fig. 5.13, as the amount of scandium is increased, the hardness of the produced foam also increased at a higher rate (0.6 wt. % Sc), which is moderate at the 0.8 wt. % Sc addition and maximum hardness is found at 1wt% of Sc. From the hardness value of the foam without Sc and scandium added foam, it is observed that

the hardness value of scandium added foam is 47% higher than the foam sample without scandium.

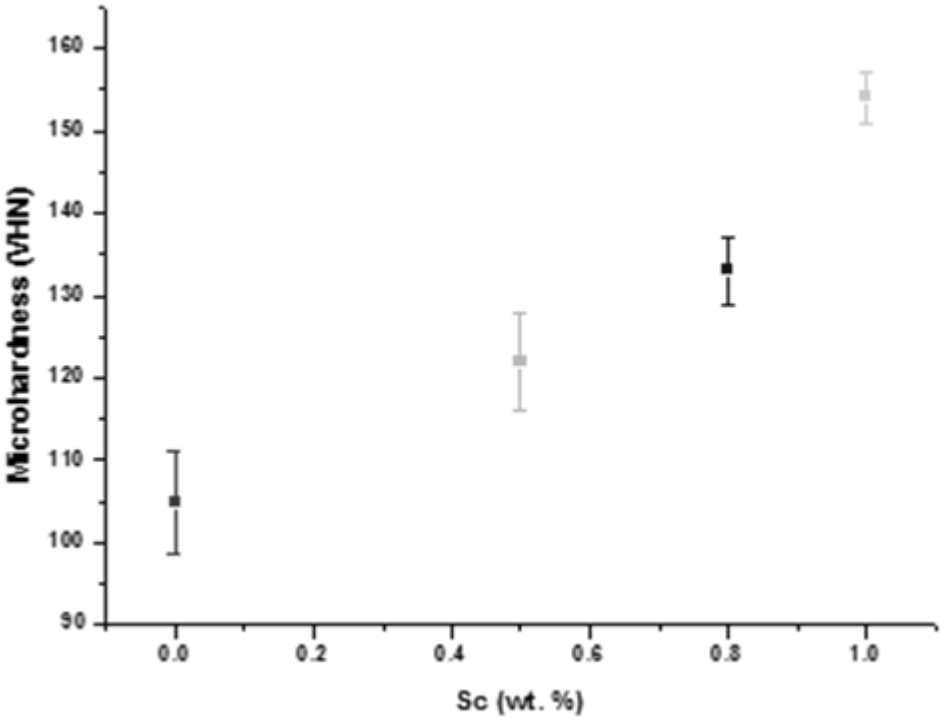

Fig. 5.13 Variations in microhardness of Al base foam with Sc addition.

Therefore, it can be easily concluded that the grain refinement results in the increase in hardness value, which further results into strengthening of the alloy.

5.4.2 Quasi-Static Compression Test

The aluminium foam with scandium master alloy has been produced. The complete detail study and discussion on the microstructural behaviour of the cell wall material with respect to level of scandium addition has been done in the previous section. From the microstructural analysis, it is found that scandium addition greatly affect the cell wall microstructure specially grain refinement. It is expected that the change in microstructural behaviour should contribute in compressive behaviour.

As discussed previously, when the foam material undergoes compression, it is observed that the collapse of the foam cell progress in the layer-by-layer from one end until full densification occurs. The compressive stress-strain curves are obtained by plotting the applied load divided by the original specimen cross-sectional area. Fig. 5.14 shows the stress-strain curves obtained from tests executed on samples of scandium added foam at different level of scandium addition i.e. 0.6, 0.8 and 1% respectively, with a reference curve of the foam produced without scandium. Table 5.3 demonstrates a summary of the foam properties i.e.

yield stress, plateau stress and energy absorption capacity, obtained from the stress strain curves and calculated, as previously described in chapter 4 in section 4.4.2.

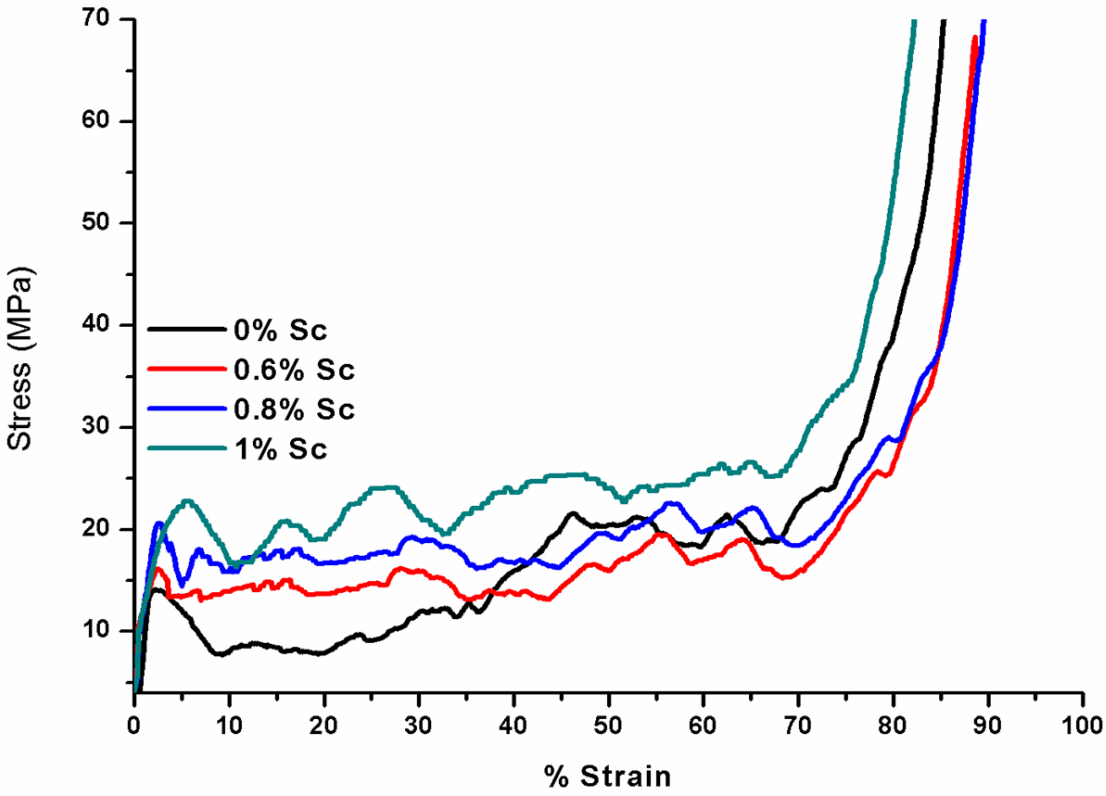

Fig. 5.14 Compressive behaviour of the foam without Sc and with Sc added sample at room temperature.

From Fig. 5.14, it is clear that the quasi-static stress-strain curve is different for different condition. From the Fig. 5.14, it can be clearly visualized that after the scandium addition results into increase in the yield stress, plateau stress and energy absorption capability considerably (Table 5.3). It can also be observed from the curve that the compressive properties are lowest for foam produced without scandium. These values are intermediate for 0.6% scandium added foam and another interesting aspect worth notice is in the case 0.6% and 0.8% scandium is more or less similar, whereas, the trend of the curve in 1% scandium is different.

Table 5.3 Summary of the mechanical properties for the Al base foam (without Sc and with Sc addition) samples.

Level of Sc addition	Average grain size (mm)	Yield strength (MPa)	Plateau stress (MPa)	Energy absorption (MJ/m^3)
0%	3.16±0.16	14.0±4.0	10.2±3.3	13.2±3.1
0.6%	4.43±0.10	16.2±1.2	14.1±1.6	15.0±2.5
0.8%	5.02±0.08	20.6±5.0	17.1±1.5	17.1±2.6
1%	5.16±0.07	22.8±3.4	20.7±2.8	19.3±1.8

Improvement in these compressive properties can be attributed to grain refinement, which leads to increase the grain boundary area which acts as a barrier to the dislocation motion when applied load and result to improved performance.

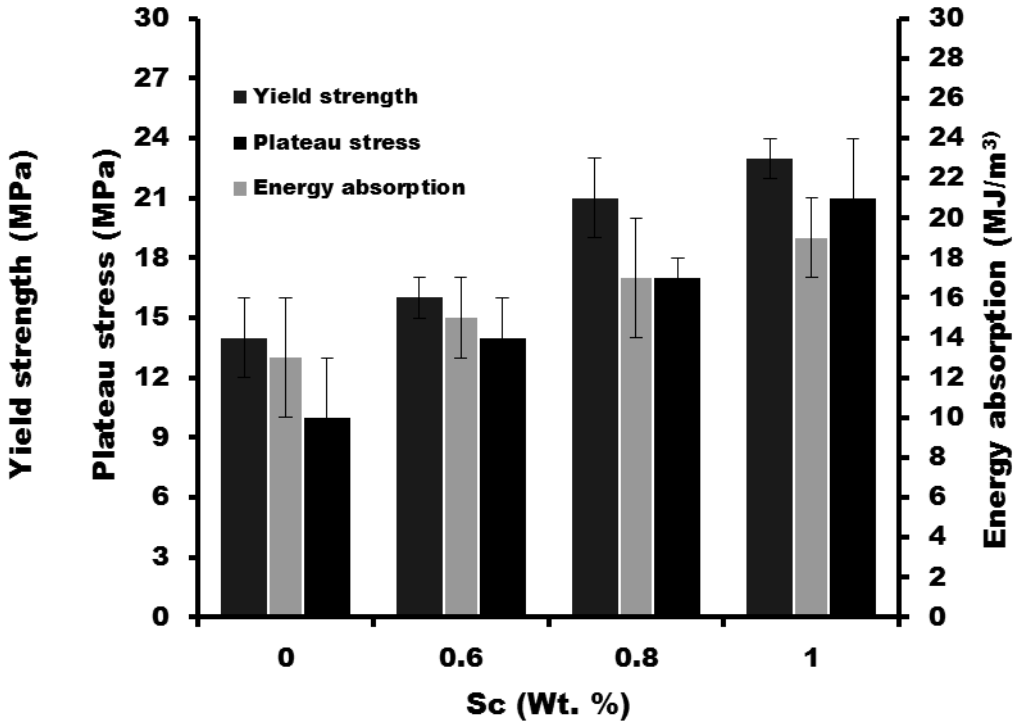

Fig. 5.15 Variations in the compressive properties of Al base foam with Sc addition.

Among all the curves, foam with 1% scandium shows the highest value in compressive test. This follows from its higher grain refinement content (Sc intermetallic content) and more refined microstructure (Figs. 5.10 (a-d)).

Fig. 5.15 shows the variations of compressive properties with respect to level of Sc addition. It is observed that for foam without Sc addition yield strength is 14 MPa whereas plateau stress and the energy absorption capacity are 10 MPa and 13 MJ/m^3 respectively. As the level of Sc addition increased, there is an increase in yield strength, plateau stress and the energy absorption. The improvement in yield strength, plateau stress and energy absorption capacity are 62%, 100% and 46% respectively. The Sc added foam showed substantial grain refinement, presence of the fine grain retards the dislocation movement and result in higher strength (as shown in Fig. 5.15).

It is evident from the literature that the Hall-Perch relation (equation 5.1) is used to explain the relationship between the yield strength and the average grain size. Yield strength of the foam with respect to variation in grain size is shown in the Fig. 5.16. Yield strength increased as amount of Sc addition increased (from 0 to 1 wt. %), yield strength for foam without Sc is 14 MPa whereas it is 23 MPa for Sc (1 wt. %) added foam. It has been explained using the Hall Petch equation which is given in equation 5.1. (Hall, 1951),(Petch, 1953).

$$\sigma_y = \sigma_o + kd^{-1/2} \ldots\ldots\ldots\ldots\ldots\ldots\ldots\ldots\ldots\ldots (5\cdot1)$$

Where; σ_o is the friction stress representing the resistance of the crystal lattice to dislocation movement, 'k' is the locking parameter that measures the hardening contribution made by grain boundaries and 'd' is the average grain diameter.

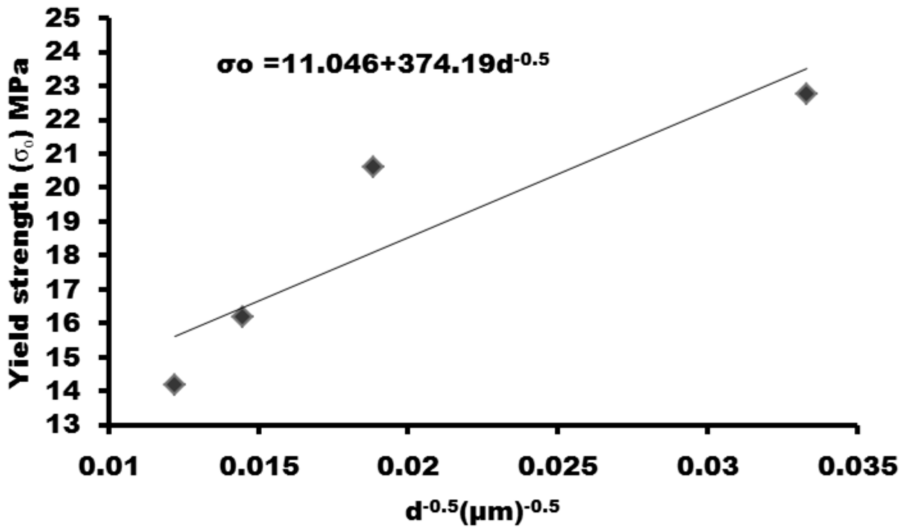

Fig. 5.16 Variations in yield strength of the Al base foam with grain size at different amount of Sc (0-1 wt. %) addition.

It can be observed from the Fig. 5.16 that there is a good fit of the data in accordance with the Hall Petch relationship. The obtained results indicate the non-basal slip as dominant mechanism in plastic deformation of cell wall structure at room temperature.

Again, these findings supports the phenomenon that the grain refinement is helpful in the improvement of mechanical properties of foam, as the compressive properties of scandium added foam demonstrate the same which encourage and prove the dependency of the properties on the cell wall microstructure. In order to explain the ductile/brittle nature of foam in all conditions, deformed samples were sectioned and examined under SEM.

5.4.3 Fractography

Fractography provide information about the nature of the fracture. In the previous chapter it is discussed that fractography in the present work is referred to the interpreted compression test (compression test of the sample up to 30% compression) and then SEM of the fracture sample has been taken, to analyse the fractured surface. Back scattered SEM image of the one of the fractured sample from interrupted compression is shown in Fig. 5.17.

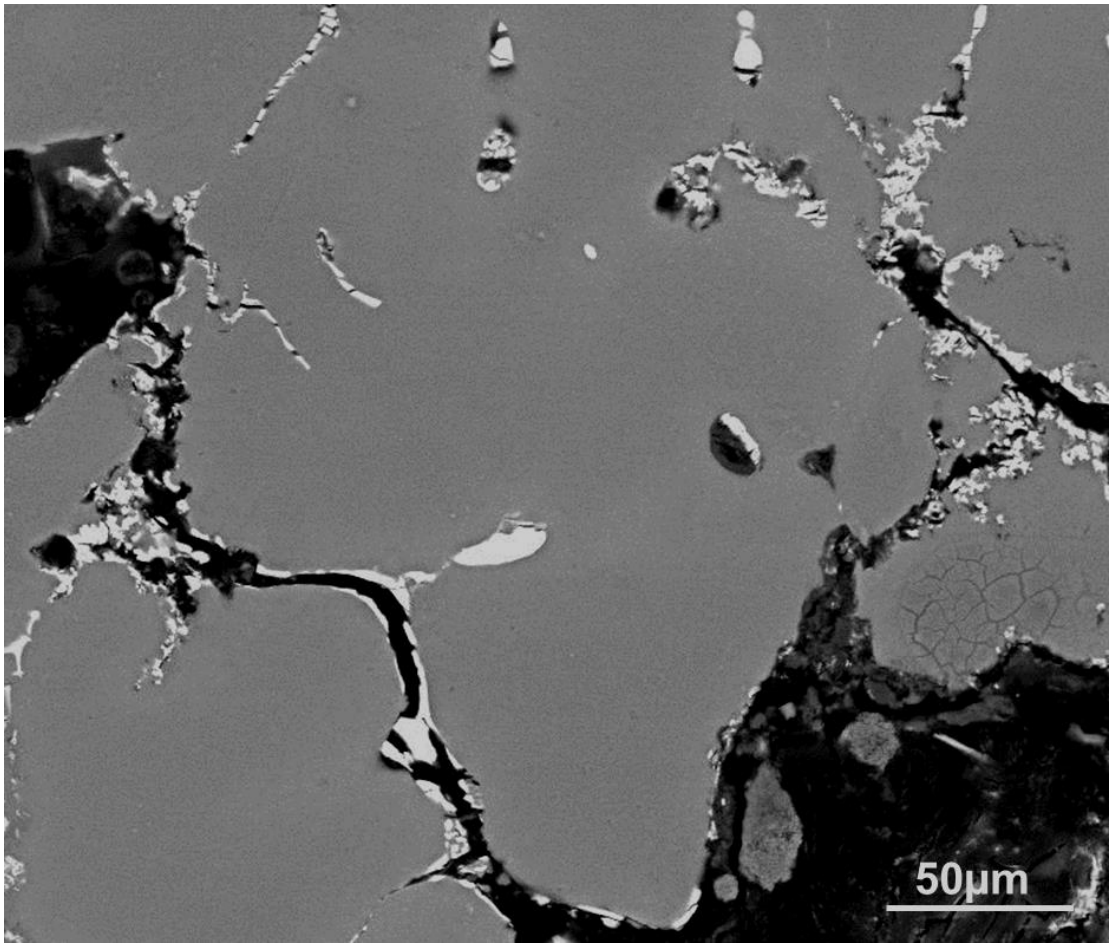

Fig. 5.17 SEM micrograph of fractured sample of scandium added foam.

From the micrograph (Fig. 5.17), it is observed that the fracture surface of scandium added foam, consist of lamellas of Al_2Cu, as well as very small dispersoids of Al-Sc intermetallic of different size, which indicate that the fracture is predominantly brittle in nature and crack start from the cell wall but the propagation is not that much severe as formerly observed in the foam produced without scandium.

5.5 Summary

1. Scandium addition has substantial effect on the microstructure i.e. addition of the scandium greatly modify the microstructure through refinement of cell wall microstructure, in terms of grain refinement.
2. As scandium amount is increased to 1%, the average grain size decreased to 30 µm which is 31 % lower than the foam without Sc.
3. The micro-hardness (VHN) of the scandium added foam enhanced with the increase in scandium addition this phenomenon of increasing is mainly attributed to the Sc intermetallic which leads to fine grain structure.
4. In the present study the different amount of scandium used to produce foam, maximum micro-hardness is observed at the 1%wt. of scandium and that is approximately 52% higher than the foam produced without scandium. This phenomenon i.e. increases in the hardness attributed to the Hall-Petch strengthening mechanism, which is mainly grain refinement produced after scandium addition.
5. From the quasi static compression test results, it is found that that the yield stress, plateau stress, and energy absorption capacity are improved after the addition of scandium as compared to foam without scandium and further improved as the addition level of scandium increases. The compressive property enhancement can be interrelated to the morphology of the cell wall, its grain size, and the presence of secondary intermetallic phase and dispersoids.

CHAPTER 6: MICROSTURCTURAL AND MECHANICAL BEHAVIOUR OF Al BASED FOAM: EFFECT OF REINFORCMENT

Introduction of reinforcement (with material having high strength and high stiffness as compared to the matrix material), is generally used to improve the specific strength of the alloy. Improvement in the properties is obtained through the alteration of the microstructural feature and mechanical behaviour.

In the previous chapters, it has been exhibited that the closed cell aluminium foam properties can be enhanced through the thermal treatment and grain refinement. To take it one step further, it is a good idea to introduce short steel fibre in the melt as a stabiliser, which is also used as a reinforcement to produce closed cell aluminium foam.

Present chapter aims to investigate the effect of copper coated short steel fibre (CCSSF) reinforcement in closed cell aluminium foam under axial compression load. It includes raw material characterisation, synthesis of the closed cell foam (reinforced by CCSSF), followed by microsturctural and mechanical characterisation. Microstructure characterisation enables the proper understanding of the structural behaviour of the produced form. The obtained result has been compared with the foam (without reinforcement) to evaluate the effect of CCSSF addition on the foaming, as well as, on the structural and mechanical behaviour. Moreover, the optimum holding time were identified through pilot experiment (60-120 sec.) and rest of the casting is done on the optimum holding time (90 sec.) and different wt.% (0.5-1.5) of CCSSF addition. Finally, chapter concludes with the outcome of the results and correlation among the microsturctural features, as well as physical and mechanical properties.

6.1 Characterisation of SSF

6.1.1 Microstructure of SSF

Shape and size (short steel fibre in present work) are the main fundamental characteristic of raw material used for reinforcement and stabilisation. In a real mass of the SSF, all fibres used for reinforcement may not have the exactly same size even though the shape may be similar. In the present study, the initial reinforcement SSF (which is used in phenolic brake pads) used for reinforcement were procured from Guru Kripa Steel Wool Industries Pvt. Ltd., New Delhi. The SSF used in the present work for reinforcement and stabilization is

approximately 5.-10 mm. in length with an average diameter of 50 µm. The chemical composition of the SSF is tabulated in the Fig. 6.1 (d) with a nominal density of 7.83 g/cm.^{3}.

The morphological study of SSF has been done using SEM. The secondary electron image of the SSF is shown in the Figs. 6.1 (a), (b), (c) and (d), which are explained in the context of their size, shape and surface morphology. Fig. 6.1 (a) shows the low magnification secondary image of the SSF which shows the appearance and length of the SSF. To reveal the shape and clear surface morphology of the SSF, image is further magnified, which shows the shape and clear surface appearance (Fig. 6.1 (b)).

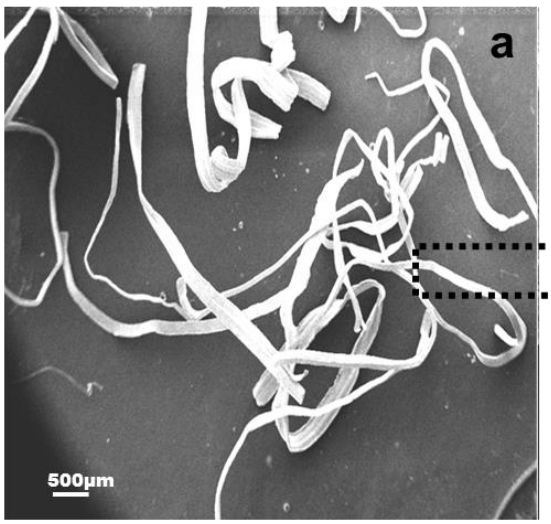

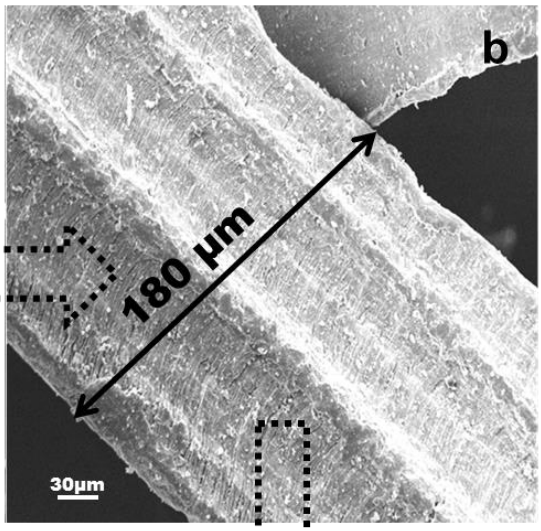

Element	wt.% c
C	0.38
Mn	0.52
Si	0.10
S	0.02
P	0.024
Fe	Bal.

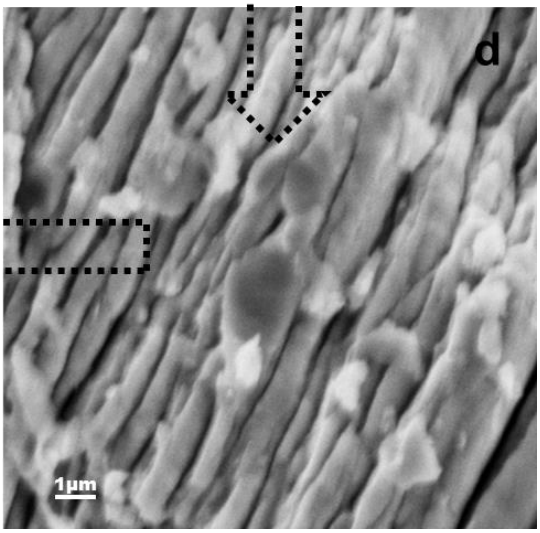

Fig. 6.1 The SSF morphology: (a) Low magnification secondary electron micrograph shape of the fibre (b) higher magnification image shows the actual shape, angular shape helps in stabilization of the foam (c) higher magnification image of the surface of the SSF, morphology of the surface shows the faceted surfaces helpful in wetting at the time of casting (d) composition of the SSF (wt. %).

From Fig 6.1 (b), it is clear that the surface of the SSF is angular in shape with rough faceted appearance. To observe the surface morphology of the SSF, image is further magnified (shown in the Fig. 6.1 (c)), which shows that the surface of the SSF is faceted. The angular shape and the faceted surface of the SSF is a major contributing factor, when it coats with copper faceted surface also improves the wetability and maintains the integrity and strength of the alloy. It is also expected that the SSF help greatly to stabilize the foam, when it added to the melt, as the shape of the fiber assist in particle interlocking and prevent drainage of liquid metal during processing.

To minimize the interface reaction at SSF and aluminium interface, a copper coating has been done on the SSF by electroless coating, following the standard procedure (Cao et al., 2006; CAO et al., 2005). SSF without coating can be react with aluminium melt which may result into brittle intermetallic which demises the performance. Copper coating can also be help to improve the wetting behaviour of the fibre during casting process as Cu usually react with aluminium and form aluminium alloy. To affirm the decomposition of the Copper, CCSSF (copper coated short steel fibre), samples are further annealed for 2 hour in tabular furnace in H_2 environment.

6.1.2 X-ray diffraction (XRD) analysis of the CCSSF

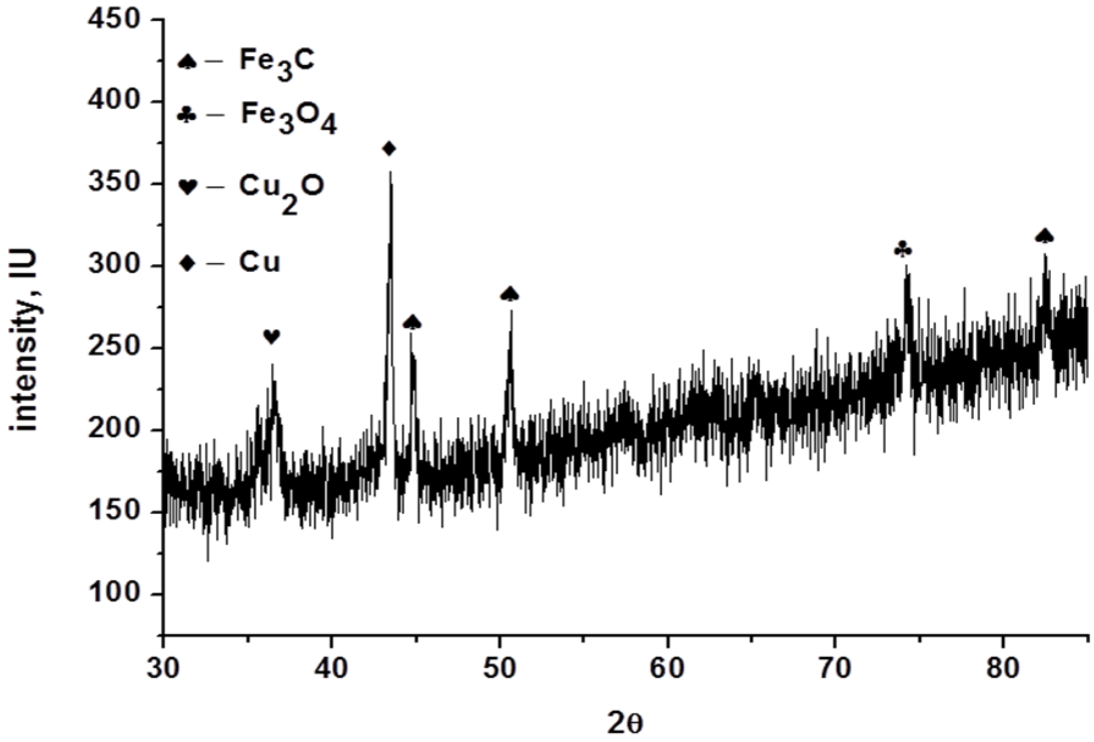

Fig. 6.2 The powder XRD pattern of CCSSF using Cu-Kα radiation

6.2 Macrostructural analysis of the CCSSF reinforced foam

CCSSF was found to be an effective stabilisation technique for forming good closed cell foam. It is capable to produce foams with good foaming height and porosity, similar to the foam produced without reinforcement, as well as, with several notable advantages. Foaming has been found to be the most effective with addition of CCSSF reinforcement. This produced foams having a fairly uniform cell structure. Low magnification digital macrograph of the foam casting with different amount of addition of CCSSF reinforcement and corresponding macrostructures of the cross section (parallel to the foaming direction) are shown in Fig. 6.3.

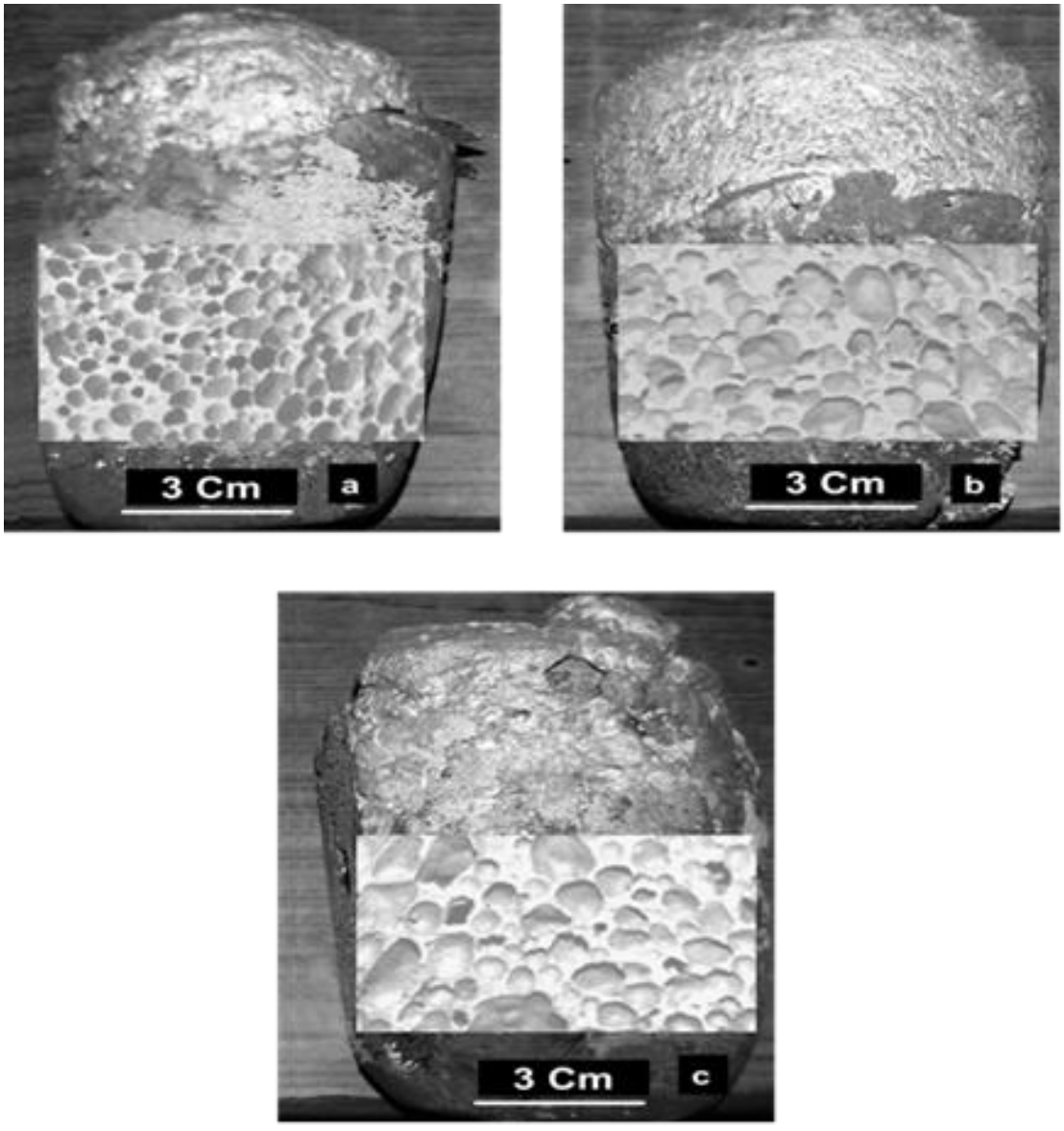

Fig. 6.3 Photographs and respective macrostructure of (a) 0.5 wt. %, (b) 1 wt. % and (c) 1.5 wt. % CCSSF reinforced foam.

It has been observed from the macrostructure that the stabilisation is improved after the addition of the CCSSF, results into stable structure with more or less similar porosity (except the point where the gas escapes and the foam collapses), which reflects in the foam of improved foaming height. It is expected that the stabilisation might be the result of low rate of drainage as CCSSF addition reacts with melt and results in the formation of secondary phases, which in turn retards the drainage.

6.3 Characterisation of the CCSSF reinforced foam

6.3.1 Introduction

It is well established fact that the stabilisation is the most considerable fact to produce good metal foam. Stabilisation has been achieved through the particle addition, particle either be added at the time of alloying or can be produced in-situ via metallurgical or chemical reactions. Stabiliser (ceramic or metallic) can be added in the foam of oxides (i.e. Al_2O_3, $MgAl_2O_4$, TiO_2 (Babcsán et al., 2004; Banhart, 2006; Chakraborty et al., 2011; Deqing and Ziyuan, 2003; Ip et al., 1999a; Kadoi et al., 2010; Körner et al., 2005a; Wübben and Odenbach, 2005)), carbides (such as SiC, B_4C, TiC (Golestanipour et al., 2011; Haesche et al., 2008; Haibel et al., 2006; Kumar and Gokhale, 2012; Mahmutyazicioglu et al., 2013; Mu et al., 2010b; Prakash et al., 1995; Ravi Kumar et al., 2014; Ravi Kumar et al., 2010; Yu et al., 2008)), borides (such as TiB_2), fly ash (Gergely and Clyne, 2000) and suspended solid particles (Babcsán et al., 2003; CAO et al., 2005; Gergely and Clyne, 2000; Guden et al., 2007; Kaptay, 2003; Mukherjee et al., 2010; Stocco et al., 2011,Mu, 2013 #893; Wübben and Odenbach, 2005). In recent years some researchers (Cao et al., 2008; Mu et al., 2011; Mu et al., 2010b; Mu et al., 2013) use carbon fibers in the melt for stabilisation purpose and found that the use of fibres improves the stability of the melt. Mu et al (Mu et al., 2013) find that the presence of fibres stimulates mechanical barrier and disjoining pressure within the melt.

Among the stabilisation technique used to minimise the drainage i.e. particle addition, fibre addition, intermetallic addition, fibre reinforcement is one of novel technique. Reinforcement technique through fibre addition is expected to be best suited technique to minimise the drainage because of its capability to render good stabilisation (through gravity abruption) which helps to minimise the local drainage. Characterisation of the SSF (previous section 6.2), revealed that the SSF have good wetting behaviour which also helps in the stabilisation of the foam.

In the present work, CCSSF reinforced foam have been characterised. Characterisation divided in two parts, first one consists of cell wall microstructure analysis particularly, cell wall

microstructure and phase formation, whereas, second part take care of its mechanical characterisation using XRD, SEM, EDS, X-ray mapping, microhardness and quasi static compression test.

6.3.2 X-ray diffraction (XRD) analysis

The XRD pattern of the CCSSF reinforced foam (as shown in Fig. 6.4) suggests that the produced closed cell foam cell wall mainly consists of $Al_{13}Fe_4$, $FeAl_3Si_2$ and Al_2Cu intermetallic phases which are present in all three CCSSF reinforced foam in a series of XRD patterns. The XRD patterns of (a) 0.5% CCSSF reinforced foam (b) 1wt.% CCSSF reinforced and (c) 1.5 wt.% CCSSF reinforced foam are mainly constituted by monoclinic $Al_{13}Fe_4$, orthorhombic $FeAl_3Si_2$, apart from these two main peaks which find in all the three type of foams, tetragonal Al_2Cu is mainly found in the 0.5% CCSSF reinforced foam.

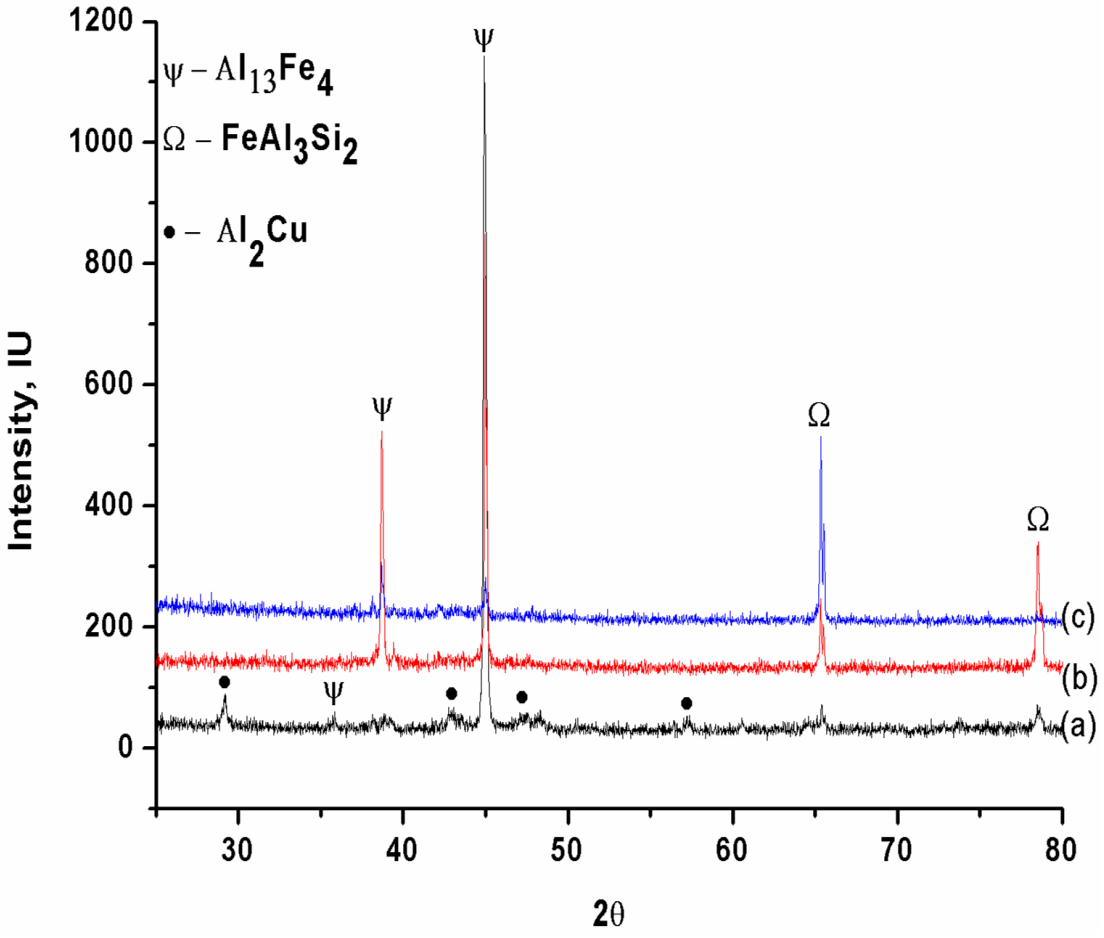

Fig. 6.4 The powder XRD patterns of: a) 0.5 wt. %, b) 1 wt. % and c) 1.5 wt. % CCSSF reinforced foams.

6.3.3 Microstructure analysis of the produced CCSSF reinforced foam

The master alloy (6061+ 4 wt. % Cu) is used to prepare metal foam, for better foamibility, foam is reinforced with varying amount (0.5-1.5 wt. %) of CCSSF, which is expected to help in improve the stability of the foam. Optical micrographs (at different magnification) of the CCSSF reinforced (0.5, 1 and 1.5 wt. %) foam are shown in the Figs. 6.5, 6.6 and 6.7.

From the optical micrograph of 0.5wt % CCSSF foam (as shown in Fig. 6.5(a), (b), (c) and (d)), it is observed that the fibers in the foam of intermetallic (intermetallic phases produce with the reaction of CCSSF and aluminium melt, numbered as 1) are distributed in the alloy matrix with Al_2Cu lamellas (numbered as 2) and Al-Ti precipitates (numbered as 3).

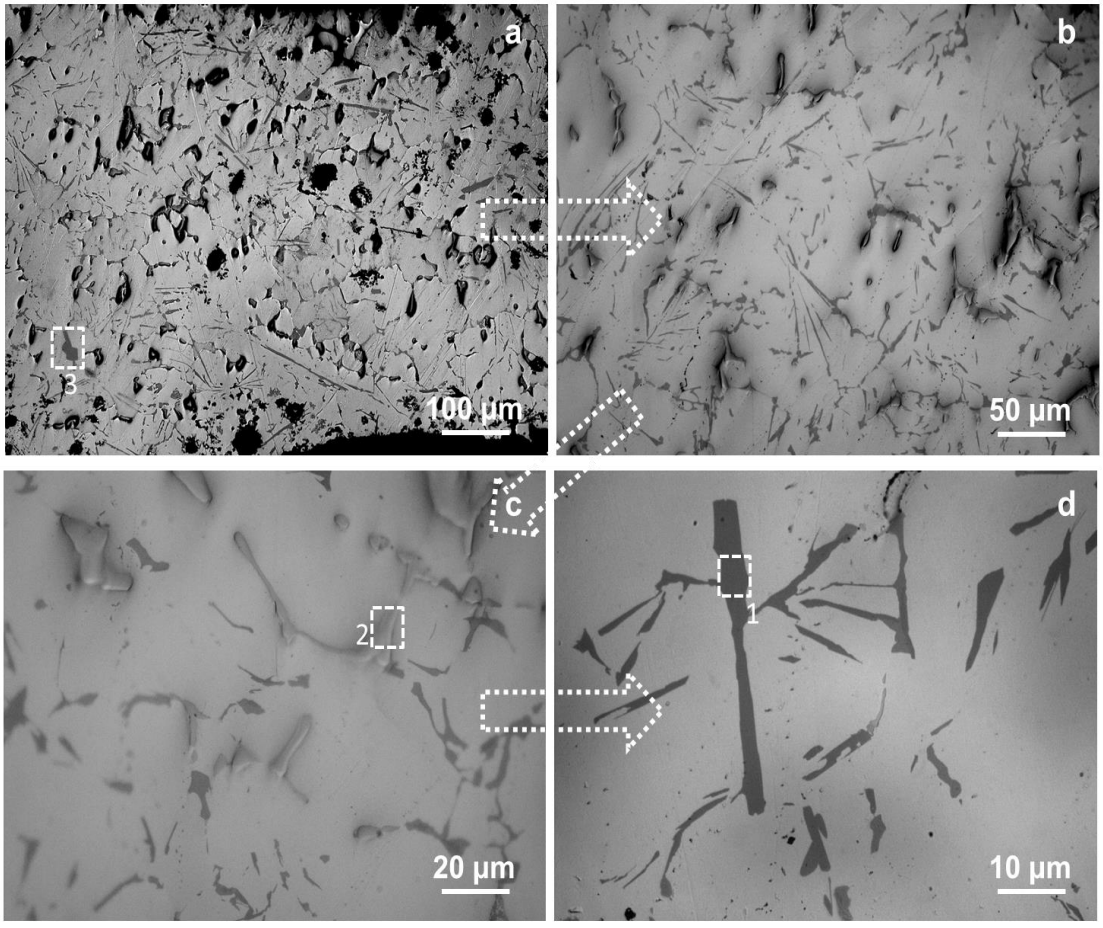

Fig. 6.5 The 0.5 wt. % CCSSF reinforced foam morphology: (a) Low magnification optical micrograph represent overall view of the cell wall (b) higher magnification for more clear morphology (c) higher magnification image of the plate like structure mainly Al_2Cu (d) higher magnification image of the plate like structure mainly represent the fibre (intermetallic foam when fibre react with Al melt).

Similar to the 0.5 wt. % CCSSF addition, optical micrographs at different magnification of the 1 wt. % CCSSF reinforced foam are shown in Figs. 6.6 ((a), (b), (c), and (d)). From the optical micrographs, it is observed that the microstructure is more or less similar to the 0.5 wt. % CCSSF reinforced foam, except amount of fibre intermetallic, which is clearly visible in Fig. 6.6 (c). From Fig. 6.6 (d), it is observed that the fibres are finer, as well as, the amount of the fiber intermetallic is increase with increase in the amount of reinforcement i.e. from (0.5wt. % to 1wt. %). It is also observed in the XRD analysis part that 1 wt. % reinforcement results in high intensity peak of the $Al_{13}Fe_4$ and $FeAl_3Si_2$ (indicated as (b) in Fig. 6.4).

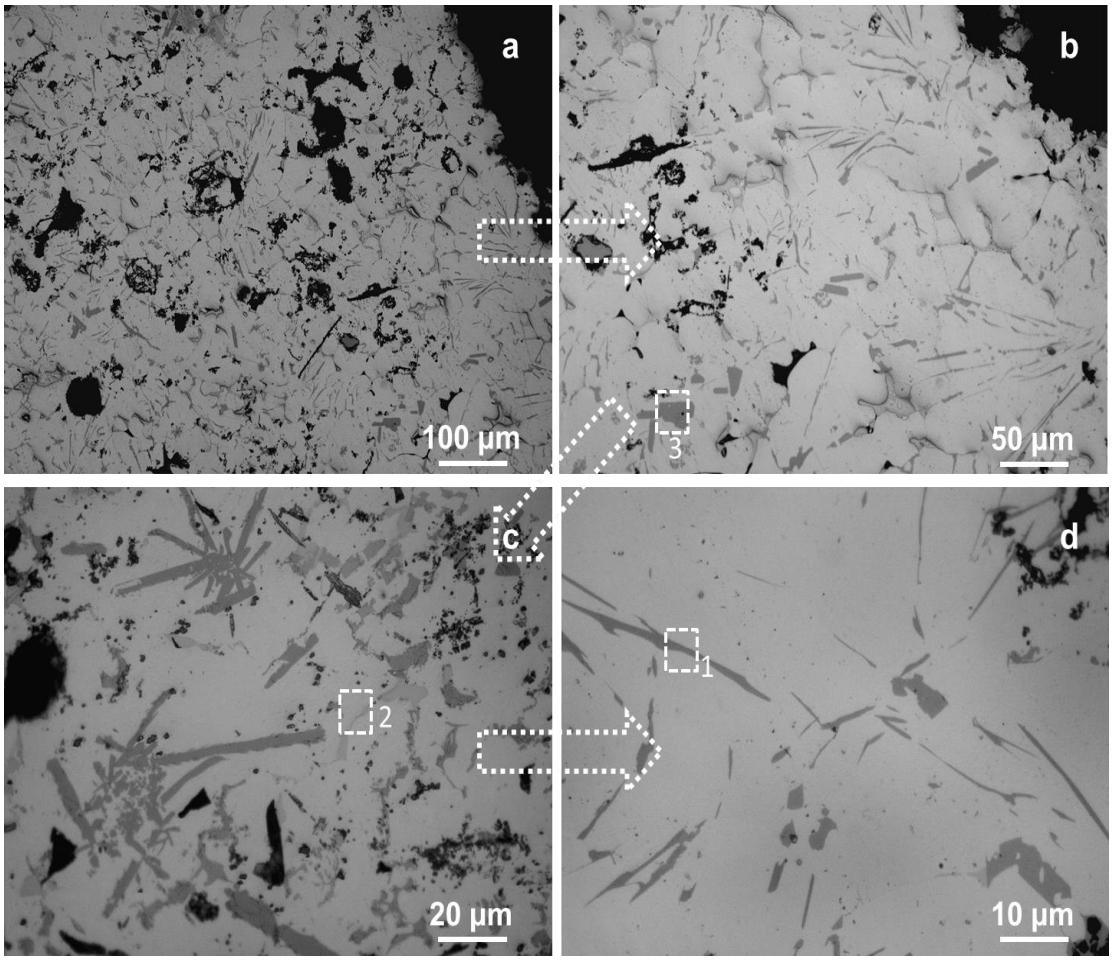

Fig. 6.6 The 1 wt. % CCSSF reinforced foam morphology: (a) Low magnification optical micrograph represent the overall view of the cell wall (b) higher magnification for more clear morphology shows the dense fibre-Al reacted intermetallic (c) higher magnification image of the plate sand branch like structure (d) higher magnification image of the plate like structure mainly represent the fibre (intermetallic foam when fibre react with Al melt).

Further increase in the amount of reinforcement to 1.5 wt. % and the effect of the same is presented in the optical micrographs (as shown in Fig. 6.7 ((a), (b), (c) and (d)). Optical micrographs at different magnification shows that the 1.5 wt. % CCSSF addition result into increase in the porosity, as well as, unreacted fibre is also clearly visible (indicated and numbered as 4).

It is worth to note that at this level of reinforcement the phases formed with fibre and aluminium melt reaction found with very low aspect ratio (as observed in all micrographs). From XRD analysis, it is observed that the amount of the $Al_{13}Fe_4$ is reduced at this level of reinforcement and amount of the $FeAl_3Si_2$ is increased (as shown in Fig. 6.4 with respective XRD peaks and indicated as (c)).

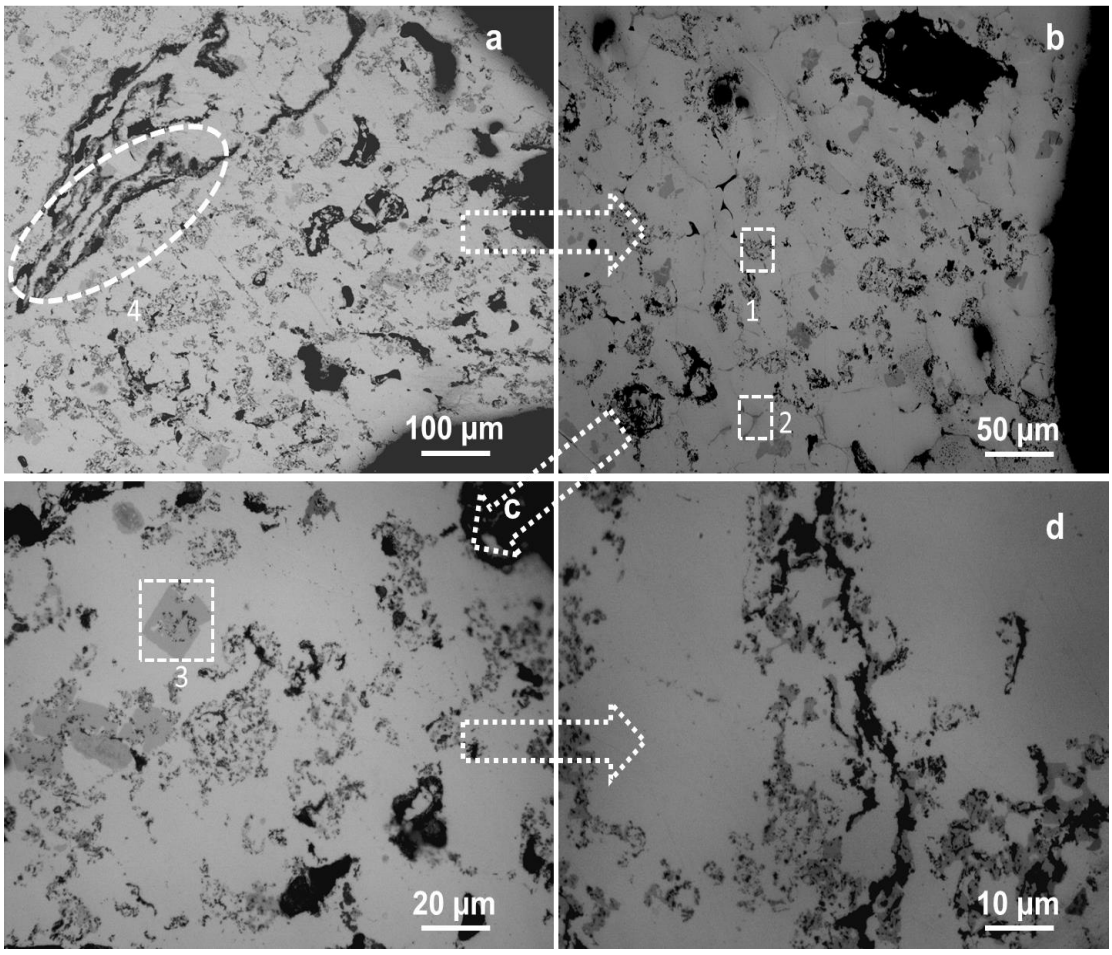

Fig. 6.7 The 1.5 wt. % CCSSF reinforced foam morphology: (a) Low magnification optical micrograph represent the overall view of the cell wall which shows some unreacted CCSSSF fiber (indicated as number 4) (b) higher magnification for more clear morphology (c) higher magnification image of low aspect ratio plate like structure and bulky structure (d) higher magnification image shows the higher

6.3.4 FE-SEM/EDS analysis of the CCSSF reinforced foam

6.3.4.1 Surface morphology of cell wall microstructure

The FE-SEM micrographs of the CCSSF reinforced foam are shown in Figs. 6.8 (a, b), 6.10 (a, b) and 6.11 (a, b). The microstructure (at two different magnification) of the 0.5 wt. % CCSSF reinforced foam is shown in the Fig. 6.8 (a, b). Fig. 6.8 (a)) shows the overall morphology of the cell wall, from this micrograph it is found that the plateau border of the cell wall consists of some plate like structure which completely cover the plateau boarder. For more clear information of this plate like structure and subsequent EDS analysis micrograph is further magnified (Fig. 6.8(b)). From magnified view it is observed that the structure which looks like a plate is actually a plate structure with some irregular branches which are free, as well as, interconnected.

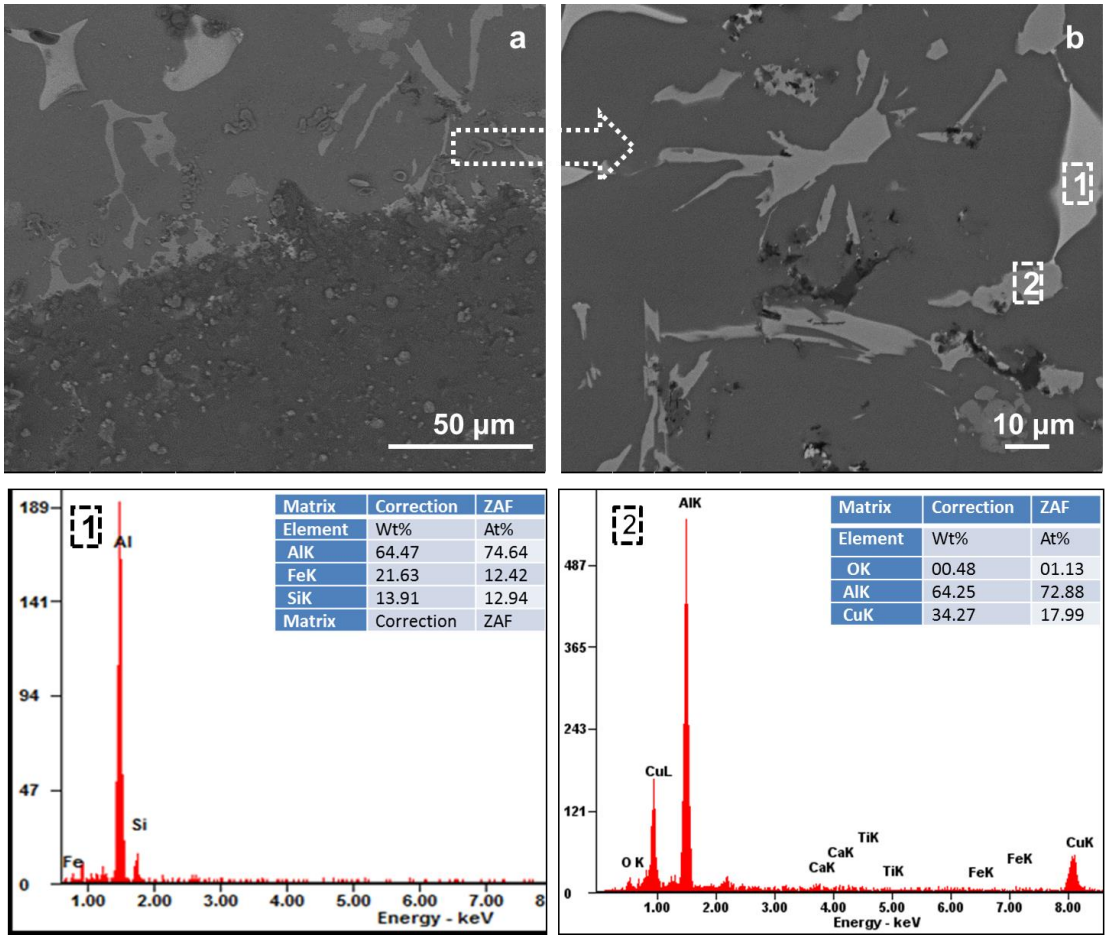

Fig. 6.8 SEM micrograph of 0.5 wt. % CCSSF reinforced foam morphology: (a) Low magnification secondary electron micrograph represent overall view of the cell wall (b) higher magnification of the plateau boarder, with respective EDS at point 1 and point 2 indicated by 1 and 2 respectively.

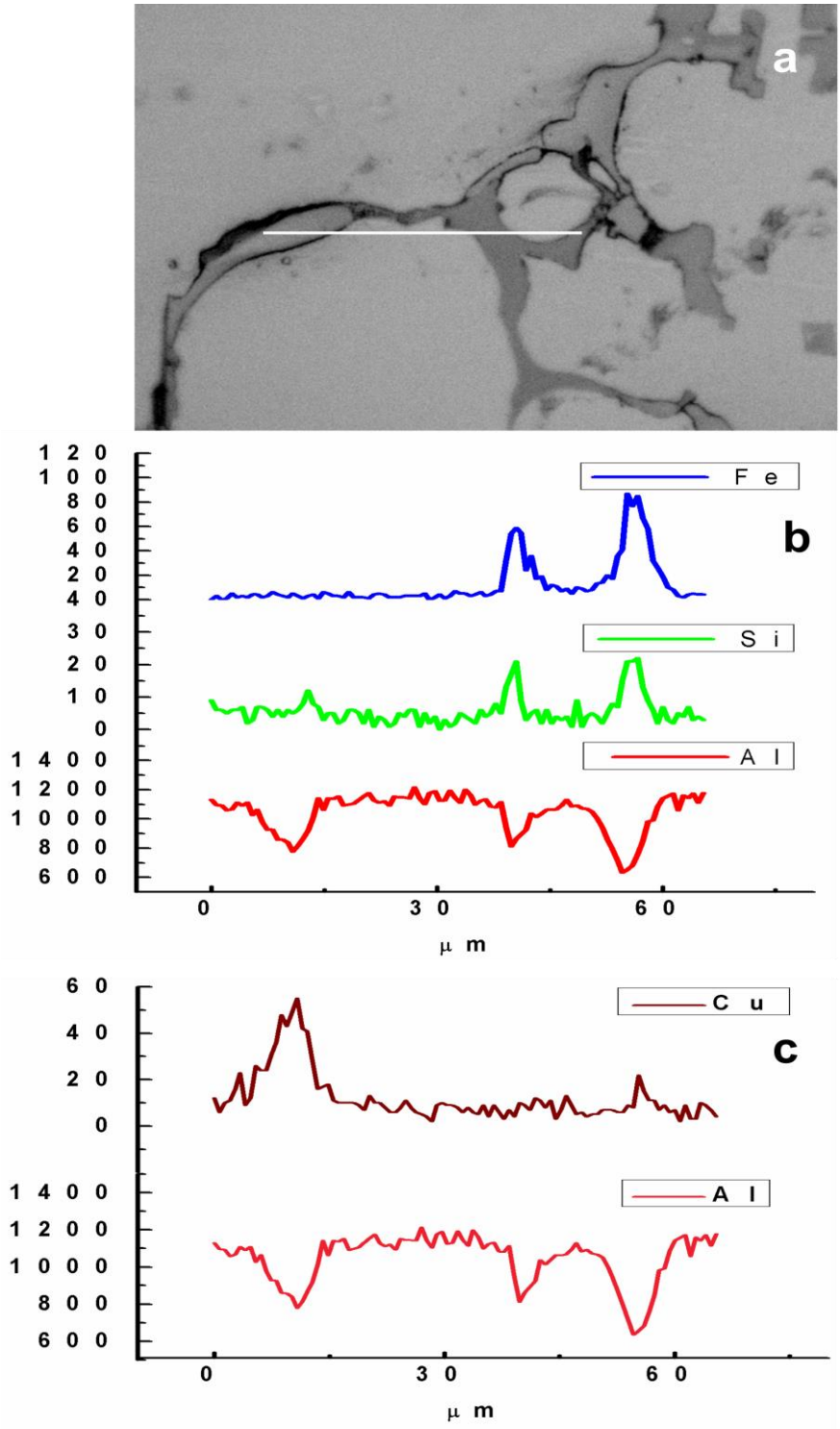

Fig. 6.9 (a) SEM micrograph, (b) EDS line scan of Fe, Si and Al, and (c) EDS line scan of Cu and Al.

It is also observed that there is slight variation in the contrast of the connected plates, which is indicated as point 1 and point 2 on Fig. 6.9. EDS analysis at point 1 and point 2 indicated that the bright plates are actually Al-Cu intermetallic and the composition is well

match with the composition of the Al_2Cu,(which can be attributed to the addition of Cu as well as, copper coated on the SSF (which may be melted during foaming process). Similarly, adjoin less bright plate like structure is actually intermetallic of Al-Fe-Si.

From EDS data presence of the Al_2Cu with small amount of oxygen is observed, the presence of oxygen suggests the probabilities of the formation of oxides at the plateau boarder of the foam. Similarly, EDS data at point 2 shows that the composition of plate like structure close to the stoichiometry of $FeAl_3Si_2$. The XRD pattern also confirms the same.

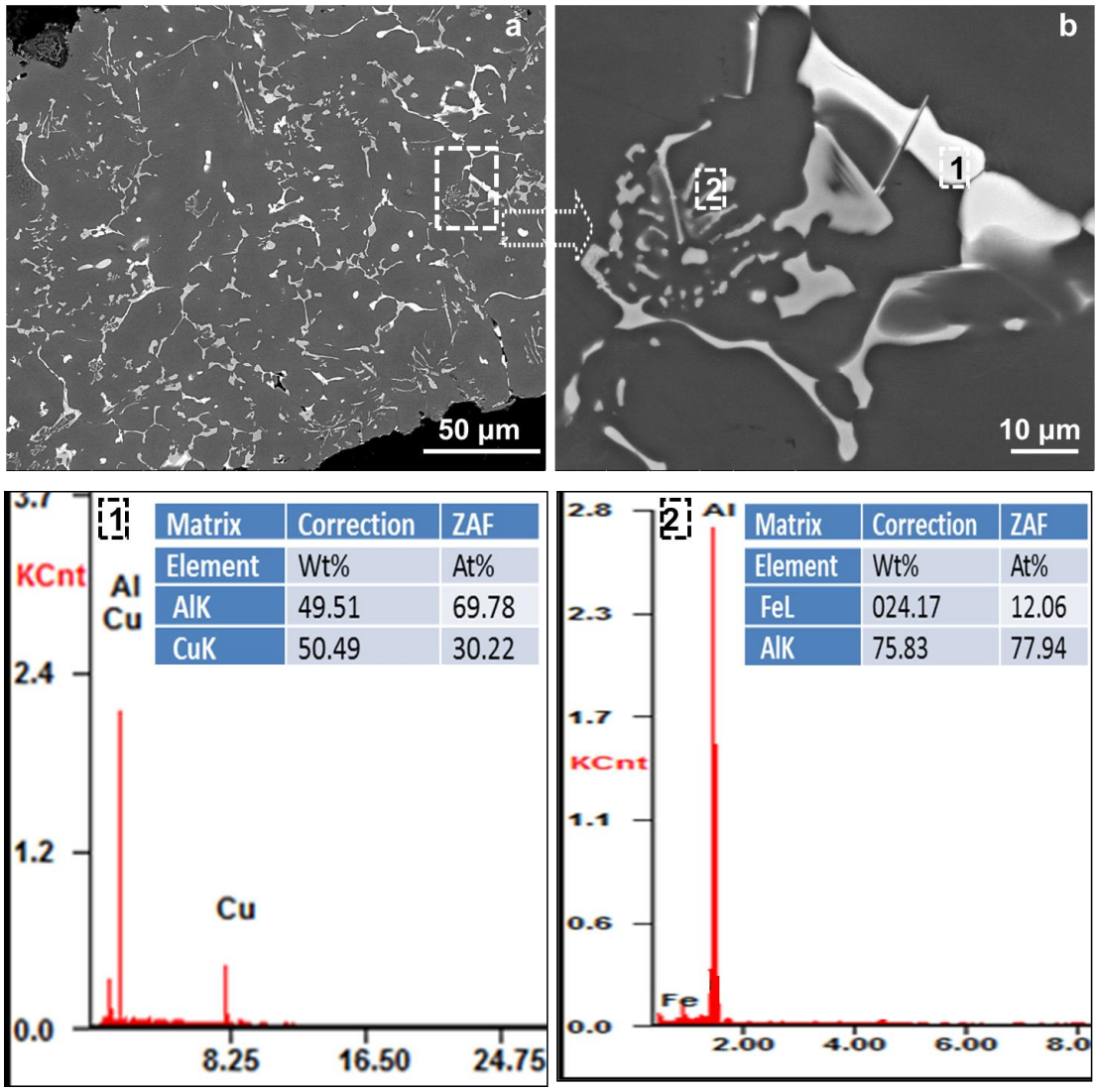

Fig. 6.10 SEM micrograph of 1 wt. % CCSSF reinforced foam morphology: (a) Low magnification secondary electron micrograph represent overall view of the cell wall (b) higher magnification of the closed packed structure, with respective EDS at point 1 and point 2 indicated by 1 and 2 respectively

EDS line scan of the plate like structure and interface of the matrix is shown in the Fig.6.9. The Al, Cu, Fe and Si EDS line scans (Fig. 6.9) has shown that the bright portion mainly consist of Al and Cu with respective peaks (as shown in the Fig. 6.9 (c)), which

indicates that the bright plates like structures are mainly Al_2Cu. Similarly, Fig. 6.9 (b) also indicates that the adjacent platen structure consists of Al, Si and Fe and their respective peaks indicate that the plate like structure (grey in shade) is $FeAl_3Si_2$.

The microstructure of the 1.0 wt. % CCSSF reinforced foam is shown in the Fig. 6.10 (a, b), (at two different magnification). Cell wall of the produced foam at low magnification (Fig. 6.10 (a)) shows that this amount of reinforcement results into some plate like structure, as well as, some closed packed tiny plates. For more clarity regarding the closed packed structure and subsequent EDS analysis micrograph is further magnified, from which (Fig. 6.10 (b)) it is observed that the closed packed structure actually consists of small plate with some irregular branches, which are free as well interconnected.

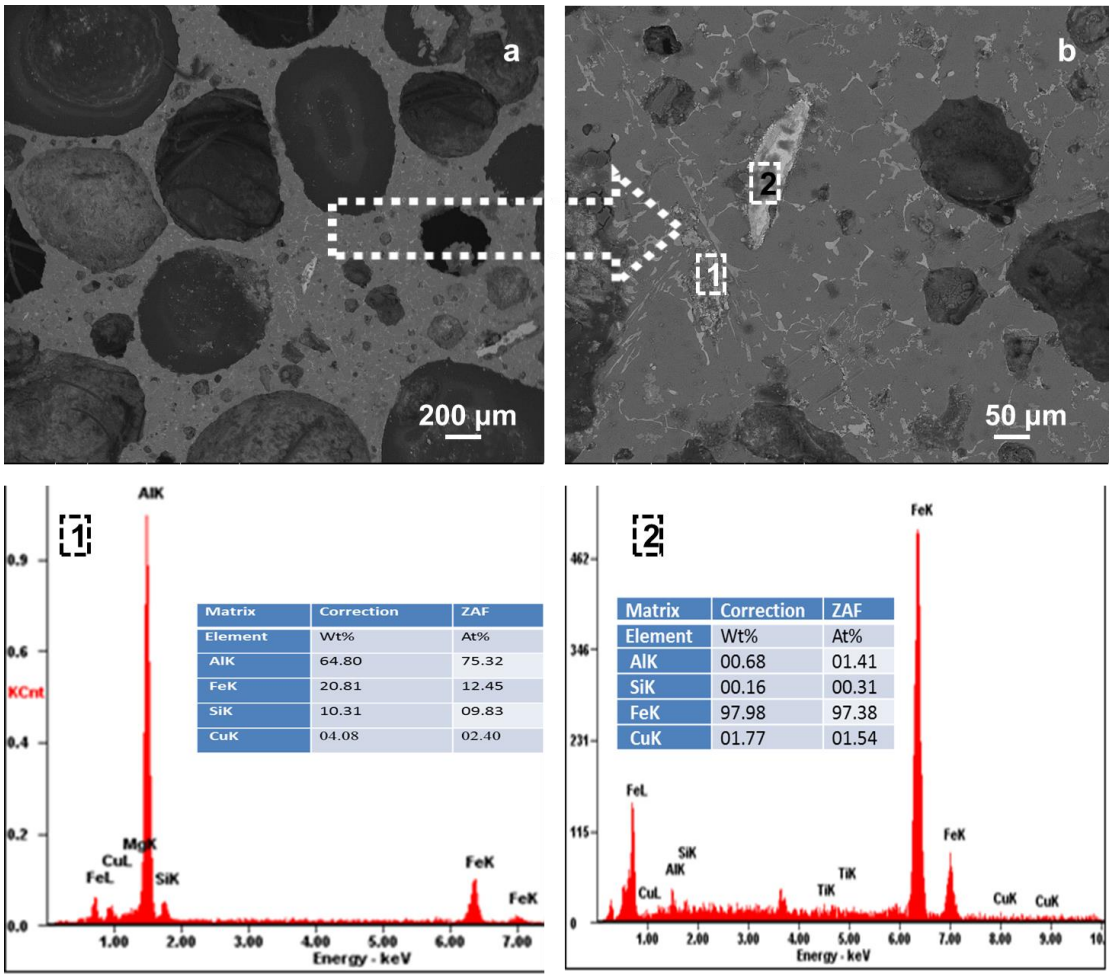

Fig. 6.11 SEM micrograph of 1.5 wt. % CCSSF reinforced foam morphology:

(a) Low magnification secondary electron micrograph represent overall view of the cell wall (b) higher magnification of the cell wall indicates the presence of unreacted fiber, with respective EDS at point 1 and point 2 indicated by 1 and 2 respectively.

The bright plates (as discussed earlier) like structure consists of Al and Cu, which is attributed to the addition of Cu, as well as, copper which is coated on the SSF may be melted during foaming process. To know the actual composition of the structure, EDS analysis has been done on the two different contrast structure, indicated as point 1 and 2 on the Fig. 6.11 (b). EDS data clearly shows the presence of Al-Cu. At point 2, EDS analysis has been done and found data suggests the presence of the Al-Fe intermetallic with the composition close to the ratio of Al_{13} Fe_4 which also affirms the finding of the pattern of XRD.

Cell wall microstructure of the 1.5 wt. % CCSSF at low magnification (Fig. 6.11(a)) shows that the cell structure which consist of platen structure (very low aspect ratio) with some unreacted fibre (as shown in the Fig.6.11 (b) and numbered as 2). For more information of the structure and the composition of the structure micrograph is further magnified. Magnified micrograph (as shown in the Fig.6.11 (b)) represents that the cell wall consist of grey plate like structure with some irregular branches, as well as, fibre, which are indicated and subsequently numbered as 1 and 2 respectively. EDS analysis at point 2 clearly indicates the presence of the fibre, with small amount of Cu. Similarly at point 1, EDS data clearly showed that the platen like structure is $FeAl_3Si_2$ with small amount of oxygen.

6.3.4.2 Cross-sectional analysis and X-ray mapping

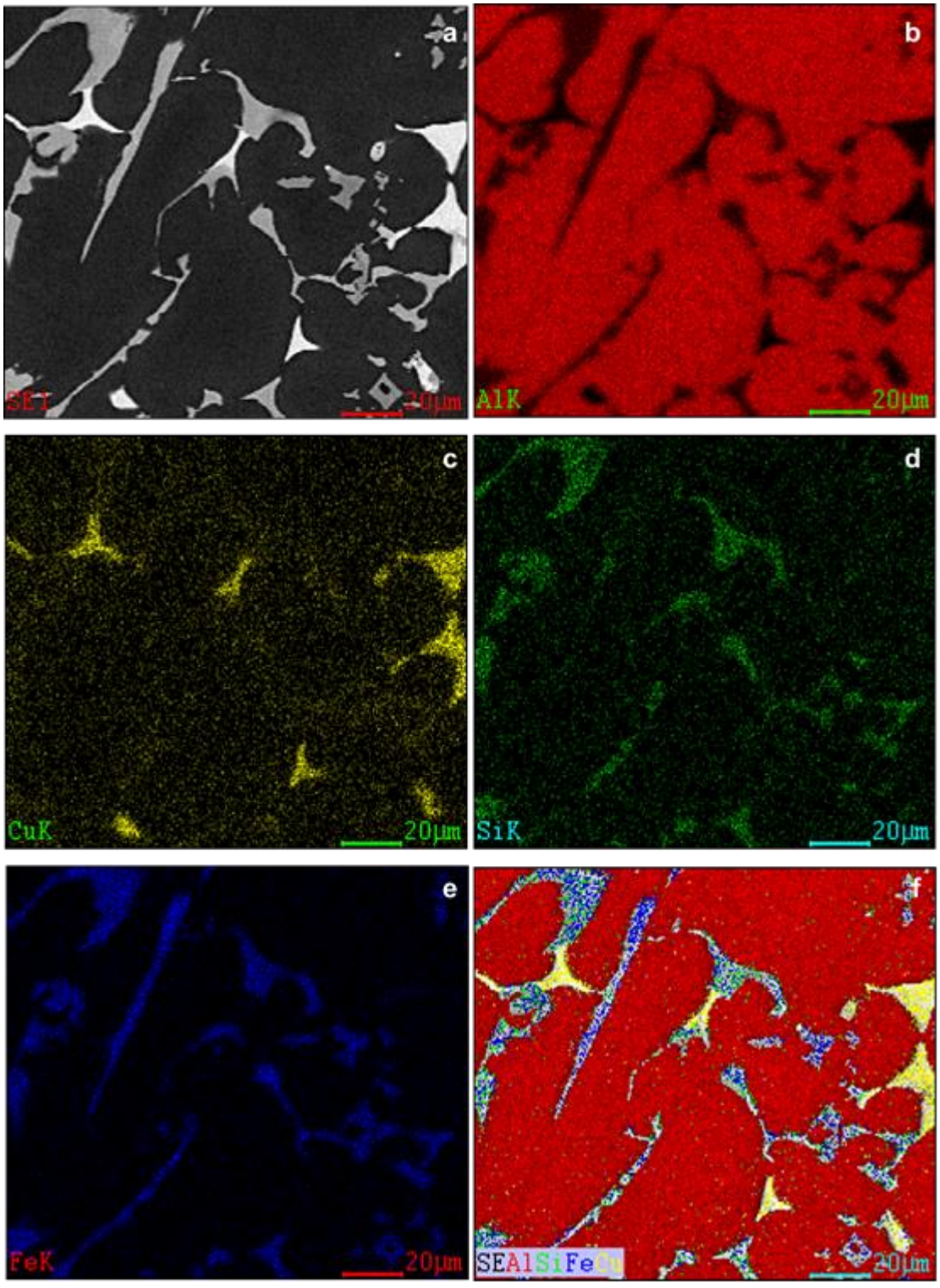

Fig. 6.12 X-ray mapping of the plate like structure connected with Al_2Cu bridge: (a) high magnification SEM micrograph, (b) EDS elemental mapping of Al, (c) EDS elemental mapping of Cu, (d) EDS elemental mapping of Si, (e)EDS elemental mapping of Fe and (f) overall EDS.

X-ray mapping of the CCSSF reinforced foam has been carried out at various points of the cell wall and shown in Fig. 6.12 and 6.13. It is clear that the large part of the cell wall is covered with $Al_{13}Fe_4$, Al_2Cu and $FeAl_3Si_2$. X-ray mapping of the reinforced foam shows (Fig. 6.12((a), (b), (c) and (d)) and Fig. 6.13((a), (b), (c) and (d))) distribution of these phases.

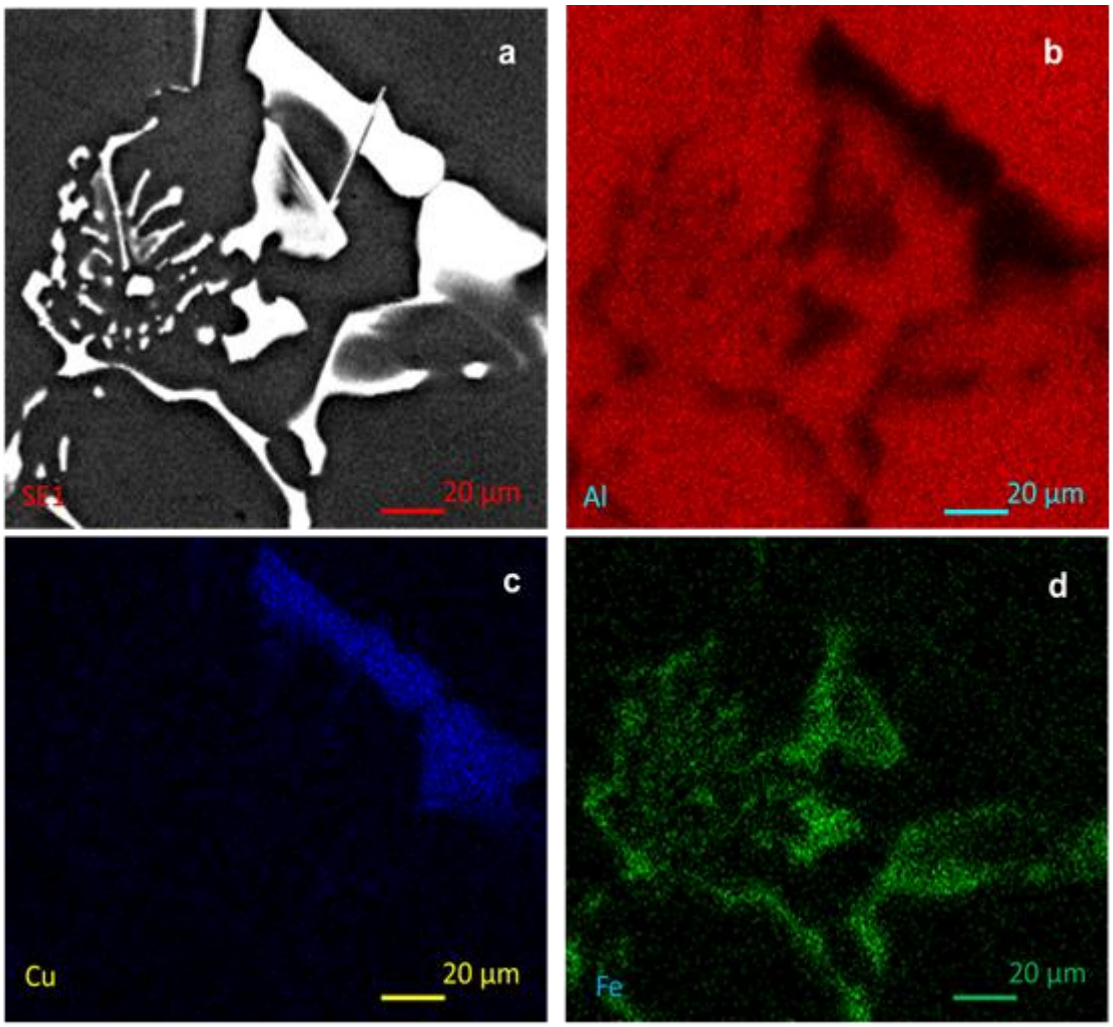

Fig. 6.13 X-ray mapping of the plate like structure with irregular branches:
(a) high magnification SEM micrograph, (b) EDS elemental mapping of Al,
(c) EDS elemental mapping of Cu and (d) EDS elemental mapping of Fe.

For more clear information, characterisation of the cell wall microstructure TEM has been employed to investigate the platen like phase. In the present study, since, the only difference in all the foam is wt.% fraction (i.e. 0.5, 1 and 1.5wt%) and slight change in the platen like phases in all the reinforced foam samples, 1wt% CCSSF foam sample was selected to be characterised by TEM. TEM specimens of the CCSSF reinforced foam (at different locations) have been prepared.

The particular image at two different magnifications refers to the structure of the plate like phase, present in the cell wall between the intermetallic particles seen in the SEM micrographs.

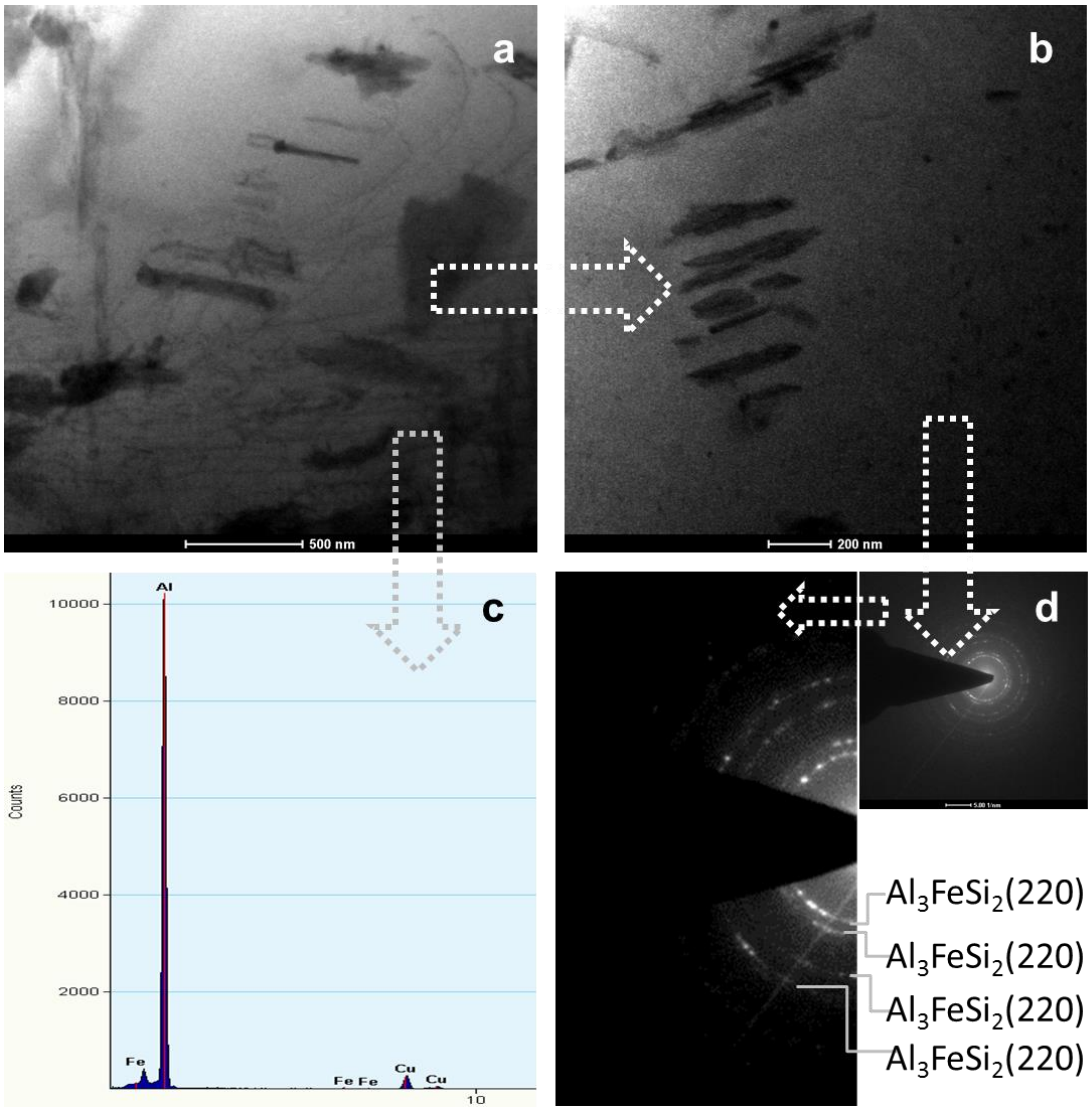

Fig. 6.14 Bright field TEM image of 1 wt. % CCSSF reinforced foam at two different magnifications (a and b), (c) STEM EDS and (d) SAED pattern

Fig. 6.14 (a), (b), (c) and (d) shows the bright field TEM micrograph, STEM EDS and SAED pattern of the 1wt. % CCSSF foam sample. Bright field TEM micrograph shown in the Fig. 6.14 (a) and (b) discloses the presence of the platen like phase on the scale of 500 and 200 nm. The SAED pattern analysis depicts that platen like phases are Al_3FeSi_2. The diffraction spots also indexed (Fig. 6.14 (d)) using JCPDS Card No. 83-0614(Al_3FeSi_2).

6.3.4.3 Inference from microstructural studies

As an overview of the results for CCSSF reinforced foam, variations in the microstructure in terms of cell wall morphology has been observed with various level of CCSSF reinforcement. Reinforcement results into stabilisation of the foam, related to the presence and distribution of phases and their distribution. Furthermore, microstructure reveals the presence of secondary phases along with Al_2Cu plates and cluster. Density of the platen structure increase, but the size of Al_3FeSi_2, Al_2Cu and $AL_{13}Fe_4$ reduce in 1.5 wt. % reinforcement, whereas the density of these phase increases and become finer. It is observed that as amount of reinforcement increase un-dissolved Fe react with adjacent Al and form $Al_{13}Fe_4$ and Al_3FeSi_2, whereas, amount of Al_2Cu is reduced. From the above discussion, it is reasonable to state that these phase originated from the reaction of undissolved SSF with the Al and further grow during the solidification and cooling.

From the cell wall morphologies, it is observed that the phases present in the foam of plates are distributed in the master alloy matrix. Limited porosity existed at the interface of phase and alloy matrix, which can be attributed to coating on the SSF improves the wetting behaviour of the SSF. Therefore, reinforcement with CCSSF improves the wetting behaviour, which results into the embedded particles more deeply in the melt and works as a barrier to the flow of the liquid melt and improves foam stability.

6.4 Mechanical Property Analysis

In the previous section 6.3, the effect of the reinforcement on the macro and microsturctural behaviour of produced foam has been described. The variations in microstructure with respect to wt. % CCSSF reinforcement has been discussed in details, comprising the results obtained in previous section. The course of action used to choose the sample i.e. number of sample for each test, dimension and subsequent calculation of the mechanical properties (i.e. energy absorption capability, plateau stress, etc.) is same, as employed in chapter 4. It should be noted that the process variable decides the morphological and microstructural features of foam, which are in turn responsible for the mechanical properties improvement. In the next section, main aim is to evaluate the mechanical property with respect to CCSSF reinforcement to support and verify the change in the microstructure mechanically.

Section 6.4 comprises of microhardness and quasi static compression test. In the initial part microhardness of foam without reinforcement and with CCSSF reinforcement (different

wt. % addition) are compared, subsequently, compression test is also performed and compared. Finally, based on the result obtained, assessment of the mechanical properties of the foam reinforced with CCSSF in comparison to foam without reinforcement has been carried out.

Therefore, the main focus of the investigation is structure-property correlation. The following sections describe the mechanical properties investigated in the present chapter.

6.4.1 Microhardness

Vickers hardness number (VHN) is measured at the same parameters which is used in the previous chapters. The microhardness value of the CCSSF reinforced foam was measured at the junction of the cell wall to investigate the variation in hardness, with respect to variation in the reinforcement.

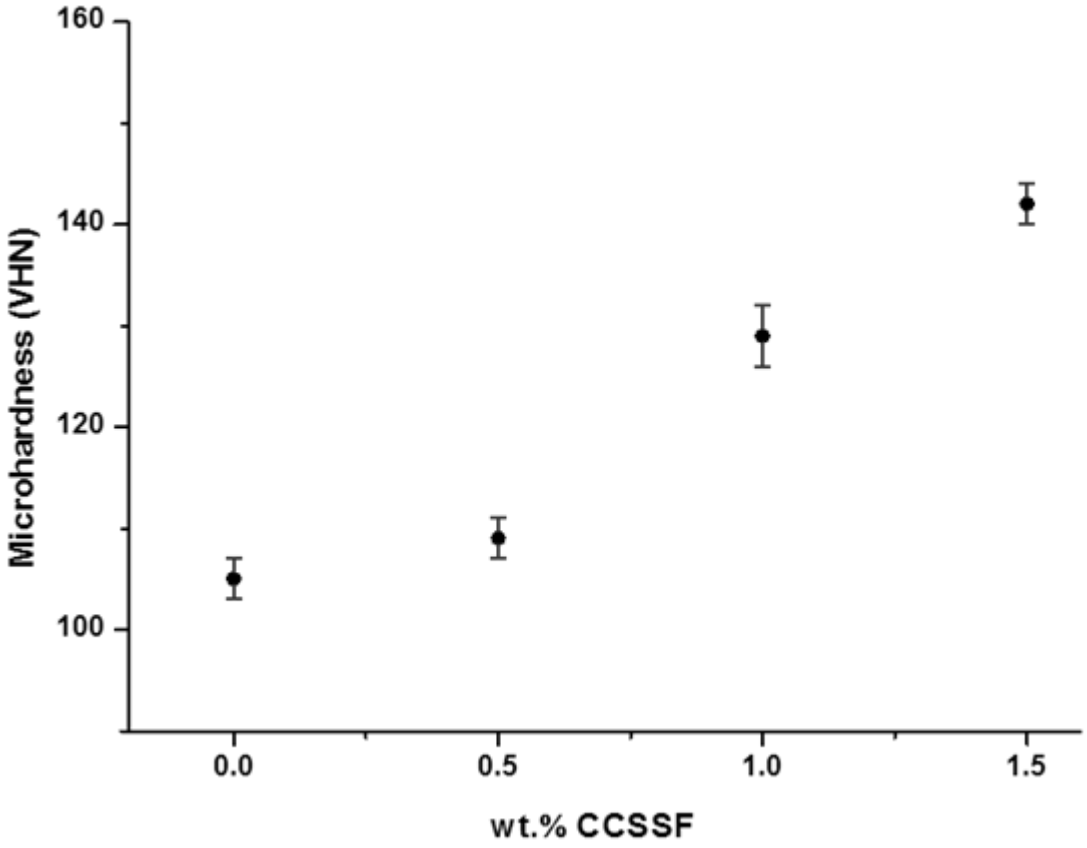

Fig. 6.15 Variations in the microhardness of the closed cell aluminium foam with reinforcement (wt. % of CCSSF).

Fig. 6.15 represents the variation in the microhardness with varying wt. % of CCSSF. It is evident from the Fig. 6.15 that the value of hardness increases with increase in wt. % of reinforcement. The average microhardness of the 0.5 wt. % CCSSF reinforced foam is slightly changed i.e. increase (in the range of 107-111VHN) than the foam without reinforcement (105 VHN).

The value of the average microhardness at 1 wt.% CCSSF reinforced foam shows different behaviour; the change in the microhardness is reasonably high (126-132 VHN) as compared to foam reinforced with 0.5wt% CCSSF and the trend is similar in the foam reinforced with 1.5 wt.% CCSSF. Therefore, it is reasonable to state that the value of microhardness is improved moderately at small amount of reinforcement and significantly higher when the produced foam reinforced with more than 1 wt. % CCSSF.

6.4.2 Quasi-Static Compression Test

The aluminium foam reinforced with CCSSF and the effect of reinforcement on the microsturctural behaviour of the cell wall matrix with respect to wt.% CCSSF reinforcement and reasonably discussed in the previous section. From the change occurred at macro and microscopic level due to the reinforcement is analysed and discussed in previous section, result shows that the reinforcement greatly change the cell wall microstructure in terms of texture appearance. Therefore, it is reasonable to anticipate the contribution of the microsturctural changes, when produced foam undergo compression load.

It is expected that when the load applied on the foam sample collapse of the cell wall progress layer by layer until densification for constant plateau region. As discussed previously, compressive stress-strain curves has been obtained by plotting the applied load divided by the original cross-sectional area of the specimen. Fig. 6.16 shows the stress-strain curves obtained from tests executed on samples of CCSSF reinforced closed cell foam at different level of reinforcement i.e. 0.5, 1 and 1.5wt% respectively, with a reference curve of the foam produced without reinforcement. The compressive properties of the reinforced foam with different wt.% of CCSSF and foam without reinforcement has been compared by measuring the yield stress, plateau stress and energy absorption capacity obtained from the stress strain curves and calculated as previously described in chapter 4 in section 4.4.2. All specimens for each condition have approximately same relative density. From Fig. 6.16, it is clear that the quasi-static stress-strain curve is different for different condition tested at constant strain rate of 1×10^{-3}.

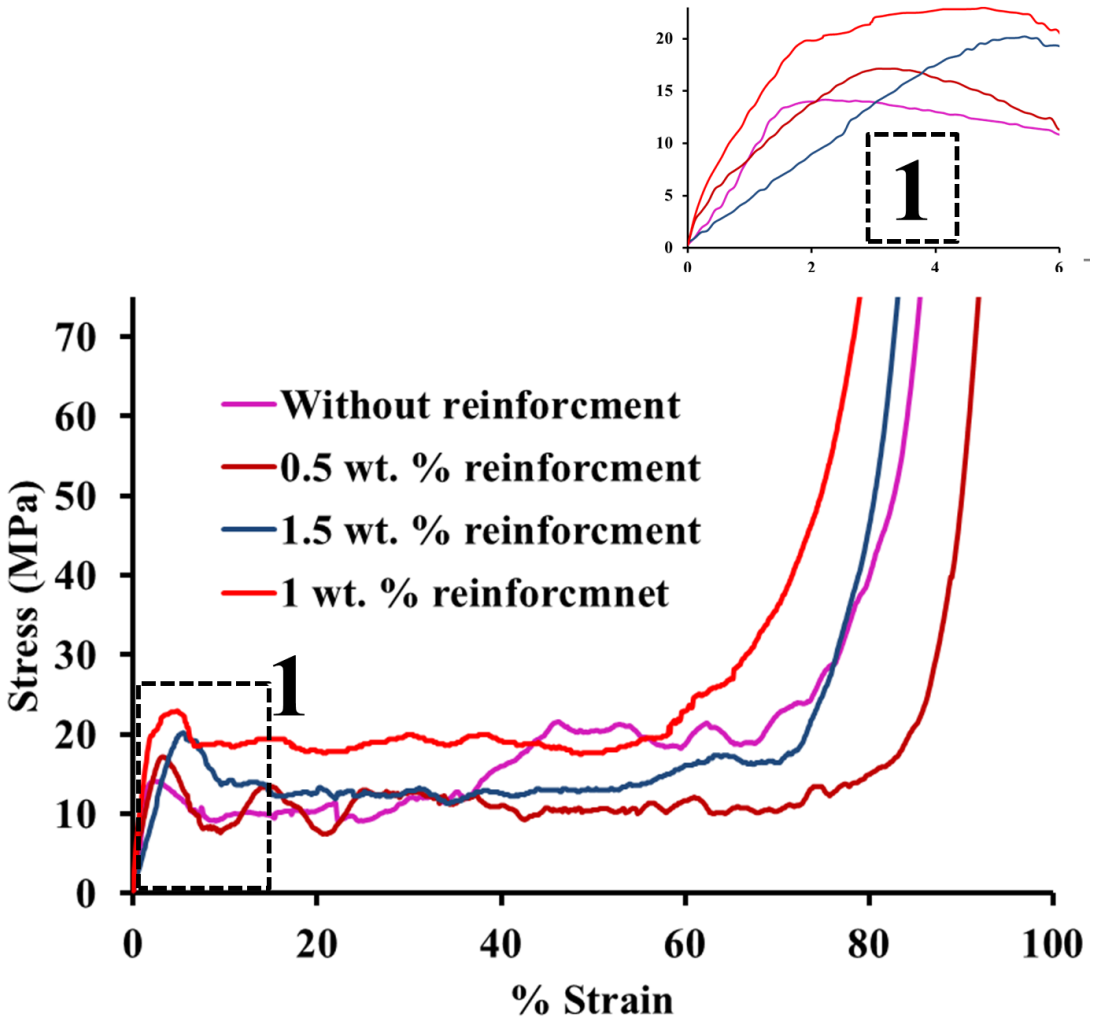

Fig. 6.16 Stress–strain curves for samples without reinforcement and with the different amount of CCSSF reinforcement compressive loading at 1×10^{-3} s^{-1} strain rate, magnified view (number as 1) of the elastic region of the curve shows the change in slope of the elastic region with respect to reinforcement.

Table 6.1 The mechanical properties of the foam sample without and with CCSSF reinforcement.

Reinforcement (wt. %)	Yield strength (MPa)	Plateau stress (MPa)	Energy absorption (MJ/mm^3)
0%	14	10	13
0.5	17	11	12
1	20	19	18
1.5	23	14	13

From the Fig. 6.16, it can be clearly visualized that after CCSSF reinforcement compressive behaviour improved, which further supported from the value of the yield stress, plateau stress and energy absorption considerably (Table 6.1).

Improvement in these compressive properties can be attributed to introduction of the CCSSF. Among all the curves, foam with 1wt. % CCSSF reinforced foam shows the highest value in compressive test. These values are intermediate for 0.5 wt.% reinforcement and a another interesting aspect worth notice is in the case 1% and 1.5 wt.% reinforcement compressive curve is smooth, the smooth stress–strain curves in indicates good compressive stability. Moreover, the change in the yield strength of the sample with 0.5,1 wt. % is moderate, whereas, in case of 1.5 wt. % CCSSF reinforced foam is higher when compared to the foam without reinforcement. Similarly, behaviour is observed in case of plateau strength, as well as, energy absorption capacity. Another interest point with noted the slope of curves in the linear region of the compression curve, it is observed that with increase (up to 1 wt. %) in the reinforcement slope is improved, after 1 wt. % of reinforcement the slope is reduced, increase in the slope of the curve shows higher elastic modulus. Improve in the elastic modulus attributed to addition of the CCSSF (up to 1 wt. %), may results into barrier to crack which pinned by reinforcing obstacles, thus crack is deviate from the straight path which further reduce the probability of the early crack formation when load is applied. After 1 wt. % addition, further increase in the reinforcement result into lower slope may be attributed to unreacted CCSSF fibre with adjacent porosity. It is clear that the as level of reinforcement of increased the stability of the foam improved (smoothness of the curve indicate the same), as well as, elastic modulus also improved (as shown in the magnified elastic region of the compressive stress strain curve). Therefore, it is reasonable to expect that the introduction of CCSSF results into improved energy absorption capability.

6.4.3 Fractography

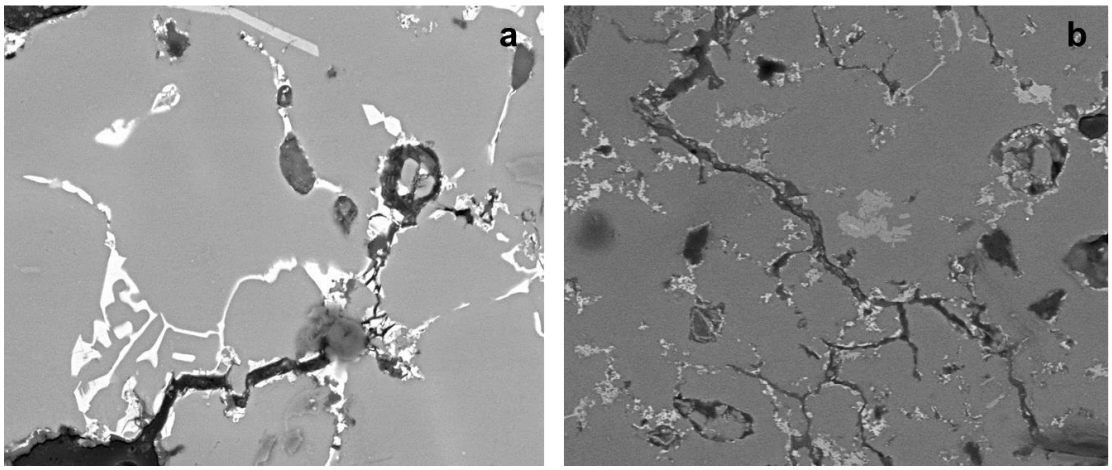

Fig. 6.17 SEM micrograph of the fractured samples (a) 1 wt. % reinforced foam and (b) 1.5 wt. % reinforced foam.

Fractography provide information about the nature of the fracture. In the present work, fractography is referred to the interpreted compression test, which is compression of the sample up to 30% compression and then SEM of the fracture sample has been taken to analyse the fractured surface. Back scattered SEM image of the fractured sample from interrupted compression is shown in Fig. 6.17. Fig.6.18 shows the backscattered electron micrograph of the fracture surface of the CCSSF foam samples. Fracture micrograph consists of lamellar, as well as, very small particles. Fig. 6.18 shows the close up of the closed packed looks structure, it is observed from this micrograph that this structure interrupt the early crack initiation.

From the micrographs, it is clear that although crack start from the cell wall but the developed CCSSF and Al melt reacted phase resist further propagation, whereas in case of 1.5 wt. % reinforcement foam crack propagation is much severe as compare to 1 wt. % reinforcement but it is not that much sever as observed in the foam produced without reinforcement.

6.5 **Summary**

CCSF has been used to produce reinforced closed cell aluminium foam and the cell wall microstructure has been characterised for macrosturctural and microsturctural features and these features are correlated with the compressive properties. The findings and conclusion of the present chapter are:

1. Reinforcement in the foam have significant effect on the drainage of the metal foam i.e. reinforcement results into less drainage due to the good wetting behaviour of the CCSSF.

2. As depicted from XRD analysis increase in wt.% of CCSSF amount of secondary phases in the platen foam, which further reduce at 1.5 wt.% CCSSF reinforcement.

3. The micro-hardness (VHN) of the CCSSF reinforced foam enhanced with the increase in CCSSF reinforcement and this phenomenon of increasing is mainly attributed to the presence of high volume fraction of secondary phase, spread in the alloy matrix.

4. From the quasi static compression test result, it can be seen that yield stress, plateau stress, and energy absorption capacity has been improved after the

reinforcement when compared with the foam without reinforcement. The compressive property improvement can be interrelated to the morphology of the cell wall and the presence of secondary intermetallic phase and dispersoids.

5. These compression test results are in agreement with the microhardness behaviour.

7.1 Introduction

Microstructural modification is a step that has the highest potential to improve the properties of the alloy in the present study cell wall material. The objectives of this thesis work were to obtain closed cell Al foam with improved performance by developing stable foam and to understand the effect of microstructural modification on the properties and stability of foam. In this thesis work, three strengthening mechanisms (post and pre-processing) are used to strengthen the cell wall material, as well as, to reduce morphological defects of the foam through the modification of the cell wall microstructure. All the changes occurred during cell wall microstructural modification are correlated with the mechanical properties through axial.

7.2 Contribution of the research work

The contributions of the research work have been divided into 3 parts.

In **part-1 (chapter-4)**, post processing techniques are used to modify the cell wall microstructure. In this technique, that is based on the thermal treatment using the phase diagram of the parent and the alloying element. Followings are the main conclusions drawn from this part of the research work:

1. Thermal treatment (post processing) has significant effect on the microstructure of the cell wall. Main phase found in the microstructure is Al_2Cu which shows age hardening behaviour when aged.

2. Thermal treatment in the present research work is a twofold process. First sample is solutionised and quenched, secondly solutionised sample further aged for different aging time and temperature. Microstructure modification is observed, as interconnected thick dendritic is break and result in non-dendritic homogenised structure as sample solutionised, whereas further aging treatment result in coarse precipitation with non-dendritic coarse grain structure.

3. Mechanical behaviour of the foam sample after post processing (thermal treatment) technique is also improved. Solutionised sample exhibit highest energy absorption capacity with lower hardness, whereas aged sample moderately higher energy absorption capacity with highest hardness due to precipitation hardening, which result in brittle fracture.

In **(chapter-5)**, grain refinement technique is used to modify the cell wall microstructure. In this technique, that is based on the grain refinement using different level of scandium (used as a grain refiner) addition. Following conclusions are drawn from this part of the research work:

1. Scandium significantly improves the cell wall microstructure. Main phase responsible for structural refinement found in the microstructure is Al_3Sc, which is a strong grain refiner.

2. Grain refinement in the present work has significant effect on the stability of the foam. At macroscopic level it is found that the use of scandium results in negligible drainage.

3. At microscopic level, it is found that the use of scandium result into grain refinement and it further improved as scandium addition level increased. At maximum level of scandium addition (i.e. 1wt. %), the grain size is reduced to 30 µm.

4. The micro-hardness (VHN) of the scandium inoculated foam enhanced with the increase in scandium addition this improvement is mainly attributed to grain refinement mechanism.

5. Compressive behaviour of grain refinement foam improved, which is reflected in the increase in the value of yield stress, plateau stress, and energy absorption capacity. The compressive property enhancement is interrelated to the morphology of the cell wall, its grain size, and the presence of secondary intermetallic phase and dispersoids.

In **(chapter-6)**, reinforcement is used to modify the strength of the foam through cell wall microstructure strengthening. In this technique, reinforcement through CCSSF has been done using different level of reinforcement (0.5, 1 and 1.5wt. %). Following conclusions are the main conclusions drawn from this part of the research work:

1. At macroscopic level, it is observed that the reinforcements play a vital role to reduce the drainage, which is attributed to resistance offered by reinforcement to liquid flow, as well as, good wetting behaviour of CCSSF.
2. Cell wall microsturctural is also modified after the reinforcement, cell wall morphology is changed to non-variant plate shape phases which mainly consist of $Al_{13}Fe_4$, Al_3FeSi_2 and $Al2_Cu$ and covered the plateau boarder of the cell wall.
3. The micro-hardness (VHN) of the CCSSF reinforced foam enhanced with the increase in CCSSF reinforcement and this phenomenon of increasing is mainly

attributed to the presence of the higher volume fraction of secondary phase, which is spread in the alloy matrix.

4. Yield stress, plateau stress, and energy absorption capacity of the reinforced foam are improved when compared with foam without reinforcement and it is attributed to the anisotropic nature of the cell wall microstructure.

At the end, author would like to conclude that these techniques provide a new concept for property enhancement through modification of the cell wall microstructure. Such a new technique would be extremely useful for property modification and would minimize the possibility of drainage for stable foam.

CHAPTER 8: SCOPE FOR FUTURE WORK

The research described here in not only led to a broad set of results but also identified a number of specific questions for additional research. The present work may be extended in one of the following directions:-

i. The work can be extended for process simulation.
ii. The work can be extended for the study of the drainage and collapse of the cell wall as well as mechanism of transport of species during the foaming through hot stage microscopy.
iii. The work can be extended for the study of the effect of the tailoring of the compositions prior to the foaming.
iv. The work can be extended for the real time study of the produced foam by designing the actual parts and testing.
v. The work can be extended for establishing the reliability and efficiency of the foaming through tomography for detection of mechanisms.
vi. The work can be extended for heat transfer phenomenon analysis which finds its wide application in the field heat and mass transfer.
vii. The work can be extended for the identification of other structural properties of the cell wall microstructure at nano level using advance techniques.

It is hoped that researchers will undertake these challenges in future to achieve the same level of intellectual satisfaction.

[1] Aguirre-Perales, L.Y., Jung, I.-H., Drew, R.A., 2012. Foaming behavior of powder metallurgical Al–Sn foams. Acta Materialia 60, 759-769.

[2] Ahmad, Z., Thambiratnam, D.P., 2009. Dynamic computer simulation and energy absorption of foam-filled conical tubes under axial impact loading. Computers & Structures 87, 186-197.

[3] Alinejad, B., Zakeri, M., 2009. A novel single-step method for fabrication of dense surface porous aluminum. Journal of Materials Processing Technology 209, 5042-5045.

[4] Alipour, M., Aghdam, B.G., Rahnoma, H.E., Emamy, M., 2013. Investigation of the effect of Al–5Ti–1B grain refiner on dry sliding wear behavior of an Al–Zn–Mg–Cu alloy formed by strain-induced melt activation process. Materials & Design 46, 766-775.

[5] Alizadeh, M., Mirzaei-Aliabadi, M., 2012. Compressive properties and energy absorption behavior of Al–Al2O3 composite foam synthesized by space-holder technique. Materials & Design 35, 419-424.

[6] Amsterdam, E., De Hosson, J.T.M., Onck, P.R., 2006. Failure mechanisms of closed-cell aluminum foam under monotonic and cyclic loading. Acta Materialia 54, 4465-4472.

[7] Andrews, E., Sanders, W., Gibson, L.J., 1999. Compressive and tensile behaviour of aluminum foams. Materials Science and Engineering: A 270, 113-124.

[8] Andrews, E.W., Gibson, L.J., 2001. The influence of crack-like defects on the tensile strength of an open-cell aluminum foam. Scripta Materialia 44, 1005-1010.

[9] Ashby, M.F., 2000. Metal foams: a design guide. Butterworth-Heinemann.

[10] Augustin, C., Öchsner, A., 2009. Commented Literature for Hollow Spheres and Hollow Sphere Structures, Multifunctional Metallic Hollow Sphere Structures. Springer, pp. 241-252.

[11] B.C., A., 1963. Methods of making foamed metal. US Patent No.3087807, 1-8.

[12] Babcsán, N., Leitlmeier, D., Degischer, H.-P., 2003. Foamability of particle reinforced aluminum melt. Materialwissenschaft und Werkstofftechnik 34, 22-29.

[13] Babcsán, N., Leitlmeier, D., Degischer, H.-P., Banhart, J., 2004. The Role of Oxidation in Blowing Particle-Stabilised Aluminium Foams. Advanced Engineering Materials 6, 421-428.

[14] Bafti, H., Habibolahzadeh, A., 2013. Compressive properties of aluminum foam produced by powder-Carbamide spacer route. Materials & Design 52, 404-411.

[15] Banhart, J., 2000. Manufacturing routes for metallic foams. Jom 52, 22-27.

[16] Banhart, J., 2001. Manufacture, characterisation and application of cellular metals and metal foams. Progress in Materials Science 46, 559-632.

[17] Banhart, J., 2006. Metal Foams: Production and Stability. Advanced Engineering Materials 8, 781-794.

[18] Banhart, J., 2012. Light-Metal Foams—History of Innovation and Technological Challenges. Advanced Engineering Materials.

[19] Banhart, J., Stanzick, H., Helfen, L., Baumbach, T., 2001. Metal foam evolution studied by synchrotron radioscopy. Applied Physics Letters 78, 1152-1154.

[20] Baumeister J., B.J., Weber M., 1996. Porous metallic material with anisotropic properties, in particular thermal and electrical conductivities. German patent DE 4,424,157, 1-4.

[21] Baumeister J., B.J., Weber M., 1997. Metallic composite and method to its production. German patent DE 4,426,627, 1-4.

[22] Baumeister J., S.H., 1991. Process for making foamed metal bodies. German Patent DE 4,101,630.

[23] Berry, C.B., 1972. Foamed Metal. Google Patents.

[24] Birol, Y., 2013. Efficiency of binary and ternary alloys from Al-Ti-B system in grain refining aluminium foundry alloys. International Journal of Cast Metals Research 26, 283-288.

[25] Bjorksten J., R.E., 1972. Method for foaming metals. US Patent 3,707,367, 1-10.

[26] Brandes, E., Brook, G., 1992. Smithells metal reference handbook. Butterworth-Heinemann London.

[27] Campana, F., Pilone, D., 2009. Effect of heat treatments on the mechanical behaviour of aluminium alloy foams. Scripta Materialia 60, 679-682.

[28] Cao, Z.-K., Li, B., Yao, G.-C., Wang, Y., 2008. Fabrication of aluminum foam stabilized by copper-coated carbon fibers. Materials Science and Engineering: A 486, 350-356.

[29] Cao, Z.-k., Liu, Y.-h., Yao, G.-c., 2006. Electroplating of carbon fibers in sulfate acidic solution. CHINESE JOURNAL OF PROCESS ENGINEERING 6, 651.

[30] CAO, Z., LIU, Y., YAO, G., 2005. Studies on copper coating on carbon fibers. Journal of Guangdong Non-Ferrous Metals 2, 496-499.

[31] Chakraborty, M., Garcia-Moreno, F., Banhart, J., 2011. Foamability of MgAl2O4 (Spinel)-Reinforced Aluminum Alloy Composites. Metallurgical and Materials Transactions A 42, 2898-2908.

[32] Chandrashekar, T., Muralidhara, M., Kashyap, K., Rao, P.R., 2009. Effect of growth restricting factor on grain refinement of aluminum alloys. The International Journal of Advanced Manufacturing Technology 40, 234-241.

[33] Chen, P.-Y., McKittrick, J., 2011. Compressive mechanical properties of demineralized and deproteinized cancellous bone. Journal of the Mechanical Behavior of Biomedical Materials 4, 961-973.

[34] Chethan, A., Garcia-Moreno, F., Wanderka, N., Murty, B., Banhart, J., 2011. Influence of oxides on the stability of zinc foam. Journal of materials science 46, 7806-7814.

[35] Cibula, A., 1949. The mechanism of grain refinement of sand castings in aluminium alloys. Journal of the Institute of Metals 76, 321.

[36] Clyne, T., Withers, P., 1995. An introduction to metal matrix composites. Cambridge University Press.

[37] Contorno, D., Filice, L., Fratini, L., Micari, F., 2006. Forming of aluminum foam sandwich panels: Numerical simulations and experimental tests. Journal of Materials Processing Technology 177, 364-367.

[38] Degischer, H.P., Körner, C., Singer, R.F., Banhart, J., Baumgärtner, F., Rausch, G., Arnold, M., Thies, M., San Marchi, C., Mortensen, A., Andersen, O., Stephani, G., 2003. Material Definitions, Processing, and Recycling, Handbook of Cellular Metals. Wiley-VCH Verlag GmbH & Co. KGaA, pp. 5-70.

[39] Demsetz, L.A., Gibson, L.J., 1987. Minimum weight design for stiffness in sandwich plates with rigid foam cores. Materials Science and Engineering 85, 33-42.

[40] Deqing, W., Weiwei, X., Xiangjun, M., Ziyuan, S., 2005. Cell structure and compressive behavior of an aluminum foam. Journal of Materials Science 40, 3475-3480.

[41] Deqing, W., Ziyuan, S., 2003. Effect of ceramic particles on cell size and wall thickness of aluminum foam. Materials Science and Engineering: A 361, 45-49.

[42] Dieter, G., 1962. Strengthening Mechanisms in Solids. ASM, Metals Park, Ohio, 279.

[43] Diop, M., Hao, H., Dong, H., Zhang, X., Yao, S., Jin, J., 2011. Modelling of solidification process of aluminium foams using lattice Boltzmann method. International Journal of Cast Metals Research 24, 158-162.

[44] Duarte, I., Banhart, J., 2000. A study of aluminium foam formation—kinetics and microstructure. Acta materialia 48, 2349-2362.

[45] Duarte, I., Oliveira, M., 2012. Aluminium Alloy Foams: Production and Properties. Powder Metallurgy, Published by InTech, Rijeka, Croatia, 47-72.

[46] Edwin Raj, R., Daniel, B.S.S., 2011. Customization of closed-cell aluminum foam properties using design of experiments. Materials Science and Engineering: A 528, 2067-2075.

[47] Edwin Raj, R., Parameswaran, V., Daniel, B.S.S., 2009. Comparison of quasi-static and dynamic compression behavior of closed-cell aluminum foam. Materials Science and Engineering: A 526, 11-15.

[48] Elliott, J.C., 1961. Metal foam and method for making. Google Patents.

[49] Evans, A.G., Hutchinson, J.W., Ashby, M.F., 1998. Cellular metals. Current Opinion in Solid State and Materials Science 3, 288-303.

[50] Fang, X., Fan, Z., 2007. A novel approach to produce Al-alloy foams. Journal of materials science 42, 7894-7898.

[51] Feng, Y., Tao, N., Zhu, Z., Hu, S., Pan, Y., 2003a. Effect of aging treatment on the quasi-static and dynamic compressive properties of aluminum alloy foams. Materials Letters 57, 4058-4063.

[52] Feng, Y., Zheng, H., Zhu, Z., Zu, F., 2003b. The microstructure and electrical conductivity of aluminum alloy foams. Materials Chemistry and Physics 78, 196-201.

[53] Fusheng, H., Zhengang, Z., 1999. The mechanical behavior of foamed aluminum. Journal of Materials Science 34, 291-299.

[54] Gao, L., Chen, Y., 2010. A study on the rare earth ore containing scandium by high gradient magnetic separation. Journal of Rare Earths 28, 622-626.

[55] Gergely, V., Clyne, B., 2000. The FORMGRIP process: foaming of reinforced metals by gas release in precursors. Advanced Engineering Materials 2, 175-178.

[56] Gergely, V., Clyne, T., 2004. Drainage in standing liquid metal foams: modelling and experimental observations. Acta Materialia 52, 3047-3058.

[57] Gergely, V., Degischer, H., Clyne, T., 2000. Recycling of MMCs and production of metallic foams. Comprehensive composite materials 3, 797-820.

[58] Gibson, L.J., Ashby, M., 1997. Cellular solids: Structure and properties. Cambridge University Press (Cambridge and New York).

[59] Gibson, L.J., Ashby, M.F., Harley, B.A., 2010. Cellular materials in nature and medicine. Cambridge University Press.

[60] Golestanipour, M., Mashhadi, H.A., Abravi, M., Malekjafarian, M., Sadeghian, M., 2011. Manufacturing of Al/SiCp composite foams using calcium carbonate as foaming agent. Materials Science and Technology 27, 923-927.

[61] Greene, S.A., Hall, I.W., Guden, M., 2002. Improving the energy absorption of closed cell aluminum foams. Journal of Materials Science Letters 21, 1591-1593.

[62] Greer, A., 2003. Grain refinement of alloys by inoculation of melts. Philosophical Transactions of the Royal Society of London. Series A: Mathematical, Physical and Engineering Sciences 361, 479-495.

[63] Guden, M., Yüksel, S., Taşdemirci, A., Tanoğlu, M., 2007. Effect of aluminum closed-cell foam filling on the quasi-static axial crush performance of glass fiber reinforced polyester composite and aluminum/composite hybrid tubes. Composite structures 81, 480-490.

[64] Guy, A.G., 1962. Physical metallurgy for engineers. Addison-Wesley Pub. Co.

[65] Haesche, M., Weise, J., Garcia-Moreno, F., Banhart, J., 2008. Influence of particle additions on the foaming behaviour of AlSi composites made by semi-solid processing. Materials Science and Engineering: A 480, 283-288.

[66] Haibel, A., Rack, A., Banhart, J., 2006. Why are metal foams stable? Applied physics letters 89, 154102.

[67] Hall, E., 1951. The deformation and ageing of mild steel: III discussion of results. Proceedings of the Physical Society. Section B 64, 747.

[68] Handbook, A., 1992. Properties and Selection: Nonferrous Alloys and Special

[69] Purpose Materials. ASM International, USA 2.

[70] Hanssen, A.G., Langseth, M., Hopperstad, O.S., 2000. Static and dynamic crushing of square aluminium extrusions with aluminium foam filler. International Journal of Impact Engineering 24, 347-383.

[71] Hardy, P.W.a.P., G.W., 1967. Method of Producing a Lightweight Foamed Metal. US Patent 3,300,296.

[72] Hatch, J.E., 1984. Aluminum: properties and physical metallurgy. ASM International.

[73] Hossein Elahi, S., Abdi, H., Shahverdi, H., 2012. Investigating viscosity variations of molten aluminum by calcium addition and stirring. Materials Letters.

[74] Huang, L., Wang, H., Yang, D., Ye, F., Lu, Z., 2012. Effects of scandium additions on mechanical properties of cellular Al-based foams. Intermetallics 28, 71-76.

[75] Huskins, E., Cao, B., Ramesh, K., 2010. Strengthening mechanisms in an Al–Mg alloy. Materials Science and Engineering: A 527, 1292-1298.

[76] Hyde, K., Norman, A., Prangnell, P., 2001. The effect of cooling rate on the morphology of primary Al_3Sc intermetallic particles in Al–Sc alloys. Acta materialia 49, 1327-1337.

[77] Ip, S., Wang, S., Toguri, J., 1999a. Aluminum foam stabilization by solid particles. Canadian Metallurgical Quarterly 38, 81-92.

[78] Ip, S.W., Wang, Y., Toguri, J.M., 1999b. Aluminum foam stabilization by solid particles. Canadian Metallurgical Quarterly 38, 81-92.

[79] Irving, B., 1997. Scandium places Aluminium Welding on a new Plateau. Welding journal 76.

[80] J., B., 1990. Porous metal body production involves compaction at low temperature followed by heating to near melting point of metal. German Patent 4,018,360, 1-5.

[81] J., B., 1992. Methods for manufacturing foamable metal bodies. US Patent 5,151,246, 1-10.

[82] J.F., P., 1960. Cellulrized light metal. US Patent 2,935,396, 1-4.

[83] JC, E., 1956. Method of producing metal foam. US Patent No.2751289, 1-6.

[84] Jeenager, V., Pancholi, V., 2014. Influence of cell wall microstructure on the energy absorption capability of aluminium foam. Materials & Design 56, 454-459.

[85] Jeenager, V., Pancholi, V., Daniel, B., 2012. The Effect of Aging on Energy Absorption Capability of Closed Cell Aluminum Foam. Advanced Materials Research 585, 327-331.

[86] Jeon, I., Katou, K., Sonoda, T., Asahina, T., Kang, K.-J., 2009. Cell wall mechanical properties of closed-cell Al foam. Mechanics of Materials 41, 60-73.

[87] Jiang, B., Wang, Z., Zhao, N., 2007. Effect of pore size and relative density on the mechanical properties of open cell aluminum foams. Scripta Materialia 56, 169-172.

[88] Jiménez, C., Garcia-Moreno, F., Pfretzschner, B., Kamm, P.H., Neu, T.R., Klaus, M., Genzel, C., Hilger, A., Manke, I., Banhart, J., 2012. Metal Foaming Studied In Situ by

Energy Dispersive X-Ray Diffraction of Synchrotron Radiation, X-Ray Radioscopy, and Optical Expandometry. Advanced Engineering Materials.

[89] Jin I., K.L., Sang H. , 1990. Method of producing lightweight foamed metal. US Patent, 1-4.

[90] Jordens, A., Cheng, Y.P., Waters, K.E., 2013. A review of the beneficiation of rare earth element bearing minerals. Minerals Engineering 41, 97-114.

[91] Jung, A., Lach, E., Diebels, S., 2014. New hybrid foam materials for impact protection. International Journal of Impact Engineering 64, 30-38.

[92] Kadoi, K., Babcsán, N., Nakae, H., 2010. Role of oxide particles in aluminum melt toward aluminum foam fabrication by the melt route, Materials Science Forum. Trans Tech Publ, 385-390.

[93] Kamm, P.H., García-Moreno, F., Jiménez, C., Banhart, J., 2013. Suitability of various complex hydrides for foaming aluminium alloys. Journal of Materials Research, 1-8.

[94] Kaptay, G., 2003. Interfacial criteria for stabilization of liquid foams by solid particles. Colloids and Surfaces A: Physicochemical and Engineering Aspects 230, 67-80.

[95] Kishimoto, S., Wang, Q., Tanaka, Y., Kagawa, Y., 2014. Compressive mechanical properties of closed-cell aluminum foam–polymer composites. Composites Part B: Engineering 64, 43-49.

[96] Konstantinidis, I.C., Papadopoulos, D.P., Lefakis, H., Tsipas, D.N., 2005. Model for determining mechanical properties of aluminum closed-cell foams. Theoretical and Applied Fracture Mechanics 43, 157-167.

[97] Körner, C., Arnold, M., Singer, R.F., 2005a. Metal foam stabilization by oxide network particles. Materials Science and Engineering: A 396, 28-40.

[98] Korner, C., Singer, R., 1999. Numerical simulation of foam formation and evolution with modified cellular automata, MetFoam 99: International Conference on Metal Foams and Porous Metal Structures, 91-96.

[99] Körner, C., Thies, M., Hofmann, T., Thürey, N., Rüde, U., 2005b. Lattice Boltzmann model for free surface flow for modeling foaming. Journal of Statistical Physics 121, 179-196.

[100] Kumar, G.V., Mukherjee, M., Garcia-Moreno, F., Banhart, J., 2013. Reduced-Pressure Foaming of Aluminum Alloys. Metallurgical and Materials Transactions A 44, 419-426.

[101] Kumar, N.R., Gokhale, A., 2012. Processing and Stability of LM25/SiCP Composite Foams. Transactions of the Indian Institute of Metals 65, 753-757.

[102] Lázaro, J., Solórzano, E., de Saja, J., Rodríguez-Pérez, M., 2013. Early anisotropic expansion of aluminium foam precursors. Journal of Materials Science, 1-11.

[103] Lehmhus, D., Banhart, J., 2003. Properties of heat-treated aluminium foams. Materials Science and Engineering: A 349, 98-110.

[104] Li, J.R., Cheng, H.F., Yu, J.L., Han, F.S., 2003. Effect of dual-size cell mix on the stiffness and strength of open-cell aluminum foams. Materials Science and Engineering: A 362, 240-248.

[105] Li, Z., Xi, C., Jing, L., Wang, Z., Zhao, L., 2014. Effect of loading rate on the compressive properties of open-cell metal foams. Materials Science and Engineering: A 592, 221-229.

[106] Lin, R., Hoch, M., 1989. The solubility of hydrogen in molten aluminum alloys. Metallurgical Transactions A 20, 1785-1791.

[107] Liu, Y., Gong, W., Zhang, X., 2014. Numerical investigation of influences of porous density and strain-rate effect on dynamical responses of aluminum foam. Computational Materials Science 91, 223-230.

[108] LM, N., 1970. Display box. German patent 2,006,445.

[109] Long, X., Khanna, S.K., 2003. Numerical simulation of residual stresses in a spot welded joint. Journal of engineering materials and technology 125, 222-226.

[110] Luong, D.D., Pinisetty, D., Gupta, N., 2013. Compressive properties of closed-cell polyvinyl chloride foams at low and high strain rates: Experimental investigation and critical review of state of the art. Composites Part B: Engineering 44, 403-416.

[111] Ma, L., Song, Z., 1998. Cellular structure control of aluminium foams during foaming process of aluminium melt. Scripta Materialia 39, 1523-1528.

[112] Mahmutyazicioglu, N., Albayrak, O., Ipekoglu, M., Altintas, S., 2013. Effects of alumina (Al2O3) addition on the cell structure and mechanical properties of 6061 foams. Journal of Materials Research 28, 2509-2519.

[113] Maine, E., Ashby, M.F., 2000. Cost estimation and the viability of metal foams. Advanced Engineering Materials 2, 205-209.

[114] Májlinger, K., Orbulov, I.N., 2014. Characteristic compressive properties of hybrid metal matrix syntactic foams. Materials Science and Engineering: A 606, 248-256.

[115] Matijasevic, B., Banhart, J., 2006. Improvement of aluminium foam technology by tailoring of blowing agent. Scripta Materialia 54, 503-508.

[116] McCartney, D., 1989. Grain refining of aluminium and its alloys using inoculants. International Materials Reviews 34, 247-260.

[117] McCormack, T.M., Miller, R., Kesler, O., Gibson, L.J., 2001. Failure of sandwich beams with metallic foam cores. International Journal of Solids and Structures 38, 4901-4920.

[118] Miyoshi, T., Hara, S., Mukai, T., Higashi, K., 2001. Development of a closed cell aluminum alloy foam with enhancement of the compressive strength. Materials transactions-JIM 42, 2118-2123.

[119] Miyoshi, T., Itoh, M., Akiyama, S., Kitahara, A., 2000. ALPORAS aluminum foam: production process, properties, and applications. Advanced engineering materials 2, 179-183.

[120] Miyoshi, T., Itoh, M., Mukai, T., Kanahashi, H., Kohzu, H., Tanabe, S., Higashi, K., 1999. Enhancement of energy absorption in a closed-cell aluminum by the modification of cellular structures. Scripta Materialia 41, 1055-1060.

[121] Monachon, C., Krug, M.E., Seidman, D.N., Dunand, D.C., 2011. Chemistry and structure of core/double-shell nanoscale precipitates in Al–6.5 Li–0.07 Sc–0.02 Yb (at.%). Acta Materialia 59, 3398-3409.

[122] Mondal, D.P., Jha, N., Badkul, A., Gul, B., Rathod, S., Das, S., 2013a. Effect of age hardening on compressive deformation behavior of Al-alloy (LM13)–cenosphere hybrid foam prepared using CaCO3 as a foaming agent. Journal of Materials Research, 1-11.

[123] Mondal, D.P., Jha, N., Gull, B., Das, S., Badkul, A., 2013b. Microarchitecture and compressive deformation behaviour of Al-alloy (LM13)–cenosphere hybrid Al-foam prepared using CaCO3 as foaming agent. Materials Science and Engineering: A 560, 601-610.

[124] Montanini, R., 2005. Measurement of strain rate sensitivity of aluminium foams for energy dissipation. International Journal of Mechanical Sciences 47, 26-42.

[125] Mostafa, A., Shankar, K., Morozov, E.V., 2013. Insight into the shear behaviour of composite sandwich panels with foam core. Materials & Design 50, 92-101.

[126] Motz, C., Pippan, R., 2001. Deformation behaviour of closed-cell aluminium foams in tension. Acta Materialia 49, 2463-2470.

[127] Mousavi, M., Cross, C., 1999. Effect of scandium and titanium–boron on grain refinement and hot cracking of aluminium alloy 7108. Science and Technology of Welding & Joining 4, 381-388.

[128] Mu, Y., Yao, G., Cao, Z., Luo, H., Zu, G., 2011. Strain-rate effects on the compressive response of closed-cell copper-coated carbon fiber/aluminum composite foam. Scripta Materialia 64, 61-64.

[129] Mu, Y., Yao, G., Liang, L., Luo, H., Zu, G., 2010a. Deformation mechanisms of closed-cell aluminum foam in compression. Scripta Materialia 63, 629-632.

[130] Mu, Y., Yao, G., Luo, H., 2010b. The dependence of damping property of fly ash reinforced closed-cell aluminum alloy foams on strain amplitude. Materials & Design 31, 1007-1009.

[131] Mu, Y., Zu, G., Cao, Z., Yao, G., Wang, Q., 2013. Metal foam stabilization by copper-coated carbon fibers. Scripta Materialia 68, 459-462.

[132] Mukherjee, M., Garcia-Moreno, F., Banhart, J., 2010. Defect generation during solidification of aluminium foams. Scripta Materialia 63, 235-238.

[133] Murty, B., Kori, S., Chakraborty, M., 2002. Grain refinement of aluminium and its alloys by heterogeneous nucleation and alloying. International Materials Reviews 47, 3-29.

[134] Nadler, J., 1999. Fabrication and Microstructure of Metal-Metal Syntactic Foams JH Nadler, KM Hurysz, JL Clark, JK Cochran, KJ Lee, and TH Sanders, Jr. School of Materials Science and Engineering Georgia Institute of Technology Atlanta, GA 30332-0245 USA. MetFoam'99, 179.

[135] Nakajima, H., 2007. Fabrication, properties and application of porous metals with directional pores. Progress in Materials Science 52, 1091-1173.

[136] Nemat-Nasser, S., Kang, W.J., McGee, J.D., Guo, W.G., Isaacs, J.B., 2007. Experimental investigation of energy-absorption characteristics of components of sandwich structures. International Journal of Impact Engineering 34, 1119-1146.

[137] Neu, T., Mukherjee, M., Moreno, F.G., Banhart, J., 2012. Magnesium and magnesium alloy foams, 7th International Conference on Porous Metals and Metallic Foams (MetFoam2011), 133.

[138] Niebylski LM, J.C., Immethun PA, 1974. Metal foam and process therefore. US Patent 3,794,481, 1-10.

[139] Niebylski LM, J.C., Lee TE, 1976. Reinforced foamed metal. US Patent US Patent 3,940,262, 1-10.

[140] Norman, A., Prangnell, P., McEwen, R., 1998. The solidification behaviour of dilute aluminium–scandium alloys. Acta Materialia 46, 5715-5732.

[141] Ohno, A., Motegi, T., Kobayashi, N., 1983. Solidification Technology in the Foundry and Casthouse. The Metals Society, London, 171.

[142] Olurin, O.B., Fleck, N.A., Ashby, M.F., 2000. Deformation and fracture of aluminium foams. Materials Science and Engineering: A 291, 136-146.

[143] Onck, P.R., 2001. Application of a continuum constitutive model to metallic foam DEN-specimens in compression. International Journal of Mechanical Sciences 43, 2947-2959.

[144] Orbulov, I.N., Ginsztler, J., 2012. Compressive characteristics of metal matrix syntactic foams. Composites Part A: Applied Science and Manufacturing 43, 553-561.

[145] Orowan, E., 1948. Symposium on Internal Stresses in Metals and Alloys. Institute of Metals, London 451.

[146] Pandey, A., Spowart, J., 2010. High Strength and High Temperature Aluminum Alloys for High Performance Applications. Minerals, Metals and Materials Society/AIME, 420 Commonwealth Dr., P. O. Box 430 Warrendale PA 15086 USA.

[147] Park, C., Nutt, S.R., 2000. PM synthesis and properties of steel foams. Materials Science and Engineering: A 288, 111-118.

[148] Park, C., Nutt, S.R., 2001a. Anisotropy and strain localization in steel foam. Materials Science and Engineering: A 299, 68-74.

[149] Park, C., Nutt, S.R., 2001b. Effects of process parameters on steel foam synthesis. Materials Science and Engineering: A 297, 62-68.

[150] Park, C., Nutt, S.R., 2002. Strain rate sensitivity and defects in steel foam. Materials Science and Engineering: A 323, 358-366.

[151] Paul, A., Ramamurty, U., 2000. Strain rate sensitivity of a closed-cell aluminum foam. Materials Science and Engineering: A 281, 1-7.

[152] Petch, N., 1953. The cleavage strength of polycrystals. J. Iron Steel Inst. 174, 25-28.

[153] Pickering, F., 1975. Basis of quantitative metallography [M] Institute of Metals. London, UK.

[154] Pinto, P., Peixinho, N., Silva, F., Soares, D., 2014. Compressive properties and energy absorption of aluminum foams with modified cellular geometry. Journal of Materials Processing Technology 214, 571-577.

[155] Polmear, J., 1995. Light Alloys - Metallurgy of the Light Metals. Arnold, London.

[156] Polonsky, L., Lipson, S., Markus, H., 1961. Light weight cellular metal. Modern Cast 65, 57-71.

[157] Prakash, O., Sang, H., Embury, J., 1995. Structure and properties of Al□ SiC foam. Materials Science and Engineering: A 199, 195-203.

[158] Quigley, B.F., Abbaschian, G.J., Wunderlin, R., Mehrabian, R., 1982. A method for fabrication of aluminum-alumina composites. Metallurgical Transactions A 13, 93-100.

[159] Rabiei, A., Hutchinson, J., Evans, A., 2000. Heat generation during the fatigue of a cellular Al alloy. Metallurgical and Materials Transactions A 31, 1129-1136.

[160] Raj, E.E., 2008. Processing and Mechanical Property Analysis of Closed-cell Aluminium Foam. PhD thesis, IIT Roorkee.

[161] Raj, R.E., Daniel, B., 2008a. Manufacturing challenges in obtaining tailor-made closed-cell structures in metallic foams. The International Journal of Advanced Manufacturing Technology 38, 605-612.

[162] Raj, R.E., Daniel, B.S.S., 2008b. Prediction of compressive properties of closed-cell aluminum foam using artificial neural network. Computational Materials Science 43, 767-773.

[163] Rajan, T., Sharma, A., 2012. Heat Treatment: Principles and Techniques. PHI Learning Pvt. Ltd.

[164] Ramachandra, S., Sudheer Kumar, P., Ramamurty, U., 2003. Impact energy absorption in an Al foam at low velocities. Scripta Materialia 49, 741-745.

[165] Ravi Kumar, N., Ramachandra Rao, N., Gokhale, A., 2014. Effect of SiC particle content on foaming and mechanical properties of remelted and diluted A356/SiC composite. Materials Science and Engineering: A.

[166] Ravi Kumar, N., Ramachandra Rao, N., Sudhakar, B., Gokhale, A., 2010. Foaming experiments on LM25 alloy reinforced with SiC particulates. Materials Science and Engineering: A 527, 6082-6090.

[167] Reglero, J.A., Solórzano, E., Rodríguez-Pérez, M.A., de Saja, J.A., Porras, E., 2010. Design and testing of an energy absorber prototype based on aluminum foams. Materials & Design 31, 3568-3573.

[168] Sahu, S., Goel, M.D., Mondal, D.P., Das, S., 2014. High temperature compressive deformation behavior of ZA27–SiC foam. Materials Science and Engineering: A 607, 162-172.

[169] Schorghuber, F., Simancik, F., Hartl, E., 1999. Method of producing molded bodies of a metal foam. Google Patents.

[170] Schwingel, D., Seeliger, H.-W., Vecchionacci, C., Alwes, D., Dittrich, J., 2007. Aluminium foam sandwich structures for space applications. Acta Astronautica 61, 326-330.

[171] Sosnick, B., 1948. PROCESS. Google Patents.

[172] Sriram, R., Vaidya, U., Kim, J.-E., 2006. Blast impact response of aluminum foam sandwich composites. Journal of Materials Science 41, 4023-4039.

[173] Stanzick, H., Klenke, J., Danilkin, S., Banhart, J., 2002a. Material flow in metal foams studied by neutron radioscopy. Applied Physics A 74, 1118-1120.

[174] Stanzick, H., Wichmann, M., Weise, J., Helfen, L., Baumbach, T., Banhart, J., 2002b. Process control in aluminum foam production using real-time X-ray radioscopy. Advanced Engineering Materials 4, 814-823.

[175] Stocco, A., Garcia-Moreno, F., Manke, I., Banhart, J., Langevin, D., 2011. Particle-stabilised foams: structure and aging. Soft Matter 7, 631-637.

[176] Sugimura, Y., Meyer, J., He, M.Y., Bart-Smith, H., Grenstedt, J., Evans, A.G., 1997. On the mechanical performance of closed cell Al alloy foams. Acta Materialia 45, 5245-5259.

[177] Sulong, M.A., Vesenjak, M., Belova, I.V., Murch, G.E., Fiedler, T., 2014. Compressive properties of Advanced Pore Morphology (APM) foam elements. Materials Science and Engineering: A 607, 498-504.

[178] Sun, Y., Burgueño, R., Vanderklok, A.J., Tekalur, S.A., Wang, W., Lee, I., 2014. Compressive behavior of aluminum/copper hybrid foams under high strain rate loading. Materials Science and Engineering: A 592, 111-120.

[179] Sun, Z., Hu, X., Sun, S., Chen, H., 2013. Energy-absorption enhancement in carbon-fiber aluminum-foam sandwich structures from short aramid-fiber interfacial reinforcement. Composites Science and Technology 77, 14-21.

[180] Surace, R., De Filippis, L.A.C., Ludovico, A.D., Boghetich, G., 2009. Influence of processing parameters on aluminium foam produced by space holder technique. Materials & Design 30, 1878-1885.

[181] Surappa, M.K., Rohatgi, P.K., 1981. Preparation and properties of cast aluminium-ceramic particle composites. Journal of Materials Science 16, 983-993.

[182] Suzuki, T., Takeuchi, S.,Yoshinaga, H., 1990. Dislocation dynamics and plasticity. In: U. Gonser (Ed.), Springer Series in Materials Science, Springer-Verlag, New York 12, 32-34.

[183] Symposium held April 13-15, San Francisco, California, U.S.A., 1998. Porous and Cellular Materials

[184] for Structural Applications. material research sociaty symposium 521.

[185] Tellkamp, V., Lavernia, E.J., Melmed, A., 2001. Mechanical behavior and microstructure of a thermally stable bulk nanostructured Al alloy. Metallurgical and Materials Transactions A 32, 2335-2343.

[186] Thiyahuddin, M.I., Gu, Y.T., Thambiratnam, D.P., Thilakarathna, H.M., 2014. Impact And Energy Absorption Of Portable Water-Filled Road Safety Barrier System Fitted With Foam. International Journal of Impact Engineering.

[187] Tolley, A., Radmilovic, V., Dahmen, U., 2005. Segregation in Al_3(Sc, Zr) precipitates in Al–Sc–Zr alloys. Scripta materialia 52, 621-625.

[188] Triantafillou, T.C., Gibson, L.J., 1987. Minimum weight design of foam core sandwich panels for a given strength. Materials Science and Engineering 95, 55-62.

[189] V., G., 2011. New Phenomenological Model for Solid Foams, in: Murín, J., Kompiš, V., Kutiš, V. (Eds.), Computational Modelling and Advanced Simulations. Springer Netherlands, 67-82.

[190] Van Dalen, M.E., Dunand, D.C., Seidman, D.N., 2005. Effects of Ti additions on the nanostructure and creep properties of precipitation-strengthened Al–Sc alloys. Acta materialia 53, 4225-4235.

[191] van Dalen, M.E., Gyger, T., Dunand, D.C., Seidman, D.N., 2011. Effects of Yb and Zr microalloying additions on the microstructure and mechanical properties of dilute Al–Sc alloys. Acta Materialia 59, 7615-7626.

[192] W.S., F., 1965. Method of making metal foam bodies. US Patent 3,214,265, 1-10.

[193] Wadley, H.N., Fleck, N.A., Evans, A.G., 2003. Fabrication and structural performance of periodic cellular metal sandwich structures. Composites Science and Technology 63, 2331-2343.

[194] Wallentowitz, H., Adam, H., 1996. Predicting the crashworthiness of vehicle structures made by lightweight design materials and innovative joining methods. International Journal of Crashworthiness 1, 163-180.

[195] Wang, S., Starink, M., 2005a. Precipitates and intermetallic phases in precipitation hardening Al–Cu–Mg–(Li) based alloys. International Materials Reviews 50, 193-215.

[196] Wang, S.C., Starink, M.J., 2005b. Precipitates and intermetallic phases in precipitation hardening Al–Cu–Mg–(Li) based alloys. International Materials Reviews 50, 193-215.

[197] Wang, Z., Li, Z., Ning, J., Zhao, L., 2009. Effect of heat treatments on the crushing behaviour and energy absorbing performance of aluminium alloy foams. Materials & Design 30, 977-982.

[198] Wicklein, M., Thoma, K., 2005. Numerical investigations of the elastic and plastic behaviour of an open-cell aluminium foam. Materials Science and Engineering: A 397, 391-399.

[199] Wilde, P., Mackie, A., Husband, F., Gunning, A., Morris, V., Fillery-Travis, A., 1999. The Role of interfacial structure and composition on foam drainage and fluid dynamics, Foams and Films: Proceedings of the International Workshop on Foams and Films, Leuven, Belgium. MIT-Verlag: Bremen, Germany, 59.

[200] Wübben, T., Odenbach, S., 2005. Stabilisation of liquid metallic foams by solid particles. Colloids and Surfaces A: Physicochemical and Engineering Aspects 266, 207-213.

[201] Xia, X., Zhao, W., Wei, Z., Wang, Z., 2012. Effects of specimen aspect ratio on the compressive properties of Mg alloy foam. Materials & Design 42, 32-36.

[202] Xu, Z.G., Fu, J.W., Luo, T.J., Yang, Y.S., 2012. Effects of cell size on quasi-static compressive properties of Mg alloy foams. Materials & Design 34, 40-44.

[203] Youssef, K., Scattergood, R., Murty, K., Koch, C., 2006. Nanocrystalline Al–Mg alloy with ultrahigh strength and good ductility. Scripta materialia 54, 251-256.

[204] Yu, S., Luo, Y., Liu, J., 2008. Effects of strain rate and SiC particle on the compressive property of SiC-Mg composite foams. Materials Science and Engineering: A 487, 394-399.

[205] Zhang, G., Wang, B., Ma, L., Wu, L., Pan, S., Yang, J., 2014. Energy absorption and low velocity impact response of polyurethane foam filled pyramidal lattice core sandwich panels. Composite Structures 108, 304-310.

[206] Zhao, R., Kim, B.G., Ryu, Y.M., Hur, B.Y., 2011a. Microstructure and Strength Properties of AZ31 Mg Alloy Foams, Materials Science Forum. Trans Tech Publ, 537-540.

[207] Zhao, W.M., Zhang, H., Li, H.P., Wang, Z.F., Zhao, Y., Zhao, R., Hur, B.Y., 2011b. Study on Fabrication, Defects and Compression Properties of Al Foams at Different Foaming Temperatures. Advanced Materials Research 214, 70-74.

[208] Zhao, Y., Liao, X., Jin, Z., Valiev, R., Zhu, Y., 2004. Microstructures and mechanical properties of ultrafine grained 7075 Al alloy processed by ECAP and their evolutions during annealing. Acta Materialia 52, 4589-4599.